5-1-2007

Behavior of Horizontally Curved Steel Tubular-Flange Bridge Girders

Zhuo Fan

Richard Sause

BEHAVIOR OF HORIZONTALLY CURVED STEEL TUBULAR-FLANGE BRIDGE GIRDERS

by

Zhuo Fan

Richard Sause

ATLSS Report No. 07-02

May 2007

ATLSS is a National Center for Engineering Research on Advanced Technology for Large Structural Systems

117 ATLSS Drive
Bethlehem, PA 18015-4729

Phone: (610)758-3525
Fax: (610)758-5902

www.atlss.lehigh.edu
Email: inatl@lehigh.edu

BEHAVIOR OF HORIZONTALLY CURVED STEEL TUBULAR-FLANGE BRIDGE GIRDERS

by

Zhuo Fan, Ph.D.
Graduate Research Assistant
Lehigh University

Richard Sause, Ph.D.
Joseph T. Stuart
Professor of Structural Engineering
Lehigh University

Sponsored by the Federal Highway Administration and the Pennsylvania Infrastructure Technology Alliance through a grant from the Pennsylvania Department of Community and Economic Development

ATLSS Report No. 07-02

May 2007

ATLSS is a National Center for Engineering Research on Advanced Technology for Large Structural Systems

117 ATLSS Drive
Bethlehem, PA 18015-4729

Phone: (610)758-3525
Fax: (610)758-5902

www.atlss.lehigh.edu
Email: inatl@lehigh.edu

Acknowledgements

This research was conducted at the Advanced Technology for Large Structural System (ATLSS) Center of Lehigh University in Bethlehem, Pennsylvania.

The research was sponsored by the Federal Highway Administration (FHWA), the Pennsylvania Infrastructure Technology Alliance (PITA) through a grant from Pennsylvania Department of Community and Economic Development, and the ATLSS Center.

The findings, opinions, and conclusions expressed in this report are the authors' and do not necessary reflect the opinions of the sponsors.

Table of Contents

List of Tables

List of Figures

Abstract

A new type of curved steel bridge girder, called a curved tubular-flange girder, with rectangular tubes as flanges, is proposed and studied in this report. A curved steel tubular-flange girder has much larger torsional stiffness than a curved I-girder and less potential for cross section distortion than a curved box-girder. Therefore, it has potential advantages compared to curved I-girders and box-girders.

A theoretical analysis method for systems of curved tubular-flange girders braced by cross frames is presented. A stress analysis method for tubular-flange girders is also provided. The behavior of curved tubular-flange girder systems is studied using the theoretical analysis method and compared to the behavior of the corresponding curved I-girder systems. A parametric study is performed using the theoretical analysis method to investigate the effects of geometric parameters on the behavior of curved tubular-flange girder systems. The studied parameters include tubular-flange width, tubular-flange depth, cross section depth, girder curvature, and the number of cross frames. Finite element analyses are conducted to verify the theoretical analysis method, to study the behavior of a curved tubular-flange girder system under dead load, and to study the behavior of a curved tubular-flange girder system with a composite concrete deck under dead and live load.

The study shows that a curved tubular-flange girder system develops much less warping normal stress and cross section rotation than a corresponding curved I-girder system. The difference is especially significant for a single curved girder under its own weight, suggesting that curved tubular-flange girders would be much easier to transport and erect than curved I-girders. As girder curvature increases, the rate of increase in the stresses and displacements for a single I-girder is much greater than for a single curved tubular-flange girder. Smaller cross frame forces develop in a tubular-flange girder system than in an I-girder system, which results in smaller cross frame members. The study also indicates that a curved tubular-flange girder system may need fewer cross frames than a curved I-girder system. Finally, for curved girder systems with a composite deck, the behavior of tubular-flange girder systems is dominated by bending stresses, while the behavior of I-girder systems includes significant warping stresses, again suggesting that the tubular-flange girder system may be more efficient.

Chapter 1 Introduction

1.1 Overview

Curved highway bridges are increasingly needed to accommodate complex highway conditions in urban and suburban areas, and to provide safe highway alignments in difficult terrain. The behavior of curved bridges is more complicated than the behavior of straight bridges because the curvature induces torsion in the bridge.

Curved steel I-girder systems or box-girder systems are often used in curved bridges. However, each of these systems has potential problems. First, stability is a major issue during construction. A single curved I-girder may not be able to support itself during erection, because the torsional stresses and displacements may be large, even under only the girder self-weight, due to the low torsional stiffness of the I-girder. Therefore, temporary shoring may be needed to erect an I-girder bridge framing system. Second, the cross frames between curved I-girders must be designed as primary load-carrying members because they work with the girders to resist the torsion carried by the bridge system. Since curved I-girders develop significant warping stress due to their low torsional stiffness, a large number of cross frames may be needed to reduce the warping stress. These cross frames may be expensive.

A box-girder has a large torsional stiffness and negligible warping stress. However, cross section distortion may occur and lead to significant distortional stresses. Thus, bracing must be used inside the box to maintain the box shape and avoid cross section distortion. The internal bracing inside a box-girder makes box-girder design, construction, and maintenance complex and expensive. Fatigue problems are also a concern for box-girders due to the potential cross section distortion and the bracing details.

In this report, a new type of curved girder, the curved tubular-flange girder, is proposed and studied. The tubular-flange girder has round, square, or rectangular tubes in place of the plate flanges of an I-girder. The web of a tubular-flange is similar to that of an I-girder. Owing to the torsional stiffness of the tubular-flanges, a tubular-flange girder has much higher torsional stiffness than an I-girder, and should have less cross-section distortion than a box-girder.

As shown later in the report, a single curved tubular-flange girder develops much smaller stresses and displacements than a single curved I-girder under self-weight or other construction loading. In addition, a curved tubular-flange girder system may require fewer cross frames than a curved I-girder system. A curved tubular-flange girder may develop cross section distortion, in particular, distortion of the web and the tubular-flanges. However, web transverse stiffeners can eliminate the web distortion.

The focus of this study is the linear elastic behavior of single curved tubular-flange girders and systems of curved tubular-flange girders braced by cross frames. A theoretical analysis method for the curved tubular-flange girder system is presented. Finite element models are developed and used to verify the accuracy of the theoretical analysis method. The analysis results for curved tubular-flange girder systems are compared with those of curved I-girder systems. A parametric study is also carried out to show the effect of cross section parameters on the behavior of curved tubular-flange girder systems.

1.2 Research Objectives

The overall objective of this report is to study the behavior of curved tubular-flange bridge girders under construction and service conditions. The specific objectives are as follows:

(1) To propose a theoretical analysis method for single curved tubular-flange girders and systems of multiple curved tubular-flange girders braced by cross frames. Displacements and stresses on the cross section are provided by the analysis method.

(2) To develop finite element models to simulate the behavior of curved tubular-flange girder systems under construction loads and live loads.

(3) To compare the behavior of curved tubular-flange girders with curved I-girders and identify advantages and disadvantages of curved tubular-flange girders.

(4) To conduct a parametric study to show the effect of cross section parameters on the behavior of curved tubular-flange girders.

(5) To study the influence of a concrete deck on a tubular-flange girder system and to study the live load behavior of a curved tubular-flange girder bridge.

1.3 Report Scope

To achieve the objectives, linear elastic analyses of systems of curved tubular-flange girders with cross frames were conducted. A theoretical analysis method for curved tubular-flange girder systems with multiple girders and cross frames is presented. Finite element analyses of curved tubular-flange girder systems are presented and used to verify the theoretical analysis method. A parametric study using both the theoretical analysis and finite element methods is presented. The study involves curved single tubular-flange girders and a tubular-flange girder system with three girders. The parametric study investigates the influence of girder geometry, including the tubular flange width, tubular-flange depth, the cross section depth, the curvature of the girders,

and the number of cross frames. The behavior of curved tubular-flange girders with a composite bridge deck under the action of live loads and dead loads is also presented.

1.4 Organization of Report

The report consists of nine chapters. Chapter 1 introduces the research and the organization of the report. Chapter 2 presents background knowledge which relates to curved tubular-flange girders. Chapter 3 presents the differential equations for simply supported single curved girders and the solutions to these equations. Chapter 4 presents the theoretical analysis method for tubular-flange girder systems with multiple girders and cross frames. Chapter 4 also presents the stress analysis of curved tubular-flange girders. In Chapter 5, the theoretical analysis method presented in Chapter 4 is used to analyze single curved tubular-flange girders and tubular-flange girder systems with multiple girders. Chapter 5 also compares curved tubular-flange girders and I-girders. Finite element simulations of curved tubular-flange system are presented in Chapter 6 and are compared with the theoretical analysis results presented in Chapter 5. The parametric study is presented in Chapter 7. The study of tubular-flange girders with a composite deck is presented in Chapter 8. Finally, Chapter 9 summarizes the research and provides conclusions.

Chapter 2 Background

The background material related to this report is reviewed in this chapter. The previous research on curved girders usually focused on concrete or steel I- or box-section girders. Research on girder cross sections with tubular flanges is limited to straight girders. In this chapter, previous research on the theory of curved open and closed section girders, and previous research on straight tubular-flange girders are briefly reviewed. Then, the analytical methods given in AASHTO Guide Specification for Horizontally Curved Highway Bridges (AASHTO 2003) are summarized. The chapter then summarizes the theory for thin-walled structural members related to this study.

2.1 Related Research

A significant amount of analytical and experimental research on curved I-girders and curved box girders has been completed. This research involves analytical methods, stability and ultimate strength analyses, and so on. Herein, only research related to the linear elastic behavior of curved tubular-flange girders (TFGs) is summarized.

Dabrowski (1968) presented the differential equations for a single curved girder and gave closed form solutions to the differential equations for curved girders with either an open cross section or a closed cross section under several different loading and boundary conditions. To determine cross section stresses, Dabrowski extended thin-walled beam theory for straight girders to curved girders. Some details of Dabrowski's work will be introduced in Section 2.4, and Chapter 3 will make a more detailed presentation of Dabrowski's results.

Kim (2005) studied straight I-shaped girders with one concrete-filled round tubular flange and one flat plate flange. His research investigated the flexural strength and stability of concrete-filled tubular flange girders (TFGs) with the tubular-flange as the compression flange. Finite element analyses and experiments were conducted. Kim listed several advantages of concrete-filled TFGs over I-girders, including: (1) a concrete-filled tubular flange provides more strength, stiffness and stability than a flat plate flange; (2) a concrete-filled TFG needs fewer diaphragms than a similar I-girder to maintain lateral torsional stability. Kim also provided design recommendations for straight concrete-filled TFGs.

Wimer (2004) conducted a design study of concrete-filled TFGs. The TFGs had a rectangular tube as the compression flange, a flat plate as the tension flange, and either a corrugated web or a flat web. A four-girder prototype bridge was considered.

Eighteen design combinations were studied. Wimer (2004) also conducted experiments and analyses of concrete-filled TFGs and he concluded that tubular flanges increase the torsional stiffness of the girder, and allow large unbraced lengths to be used in bridges with TFGs.

Richardson et al. (1963) presented a rigorous theoretical analysis method to determine the internal forces and stresses for each girder in a curved I-girder system. They separated the I-girder system into individual girders. The unknown interaction forces between the girders and cross frames were treated as external forces applied to the individual girders. Cross frame deflections were considered. Since there are two equilibrium equations and two displacement compatibility equations for each cross frame, a series of simultaneous linear equations are obtained, and then, the unknown interaction forces are determined by solving these equations.

2.2 Analytical Methods for Curved Girders

Both approximate and refined analytical methods have been proposed for the analysis of curved bridges in the AASHTO Guide Specification of Horizontally Curved Steel Girders (AASHTO 2003). The approximate analytical methods are usually used for preliminary analysis and the refined methods are used for final or detailed analysis.

2.2.1 Approximate Methods

The V-load method (U.S. Steel Corporation 1984) is a widely used approximate method for the analysis of curved I-girder bridges and is best suited for the analyses needed for preliminary design.

2.2.2 Refined Methods

Two refined methods of analyses are summarized here briefly, namely the classic theoretical method and the finite element method. The classic theoretical method was summarized by Zureick and Naqib (1997). This method solves differential equations for a curved bridge girder to obtain the internal forces and displacements of the girders. The solution is a closed form or a convergent series solution of the differential equations. Then, thin-walled member theory is used to determine the cross section stresses. However, the classic theoretical method has some limitations. Solutions of the differential equations may be very difficult or impossible for some loading and boundary conditions. And also, thin-walled member theory may not be applicable to all cases of the curved bridge girders.

The finite element method is a widely used refined method for the analysis of curved girder bridge system. This method can be applied to various girder configurations under different loading and boundary conditions. The disadvantage of the finite element method is the time and effort needed to build the finite element model.

2.3 Theory for In-Plane Bending of Thin-Walled Girders

This section summarizes thin-walled member theory that is needed for the analysis of stresses and displacements of bridge girders.

2.3.1 Bending Normal Stress

The normal stress due to bending about one principle x-axis is linearly distributed across the cross section. Here, it is assumed that the x-axis is horizontal and the y-axis is vertical (see **Figure 2.1**). The normal stress at any point on the cross section is:

$$\sigma_x = \frac{M_x}{I_x} y \tag{2.1}$$

where, a tensile normal stress is positive; I_x is the moment of inertia about x-axis; and the bending moment about the x-axis, M_x, is:

$$M_x = -EI_x \frac{d^2 v}{dz^2}$$

where, E is the elastic modulus; v is the displacement in y-axis direction. The sign convention for M_x and v are shown in **Figure 2.1**.

2.3.2 Shear Stress

The shear stress related to the bending of a thin-walled girder is different for a girder with an open cross section and a girder with a closed cross section.

2.3.2.1 Thin-Walled Girder with Open Cross Section

The shear stress on an open cross section is parallel to the wall of the cross section and uniformly distributed across the thickness of the wall. Assuming bending about a horizontal x-axis, the associated shear stress is:

$$\tau_v = -\frac{V_y}{I_x t} \int_0^s yt \cdot ds \tag{2.2}$$

where, τ_v is the shear stress due to the vertical shear force; V_y is the vertical shear force; t is the wall thickness; s is the contour coordinate along the centerline of the cross section wall (see **Figure 2.2**). The origin, o, of the contour coordinate, s, is an arbitrary point at the centerline of the cross section wall. Usually, one end point of the open section is taken as the origin, o, as shown in **Figure 2.2**. Eq. (2.2) gives the shear stress, τ_v, at a distance s from the origin of the contour coordinate.

2.3.2.2 Thin-Walled Girder with Closed Cross Section

The shear stress on a closed cross section can be treated as having two components. The first component is the shear stress on an associated open cross section, which is obtained by making a cut at any point on the closed cross section. The second component is a constant shear flow around the closed cross section to prevent a discontinuity in the longitudinal warping displacement at the cut in the associated open section member. Thus, the total shear stress on the closed section is:

$$\tau_v = \tau_{vc} + \tau_{vo} \tag{2.3}$$

where, τ_v is the total shear stress due to the vertical shear force; τ_{vc} is the constant shear stress; τ_{vo} is the shear stress on the associated open cross section, which can be determined using Eq. (2.2). The constant shear τ_{vc} is determined as follows. At the cut made in the closed section to create the associated open section member, the relative warping displacement is:

$$w = \int_0^e \frac{\tau_v}{G} \cdot ds$$

where, G is the shear modulus. The origin, o, of the contour coordinate, s, is arranged to be on one side of the cut, and the end, e, of the contour coordinate is arranged to be on the other side of the cut, as shown in **Figure 2.3**. The integral is taken from o to e. For the closed cross section, w must be zero. Thus,

$$\oint \frac{\tau_v}{G} \cdot ds = 0 \tag{2.4}$$

The integral in Eq. (2.4) is calculated from the origin around the centerline of the cross section and back to the origin.

By substituting Eq. (2.3) into Eq. (2.4), the constant shear flow is obtained as follows:

$$\tau_{vc} t = \frac{\oint \tau_{vo} ds}{\oint (1/t) ds} \tag{2.5}$$

So, the shear stress on the closed section is equal to:

$$\tau_{vt} = \frac{\oint \tau_{vo} ds}{t \cdot \oint (1/t) ds} - \frac{V_y}{I_x t} \int_0^s y \cdot t ds \tag{2.6}$$

2.4 Theory for Torsion of Thin-Walled Girders

The torsion theory for thin-walled girders presented in this section is based on Dabrowski (1968) and Galambos (1968). Dabrowski (1968) used this theory in the analysis of curved girders. The theory assumes that the cross section shape is preserved, the displacements and deformations are small and the material is linear elastic.

2.4.1 Thin-Walled Girders with Open Section

Torsion is usually treated as consisting of two components, uniform torsion and non-uniform torsion.

2.4.1.1 Uniform Torsion

Under uniform torsion, also called St. Venant torsion, the twist angle per length is constant along the girder. The longitudinal warping displacements are also constant along the girder. Only shear stress is induced, and the corresponding torque is called St.Venant torque. The St. Venant torque is:

$$M_{st} = GJ\frac{d\varphi}{dz} \tag{2.7}$$

where, M_{st} is the St. Venant torque on the cross section; φ is the twist angle; J is the torsion constant and is (for a thin-walled cross section):

$$J = \frac{1}{3}\int_s t^3 ds \tag{2.8}$$

The St. Venant shear stress distribution on a thin-walled open cross section is parallel to the walls of the cross section and varies linearly across the thickness of the walls. The maximum shear stress on a wall is equal to:

$$\tau_{st} = \frac{M_{st}}{J}\cdot t \tag{2.9}$$

where, τ_{st} is the St. Venant shear stress on the wall; t is the wall thickness.

2.4.1.2 Non-Uniform Torsion

Under non-uniform torsion, also called warping torsion, the warping deformation is constrained. Both the rate of change of the twist angle, $\frac{d\varphi}{dz}$, and the longitudinal warping displacement, w, vary along the length of the girder. As a result, in

addition to the St. Venant shear stress, longitudinal warping normal stress and shear stress are induced under non-uniform torsion.

Warping Normal Stress

The warping normal stress results from the restrained warping displacements along the girder and can be expressed as follows:

$$\sigma_w = E \cdot \omega_n \cdot \frac{d^2\varphi}{dz^2} \tag{2.10}$$

where, ω_n is the normalized unit warping and is defined as:

$$\omega_n(s) = \frac{1}{A}\int_0^e \omega_0(s)t(s)ds - \omega_0(s) \tag{2.11}$$

where, A is the cross section area; e is the contour coordinate at the end point of the open section member; ω_0 is the unit warping with respect to the shear center of the cross section and is defined as

$$\omega_0(s) = \int_0^s \rho_0 ds \tag{2.12}$$

where, ρ_0 is the perpendicular distance between the tangent to a point on the cross section and the shear center (S.C. in **Figure 2.2**).

For convenience, the concept of a bimoment is introduced, and is defined from the warping normal stress as follows:

$$B = -\int_0^e \sigma_w \omega_n t ds \tag{2.13}$$

Substituting Eq. (2.10) into Eq. (2.13) yields:

$$B = -EI_w \frac{d^2\varphi}{dz^2} \tag{2.14}$$

where, I_w is the warping moment of inertia, equal to:

$$I_w = \int_0^e \omega_n^2 t ds \tag{2.15}$$

The warping normal stress represented in term of the bimoment is:

$$\sigma_w = -\frac{B}{I_w} \cdot \omega_n \tag{2.16}$$

Warping Shear Stress

As the warping normal stress varies along the length of the girder, warping shear stress is induced. The warping shear flow is:

$$\tau_w t = -ES_w \frac{d^3\varphi}{dz^3} \tag{2.17}$$

where, τ_w is the warping shear stress; S_w is the warping static moment, equal to:

$$S_w = \int_0^s \omega_n \cdot t ds \tag{2.18}$$

The contribution of the warping shear stress to resisting torsion is called the warping torque. By the integration of the warping shear flow about the shear center, the warping torque is obtained as:

$$M_w = \int_0^e \tau_w t \cdot \rho_0 ds = -EI_w \frac{d^3\varphi}{dz^3} \tag{2.19}$$

The warping shear stress can be expressed in term of the warping torque as:

$$\tau_w = \frac{M_w}{I_w t} \cdot S_w \tag{2.20}$$

From Eq. (2.14) and Eq. (2.19), the relation between the bimoment and warping torque is shown to be:

$$M_w = \frac{dB}{dz} \tag{2.21}$$

2.4.1.3 Total Torque

The total torque for a thin-walled open section girder is the sum of the St. Venant torque and the warping torque. That is

$$M_z = GJ\frac{d\varphi}{dz} - EI_w\frac{d^3\varphi}{dz^3} \tag{2.22}$$

where, M_z is the total torque.

2.4.2 Thin-Walled Girders with Closed Cross Sections

Similar to open section girders, torsion of girders with closed cross sections is usually treated as having two components, uniform torsion and non-uniform torsion.

2.4.2.1 Uniform Torsion

Uniform torsion of a closed section girder induces only shear flow. The uniform torsion shear stress distribution is different for a closed section and an open section girder. For the closed cross section, a constant shear flow around the cross section develops under uniform torsion, which is equal to:

$$\tau_{st} t = \frac{M_{st}}{2A_e} \tag{2.23}$$

where, τ_{st} is the St. Venant shear stress on the section; A_e is the area enclosed by the centerline of the closed section walls.

The torsion constant for a closed section is:

$$J = \frac{4A_e^2}{\oint (1/t)ds} \tag{2.24}$$

2.4.2.2 Non-Uniform Torsion

Non-uniform torsion of a closed section beam induces both warping normal stress and warping shear stress.

Warping Normal Stress

Benscoter (1954) presented an approximate solution for a thin-walled girder with a closed cross section. In this solution, the warping displacement is assumed to be:

$$w = \omega_n \cdot \frac{df(z)}{dz}$$

where, w is the warping displacement; f(z) is a dimensionless warping function; ω_n is the normalized unit warping for the closed section and is defined as:

$$\omega_n(s) = \frac{2A_e}{\oint \frac{ds}{t}} \int_0^s \frac{ds}{t} - \omega_0(s) \tag{2.25}$$

where, $\omega_0(s)$ has the same definition as given previously for a girder with an open section, and is given by Eq. (2.12). The starting point of integral, o, where s = 0, in Eq. (2.25) can be an arbitrary point on the cross section. Thus, the warping normal stress is given as follows:

$$\sigma_w = E \cdot \frac{dw}{dz} = E \cdot \omega_n \cdot \frac{d^2 f}{dz^2} \tag{2.26}$$

where, σ_w is the warping normal stress.

The bimoment for a girder with a closed section is:

$$B = -\int_0^s \sigma_w \omega_n t ds = -EI_w \frac{d^2 f}{dz^2} \tag{2.27}$$

where, I_w is the warping moment of inertia for a girder with a closed section as follow:

$$I_w = \int \omega_n{}^2 \cdot t ds \tag{2.28}$$

The warping normal stress is given in terms of the bimoment as follows:

$$\sigma_w = -\frac{B}{I_w} \cdot \omega_n \tag{2.29}$$

Warping Shear Stresses

The warping shear flow is in equilibrium with the normal stress. The warping shear flow is expressed with respect to the warping function as:

$$\tau_w t = -E\bar{S}_w \frac{d^3 f}{dz^3} \tag{2.30}$$

where, τ_w is the warping shear stress; $\bar{S}_w$ is the secondary warping moment.
Then the warping torque is obtained as:

$$M_w = \int_0^s \tau_w t \cdot \rho_0 ds = -EI_w \frac{d^3 f}{dz^3} \tag{2.31}$$

The warping shear stress can be expressed in term of warping torque as:

$$\tau_w = \frac{M_w}{I_w \cdot t} \cdot \bar{S}_w \tag{2.32}$$

where, τ_w is the warping shear stress. $\bar{S}_w$ for a girder with a closed cross section is considered to have two parts, namely, a statically determinate part and a statically indeterminate part (Benscoter,1954). $\bar{S}_w$ is expressed as follows:

$$\bar{S}_w = S_{wi} - S_w \tag{2.33}$$

where, S_{wi} is the warping indeterminate moment; S_w is the warping statical moment and is determined by the following equation:

$$S_w = \int_0^s \omega_n \cdot t ds \tag{2.34}$$

To maintain continuity of warping displacements for a closed section, the secondary shear flow has to satisfy the following equation (Benscoter, 1954):

$$\oint \tau_w t \cdot \frac{ds}{t} = 0 \tag{2.35}$$

Substituting Eq. (2.32) into Eq. (2.35), the following equation is obtained:

$$\oint S_{wi} \frac{ds}{t} = \oint S_w \frac{ds}{t} \tag{2.36}$$

By integrating Eq. (2.36), S_{wi} is determined and then $\bar{S}_w$ can be determined from Eq. (2.33).

2.4.2.3 Total Torque

The total torque for a closed section girder is the summation of the uniform torque and non-uniform torque and is expressed as below:

$$M_z = GJ\frac{d\varphi}{dz} - EI_w\frac{d^3f}{dz^3} \tag{2.37}$$

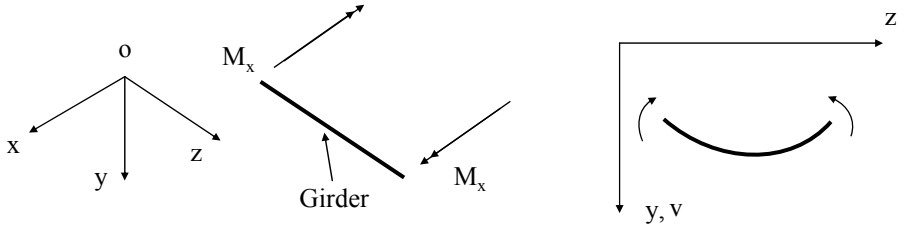

(a) Positive bending moment (b) Curvature in yz plane

Figure 2.1 Bending Moment and Curvature Sign Convention

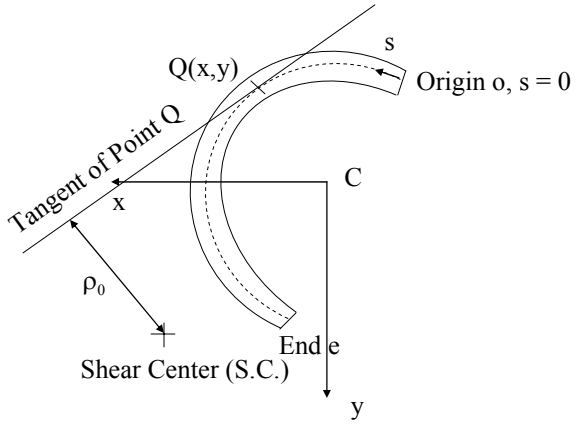

Figure 2.2 Contour Coordinate and Tangential Distances on Cross Section

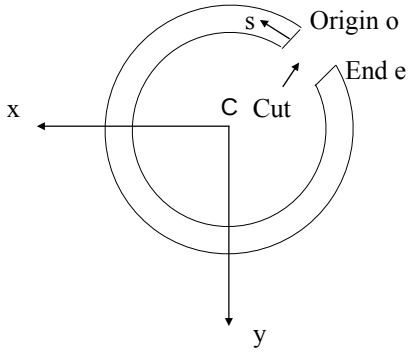

Figure 2.3 Associate Open Section for a Closed Section

Chapter 3 Analytical Solutions to Differential Equations

A detailed discussion of the differential equations of equilibrium and the analytical solution of these equations for a simply supported curved girder is provided in this chapter.

3.1. Differential Equations for Curved Girders

The differential equations for a simply supported curved girder subjected to uniformly distributed loads are presented by Dabrowski (1968). In this chapter, the theory for thin-walled girders presented in Chapter 2, with all of the assumptions given there, is extended for curved girders. The derivation of differential equations in this section follows that of Dabrowski (1968). Dabrowski makes the following additional assumptions: the curved girder is radially supported at the ends, and the cross section dimensions (width and depth) are small in comparison to the span length and the radius of curvature.

Figure 3.1 shows a differential element of a curved thin-walled girder subjected to uniform loads. The centroid of the cross-section is the origin of the coordinate system. The cross-section is singly symmetric and the coordinate of the shear center is $(0, y_0)$. The x-axis is located in the plane of the curvature of the girder and is directed toward the center of curvature. The y-axis is perpendicular to the plane of the curvature and the positive direction is downward. The z-axis is in the direction of the tangent of the curved girder. A distributed radial load, $p_x(z)$, and a vertical load, $p_y(z)$, as well as a distributed torque, $m_z(z)$, are applied at the shear center of the cross-section. The shear forces,V_x, V_y, and the total torque, M_z, also act at the shear center. The bending moments, M_x, M_y, and the axial force N act at the centroid of the cross-section.

From equilibrium of forces in the directions of the x-, y-, and z-axis respectively, the differential equations of equilibrium for a curved girder subjected to distributed loads are as follows:

x-axis:
$$\frac{dV_x}{dz} + \frac{N}{R} + p_x(z) = 0 \tag{3.1}$$

y-axis:
$$\frac{dV_y}{dz} + p_y(z) = 0 \tag{3.2}$$

z-axis:
$$\frac{dN}{dz} - \frac{V_x}{R} = 0 \tag{3.3}$$

where, R is the radius of curvature of the curved girder. Additional differential equations of equilibrium based on the moments about x-, y-, and z-axis are as follows:

x-axis: $$\frac{dM_x}{dz} + \frac{1}{R}(M_z + V_x y_0) - V_y = 0 \tag{3.4}$$

y-axis: $$\frac{dM_y}{dz} - V_x = 0 \tag{3.5}$$

z-axis: $$\frac{dM_z}{dz} - \frac{1}{R}(M_x + Ny_0) + m_z(z) = 0 \tag{3.6}$$

where, y_0 is the y-axis coordinate of the shear center.

3.2. Solutions of Differential Equations

Dabrowski (1968) provided solutions of the differential equations of equilibrium, but did not present many of the details involved in developing the solutions. Here, Dabrowski's results are reviewed with additional details provided.

In the following subsections, the differential equation solutions for a single span curved girder with an open cross section and a closed section under uniformly distributed and concentrated loads are presented, respectively. The applied distributed loads include a uniformly distributed vertical load, p_y, and a uniformly distributed torque, m_z. The applied concentrated loads included the vertical load, P, and the torque, T. Simply-supported boundary condition are assumed, with each end free to warp, but restrained against twist.

3.2.1. Primary Bending Moment

3.2.1.1 Differential Equations

Considering only the equilibrium equations involving the uniformly distributed load p_y, and the uniformly distributed torque, m_z, Eqs. (3.2), (3.3) and (3.6) are rewritten as:

$$\frac{dV_y}{dz} = -p_y \tag{3.6}$$

$$\frac{V_x}{R} = \frac{dN}{dz} \tag{3.7}$$

$$\frac{dM_z}{dz} = \frac{1}{R}(M_x + Ny_0) - m_z \tag{3.8}$$

Replacing the term $\frac{V_x}{R}$ in Eq. (3.4) with Eq. (3.7) and taking the first derivative, results in the following:

$$\frac{d^2M_x}{dz^2} + \frac{dM_z}{Rdz} + \frac{d^2N}{dz^2}y_0 - \frac{dV_y}{dz} = 0 \tag{3.9}$$

Substituting Eq. (3.8) and Eq. (3.6) into Eq. (3.9), results in a differential equation relating the bending moment and the axial load to the applied loads as follows:

$$\frac{d^2M_x}{dz^2} + \frac{M_x + Ny_0}{R^2} - \frac{m_z}{R} + \frac{d^2N}{dz^2}y_0 + p_y = 0 \tag{3.10}$$

For a simply-supported curved girder with no axial load applied along the z-axis and no radial load $p_x(z)$, the axial force is zero. Thus, Eq. (3.10) is simplified to:

$$\frac{d^2M_x}{dz^2} + \frac{M_x}{R^2} = \frac{m_z}{R} - p_y \tag{3.11}$$

Eq. (3.11) is the differential equation relating the bending moment of a curved girder to the uniformly distributed vertical load and torque.

When a curved girder is subjected to a concentrated vertical load, P, and torque, T, applied at position z_0, the fundamental differential equation can be written based on the equation for distributed loads and torque. The concentrated loads are treated as a special case of distributed loads using the Dirac Delta function as follows:

$$p_y(z) = P\delta(z - z_0) \tag{3.12a}$$

$$m_z(z) = T\delta(z - z_0) \tag{3.12b}$$

The equivalent distributed vertical load in Eq. (3.12a) and equivalent distributed torque in Eq. (3.12b) are equal to P and T respectively, acting at position z_0. When z is not equal to z_0, the equivalent distributed loads $p_y(z)$ and $m_z(z)$ are both zero.

Replacing p_y and m_z in Eq. (3.11) with Eqs. (3.12a) and (3.12b), the differential equation for a concentrated vertical load, P, and torque, T, is as follows:

$$\frac{d^2M_x}{dz^2} + \frac{M_x}{R^2} = \left(\frac{T}{R} - P\right)\delta(z - z_0) \tag{3.13}$$

3.2.1.2 Solutions of Differential Equations

The complete solution of a differential equation is the summation of the homogeneous solution and the particular solution.

The homogenous equations for Eqs. (3.11) and (3.13) are the same and are equal to:

$$\frac{d^2 M_x}{dz^2} + \frac{M_x}{R^2} = 0$$

The homogenous solution, M_{xh}, is:

$$M_{xh} = C_1 \cos(\frac{z}{R}) + C_2 \sin(\frac{z}{R}) \tag{3.14}$$

The coefficients C_1 and C_2 are determined later from the boundary conditions.

The particular solutions, M_{xp}, for Eqs. (3.11) and (3.13) are as follows. For the uniformly distributed load, p_y, and torque, m_z:

$$M_{xp} = m_z \cdot R - p_y \cdot R^2 \tag{3.15}$$

For the concentrated vertical load, P, and concentrated torque, T:

$$z < z_0 \qquad M_{xp} = 0 \tag{3.16a}$$

$$z > z_0 \qquad M_{xp} = (T - PR)\sin(\frac{z - z_0}{R}) \tag{3.16b}$$

Thus, the complete solution for the bending moment is as follows. For the uniformly distributed loads, p_y, and torque, m_z, the bending moment is:

$$M_x = C_1 \cos(\frac{z}{R}) + C_2 \sin(\frac{z}{R}) + m_z \cdot R - p_y \cdot R^2 \tag{3.17}$$

For the concentrated load, P, and torque, T, applied at position z_0, the bending moment is:

$$z < z_0 \qquad M_x = C_1 \cos(\frac{z}{R}) + C_2 \sin(\frac{z}{R}) \tag{3.18a}$$

$$z > z_0 \quad M_x = C_1 \cos(\frac{z}{R}) + C_2 \sin(\frac{z}{R}) + (T - P_y R)\sin(\frac{z - z_0}{R}) \tag{3.18b}$$

The boundary conditions for the simply supported girder require that the bending moment is equal to zero at each end of the girder.

$$z = 0 \quad M_x(z = 0) = 0 \tag{3.19a}$$

$$z = L \quad M_x(z = L) = 0 \tag{3.19b}$$

Substituting Eqs. (3.19) into Eqs. (3.17) and (3.18) respectively, the coefficients C_1 and C_2 can be determined. Thus, the complete solutions for the bending moment of a single span curved girder with simple supports are expressed as follows. For the uniformly distributed vertical load, p_y, and torque, m_z, the bending moment is:

$$M_x = (p_y R^2 - m_z R) \cdot (\frac{\sin(\frac{z}{R}) + \sin(\frac{L - z}{R})}{\sin(\frac{L}{R})} - 1) \tag{3.20}$$

For the concentrated load, P, and torque, T, applied at position z_0, the bending moment is:

$$z < z_0 \qquad M_x = (PR - T)\frac{\sin(\frac{L - z_0}{R})}{\sin(\frac{L}{R})} \cdot \sin(\frac{z}{R}) \tag{3.21a}$$

$$z > z_0 \qquad M_x = (PR - T)\frac{\sin(\frac{z_0}{R})}{\sin(\frac{L}{R})} \cdot \sin(\frac{L - z}{R}) \tag{3.21b}$$

3.2.2 Primary Shear Forces

The lateral shear force, V_x, can be determined for Eq. (3.3). With no lateral load, p_x, and no axial force N, the result is:

$$V_x = 0 \tag{3.22}$$

The vertical shear force V_y can be determined by integration of Eq. (3.2) as follows:

$$V_y = \int_0^z p_y dz + C \tag{3.23}$$

3.2.3 Torsion of Girder with Open Cross Section

3.2.3.1 Differential Equations

The total torque M_z on a cross-section is assumed to consist of two components, the St. Venant torque M_{st} and the warping torque M_w. The fundamental differential equations are developed as follows. The total torque is:

$$M_z = M_{st} + M_w \tag{3.24}$$

The St. Venant torque for the open section girder is given by Eq. (2.7), as follows:

$$M_{st} = GJ\frac{d\varphi}{dz}$$

The warping torque for the open section girder is given by Eq. (2.19), as follows:

$$M_w = -EI_w\frac{d^3\varphi}{dz^3}$$

Substituting Eqs. (2.7) and (2.19) into Eq. (3.24), the total torque is rewritten in terms of the twist angle, φ, as follows:

$$M_z = GJ\frac{d\varphi}{dz} - EI_w\frac{d^3\varphi}{dz^3} \tag{3.25}$$

Substituting Eq. (3.25) into Eq. (3.8) with the axial force, N, equal to zero for a simply supported curved girder, the differential equation expressed in terms of the twist angle is as follows:

$$\frac{d^4\varphi}{dz^4} - \lambda^2\frac{d^2\varphi}{dz^2} = \frac{1}{EI_w}\left(m_z - \frac{M_x}{R}\right) \tag{3.26}$$

where, $\lambda = \sqrt{\frac{GJ}{EI_w}}$. This differential equation is used for a curved girder subjected to the distributed vertical load, p_y, and torque, m.

For the concentrated vertical load, P, and torque, T, the fundamental differential equation can be written based on the equation for distributed load and torque. The concentrated loads can be expressed using the Dirac Delta function as in Eq. (3.12a) and (3.12b). Replacing m_z in Eq. (3.26) with Eq. (3.12b), the differential equation for the concentrated loading case is:

$$\frac{d^4\varphi}{dz^4} - \lambda^2 \frac{d^2\varphi}{dz^2} = \frac{1}{EI_w}[T\delta(z - z_0) - \frac{M_x}{R}] \tag{3.27}$$

If both distributed loads and concentrated loads are applied to the curved girder, the differential equation, based on Eqs. (3.26) and (3.27), is:

$$\frac{d^4\varphi}{dz^4} - \lambda^2 \frac{d^2\varphi}{dz^2} = \frac{1}{EI_w}[m_z + T\delta(z - z_0) - \frac{M_x}{R}] \tag{3.28}$$

If the bending moment, M_x, is known, the twist angle can be solved from the differential equation. Then, the St. Venant torque, the warping torque and the total torque on a cross section can be determined by Eqs. (2.7), (2.19) and (3.24) respectively.

3.2.3.2 Solutions of Differential Equations

The homogeneous equation is:

$$\frac{d^4\varphi}{dz^4} - \lambda^2 \frac{d^2\varphi}{dz^2} = 0 \tag{3.29}$$

The solution of this homogeneous equation is:

$$\varphi = C_1 \sinh \lambda z + C_2 \cosh \lambda z + C_3 z + C_4 \tag{3.30}$$

where, coefficients C_1 to C_4 are determined later from the boundary conditions.

The particular solutions for Eqs. (3.26) and (3.27) can be obtained by analogy to a straight girder with a thin-walled open cross section. Thus, the particular solutions for the twist angle for a curved girder are as follows. For the uniformly distributed torque, m_z, the particular solution is:

$$\varphi_p = -\frac{m_z}{2GJ} z^2 \tag{3.31}$$

For the concentrated torque, T, the particular solution is:

$$0 < z < z_0 \qquad \varphi_p = 0 \tag{3.32a}$$

$$z > z_0 \qquad \varphi_p = \frac{T}{GJ}\left[\frac{\sinh \lambda(z - z_0)}{\lambda} - (z - z_0)\right] \tag{3.32b}$$

The term $-\frac{M_x}{R}$ may be considered as a series of concentrated torques applied along the whole length of the girder. The particular solution due to the term $-\frac{M_x}{R}$ is:

$$z > \bar{z}_0 \quad \varphi_p = \int_0^z \frac{M_x(\bar{z}_0)}{RGJ}\left[\left(\frac{\sinh \lambda(z - \bar{z}_0)}{\lambda} - (z - \bar{z}_0)\right]d\bar{z}_0\right. \tag{3.33}$$

where, $\bar{z}_0$ is the position of the applied equivalent torque $-\frac{M_x(\bar{z}_0)}{R}$. For a simply-supported curved girder, the bending moment M_x is given by Eqs. (3.20) or (3.21). Substituting Eq. (3.20) or (3.21) into the Eq. (3.33), the particular solution can be obtained by integration. Hence, the complete solution of the twist angle for the curved girder is:

$$\varphi = C_1 \sinh \lambda z + C_2 \cosh \lambda z + C_3 z + C_4 + \varphi_p \tag{3.34}$$

Substituting Eqs. (3.31), (3.32) and (3.33) into Eq. (3.34), the complete solution for a curved girder subjected to uniformly distributed loads and concentrated loads, respectively, is as follows. For the uniformly distributed vertical load, p_y, and torque, m_z, the twist angle is:

$$\varphi = C_1 \sinh \lambda z + C_2 \cosh \lambda z + C_3 z + C_4 - \frac{m_z}{2GJ} z^2 - \int_0^z \frac{M_x}{RGJ}\left[\frac{\sinh \lambda(z - \bar{z}_0)}{\lambda} - (z - \bar{z}_0)\right]d\bar{z}_0 \tag{3.35}$$

where, the bending moment M_x is given by Eq. (3.20).

For the concentrated vertical load, P_y, and torque, T, applied at the position z_0, the twist angle is:

$0 < z < z_0$

$$\varphi = C_1 \sinh \lambda z + C_2 \cosh \lambda z + C_3 z + C_4 - \int_0^z \frac{M_x}{RGJ}[\frac{\sinh \lambda(z - \bar{z}_0)}{\lambda} - (z - \bar{z}_0)]d\bar{z}_0$$

(3.36a)

$z > z_0$

$$\varphi = C_1 \sinh \lambda z + C_2 \cosh \lambda z + C_3 z + C_4 + \frac{T}{GJ}[\frac{\sinh \lambda(z - z_0)}{\lambda} - (z - z_0)]$$

$$- \int_0^z \frac{M_x}{RGJ}[\frac{\sinh \lambda(z - \bar{z}_0)}{\lambda} - (z - \bar{z}_0)]d\bar{z}_0 \qquad (3.36b)$$

where, the bending moment M_x is given by Eq. (3.21).

The boundary conditions for a simply supported curved girder are as follows:

$$z = 0 \qquad \varphi(0) = 0 \qquad \frac{d^2\varphi(0)}{dz^2} = 0 \qquad (3.37a)$$

$$z = L \qquad \varphi(L) = 0 \qquad \frac{d^2\varphi(L)}{dz^2} = 0 \qquad (3.37b)$$

At the two end cross sections, the warping is free, but the twist is restrained. That means the bimoment and the twist angle at each end are zero.

Substituting the equations for the boundary conditions, Eqs. (3.37), into Eq. (3.35) or Eqs. (3.36), the coefficients C_1, C_2, C_3 and C_4 are determined. The solution for the twist angle of a simply-supported curved girder is as follows. For the uniformly distributed load, p_y, and torque, m_z, the twist angle is:

$$\varphi = \frac{m_z(1-\eta) + p_y R\eta}{GJ\lambda^2}(\frac{\sinh \lambda z + \sinh \lambda(L-z)}{\sinh \lambda L} - 1)$$
$$- \frac{p_y R^3 - m_z R^2}{GJ}(1-\eta)(\frac{\sin(\frac{z}{R}) + \sin(\frac{L-z}{R})}{\sin(\frac{L}{R})} - 1) + \frac{p_y R}{2GJ} z(L-z)$$

(3.38)

where, η is a dimensionless parameter and is equal to:

$$\eta = \frac{1}{1+(\lambda R)^2} \tag{3.39}$$

For the concentrated load P and torque T applied at position z_0, the twist angle is:

$0 < z < z_0$

$$\varphi = \frac{TR - PR^2}{GJ}(1-\eta)\frac{\sin(\frac{L-z_0}{R})}{\sin(\frac{L}{R})}\sin(\frac{z}{R}) + \frac{PR}{GJ}\frac{(L-z_0)}{L}z - \frac{T(1-\eta)+PR\eta}{GJ\cdot\lambda}\frac{\sinh\lambda(L-z_0)}{\sinh\lambda L}\sinh\lambda z \tag{3.40a}$$

$z_0 < z < L$

$$\varphi = \frac{TR - PR^2}{GJ}(1-\eta)\frac{\sin(\frac{z_0}{L})}{\sin(\frac{L}{R})}\sin(\frac{z}{R}) + \frac{PR}{GJ}\frac{z_0}{L}z - \frac{T(1-\eta)+PR\eta}{GJ\cdot\lambda}\frac{\sinh\lambda z_0}{\sinh\lambda L}\sinh\lambda z \tag{3.40b}$$

According to Eqs. (3.24), (2.7) and (2.19), the total torque, the St. Venant torque and the warping torque at a cross section can be determined completely from the twist angle. Hence, the torques for the curved thin-walled open-section girders are as follows. For the uniformly distributed load, p_y, and torque, m_z, the St. Venant torque is:

$$M_{st} = (m_z R - p_y R^2)(1-\eta)\frac{\cos(\frac{z}{L}) - \cos(\frac{L-z}{R})}{\sin(\frac{L}{R})} - p_y R\frac{2z-L}{2} + [m_z(1-\eta)+pR\eta]\frac{\cosh(\lambda z) - \cosh[\lambda(L-z)]}{\lambda\sinh(\lambda L)} \tag{3.41}$$

The warping torque is:

$$M_w = -\frac{m_z(1-\eta)+p_y R\eta}{\lambda}\frac{\cosh(\lambda z - \cosh[\lambda(L-z)]}{\sinh\lambda L} + (m_z R - p_y R^2)\eta\frac{\cos(\frac{z}{R}) - \cos(\frac{L-z}{R})}{\sin(\frac{L}{R})} \tag{3.42}$$

The total torque is:

$$M_z = (m_z R - p_y R^2)\frac{\cos(\frac{z}{R}) - \cos(\frac{L-z}{R})}{\sin(\frac{L}{R})} - p_y R^2 \frac{\frac{z}{R} - (\frac{L-z}{R})}{2} \tag{3.43}$$

For the concentrated vertical load, P, and torque, T, applied at position z_0, the St. Venant torque is:

$0 < z < z_0$

$$M_{st} = (T - PR)(1-\eta)\frac{\sin(\frac{L-z_0}{R})}{\sin(\frac{L}{R})}\cos(\frac{z}{R}) + PR\frac{(L-z_0)}{L} - [T(1-\eta) + PR\eta]\frac{\sinh\lambda(L-z_0)}{\sinh\lambda L}\cosh\lambda z \tag{3.44a}$$

$z_0 < z < L$

$$M_{st} = -(T - PR)(1-\eta)\frac{\sin(\frac{z_0}{R})}{\sin(\frac{L}{R})}\cos(\frac{L-z}{R}) - PR\frac{z_0}{L} + [T(1-\eta) + PR\eta]\frac{\sinh\lambda z_0}{\sinh\lambda L}\cosh\lambda(L-z) \tag{3.44b}$$

The warping torque is:

$0 < z < z_0$

$$M_w = [T(1-\eta) + PR\eta]\frac{\sinh\lambda(L-z_0)}{\sinh\lambda L}\cosh\lambda z + (T - PR)\eta\frac{\sin(\frac{L-z_0}{R})}{\sin(\frac{L}{R})}\cos(\frac{z}{R}) \tag{3.45a}$$

$z_0 < z < L$

$$M_w = -[T(1-\eta) + PR\eta]\frac{\sinh\lambda z_0}{\sinh\lambda L}\cosh\lambda(L-z) - (T - PR)\eta\frac{\sin(\frac{z_0}{R})}{\sin(\frac{L}{R})}\cos(\frac{L-z}{R}) \tag{3.45b}$$

The total torque is:

$0 < z < z_0$

$$M_z = (T - PR)\frac{\sin(\frac{L - z_0}{R})}{\sin(\frac{L}{R})}\cos(\frac{z}{R}) + PR\frac{L - z_0}{L} \tag{3.46}$$

$z_0 < z < L$

$$M_z = -(T - PR)\frac{\sin(\frac{z}{R})}{\sin(\frac{L}{R})}\cos(\frac{L - z}{R}) - PR\frac{z_0}{L} \tag{3.47}$$

3.2.3.3 Bimoment

Eq. (2.14) gives the bimoment for a girder with an open cross section as:

$$B = -EI_w\frac{d^2\varphi}{dz^2}$$

Since the twist angle is known from the differential equation solution, the bimoment, B, can be determined by substituting Eq. (3.38) or Eqs. (3.39) into Eq. (2.14). The bimoment expressions for a simply-supported curved girder with an open cross section subjected to uniformly distributed loads and concentrated loads are as follows. For the uniformly distributed vertical load, p_y, and torque, m_z, the bimoment is:

$$B = -\frac{m_z(1-\eta) + p_y R\eta}{\lambda_c{}^2}\left(1 - \frac{\sinh(\lambda_c z) + \sinh[\lambda_c(L - z)]}{\sinh(\lambda_c L)}\right) +$$

$$(m_z R^2 - p_y R^3)\eta\left(\frac{\sin(\frac{z}{R}) + \sin(\frac{L - z}{R})}{\sin(\frac{L}{R})} - 1\right) \tag{3.48}$$

For the concentrated vertical load, P, and torque, T, applied at position z_0, the bimoment is:

$0 < z < z_0$

$$B = \frac{T(1-\eta)+PR\eta}{\lambda}\frac{\sinh[\lambda(L-z_0)]}{\sinh(\lambda L)}\sinh(\lambda z) + (TR - PR^2)\eta\frac{\sin(\frac{L-z_0}{R})}{\sin(\frac{L}{R})}\sin(\frac{z}{R}) \tag{3.49}$$

$z_0 < z < L$

$$B = \frac{T(1-\eta)+PR\eta}{\lambda}\frac{\sinh(\lambda z_0)}{\sinh(\lambda L)}\sinh[\lambda(L-z)] + (TR - PR^2)\eta\frac{\sin(\frac{z_0}{R})}{\sin(\frac{L}{R})}\sin(\frac{L-z}{R}) \tag{3.50}$$

3.2.4 Torsion of Girder with Closed Cross Section

The warping torque for a girder with a closed cross section is related to the warping function f(z), rather than the twist angle, $\varphi(z)$, as shown in Eq. (2.31):

$$M_w = -EI_w\frac{d^3f}{dz^3}$$

So the warping function has to be determined before the warping torque can be determined.

3.2.4.1 Differential Equations in Terms of Warping Function

The total torque for a closed cross section girder is given by Eq. (2.33) as:

$$M_z = GJ\frac{d\varphi}{dz} - EI_w\frac{d^3f}{dz^3}$$

The relationship between the twist angle and the warping function is given by Dabrowski (1968) as:

$$\frac{d\varphi}{dz} = \mu\frac{df}{dz} + \frac{M_z}{GI_c} \tag{3.51}$$

where, μ is a warping shear parameter, defined as:

$$\mu = 1 - \frac{J}{I_c} \tag{3.52}$$

I_c is the central moment of inertia, which is:

$$I_c = \int_A \rho_0^2 dA \tag{3.53}$$

where ρ_0 is as defined in Chapter 2. Substituting Eq. (3.51) into the total torque Eq. (2.33) yields a differential equation with regard to the warping function:

$$\mu GJ \frac{df}{dz} - EI_w \frac{d^3 f}{dz^3} = \mu M_z \tag{3.54}$$

After differentiating Eq. (3.54) once and substituting Eq. (3.8) into Eq. (3.54), the differential equation in terms of the warping function is obtained as follows:

$$\frac{d^4 f}{dz^4} - \lambda_c^2 \frac{d^2 f}{dz^2} = \frac{\mu}{EI_w}\left(m_z - \frac{M_x}{R}\right) \tag{3.55}$$

where, $\lambda_c = \sqrt{\mu \frac{GJ}{EI_w}}$.

3.2.4.2 Warping Torque and Bimoment

Comparing Eq. (3.26) to Eq. (3.55) shows that the differential equation for a girder with a closed cross section has the same form as that for a girder with an open cross section. The only difference is the constant μ, which amplifies the applied loads and appears in the constant λ_c. That is, the applied loads, p_y, m_z, P, and T become μp_y, μm_z, μP, and μT, and λ is replaced by λ_c. In addition, the boundary conditions for a girder with a closed cross section differ from the boundary conditions for a girder with an open cross section. The simple support boundary conditions are:

$$z = 0 \qquad \varphi(0) = 0 \qquad \frac{d^2 f(0)}{dz^2} = 0 \tag{3.56a}$$

$$z = L \qquad \varphi(L) = 0 \qquad \frac{d^2 f(0)}{dz^2} = 0 \tag{3.56b}$$

The procedure used to determine the twist angle can be used to determine the warping function f(z). After the warping function is determined, the bimoment for a closed cross section can be determined by Eq. (2.27), which is:

$$B = -EI_w \frac{d^2 f}{dz^2}$$

The results show that the bimoment is as follows. For the uniformly distributed vertical load, p_y, and torque, m_z, the bimoment is:

$$B = -\mu \frac{m_z(1-\eta) + p_y R\eta}{\lambda_c{}^2}\left(1 - \frac{\sinh(\lambda_c z) + \sinh[\lambda_c (L-z)]}{\sinh(\lambda_c L)}\right) + \mu(m_z R^2 - p_y R^3)\eta\left(\frac{\sin(\frac{z}{R}) + \sin(\frac{L-z}{R})}{\sin(\frac{L}{R})} - 1\right) \tag{3.57}$$

For the concentrated vertical load, P, and torque, T, applied at position z_0, the bimoment is :

$0 < z < z_0$

$$B = \frac{\mu T(1-\eta) + PR\eta}{\lambda_c}\frac{\sinh[\lambda_c (L-z_0)]}{\sinh(\lambda_c L)}\sinh(\lambda_c z) + \mu(TR - PR^2)\eta\frac{\sin(\frac{L-z_0}{R})}{\sin(\frac{L}{R})}\sin(\frac{z}{R}) \tag{3.58a}$$

$z_0 < z < L$

$$B = \frac{\mu T(1-\eta) + PR\eta}{\lambda_c}\frac{\sinh(\lambda_c z_0)}{\sinh(\lambda_c L)}\sinh[\lambda_c (L-z)] + \mu(TR - PR^2)\eta\frac{\sin(\frac{z_0}{R})}{\sin(\frac{L}{R})}\sin(\frac{L-z}{R}) \tag{3.58b}$$

As given in Eq. (2.21), $M_w = \frac{dB}{dz}$, so the warping torque for a closed cross section girder is as follows. For the uniformly distributed vertical load, p_y, and torque, m_z, the warping torque is:

$$M_w = -\mu \frac{m_z(1-\eta) + p_y R\eta}{\lambda_c} \frac{\cosh(\lambda_c z - \cosh[\lambda_c (L-z)]}{\sinh \lambda_c L} + \mu(m_z R - p_y R^2)\eta \frac{\cos(\frac{z}{R}) - \cos(\frac{L-z}{R})}{\sin(\frac{L}{R})}$$

(3.59)

For the concentrated vertical load, P, and torque, T, applied at position z_0, the warping torque is:

$0 < z < z_0$

$$M_w = \mu[T(1-\eta) + PR\eta] \frac{\sinh \lambda_c (L - z_0)}{\sinh \lambda_c L} \cosh \lambda_c z + \mu(T - PR)\eta \frac{\sin(\frac{L - z_0}{R})}{\sin(\frac{L}{R})} \cos(\frac{z}{R})$$

(3.60a)

$z_0 < z < L$

$$M_w = -\mu[T(1-\eta) + PR\eta] \frac{\sinh \lambda_c z_0}{\sinh \lambda_c L} \cosh \lambda_c (L - z) - \mu(T - PR)\eta \frac{\sin(\frac{z_0}{R})}{\sin(\frac{L}{R})} \cos(\frac{L-z}{R})$$

(3.60b)

3.2.4.3 St.Venant Torque

The total torque is determined by Eq. (3.43) or Eqs. (3.46). Then, the St.Venant torque can be obtained for a girder with a closed cross section as follows:

$$M_{st} = M_z - M_w$$

3.2.4.4 Twist Angle

The twist angle is determined by integrating Eq. (3.51), after the warping function f(z) and the total torque are known. The twist angle is as follows. For the uniformly distributed load, p_y, and torque, m_z, the twist angle is:

$$\varphi = C_{\varphi m} \cdot m_z + C_{\varphi p} \cdot p_y$$

where,

$$C_{\varphi m} = \frac{1}{GJ}\left[R^2 \cdot C_{\varphi 1} - \mu \cdot \frac{(1-\eta)}{\lambda_c{}^2} \cdot C_{\varphi 2} \right]$$

$$C_{\varphi p} = \frac{1}{GJ}\left[-R^3 \cdot C_{\varphi 1} + \frac{R^3}{2} \cdot \frac{z(L-z)}{R^2} - \mu \cdot \frac{R \cdot \eta}{\lambda_c{}^2} \cdot C_{\varphi 2} \right]$$

$$C_{\varphi 1} = (1 - \mu \cdot \eta) \cdot \left[\frac{\sin(\frac{z}{R}) + \sin(\frac{L-z}{R})}{\sin(\frac{L}{R})} - 1 \right]$$

$$C_{\varphi 2} = \left[1 - \frac{\sinh(\lambda_c z) + \sinh[\lambda_c (L-z)]}{\sinh(\lambda_c L)} \right]$$

For the concentrated vertical load, P, and torque, T, applied at position z_0, the twist angle is:

$0 < z < z_0$

$$\varphi = C_{\varphi T1} \cdot T + C_{\varphi P1} \cdot P$$

where,

$$C_{\varphi T1} = \frac{1}{GJ}\left[R \cdot C_{\varphi 3} - \mu \cdot \frac{1-\eta}{\lambda_c} \cdot C_{\varphi 4} \right]$$

$$C_{\varphi P1} = \frac{1}{GJ}\left[-R^2 \cdot C_{\varphi 3} + \frac{R^2 (L - z_0) \cdot z}{R \cdot L} - \mu \frac{R \cdot \eta}{\lambda_c} \cdot C_{\varphi 4} \right]$$

$$C_{\varphi 3} = (1 - \mu \cdot \eta) \cdot \frac{\sin(\frac{L-z_0}{R})}{\sin(\frac{L}{R})} \cdot \sin(\frac{z}{R})$$

$$C_{\varphi 4} = \frac{\sinh[\lambda_c (L - z_0)]}{\sinh(\lambda_c L)} \cdot \sinh(\lambda_c z)$$

$z_0 < z < L$

$$\varphi = C_{\varphi T2} \cdot T + C_{\varphi P2} \cdot P$$

where,

$$C_{\varphi T2} = \frac{1}{GJ}\left[R \cdot C_{\varphi 5} - \mu \cdot \frac{1-\eta}{\lambda_c} \cdot C_{\varphi 6} \right]$$

$$C_{\varphi P2} = \frac{1}{GJ}\left[-R^2 \cdot C_{\varphi 5} + \frac{R \cdot z_0 \cdot (L-z)}{L} - \mu \cdot \frac{R \cdot \eta}{\lambda_c} \cdot C_{\varphi 6} \right]$$

$$C_{\varphi 5} = (1 - \mu \cdot \eta) \cdot \frac{\sin(\frac{z_0}{R})}{\sin(\frac{L}{R})} \cdot \sin(\frac{L-z}{R})$$

$$C_{\varphi 6} = \frac{\sinh(\lambda_c z_0)}{\sinh(\lambda_c L)} \cdot \sinh[\lambda_c (L-z)]$$

3.3. Vertical Displacement for Curved Girders

This section summarizes the solution for the vertical displacement for single span curved girders, which was presented by Dabrowski (1968).

3.3.1. Longitudinal Strain and Normal Stress

The longitudinal strain in the z-axis direction for a curved girder comes from bending, torsion, axial displacement and radius displacement. The strain due to the torsion is different for open section and closed section girders. In the following section, the longitudinal strains for an open section girder and a closed section girder will be presented separately.

Open Section Girder

The strain due to bending of a curved girder is similar to the bending strain for a straight girder and is:

$$\varepsilon_b = -\frac{d^2u}{dx^2}x + \frac{d^2v}{dy^2}y \tag{3.61}$$

where, u is the displacement in the radial or x-axis direction; and v is the displacement in the vertical or y-axis direction.

Torsion produces a longitudinal strain, which is equal to:

$$\varepsilon_t = -\frac{d^2\varphi}{dz^2}\omega_n \tag{3.62}$$

Assuming that the cross section dimensions are small compared to the radius of curvature of the girder, the strain due to the radial displacement is:

$$\varepsilon_u = -\frac{u + (y - y_0)\theta}{R^2}(R + x) \tag{3.63}$$

where, θ is the total rotation angle of the cross section and is:

$$\theta = \varphi - \frac{v}{R} \tag{3.64}$$

The strain due to axial displacement at the cross section centroid is the derivative of the axial displacement.

$$\varepsilon_a = \frac{dw}{dz} \tag{3.65}$$

where, w is the axial displacement at the cross section centroid in the z-axis direction. Thus, the total longitudinal strain of the curved girder is a summation of the previous four strains which are given by Eqs. (3.61), (3.62), (3.63), and (3.64) respectively. The total longitudinal strain is:

$$\varepsilon = -\frac{d^2u}{dx^2}x + \frac{d^2v}{dy^2}y - \frac{d^2\varphi}{dz^2}\omega_n + \frac{dw}{dz} - \frac{u + (y - y_0)\theta}{R^2}(R + x) \tag{3.66}$$

The normal stress σ is equal to:

$$\sigma = E \cdot \varepsilon \tag{3.67}$$

Substituting Eq. (3.66) into Eq. (3.67), the normal stress for a curved girder with an open cross section is:

$$\sigma = E \cdot [-\frac{d^2u}{dx^2}x + \frac{d^2v}{dy^2}y - \frac{d^2\varphi}{dz^2}\omega_n + \frac{dw}{dz} - \frac{u + (y - y_0)\theta}{R^2}(R + x)] \tag{3.68}$$

Closed Section Girder

For a girder with a closed cross section, the warping shear deformations affect the warping displacement. The warping shear deformations were accounted for in the warping function f(z). The warping displacement is expressed as:

$$w = -\frac{df}{dz}\omega_n$$

Thus, the longitudinal strain due to torsion is:

$$\varepsilon_t = \frac{dw}{dz} = -\frac{d^2 f}{dz^2}\omega_n$$

The other contributions to the longitudinal strain for a closed section girder are the same as those for an open section girder, and the total strain is:

$$\varepsilon = -\frac{d^2 u}{dx^2}x + \frac{d^2 v}{dy^2}y - f''\omega_n + w_z' - \frac{u + (y - y_0)\theta}{r^2}(r + x)$$

Then the normal stress is equal to:

$$\sigma = E \cdot [-\frac{d^2 u}{dx^2}x + \frac{d^2 v}{dy^2}y - \frac{d^2 f}{dz^2}\omega_n + \frac{dw}{dz} - \frac{u + (y - y_0)\theta}{R^2}(R + x)]$$

3.3.2. Differential Equations

The bending moments M_x, M_y and the axial force N are equal to:

$$M_x = -\int_A \sigma y \, dA \tag{3.69}$$

$$M_y = \int_A \sigma x \, dA \tag{3.70}$$

$$N = \int_A \sigma \, dA \tag{3.71}$$

Introducing the normal stress into Eqs. (3.69), (3.70) and (3.71), the relationship between the stress resultants and the displacements are obtained:

$$M_x = -E\left[I_x\left(\frac{d^2 v}{dy^2} - \frac{\theta}{R}\right) - I_{xy}\left(\frac{d^2 u}{dx^2} + \frac{u}{R^2}\right) + \left(I_x \cdot y_0 - \int_A y^2 x \cdot dA \right)\frac{\theta}{R^2}\right] \tag{3.72}$$

$$M_y = -E\left[I_y\left(\frac{d^2 u}{dx^2} + \frac{u}{R^2}\right) - I_{xy}\left(\frac{d^2 v}{dy^2} - \frac{\theta}{R}\right) - \left(I_y \cdot y_0 - \int_A x^2 y \cdot dA \right)\frac{\theta}{R^2}\right] \tag{3.73}$$

$$N = EA\left(\frac{dw}{dz} - \frac{u - y_0\theta}{R}\right) - EI_{xy}\frac{\theta}{R^2} \tag{3.74}$$

For a simply supported girder under only vertical load, the bending moment M_y and the axial load N are equal to zero. Setting Eqs. (3.73) and (3.74) equal to zero, respectively, leads to the following:

$$\frac{d^2u}{dx^2}+\frac{u}{R^2}=\frac{I_{xy}}{I_y}\left(\frac{d^2v}{dy^2}-\frac{\theta}{R}\right)+\left(y_0-\frac{\int_A x^2 y\cdot dA}{I_y}\right)\frac{\theta}{R^2} \tag{3.75}$$

$$\frac{dw}{dz}-\frac{u-y_0\theta}{R}=\frac{I_{xy}}{A}\frac{\theta}{R^2} \tag{3.76}$$

Assuming that the radius of the girder curvature is much greater than the cross section dimensions, the right hand side of Eq. (3.76) is approximately to zero. Then, the strain due to the torsion from Eq. (3.65) can be expressed as:

$$\varepsilon_t=\frac{dw}{dz}=\frac{u-y_0\theta}{R} \tag{3.77}$$

Substituting Eqs. (3.75) and (3.64) into Eq. (3.72), a differential equation with respect to the vertical displacement v and the twist angle φ is obtained as follow:

$$\frac{d^2v}{dy^2}+(1-\frac{\rho}{\psi})\frac{v}{R^2}=-\frac{M_x}{\psi EI_x}+(1-\frac{\rho}{\psi})\frac{\varphi}{R} \tag{3.78}$$

where, ψ and ρ are both dimensionless coefficients related to the cross section shape and are defined as:

$$\psi=1-\frac{I_{xy}^2}{I_xI_y},$$

$$\rho=\frac{1}{RI_xI_y}(I_{xy}\int_A x^2 y dA-I_y\int_A y^2 x dA)$$

ψ equals 1 for singly-symmetric and doubly-symmetric cross sections. ρ is zero for singly-symmetric and doubly-symmetric sections. Hence, Eq. (3.78) can be rewritten for symmetric cross sections as:

$$\frac{d^2v}{dy^2}+\frac{v}{R^2}=-\frac{M_x}{EI_x}+\frac{\varphi}{R} \tag{3.79}$$

For asymmetric cross sections, the quotient ρ/ψ is very small relative to 1, and assuming that the cross section dimensions are small in comparison to the radius of the girder curvature, the term ρ in Eq. (3.78) may be neglected. Eq. (3.79) is valid for both open and closed sections.

3.3.3 Solutions of Differential Equation for Vertical Displacement

Results for the bending moment M_x and the twist angle φ in Eq. (3.79) were given earlier in this chapter. So the vertical displacement, v, can be determined by solving Eq. (3.79). The boundary conditions for a simply supported curved girder are:

$$z = 0 \qquad v(0) = 0 \tag{3.80a}$$

$$z = L \qquad v(L) = 0 \tag{3.80b}$$

By introducing the bending moment and the twist angle into Eq. (3.79) and integrating twice, the vertical displacement v can be determined. Since the twist angle is different for open and closed cross sections, the expression for the vertical displacement, v, is also different for open and closed cross sections.

3.3.3.1 Solution for Girder with Open Cross Section

For the uniformly distributed load, p_y, and torque, m_z, the vertical displacement is:

$$v = C_{vm} \cdot m_z + C_{vp} \cdot p_y$$

where,

$$C_{vm} = \frac{1}{EI_x}\left[-R^3 \cdot C_{v1} + \chi \frac{R(1-\eta)}{\lambda^2} \cdot C_{v2}\right]$$

$$C_{vp} = \frac{1}{EI_x}\left[R^4 \cdot C_{v1} - \chi \cdot R^4 \cdot \left[\frac{\sin(\frac{z}{R}) + \sin(\frac{L-z}{R})}{\sin(\frac{L}{R})} - 1 - \frac{\frac{z}{R}(\frac{L-z}{R})}{2}\right] + \chi \cdot \frac{R^2 \cdot \eta}{\lambda^2} \cdot C_{v2}\right]$$

$$C_{v1} = \left[\frac{1}{\psi} + \chi(1-\eta)\right] \cdot \left[1 + \frac{\frac{z}{R}\cos(\frac{z}{R}) + \frac{L-z}{R}\cos(\frac{L-z}{R})}{2\sin(\frac{L}{R})} - (1 + \frac{\frac{L}{R}}{2\tan(\frac{L}{R})}) \frac{\sin(\frac{z}{R}) + \sin(\frac{L-z}{R})}{\sin(\frac{L}{R})}\right]$$

$$C_{v2} = \left[(1-\eta)\frac{\sin(\frac{z}{R}) + \sin(\frac{L-z}{R})}{\sin(\frac{L}{R})} - 1 + \eta\frac{\sinh(\lambda z) + \sinh[\lambda(L-z)]}{\sinh(\lambda L)} \right]$$

where, $\chi = \frac{EI_x}{GJ}$

For the concentrated vertical load, P, and torque, T, the vertical displacement is:

$0 < z < z_0$

$$v = C_{vT1} \cdot T + C_{vP1} \cdot P$$

$$C_{vT1} = \frac{1}{EI_x}\left[-R^2 \cdot C_{v3} + \chi \cdot \eta \cdot R^2 (1-\eta) \cdot C_{v4} \right]$$

$$C_{vP1} = \frac{1}{EI_x}\left[R^3 \cdot C_{v3} - \chi \cdot R^3 \cdot \left[\frac{\sin(\frac{L-z_0}{R})}{\sin(\frac{L}{R})}\sin(\frac{z}{R}) - \frac{(\frac{L-z_0}{R})\cdot z}{L} \right] + \chi\eta^2 R^3 \cdot C_{v4} \right]$$

$$C_{v3} = \frac{\frac{1}{\psi} + \chi(1-\eta)}{2}[\frac{\sin(\frac{L-z_0}{R})}{\sin(\frac{L}{R})}\frac{z}{R}\cos(\frac{z}{R}) - (\frac{z_0}{R}\cos(\frac{L-z_0}{R}) + \sin(\frac{L-z_0}{R}) - \frac{L}{R}\frac{\sin(\frac{z_0}{R})}{\sin(\frac{L}{R})})\frac{\sin(\frac{z}{R})}{\sin(\frac{L}{R})}]$$

$$C_{v4} = (\frac{\sin(\frac{L-z_0}{R})}{\sin(\frac{L}{R})}\sin(\frac{z}{R}) - \frac{\sinh\lambda(L-z_0)}{\lambda R \sinh\lambda L}\sinh\lambda z)$$

$z_0 < z < L$

$$v = C_{vT2} \cdot T + C_{vP2} \cdot P$$

where,

$$C_{vT2} = \frac{1}{EI_x}\left[-R^2 \cdot C_{v5} + \chi\eta R^2(1-\eta)\cdot C_{v6}\right]$$

$$C_{vP2} = \frac{1}{EI_x}\left[R^3 \cdot C_{v5} - \chi R^3\left[\frac{\sin(\frac{z_0}{R})}{\sin(\frac{L}{R})}\sin(\frac{L-z}{R}) - \frac{z_0(L-z)}{R\cdot L}\right] + \chi\eta^2 R^3 \cdot C_{v6}\right]$$

$$C_{v5} = \frac{\frac{1}{\psi}+\chi(1-\eta)}{2}\left\{\frac{\sin(\frac{z_0}{R})}{\sin(\frac{L}{R})}(\frac{L-z}{R})\cos(\frac{L-z}{R}) - \left[(\frac{L-z}{R}\cos(\frac{z_0}{R}) + \sin(\frac{z_0}{R}) - \frac{L}{R}\frac{\sin(\frac{L-z_0}{R})}{\sin(\frac{L}{R})})\right]\cdot\frac{\sin(\frac{L-z}{R})}{\sin(\frac{L}{R})}\right\}$$

$$C_{v6} = \frac{\sin(\frac{z_0}{R})}{\sin(\frac{L}{R})}\sin(\frac{L-z}{R}) - \frac{\sinh(\lambda z_0)}{\lambda R\sinh(\lambda L)}\sinh[\lambda(L-z)]$$

3.3.3.2 Solution for Girder with Closed Cross Section

For the uniformly distributed load, p_y, and torque, m_z, the vertical displacement is:

$$v = C_{vmc}\cdot m_z + C_{vpc}\cdot p_y$$

where,

$$C_{vmc} = \frac{1}{EI_x}\left[-R^3\cdot C_{v7} + \mu\cdot\chi\frac{R(1-\eta)}{\lambda_c^{\,2}}\cdot C_{v8}\right]$$

$$C_{vpc} = \frac{1}{EI_x}\left[R^4\cdot C_{v7} - \chi\cdot R^4\cdot[\frac{\sin(\frac{z}{R})+\sin(\frac{L-z}{R})}{\sin(\frac{L}{R})} - 1 - \frac{z(L-z)}{2R^2}] + \mu\cdot\chi\cdot\frac{R^2\cdot\eta}{\lambda_c^{\,2}}\cdot C_{v8}\right]$$

$$C_{v7} = \left[\frac{1}{\psi} + \chi(1-\mu\cdot\eta)\right]\cdot\left[1+\frac{\frac{z}{R}\cos(\frac{z}{R})+\frac{L-z}{R}\cos(\frac{L-z}{R})}{2\sin(\frac{L}{R})} - (1+\frac{\frac{L}{R}}{2\tan(\frac{L}{R})})\frac{\sin(\frac{z}{R})+\sin(\frac{L-z}{R})}{\sin(\frac{L}{R})}\right]$$

$$C_{v8} = \left[(1-\eta)\frac{\sin(\frac{z}{R})+\sin(\frac{L-z}{R})}{\sin(\frac{L}{R})} - 1 + \eta\frac{\sinh(\lambda_c z)+\sinh[\lambda_c(L-z)]}{\sinh(\lambda_c L)}\right]$$

For the loading case with concentrated vertical load, P, and torque, T, the vertical displacement is:

$0 < z < z_0$

$$v = C_{vTc1}\cdot T + C_{vPc1}\cdot P$$

where,

$$C_{vTc1} = \frac{1}{EI_x}\left[-R^2\cdot C_{v9} + \mu\cdot\chi\cdot\eta\cdot R^2(1-\eta)\cdot C_{v10}\right]$$

$$C_{vPcl} = \frac{1}{EI_x}\left[R^3\cdot C_{v9} - \chi\cdot R^3\cdot\left[\frac{\sin(\frac{L-z_0}{R})}{\sin(\frac{L}{R})}\sin(\frac{z}{R}) - \frac{(\frac{L-z_0}{R})\cdot z}{L}\right] + \mu\cdot\chi\cdot\eta^2\cdot R^3\cdot C_{v10}\right]$$

$$C_{v9} = \frac{\frac{1}{\psi}+\chi(1-\mu\eta)}{2}\left\{\frac{\sin(\frac{L-z_0}{R})}{\sin(\frac{L}{R})}\frac{z}{R}\cos(\frac{z}{R}) - \left[\frac{z_0}{R}\cos(\frac{L-z_0}{R})+\sin(\frac{L-z_0}{R})-\frac{L}{R}\frac{\sin(\frac{z_0}{R})}{\sin(\frac{L}{R})}\right]\frac{\sin(\frac{z}{R})}{\sin(\frac{L}{R})}\right\}$$

$$C_{v10} = \frac{\sin(\frac{L - z_0}{R})}{\sin(\frac{L}{R})} \sin(\frac{z}{R}) - \frac{\sinh \lambda_c (L - z_0)}{\lambda_c R \sinh(\lambda_c L)} \sinh(\lambda_c z)$$

$z_0 < z < L$

$$v = C_{vTc2} \cdot T + C_{vPc2} \cdot P$$

where,

$$C_{vTc2} = \frac{1}{EI_x} \left[- R^2 \cdot C_{v11} + \mu \chi \eta R^2 (1 - \eta) \cdot C_{v12} \right]$$

$$C_{vPc2} = \frac{1}{EI_x} \left[R^3 \cdot C_{v11} - \chi R^3 \left[\frac{\sin(\frac{z_0}{R})}{\sin(\frac{L}{R})} \sin(\frac{L - z}{R}) - \frac{z_0 (L - z)}{R \cdot L} \right] + \mu \chi \eta^2 R^3 \cdot C_{v12} \right]$$

$$C_{v11} = \frac{\frac{1}{\psi} + \chi(1 - \mu\eta)}{2} \left[\frac{\sin(\frac{z_0}{R})}{\sin(\frac{L}{R})} (\frac{L - z}{R}) \cos(\frac{L - z}{R}) \right] - \left[\frac{L - z}{R} \cos(\frac{z_0}{R}) + \sin(\frac{z_0}{R}) - \frac{L}{R} \frac{\sin(\frac{L - z_0}{R})}{\sin(\frac{L}{R})} \right] \cdot \frac{\sin(\frac{L - z}{R})}{\sin(\frac{L}{R})}$$

$$C_{v12} = \frac{\sin(\frac{z_0}{R})}{\sin(\frac{L}{R})} \sin(\frac{L - z}{R}) - \frac{\sinh(\lambda_c z_0)}{\lambda_c R \sinh(\lambda_c L)} \sinh[\lambda_c (L - z)]$$

3.4 Cross Section Rotation for Curved Girders

This section summarizes the solution for the cross section rotation for single span curved girders, which was presented by Dabrowski (1968). The rotation of a curved girder cross section differs from that of a straight girder. For a straight girder, the cross section rotation is equal to the cross section twist angle. However, for a curved

girder, the vertical displacement contributes to the rotation. The rotation of the cross section is determined by Eq. (3.64) as follows:

$$\theta = \varphi - \frac{v}{R}$$

Since the twist angle and vertical displacement are as given in the previous sections of this chapter, the cross section rotation can be determined by Eq. (3.64) using the previous results.

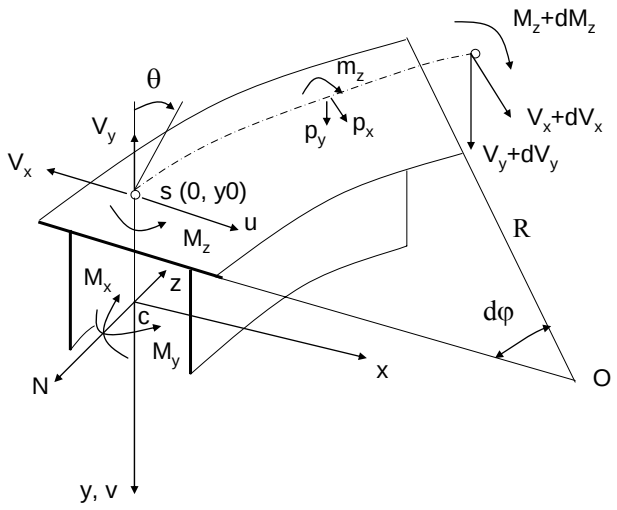

Figure 3.1 Free Body Diagram of Differential Element

Chapter 4 Linear Elastic Theoretical Analysis

The behavior of a curved girder bridge structure differs from that of individual girders because the cross-frames between girders resist the cross section rotation. A theoretical analysis method is proposed in this chapter to analyze a curved bridge structure composed of multiple curved girders connected by cross frames. In this method, the bridge structure is treated as a set individual curved girders, with the vertical forces and torques carried by the cross frames between girders treated as loads applied to each girder. The response of each girder to these vertical forces and torques, as well as the applied loads, is determined using the equations developed in Chapter 3. A set of equations are written for each girder, with the vertical forces and torques carried by the cross frames as unknowns. The equations are solved for these unknowns and then each girder is analyzed in detail. To illustrate the theoretical method, a simply supported curved multiple-girder bridge subjected to a uniformly distributed load p and torque m is analyzed.

4.1 Theoretical Analysis Method

The theoretical analysis method for curved girder bridges presented in this chapter is based on the following assumptions:

(1) The cross section of each curved girder remains plane under bending.
(2) Cross section distortion and shear lag in each curved girder is neglected.
(3) The bending normal stresses are assumed to be linearly distributed through the depth of the cross section.
(4) The cross frames are assumed to be rigid and to be rigidly connected to the girders.

The theoretical analysis method is developed in four steps.

(1) Each girder is isolated from the structure. The forces at the interface between the girder and the cross frames are treated as external concentrated forces applied to each girder at the cross sections braced by the cross frames (see **Figure 4.1**). Thus, there are two types of load applied to each girder: the actual applied loads and the concentrated forces from the cross frames.
(2) The concentrated forces acting on the girders from the cross frames are determined. Initially, the concentrated vertical force and torque acting on each girder at each cross frame location are unknown. They are determined by solving a set of equilibrium equations and displacement compatibility equations between the cross frames and the girders.
(3) The internal forces and deflections for each girder are determined, using results from Chapter 3.
(4) Thin-walled member theory is used to conduct the cross section stress analysis for each girder, and the stresses are obtained for each girder in the bridge.

4.1.1 Cross Frame Forces

For convenience, the concentrated vertical forces and torques acting on the girders at the interface with the cross frames are simply called cross frame forces. These forces are determined by solving a set of equilibrium equations and displacement compatibility equations for the cross frames and the girders. **Figure 4.1** shows a free body diagram of a typical cross frame and the cross frame forces between the adjacent girders and the cross frame. All forces shown in **Figure 4.1** are acting in the positive direction.

4.1.1.1 Displacement Compatibility Equations

Based on the assumption that each cross frame is rigid and is rigidly connected to the adjacent girders, the following two displacement compatibility equations are written for each cross frame, which connects two adjacent girder, i and (i+1):

(i) The difference in the vertical displacements for the ith girder and the (i+1)th girder is equal to the rotation of the (i+1)th girder multiplied by the space between girder i and (i+1).

$$v^{(i)} - v^{(i+1)} = \theta^{(i+1)} \cdot S_p \tag{4.1a}$$

(ii) The rotation of the ith girder is equal to the rotation of the (i+1)th girder at the braced cross section.

$$\theta^{(i)} = \theta^{(i+1)} \tag{4.1b}$$

where, $v^{(i)}$ and $\theta^{(i)}$ are the vertical displacement and the total rotation of the ith girder respectively at the braced cross section; $v^{(i+1)}$ and $\theta^{(i+1)}$ are the vertical displacement and the total cross section rotation of the (i+1)th girder respectively at the braced cross section; S_p is the girder spacing. **Figure 4.2** shows the displacements of the cross section of each girder at the cross frame location. Eqs. (4.1a) and (4.1b) are written for each cross frame. If the bridge has n_g girders and j cross frames in a cross section (where $j = n_g - 1$), there will be 2j displacement compatibility equations.

4.1.1.2 Constitutive Equations

Using the principle of superposition, the total cross section rotation and the vertical displacement of the cross section of a typical interior girder at the location of the cross frame can be expressed in terms of the applied loads and the cross frame forces. Here, it is assumed that the applied loads are the uniformly distributed load p and torque m.

$$\theta^{(i)} = a_{k1}^{(i)} \cdot p^{(i)} + a_{k2}^{(i)} \cdot m^{(i)} + a_{k3}^{(i)} \cdot V_g^{(i,1)} + a_{k4}^{(i)} \cdot M_{z,g}^{(i,1)} + a_{k5}^{(i)} \cdot V_g^{(i,2)} + a_{k6}^{(i)} \cdot M_{z,g}^{(i,2)} \qquad (4.2a)$$

$$v^{(i)} = a_{(k+1)1}^{(i)} \cdot p^{(i)} + a_{(k+1)2}^{(i)} \cdot m^{(i)} + a_{(k+1)3}^{(i)} \cdot V_g^{(i,1)} + a_{(k+1)4}^{(i)} \cdot M_{z,g}^{(i,1)} + a_{(k+1)5}^{(i)} \cdot V_g^{(i,2)} + a_{(k+1)6}^{(i)} \cdot M_{z,g}^{(i,2)} \qquad (4.2b)$$

where, a_{kq} is an influence coefficient corresponding to each type of force. These coefficients are the rotation or the vertical deflection due to a unit load. The results given in Chapter 3 provide these influence coefficients. $V_g^{(i,1)}$ and $V_g^{(i,2)}$ are the vertical force on the ith girder from its left and right side cross frames, respectively; $M_{z,g}^{(i,1)}$ and $M_{z,g}^{(i,2)}$ are the torque on the ith girder from its left and right side cross frames, respectively.

Since there is no cross frame on the left side of the inner girder (girder 1) of the bridge, the cross frame forces $M_{z,g}^{(1,1)}$ and $V_g^{(1,1)}$ are zero. Therefore, for the inner girder, the total cross-section rotation and the vertical displacement of the cross section at the cross frame location can be expressed as:

$$\theta^{(1)} = a_{11}^{(1)} \cdot p^{(1)} + a_{12}^{(1)} \cdot m^{(1)} + a_{15}^{(1)} \cdot V_g^{(1,2)} + a_{16}^{(1)} \cdot M_{z,g}^{(1,2)} \qquad (4.2c)$$

$$v^{(1)} = a_{21}^{(1)} \cdot p^{(1)} + a_{22}^{(1)} \cdot m^{(1)} + a_{25}^{(1)} \cdot V_g^{(1,2)} + a_{26}^{(1)} \cdot M_{z,g}^{(1,2)} \qquad (4.2d)$$

Similarly, the cross frame forces $M_{z,g}^{(n,2)}$ and $V_g^{(n,2)}$ on the right side of the outer girder (girder n) are zero. Therefore, for the outer girder, the total cross section rotation and the vertical displacement of the cross section at the cross frame location can be expressed as:

$$\theta^{(n)} = a_{(2n-1)1}^{(n)} \cdot p^{(n)} + a_{(2n-1)2}^{(n)} \cdot m^{(n)} + a_{(2n-1)3}^{(n)} \cdot V_g^{(n,1)} + a_{(2n-1)4}^{(n)} \cdot M_{z,g}^{(n,1)} \qquad (4.2e)$$

$$v^{(n)} = a_{2n1}^{(n)} \cdot p^{(n)} + a_{2n2}^{(n)} \cdot m^{(n)} + a_{2n3}^{(i)} \cdot V_g^{(i,1)} + a_{2n4}^{(i)} \cdot M_{z,g}^{(i,1)} \qquad (4.2f)$$

By substituting Eqs. (4.2) into Eqs. (4.1a) and (4.1b) for the pair of girders attached to each cross frame, the two deflection compatibility equations at each cross frame location are expressed in terms of the unknown cross frame forces. Since there are 4 unknown cross frame forces for each cross frame, as shown in Figure 4.1, 2j compatibility equations with 4j unknown cross frame forces are obtained for each cross section of the bridge having j cross frames.

4.1.1.3 Equilibrium Equations

The equilibrium equations for each cross frame (see **Figure 4.1**) can be written as:

$$V_c^{(i,2)} + V_c^{(i+1,1)} = 0 \tag{4.3a}$$

$$M_{z,c}^{(i,2)} + M_{z,c}^{(i+1,1)} - V_c^{(i+1,1)} \cdot S_p = 0 \tag{4.3b}$$

The forces at the interface between the girder and the cross frame are equal and opposite to each other and are expressed as follows:

$$V_g^{(i,2)} = V_c^{(i,2)} \tag{4.4a}$$

$$V_g^{(i+1,1)} = V_c^{(i+1,1)} \tag{4.4b}$$

$$M_{z,g}^{(i,2)} = M_{z,c}^{(i,2)} \tag{4.4c}$$

$$M_{z,g}^{(i+1,1)} = M_{z,c}^{(i+1,1)} \tag{4.4d}$$

Substituting Eqs. (4.4) into Eqs. (4.3), the relationship between the cross frame forces on girder i and girder i+1 are presented in the following equations:

$$V_g^{(i,2)} + V_g^{(i+1,1)} = 0 \tag{4.5a}$$

$$M_{z,g}^{(i,2)} + M_{z,g}^{(i+1,1)} - V_g^{(i+1,1)} \cdot S_p = 0 \tag{4.5b}$$

For convenient later use, Eqs. (4.5a) and (4.5b) are rewritten as follows:

$$V_g^{(i,2)} = -V_g^{(i+1,1)} \tag{4.6a}$$

$$M_{z,g}^{(i,2)} = -M_{z,g}^{(i+1,1)} + V_g^{(i+1,1)} \cdot S_p \tag{4.6b}$$

Eqs. (4.6a) and (4.6b) are written for each cross frame. If the bridge has n_g girders and j cross frames in a braced cross section (where, again, $j = n_g - 1$), there will be 2j equilibrium equations. Thus, the 2j equilibrium equation, combined with the 2j displacement compatibility equations, provide a total of 4j simultaneous equations for determining the 4j unknown cross frame forces at a bridge cross section with cross frames. If the bridge has n_c interior cross sections (not including the end cross frames) with j cross frames at each section, the same procedure can be applied to each such bridge cross section. Thus, a total of $4n_cj$ linear simultaneous equations with $4n_cj$

unknown cross frame forces are obtained and can be solved to determine the cross frame forces.

4.1.2 Internal Forces

After the cross frame forces are determined, the total set of forces acting on each curved girder, including the actual applied loads and the concentrated forces at the cross frames, are known. Each curved girder develops internal forces, namely, bending moment, shear force, and torque, as discussed in Chapter 3. The internal forces that develop under uniform or concentrated loads and torques were given in Chapter 3. Using the principle of superposition, the internal forces for each girder are determined from the uniform and concentrated loads acting on each girder.

4.2 Stress Analysis

The stresses in the curved girders are determined from the internal forces using the thin-walled member theory, summarized in Chapter 2. The stress analysis is different for open cross section and closed cross section girders. As noted in Chapter 1, the behavior of curved tubular-flange girders are compared with the behavior of curved I-girders in this report, so the stress analysis of curved I-girders is summarized in this chapter. Since an I-girder is an open section girder, the thin-walled open section theory is used. The cross section of the tubular-flange girder includes closed section components (the tubular flanges) and an open section component (the web). Therefore, the stress analysis of a tubular-flange girder involves both thin-walled open and closed section theory. The stress analysis methods are introduced separately for curved I-girders and curved tubular-flange girders in the following sections.

4.2.1 Stress Analysis of Curved I-Girders

The stresses on a curved I-girder cross section considered in this study are the normal stress due to the vertical (primary) bending, the normal stress due to the warping torsion, the shear stress due to the vertical shear force, the shear stress due to the warping torsion, and the shear stress due to the St. Venant torsion (see **Figure 4.3**).

Normal Stress Due to Vertical (Primary) Bending

The vertical (primary) bending normal stress for a curved I-girder is assumed to be similar to that of a straight I-girder. The influence of the girder curvature is neglected, and the primary bending normal stress is determined by Eq. (2.1) as follows:

$$\sigma_x = \frac{M_x}{I_x} y$$

Normal Stress Due to Warping Torsion

The warping normal stress is determined from Eq. (2.16) as follows:

$$\sigma_w = -\frac{B}{I_w} \cdot \omega_n$$

where, the normalized unit warping, ω_n is as shown in **Figure 4.4**.

Shear Stress Due to Vertical Shear Force

The shear stress due to the vertical shear force is parallel to the walls of the cross section and uniformly distributed across the thickness of the walls. The shear stress is determined by Eq. (2.2) as follows:

$$\tau_v = -\frac{V_y}{I_x t} \int_0^s yt \cdot ds$$

Shear Stress Due to Warping Torsion

As the warping normal stress varies along the length of the girder, warping shear stress is induced and the shear stress is determined from Eq.(2.20) as follows:

$$\tau_w = \frac{M_w}{I_w t} \cdot S_w$$

where, the warping static moment S_w for the I-girder is shown in **Figure 4.4**.

After completing the integration shown in Eq. (2.15), the warping moment of inertia for a doubly symmetric I-girder can be expressed as follows:

$$I_w = \frac{I_{yf} \cdot h^2}{4} \tag{4.7}$$

where, h is the centerline distance between the flanges; I_{yf} is the moment of inertia of the flange about y-axis as follows:

$$I_{yf} = \frac{b_f{}^3 t_f}{6}$$

Shear Stress Due to St. Venant Torsion

The St. Venant shear stress distribution is parallel to the walls of the cross section and varies linearly across the thickness of the walls, t. The shear stress is determined by Eq. (2.9) as follows:

$$\tau_{st} = \frac{M_{st}}{J} \cdot t$$

where, the torsion constant, J, is given by Eq. (2.8).

4.2.2 Stress Analysis of Curved Tubular-Flange Girders

The stresses on a curved tubular-flange girder cross section considered in this study are the normal stress due to the vertical (primary) bending, the normal stress due to the warping torsion, the shear stress due to the vertical shear force, the shear stress due to the warping torsion, and the shear stress due to the St. Venant torsion. Only doubly symmetric tubular-flange girder cross sections are considered in this study.

Figure 4.5(a) shows a tubular-flange girder cross section and dimensions. Herein, h is the distance between the centerlines of the tube top and bottom walls, which is equal to the cross section depth less the tube thickness; h_0 is the distance between the centroids of the top and bottom tubular flanges; b_f is the tube width; and d_f is the tube depth with respect to the centerlines of the tube walls. Several specific points on the tube are numbered for easily describing the stresses at those points. Points 2, 3, 4, 5 identify the four corner points of each tube respectively. Points 1 and 6 are the middle points of the tube walls.

Normal Stress Due to Vertical (Primary) Bending

Based on beam theory, the normal stress is linearly distributed through the depth of the cross section. Thus, the primary bending normal stress for a tubular-flange girder is similar to that of an I-girder and is determined by Eq. (2.1). **Figure 4.5(b)** shows the bending normal stress distribution for a cross section under positive bending moment.

$$\sigma_x = \frac{M_x}{I_x} y$$

Normal Stress Due to Warping Torsion

The warping normal stress for a tubular-flange girder is determined from Eq. (2.29) as follows:

$$\sigma_w = -\frac{B}{I_w} \cdot \omega_n$$

The normalized unit warping ω_n is calculated by Eq. (2.26) as follows:

$$\omega_n(s) = \frac{2A_e}{\oint \frac{ds}{t}} \int_0^s \frac{ds}{t} - \omega_0(s)$$

The integral expressions in Eq. (2.26) only relate to the closed part of the cross section. The normalized unit warping for a tubular-flange girder cross section with any size rectangular tube is given in **Figure 4.6**, where, n is the aspect ratio of the tubular-flange and is equal to d_f/b_f.

It is observed that the normalized unit warping ω_n of the tubular-flange girder can be decomposed into two parts: ω_{ng} and ω_{nl}, as shown in **Figure 4.7(a)** and **Figure 4.7(b)**. ω_{ng} in **Figure 4.7(a)** is defined as the global normalized unit warping. It is similar to the normalized unit warping of an I-girder with the tubular flange centroid distance, h_0, (see **Figure 4.7(c)**). ω_{nl} is defined as the local normalized unit warping, and is equal to the normalized unit warping of the flange tube (see **Figure 4.7(d)**).

The warping moment of inertia is calculated from Eq. (2.28) as follows:

$$I_w = \int \omega_n^2 \cdot t ds$$

A general formula for the warping moment of inertia I_w of a tubular-flange girder with any size rectangular tube is as follows:

$$I_w = \frac{h_0^2 \cdot b_f^3 \cdot t_f}{12}(1+3n) + \frac{n^2 \cdot (1-n)^2 \cdot b_f^5 \cdot t_f}{12(1+n)} \tag{4.8}$$

where, t_f is the thickness of the tubular flange.

Similarly, the warping moment of inertia of a tubular-flange girder may also be separated into two parts. The first term in Eq. (4.8) can be written as:

$$I_{wg} = \frac{I_{yf} \cdot h_0^2}{4} \tag{4.9}$$

where, I_{wg} is the global warping moment of inertia; I_{yf} is the tubular-flange moment of inertia about the y-axis, which is equal to:

$$I_{yf} = \frac{b_f^3 \cdot t_f}{3} \cdot (1 + 3n)$$

Eq. (4.9) is similar to the warping moment of inertia for an I-girder (Eq. (4.7)) with the tubular flange centroid distance, h_0, used in place of the flange centerline spacing. The second term of Eq. (4.8) is equal to twice the warping moment of inertia of the flange tube about its own shear center, since there are two tubes in the cross section. This term is defined as the local warping moment of inertia and is calculated as follows:

$$I_{wl} = \frac{n^2 (1-n)^2 b_f^5 \cdot t_f}{12} \tag{4.10}$$

Comparing the global warping moment of inertia, I_{wg}, to the local warping moment of inertia, I_{wl}, it is suggested that I_{wl} is relatively very small and possibly negligible. This possibility is studied here. Assume that if the ratio of I_{wl} to I_{wg} is less than 5%, then I_{wl} is small enough to be neglected. That is:

$$\frac{I_{wl}}{I_{wg}} \le 5\% \tag{4.11}$$

Substituting Eqs. (4.9) and (4.10) into Eq. (4.11), the following equation is obtained:

$$\frac{h_0}{b_f} \ge \sqrt{\frac{20 \cdot n^2 (1-n)^2}{(1+n) \cdot (1+3n)}} \tag{4.12}$$

Since $h_0 = h - d_f$, Eq. (4.12) can be expressed as a ratio of h/b_f as follows:

$$\frac{h}{b_f} \ge \sqrt{\frac{20 \cdot n^2 (1-n)^2}{(1+n) \cdot (1+3n)}} + n \tag{4.13}$$

where, as noted earlier, $n = d_f/b_f$. If Eq. (4.12) or Eq. (4.13a) is satisfied, I_{wl} is less than 5% of I_{wg}. In addition, to avoid overlap of the top and bottom tubes, h has to greater than or equal to $2d_f$, that is, $h \ge 2d_f$. For $d_f = nb_f$, the following equation is obtained:

$$\frac{h}{b_f} \ge 2n \tag{4.14}$$

Therefore, if the ratio of h/b_f satisfies both Eqs. (4.13) and Eqs. (4.14), then I_{wl} can be neglected. **Figure 4.8** plots h/b_f versus n from Eqs. (4.13) and (4.14), treating the equations as equalities. The inequalities are satisfied for h/b_f values above the plotted curves. **Figure 4.8** shows that for $n \le 0.55$, as long as Eq. (4.13) is satisfied, that is, the

value of h/b_f is located on or above Curve I, Eq. (4.14) is automatically satisfied. Therefore, for h/b_f satisfying Eq. (4.13) and $n \le 0.55$, I_{wl} is negligible; **Figure 4.8** also shows that for $0.55 \le n \le 1$, as long as Eq.(4.14) is satisfied, that is, the value of h/b_f is located on or above Curve II, Eq. (4.13) is automatically satisfied and I_{wl} is negligible. Note that Figure 4.8 considers only cases where $n \le 1$. Practical cross sections will satisfy Eqs. (4.13) and (4.14), and thus, the warping moment of inertia for the tubular-flange girder can be expressed simply as:

$$I_w = \frac{I_{yf} \cdot h_0^2}{4} \tag{4.15}$$

For the results presented later in the report, this simplification was not used.

Shear Stress Due to Vertical Shear Force

As noted earlier, the cross section of a tubular-flange girder includes closed section components (the tubular flanges) and an open section component (the web). The shear stress on the tubular flange cross sections is assumed to follow the thin-walled closed section theory and the shear stress on the web cross section follow the thin-walled open section theory. First, for the tubular flanges, an equivalent open section is obtained by making a cut on each tubular-flange. The shear stress on this open section is determined using the thin-walled open section theory (Eq. (2.2)) as follows:

$$\tau_{vo} = -\frac{V_y}{I_x t}\int_0^s y \cdot t ds$$

Then, the thin-walled closed section theory is applied and the constant shear flow on the tubular-flange is determined by Eq. (2.5) as follows:

$$\tau_{vc} = \frac{\oint \tau_{vo} ds}{1/t \cdot \oint (1/t) ds}$$

Thus, the shear stress due to the vertical shear force on the tubular-flange cross section is equal to:

$$\tau_{vt} = \frac{\oint \tau_{vo} ds}{t \cdot \oint (1/t) ds} - \frac{V_y}{I_x t}\int_0^s y \cdot t ds$$

Figure 4.9 shows the vertical shear stress distribution. The vertical shear stresses are symmetric about the x-axis and anti-symmetric about the y-axis. The maximum stress occurs at the point where the web and the flange join (Point 6).

Shear Stress Due to Torsion

The shear stress in a tubular flange girder under torsion is treated in two parts. One part is the "primary" shear stress which is determined from uniform torsion theory. The other part is the "secondary" shear stress, which is determined by the continuity condition of the axial displacements (Benscoter 1954).

Shear Stress Due to Uniform Torsion (Primary Shear Stress)

The uniform torsion stress is proportional to the torsional rigidity GJ. The total uniform torque acting on the cross section, M_{st}, can be divided into three parts, which are proportional to the torsional rigidity of the top tubular flange, the bottom tubular flange and the web, respectively. However, the web torsional rigidity is much smaller than that of each tubular flange and is neglected in the present study. For a doubly symmetric tubular flange girder, the uniform torque carried by one tubular flange is equal to half of the total uniform torque acting on the cross section. Uniform torsion produces a constant shear flow around each closed tubular flange. This shear flow is constant across the thickness of the tube walls. Therefore, the shear stress is given as:

$$\tau_{st} = \frac{M_{st}}{4A_e t} \tag{4.16}$$

where, M_{st} is the St.Venant torque; A_e is the area enclosed by the tubular flange; t is the wall thickness.

Shear Stress Due to Warping Torsion (Secondary Shear Stress)

The secondary shear stress is determined by Eq. (2.32) as follows:

$$\tau_w = \frac{M_w}{I_w t} \cdot \bar{S}_w$$

The secondary warping moment $\bar{S}_w$ for the tubular-flange girder can be expressed using Eq. (2.33):

$$\bar{S}_w = S_{wi} - S_w$$

where, S_{wi} is the warping indeterminate moment; S_w is the warping statical moment and is determined by Eq. (2.34):

$$S_w = \int_0^s \omega_n \cdot t ds$$

S_{wi} is determined by Eq. (2.36):

$$\oint S_{wi}\frac{ds}{t} = \oint S_w \frac{ds}{t}$$

Herein, the warping indeterminate moment S_{wi} is assumed constant for a tubular-flange girder and then can be obtained by solving Eq. (2.36) as follows:

$$S_{wi} = \frac{\oint \frac{S_w}{t} ds}{\oint \frac{ds}{t}}$$

Thus, substituting S_{wi} and S_w into Eq. (2.33), the secondary warping moment for the tubular-flange girder is determined as follows:

$$\bar{S}_w = \frac{\oint \frac{S_w}{t} ds}{\oint \frac{ds}{t}} - S_w \qquad (4.17)$$

Figure 4.10(a) shows the secondary warping moment $\bar{S}_w$ for the tubular-flange girder. Similar to the normalized unit warping, ω_n, $\bar{S}_w$ can be decomposed into two parts: the global normalized warping moment $\bar{S}_{wg}$ (see **Figure 4.10(b)**) and the local warping moment $\bar{S}_{wl}$ (see **Figure 4.10(c)**).

Assuming that if the ratio of $\bar{S}_{wl}/\bar{S}_{wg}$ is less than or equal to 5%, then $\bar{S}_{wl}$ is negligible. Since $\bar{S}_w$ varies along the wall, only the maximum value $\bar{S}_{wl1}$ and $\bar{S}_{wg1}$ are compared. That is:

$$\frac{\bar{S}_{wl1}}{\bar{S}_{wg1}} \le 5\% \qquad (4.18)$$

Substituting $\bar{S}_{wl1}$ and $\bar{S}_{wg1}$ into Eq. (4.18), the following equation is obtained:

$$\frac{h}{b_f} \ge \frac{20 \cdot n \cdot (1-n)}{3(1+n)} + n \qquad (4.19)$$

If the ratio of h/b_f satisfies both Eq. (4.14) and Eq. (4.19), $\bar{S}_{wl}$ is negligible. **Figure 4.11** plots h/b_f versus n from Eqs. (4.14) and (4.19), treating the equations as equalities. The inequalities are satisfied for h/b_f values above the plotted curves. **Figure 4.11** shows

that for $n \leq 0.74$, if Eq. (4.19) is satisfied, then Eq. (4.14) is automatically satisfied and $\bar{S}_{wl}$ is negligible; for $n > 0.74$, if Eq. (4.14) is satisfied, then Eq. (4.19) is automatically satisfied and $\bar{S}_{wl}$ is negligible. For the results presented later in the report, $\bar{S}_{wl}$ was not neglected.

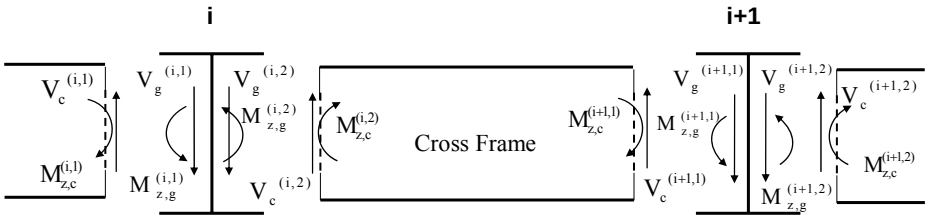

Figure 4.1 Cross Frame Forces

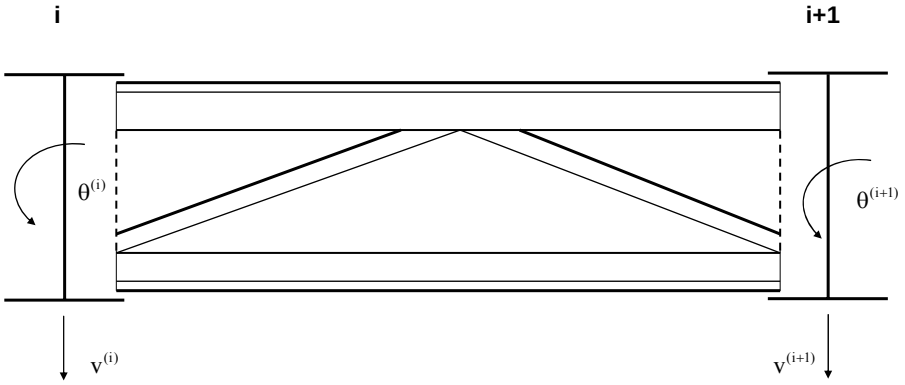

Figure 4.2 Braced Cross Section Deflections at Cross Frame

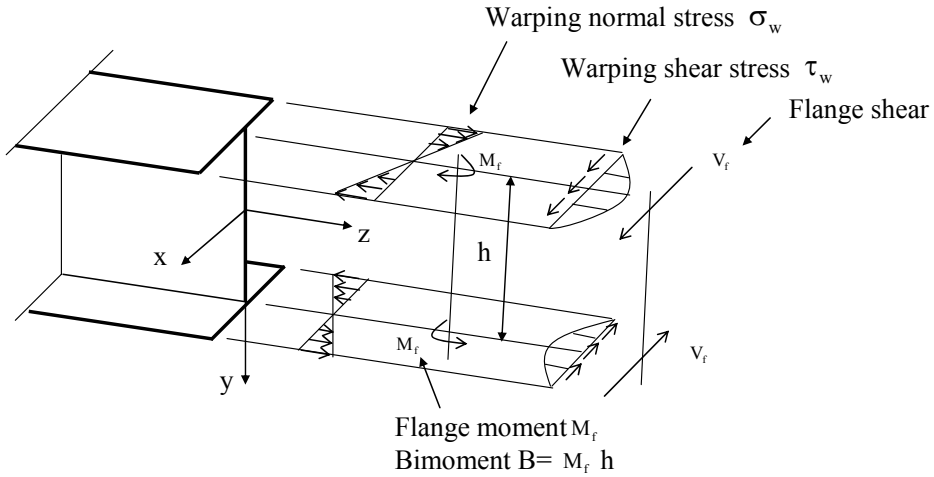

Figure 4.3 Warping Stress, Stress Resultant and Bimoment

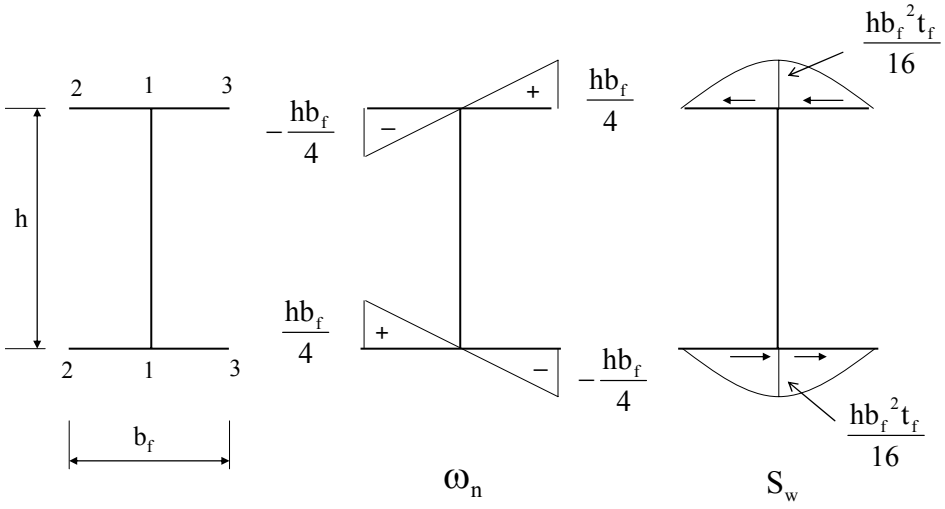

Figure 4.4 Normalized Unit Warping and Warping Static Moment

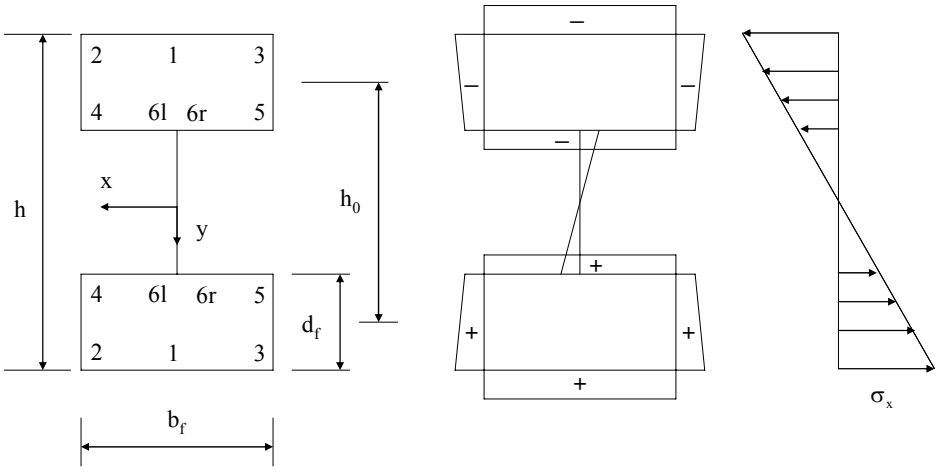

(a) Tubular-flange cross section (b) Bending normal stress distribution

Figure 4.5 Primary Bending Normal Stress

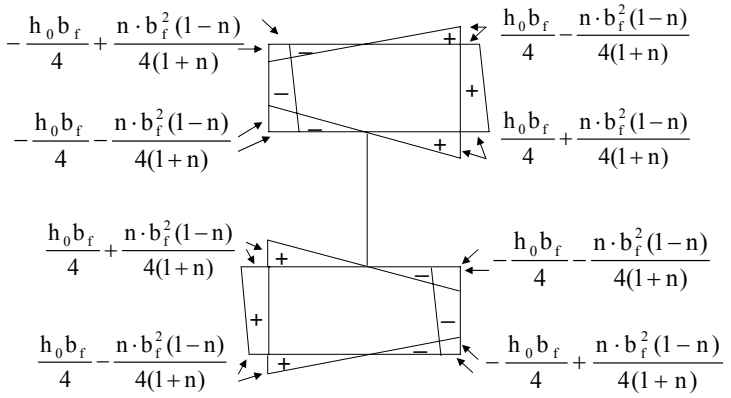

Figure 4.6 Normalized Unit Warping ω_n

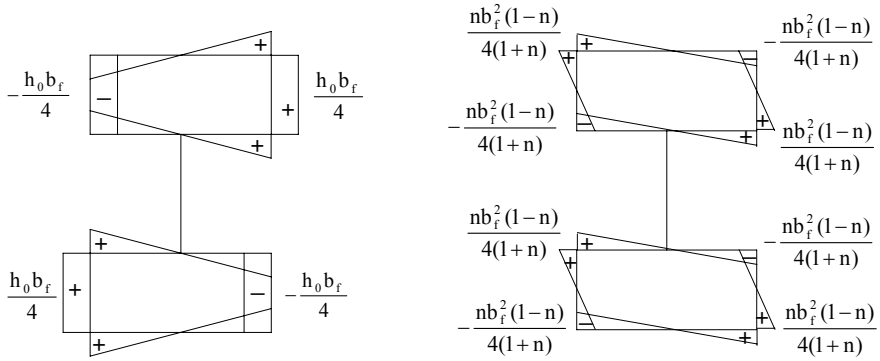

(a) Global warping ω_{ng} (b) Local warping ω_{nl} ($d_f < b_f$)

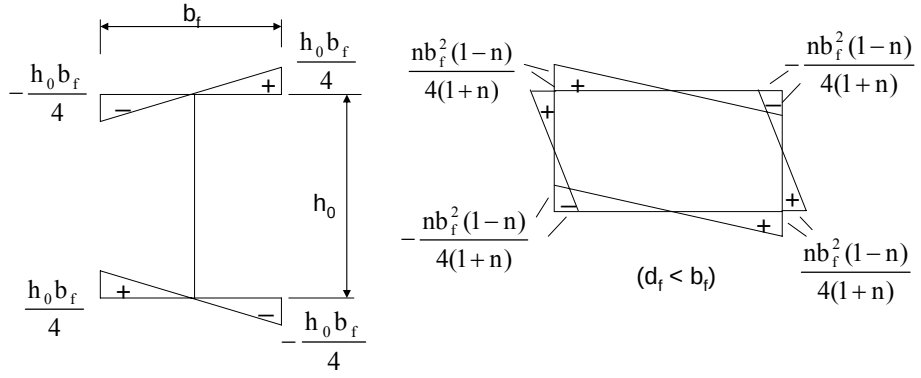

(c) ω_n for I-girder (d) ω_n for rectangular tube

Figure 4.7 Global and Local Normalized Unit Warping

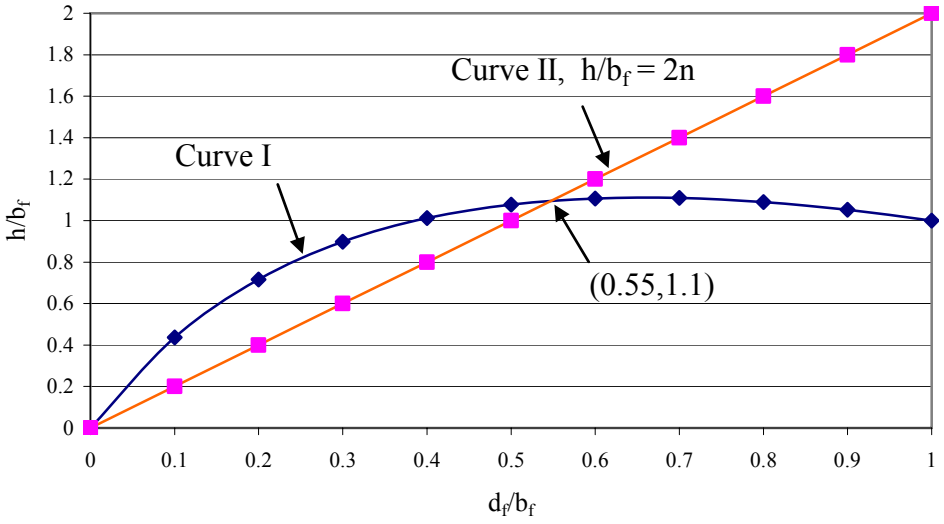

Figure 4.8 Ratio of h/b_f vs.Ratio of d_f/b_f

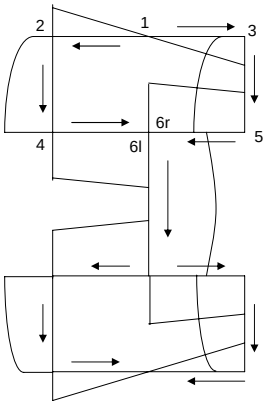

$$\tau_{v1} = 0\ ,\ \tau_{v2} = \frac{V_y}{I_x}\cdot\frac{t_f\cdot b_f}{2}\cdot\left(\frac{h_0}{2}+\frac{d_f}{2}\right)$$

$$\tau_{v3} = -\frac{V_y}{I_x}\cdot\frac{t_f\cdot b_f}{2}\cdot\left(\frac{h_0}{2}+\frac{d_f}{2}\right)$$

$$\tau_{v4} = \frac{V_y}{I_x}\cdot\frac{t_f\cdot b_f}{2}\cdot\left(\frac{h_0}{2}+\frac{d_f}{2}\right)+\frac{V_y}{I_x}\cdot\frac{h_0\cdot d_f\cdot t_f}{2}$$

$$\tau_{v5} = -\frac{V_y}{I_x}\cdot\frac{t_f\cdot b_f}{2}\cdot\left(\frac{h_0}{2}+\frac{d_f}{2}\right)-\frac{V_y}{I_x}\cdot\frac{h_0\cdot d_f\cdot t_f}{2}$$

$$\tau_{v6}^{l} = \frac{V_y}{I_x}\cdot\frac{t_f\cdot b_f\cdot h_0}{2}+\frac{V_y}{I_x}\cdot\frac{h_0\cdot d_f\cdot t_f}{2}$$

$$\tau_{v6}^{r} = -\frac{V_y}{I_x}\cdot\frac{t_f\cdot b_f\cdot h_0}{2}-\frac{V_y}{I_x}\cdot\frac{h_0\cdot d_f\cdot t_f}{2}$$

Figure 4.9 Vertical Shear Stress Distribution

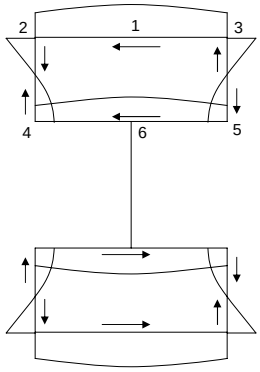

$$\bar{S}_{w1} = \frac{h_0}{2}\cdot\left(\frac{b_f{}^2 t_f}{8} + \frac{b_f t_f d_f}{4}\right) - \frac{b_f{}^3 n(1+n-2n^2)t_f}{48(1+n)}$$

$$\bar{S}_{w2} = \frac{h_0}{2}\cdot\frac{b_f t_f d_f}{4} + \frac{b_f{}^3 n(1-n)^2 t_f}{24(1+n)},\ \bar{S}_{w3} = \bar{S}_{w2}$$

$$\bar{S}_{w4} = -\frac{h_0}{2}\cdot\frac{b_f t_f d_f}{4} + \frac{b_f{}^3 n(1-n)^2 t_f}{24(1+n)},\ \bar{S}_{w5} = \bar{S}_{w4}$$

$$\bar{S}_{w6} = -\frac{h_0}{2}\cdot\left(\frac{b_f{}^2 t_f}{8} + \frac{b_f t_f d_f}{4}\right) - \frac{b_f{}^3 n(1+n-2n^2)t_f}{48(1+n)}$$

(a) Warping moment $\bar{S}_w$

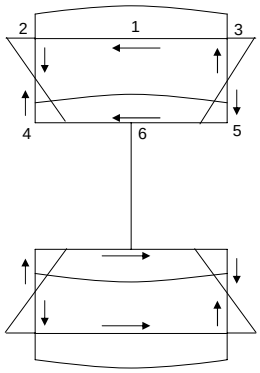

$$\bar{S}_{wg1} = \frac{h_0}{2}\cdot\left(\frac{b_f{}^2 t_f}{8} + \frac{b_f t_f d_f}{4}\right)$$

$$S_{wg2} = \frac{h_0}{2}\cdot\frac{b_f t_f d_f}{4},\ S_{wg3} = S_{wg2}$$

$$S_{wg4} = -\frac{h_0}{2}\cdot\frac{b_f t_f d_f}{4},\ S_{wg5} = S_{wg4}$$

$$S_{wg6} = -\frac{h_0}{2}\cdot\left(\frac{b_f{}^2 t_f}{8} + \frac{b_f t_f d_f}{4}\right)$$

(b) Global warping moment $\bar{S}_{wg}$

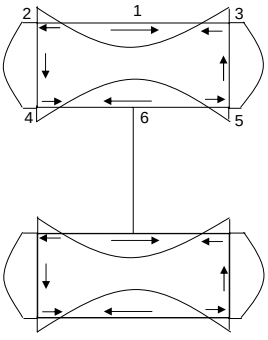

$$\bar{S}_{wl1} = -\frac{b_f{}^3 n(1+n-2n^2)t_f}{48(1+n)}$$

$$\bar{S}_{wl2} = \frac{b_f{}^3 n(1-n)^2 t_f}{24(1+n)}$$

$$\bar{S}_{wl3} = \bar{S}_{wl4} = \bar{S}_{wl5} = \bar{S}_{wl2}$$

$$\bar{S}_{wl6} = \bar{S}_{wl1}$$

(c) Local warping moment $\bar{S}_{wl}$

Figure 4.10 Normalized Warping Moment

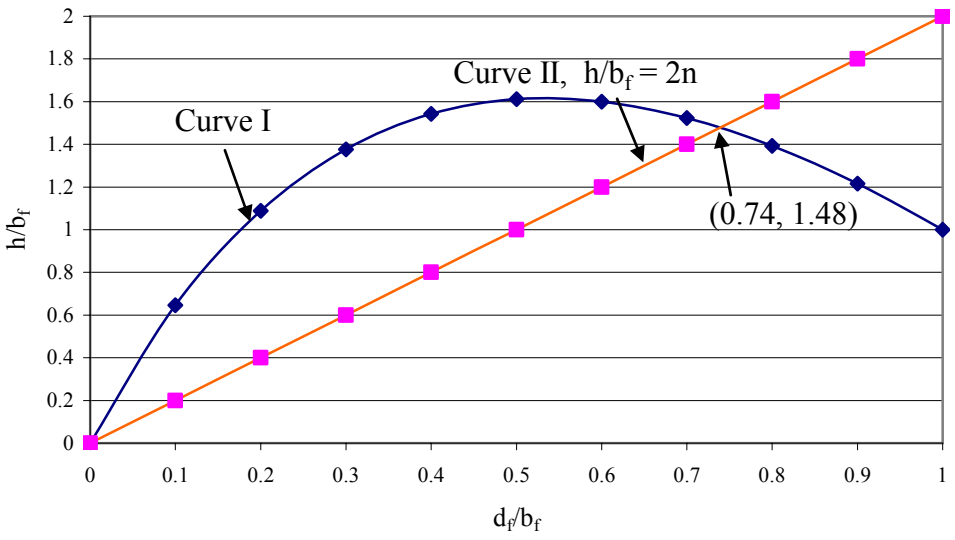

Figure 4.11 Ratio of h/b_f vs.Ratio of d_f/b_f

Chapter 5 Theoretical Analysis Results

Analyses of curved tubular-flange girder bridge systems are presented in this chapter. The theoretical method discussed in Chapter 4 is used. A single girder, a two-girder system and a three-girder system are studied, respectively. The loading and support conditions represent conditions that might occur during construction of a bridge. Specifically, the analysis of the single girder system represents a single bridge girder placed on its bearings and laterally braced at the bearings without intermediate bracing along the span. The two- and three-girder systems represent two-girder and three-girder bridges during the placement of the bridge deck after the cross frames are in place. Each girder system is simply-supported at the girder ends and subjected to uniformly distributed vertical loads. Comparisons with curved I-girder systems are presented at the end of the chapter.

5.1 Bridge Configuration, Girder Dimensions, and Applied Loads

5.1.1 Bridge Configuration

Figure 5.1 shows a schematic of the cross section of the three-girder bridge system, including the girder spacing and the overhang. For the two-girder bridge system, the girder spacing and the overhang width are the same as for the three-girder system. The configuration of these curved girder systems is based on a curved I-girder test specimen used in FHWA tests (Zureick and Naqib 1999). The FHWA test specimen was a curved three-girder system with girders and cross frames arranged as shown schematically in **Figure 5.2**. The span, radius and weight of each FHWA test specimen girder were as shown in **Table 5.1**. The ratio of the overall span to the radius of curvature (L/R) of the girders was 0.45. Three intermediate cross frames were used along the span length and the ratio of the unbraced length to the radius of curvature (L_b/R) was 0.1125 for each girder. The cross frames shown schematically in **Figure 5.2** were made from 5-in diameter steel tubes with ¼ in. wall thickness. In all cases, the girders and cross frames were assumed to be made of steel with an elastic modulus of 29000 ksi and Poison's ratio of 0.3.

5.1.2. I-Girder Dimensions

To enable the behavior of the curved tubular-flange girder systems to be compared against the behavior of curved I-girder systems, corresponding curved I-girders were also analyzed using the theoretical method presented in Chapter 4. The cross-section dimensions of the three doubly-symmetric curved I-girders, denoted G1, G2, G3, are given in **Table 5.2**. For the single girder study, girder G2 is used. Girders G1 and G2 are used for the two-girder system and girders G1, G2 and G3 are used for the three-girder system.

5.1.3. Tubular-Flange Girder Dimensions

The three curved tubular-flange girders, denoted TG1, TG2, and TG3, are designed to have the same girder weight and cross section depth as the corresponding curved I-girders G1, G2 and G3 respectively. The dimensions of the doubly-symmetric tubular-flange girders are given in **Table 5.3**. Girder TG2 is used for the single girder. Girders TG1 and TG2 are used for the two-girder system and girders TG1, TG2 and TG3 are used for the three-girder system.

5.1.4 Applied Loads

The loads considered for analyses of the girders under construction conditions include only the dead load. During the placement of the cast-in-place concrete deck, the concrete deck does not contribute to the resistance of the system and is treated as a dead load applied on each bridge girder. Since the overhangs equal half the spacing between the girders and the overhangs do not add torsion to the external and internal girders (see **Figure 5.1**). Only uniformly distributed vertical loads are applied to each girder. The dead load includes the following items:

An 8-in thick concrete slab with a concrete unit weight of 150 lbs/ft^3.
Concrete hauches with an estimated weight of 40 lbs/ft.
Stay-in-place deck forms with a weight of 16 lbs/ft^2.
Cross frames with an estimated weight of 10% of the girder self-weight.
The girder self-weight (see **Table 5.1**).

For the single girder study, the dead load that is applied during construction is actually only the girder self-weight, given in **Table 5.1**. For the two-girder system, the full dead load applied to girder TG1 and TG2 is 105 lbs/in and 110 lbs/in, respectively. For the three-girder system, the full dead load applied to girder TG1, TG2 and TG3 is 105 lbs/in, 110 lbs/in and 129 lbs/in, respectively. The analysis of the single girder under the full dead load (110 lbs/in) was conducted for the purpose of comparison with the two-girder and three-girder system results. Therefore, two types of dead loads are considered for the single girder study, namely, girder self-weight only and full dead load.

5.2. Analysis Results for Curved Tubular-Flange Girder Systems

The stresses and displacements at only critical points in the girders are presented in the plots shown in the following sections. These important points on the cross section are labeled in **Figure 4.4** and **Figure 4.5**. The analysis results for the corresponding curved I-girder are presented along with the curved tubular-flange girder results in the plots for the purpose of comparison. The following notation is used in legends for the plots: GN, which indicates the result for the corresponding curved I-girder, where N is the girder number, either 1,2 or 3; TGN, which indicates the result for the corresponding curved tubular-flange girder, where N is the girder number, either 1,2 or 3.

5.2.1 Single Curved Tubular-Flange Girder

During the construction stage, curved girders could be erected individually without shoring, and therefore, they would carry dead loads before cross frames are installed. As mentioned in Section 5.1.4, two types of dead loads are considered for the single curved tubular-flange girder study. One is the single girder self-weight, which is the actual load applied on a single curved tubular-flange girder during construction and the other is the full dead load given in Section 5.1.4, which is an imaginary dead load applied on a single curved tubular-flange girder to enable comparison of the single girder results with the two-and three-girder system results. Since the analysis is linear elastic, the stresses and displacements under these two types of dead load are the same and only the magnitude of the stresses and displacements change. So the results for the single curved tubular-flange girder under the full dead load are plotted in **Figure 5.3** through **Figure 5.12**. To find the results for girder self-weight only, the results in these figures can be multiplied by the factor 0.182. The maximum stresses and displacements for the single curved tubular-flange girder under the girder self-weight are presented in **Table 5.4**. The discussion in this section is based on the results under the full dead load. Since the cross section is doubly symmetric, stresses in the top and bottom flange are symmetric or anti-symmetric, so the plots show only stresses at the critical points in the girder top flange and the displacements at the cross section centroid. The plots also show I-girder results which are discussed later.

The analysis results indicate that the warping stress is not significant and the bending stress is dominant in the simply supported single curved tubular-flange girder. For the girder that was studied, the warping normal stress equals only 7% of the bending normal stress. The maximum total normal stress in the top flange occurs at Point 2 (P2) of the midspan cross-section. For shear stresses, the results show that the warping shear stress is negligible and the St. Venant stress dominates the total shear stress. Unlike in the I-girder, the tubular flanges also carry a small amount of vertical shear, so the vertical shear stress is considered in calculating the total shear stress in the tubular flange. The maximum total shear stress in the top flange occurs at the right side of Point 6 (P6r) at the two end cross sections. Since the total normal stress is much larger than the total shear stress in the single curved tubular-flange girder, the maximum Von-Mises stress in the top flange occurs at P2 of the midspan cross-section, where the shear stresses are zero. Therefore, only the total normal stress contributes to the maximum Von-Mises stress at this location. The maximum vertical displacement occurs at midspan and is 1/250 of the arc span length of the girder (L). The maximum cross section rotation occurs at midspan and equal to 0.0303 rad. Since the cross section depth is 50.375 in., as shown in **Table 5.3**, this maximum cross section rotation results in a relative horizontal displacement between the top and bottom flanges of 1.53 in. The ratio of the relative horizontal displacement to the cross section width, which is 20 in., is 1/13.

5.2.2 Two Curved Tubular-Flange Girder System

In a two-girder bridge system, the cross frames restrain the cross-section rotation of the girders, but they also increase the vertical load on the outer girder and decrease the vertical load on the inner girder. Since the internal forces on the inner girder are smaller than those on the outer girder, the outer girder is usually designed to have larger capacity. **Figure 5.13** through **Figure 5.32** presents the stresses at the critical points and the displacements at the centroids of the two girders in the two-girder system.

The analysis results show that the interaction of the cross frames with the girders increases the warping normal stress and warping shear stress in the regions near the braced cross section relative to the results for a single girder. The cross sections with the largest warping shear stress are the interior braced cross sections in the two-girder system. For the single girder, the largest warping shear stress is at the end cross sections. However, the bending normal stresses are still much larger than the warping normal stresses. The St.Venant shear stresses are still much larger than both the warping shear stresses and the vertical shear stresses. For the inner girder (TG1), the maximum total normal stress occurs at P2 in the region near the midspan. For the outer girder, the maximum total normal stress occurs at Point 3 (P3) at the midspan. For both girders in the two-girder system, the St. Venant shear stress is the dominant part of the total shear stress and the total normal stress is still much larger than the total shear stress. The maximum total shear stress occurs at the two end cross sections, and the maximum Von-Mises stress is dominated by the total normal stress, and is essentially equal in magnitude to the maximum total normal stress.

Comparing to the single girder (see **Table 5.5**), the maximum total normal stress is reduced for the inner girder, but increased for the outer girder. The maximum total shear stress in both girders of the two-girder system is smaller than the maximum total shear stress of the single girder. The change in the maximum Von-Mises stress, relative to the single girder case, is similar to the change in the maximum total normal stress for both girders. The cross section rotations of both girders are reduced in the two-girder system due to the restraint from the cross frames. Relative to the single girder, the vertical displacement is reduced for the inner girder, but increased for the outer girder, since the cross frames decrease the vertical load on the inner girder and increase the vertical load on the outer girder.

Hence, it is concluded for the two-girder system that the cross frames transfer loads from the inner girder to the outer girder, thus as shown, the outer tubular-flange girder needs to be designed with a larger capacity than the inner girder.

5.2.3 Three Curved Tubular-Flange Girder System

For the three-girder system, the stresses at the critical points and the displacements at the centroids are presented in **Figure 5.33** through **Figure 5.62**.

Similar to the single girder and the two-girder system, the bending normal stress is much larger than the warping normal stress in the three-girder system. The maximum total normal stress for each girder occurs at P3 of the midspan cross section. The maximum total shear stress for each girder occurs at the two end cross sections. The maximum Von-Mises stress for each girder is essentially the same magnitude as the maximum total normal stress and occurs at P3 of the midspan cross section. The largest stresses and displacements in the three-girder system occur in the outer girder (TG3). Comparing to the single and two-girder system (see **Table 5.5**), the analysis results show that the total normal stress, the total shear stress, and the displacement of the inner girder and the middle girder in the three-girder system are smaller than the results of the associated girders in the single girder and the two-girder system respectively. The largest stresses and displacements among the three girders in the three-girder system are smaller than the largest stresses and deflections in the single and two-girder system. In addition, unlike the single girder, the warping shear stress is not negligible in the two- and three-girder systems. However, the warping shear stress at the end cross sections is small enough to be ignored relative to the total shear stress. Since the maximum total shear stress for each girder occurs at the end cross sections, the contribution of the warping shear stress to the maximum total shear stress is negligible.

5.2.4 Summary of Findings from Results

Based on the analysis of the single girder and the two- and three-girder systems, it is observed that the critical stresses and displacements in the three-girder system are smaller than those in the two-girder system and the single girder. For the two-girder system, the outer girder has the largest stress and displacement demands due to the load transfer from the inner girder to the outer girder. For the three-girder case, the torsional stiffness of the bridge system is significantly increased, so the stresses and displacements, especially the St.Venant shear stress and the cross section rotation, are reduced, compared to those of the two-girder system and the single girder.

5.3 Comparison with Curved I-Girder System

As noted in Section 5.1, the I-girders have the same self-weight and cross section depth as the corresponding tubular-flange girders. As a result of these similarities and the differing cross section shapes, the curved I-girders have a larger flexural rigidity and smaller St.Venant torsional constant than the corresponding curved tubular-flange girders. Therefore, for the two- and three-girder systems, the curved I-girders tend to have a smaller bending normal stress and vertical displacement than the corresponding curved tubular-flange girder. However, the curved tubular-flange girders have much lower warping normal stress and less cross section rotation than the corresponding curved I-girders. For the curved tubular-flange girder, the bending normal stress is dominant, and is much larger than the warping normal stress and the shear stresses. For the curved I-girder, the warping normal stress can be very large and is larger than the bending normal stress for the single girder case. The St.Venant shear stress is small for the I-girder, except for the single girder case. The vertical shear stress

is negligible in the I-girder flange. A detailed discussion of these comparisons is as follows.

The analysis results for the single tubular-flange girder and I-girder under the girder self-weight are used for the comparison in this section (see **Table 5.4**). For the single girder case, the single curved I-girder is not capable of carrying the girder self-weight due to its low torsional stiffness, and the displacements are very large. The vertical displacement of the I-girder is 1/71 of the arc span length. The cross section rotation of the single I-girder is 0.307 rad. The relative horizontal displacement between the top and bottom flanges due to this cross section rotation is 15.5 in., which is 77% of the I-girder cross section width, i.e. 20 in. The total normal stress and total shear stress for the single curved I-girder are also significantly larger than those of the corresponding tubular-flange girder. The single curved tubular-flange girder is much better in resisting the girder self-weight due to its higher torsional stiffness. The single tubular-flange girder develops much smaller stresses and displacements than the corresponding single curved I-girder. The vertical displacement of the single curved tubular-flange girder is 1/1400 of the girder arc span length. The cross section rotation of the single tubular-flange girder is 5.52×10^{-3} rad. and the resulting relative horizontal displacement between the top and bottom flange is 0.28 in., which is 1/71 of the cross section width, 20 in. So, the single curved tubular-flange girder develops small stresses and displacements under the girder self-weight. Hence, unlike the single curved I-girder, the single curved tubular-flange girder is capable of supporting itself. Temporary bracing or shoring may not be needed for a single curved tubular-flange girder as the girder is erected.

For the two-girder systems, the increase in vertical load on the outer girder and decrease in vertical load on the inner girder are greater for the I-girder system than the tubular-flange girder system due to the low torsional stiffness of the I-girder. Thus, the bending normal stress in the inner I-girder is much less than that in the inner tubular-flange girder (see **Figure 5.13**), while the bending normal stress of the outer I-girder and the outer tubular-flange girder are similar (see **Figure 5.23**). The warping normal stresses for the inner and outer I-girders are larger than the warping normal stress in the inner and outer tubular-flange girders, respectively. Since the warping normal stress magnitude is similar to the bending normal stress magnitude for the I-girder, the warping normal stress has a large influence on the total normal stress of the I-girder (see **Figure 5.15** and **Figure 5.25**). The warping normal stress varies significantly along the span. As a result, the total normal stress along the span has a large variation for the curved I-girders, especially for the outer girder. However, the warping normal stress has a very small contribution to the total normal stress for the tubular-flange girder. So the variation of the total normal stress along the span follows the bending normal stress and the girder cross-section is used more efficiently. The maximum total normal stress for the outer I-girder is larger than that for the outer tubular-flange girder due to the significant warping normal stress developed in the I-girder (see **Table 5.6**).

For the two-girder systems, the St.Venant and vertical shear stresses in the I-girders are both smaller than those of the tubular-flange girders. So the total shear

stresses in the curved I-girders are smaller than those in the tubular-flange girders (see **Table 5.6**). The tubular-flange girder system develops less cross section rotation (see **Table 5.6**) than the curved I-girder system due to the larger torsional stiffness of the tubular-flange girders. The vertical displacement for the inner tubular-flange girder is larger than that for the inner I-girder (see **Table 5.6**). However, the vertical displacement for the outer tubular-flange girder is smaller than that for the outer I-girder.

For the three-girder systems, the comparisons are similar to those for the two-girder systems. The bending normal stresses for the three tubular-flange girders are larger than those of the corresponding three I-girders. The warping normal stresses for the tubular-flange girders are much less than those of the I-girders, especially for the middle and outer girder. The total normal stress for the inner tubular-flange is larger than for the inner I-girder, since the bending normal stress has more influence on the total normal stress (see **Table 5.7**). However, the maximum total normal stresses for the middle and outer tubular-flange girder are less than those for the middle and outer I-girder, respectively (see **Table 5.7**). The differences in total normal stress between the tubular-flange girders and the I-girders are reduced with respect to the two-girder case. Similar to the two-girder systems, the total normal stress along the span has a large variation for the curved I-girders.

For the three-girder systems, the St.Venant shear stress and total shear stress for the tubular-flange girders are larger than those for the I-girders (see **Table 5.7**). The cross section rotation of the tubular-flange girders is smaller than those of the I-girders due to the higher torsional stiffness of tubular-flange girders (see **Table 5.7**). However, the vertical displacement due to bending for the three girders is much larger than the component due to the cross section rotation. As a result, the vertical displacement of the tubular-flange girders is larger than that of the I-girders (see **Table 5.7**).

Table 5.8 presents the cross frame forces, which are the concentrated vertical forces and torques on the girders at the interface between the girders and the cross frames. These forces are equal and opposite to the vertical forces and bending moments carried by cross frames. The maximum cross frame forces for the cross frame between TG1/G1 and TG2/G2 as well as between TG2/G2 and TG3/G3 are given. The results show that the forces carried by the cross frames for the tubular-flange girder system are smaller than for the I-girder system. Because the tubular-flange girder has higher torsional stiffness than the I-girder, smaller cross frame forces develop in the tubular-flange girder system. As a result, the cross frames in tubular-flange girder systems can be designed with smaller members.

Based on the previous discussion, the findings of the study are summarized as follows: (1) a single curved tubular-flange girder can carry the girder self-weight, and there appears to be no need for temporary shoring or support as the girders are erected, however, a single curved I-girder needs temporary shoring or support to carry the girder self-weight; (2) a curved I-girder is better at resisting bending, but develops very large warping normal stress and cross section rotation, while the curved tubular-flange girder

is effective at resisting torsion, and develops small warping normal stress and cross section rotation; (3) the bending normal stress is the major part of the total normal stress for a curved tubular-flange girder, but the warping normal stress and the bending normal stress have similar contributions to the total normal stress for a curved I-girder. As a result, the total normal stress is more uniform over the span for a curved tubular-flange girder, but the total normal stress varies widely over the span for a curved I-girder; (4) the warping shear stress is negligible for a single curved tubular-flange girder, however, for the two- and three-girder systems, the warping shear stress is large at the braced cross sections, but its contribution to the maximum total shear stress at the end cross sections is negligible; (5) Compared to the I-girder system, the tubular-flange girder system develops smaller cross frame forces, which would permit smaller size of cross frame members in tubular-flange girder systems.

Table 5.1 Girder Geometry and Weight

Girders	Span (ft)	Radius (ft)	Weight (lb/in)
G1 / TG1	86.093	191.25	15.40
G2 / TG2	90.000	200.00	20.02
G3 / TG3	93.938	208.75	36.96

Table 5.2 Curved I-Girder Dimensions

Girders	Flanges(in)	Web (in)	Depth (in)
G1	16 x 17/16	48 x 7/16	50.125
G2	20 x 19/16	48 x 1/2	50.375
G3	24 x 9/4	48 x 1/2	52.500

Table 5.3 Curved Tubular-Flange Girder Dimensions

Girders	Tubular Flange (in)	Web (in)	Depth (in)
TG1	16 x 8 x 0.421	33.283 x 7/16	50.125
TG2	20 x 10 x 0.489	29.398 x 7/16	50.375
TG3	24 x 12 x 0.823	26.853 x 8/16	52.500

Table 5.4 Maximum Stresses and Displacements for Single Girder

Girders	σ_x (ksi)	τ_t (ksi)	v (in)	θ (rad)
TG2	-3.155	-0.883	-0.764	0.00552
G2	-20.243	-11.847	-15.52	0.307

Note: σ_x is the total normal stress; τ_t is the total shear stress;
v is the vertical displacement; θ is the cross section rotation.

Table 5.5 Maximum Stress and Displacements of Curved Tubular-flange Girders

Girders		σ_x (ksi)	τ_t (ksi)	v (in)	θ (rad)
Single Girder	TG2	-17.33	-7.55	-4.20	0.030
Two-Girder System	TG1	-10.84	-4.71	-2.58	0.020
	TG2	-24.05	-6.28	-4.84	0.020
Three-Girder System	TG1	-10.21	-2.23	-1.77	0.0044
	TG2	-13.94	-2.64	-2.48	0.0044
	TG3	-17.71	-3.00	-3.19	0.0044

Note: σ_x is the total normal stress; τ_t is the total shear stress;
v is the vertical displacement; θ is the cross section rotation.

Table 5.6 Maximum Stresses and Displacements for Two-Girder Systems

Girders	σ_x (ksi)	τ_t (ksi)	v (in)	θ (rad)
TG1	-10.84	-4.71	-2.58	0.020
TG2	-24.05	-6.28	-4.84	0.020
G1	2.52	-1.61	-1.86	0.038
G2	-40.47	-3.17	-5.84	0.042

Note: σ_x is the total normal stress; τ_t is the total shear stress;
v is the vertical displacement; θ is the cross section rotation.

Table 5.7 Maximum Stresses and Displacements for Three-Girder Systems

Girders	σ_x (ksi)	τ_t (ksi)	v (in)	θ (rad)
TG1	-10.21	-2.23	-1.77	0.0044
TG2	-13.94	-2.64	-2.48	0.0044
TG3	-17.71	-3.00	-3.19	0.0044
G1	-8.30	-0.83	-1.12	0.0086
G2	-15.41	-1.07	-1.89	0.0093
G3	-20.52	-2.05	-2.66	0.0093

Note: σ_x is the total normal stress; τ_t is the total shear stress;
v is the vertical displacement; θ is the cross section rotation.

Table 5.8 Maximum Cross Frame Forces

Cross Frame	Vertical Force (kip)	Moment (kip-in)
TG1 – TG2	16.36	1116
TG2 – TG3	22.86	2476
G1 – G2	22.67	1893
G2 – G3	31.91	3958

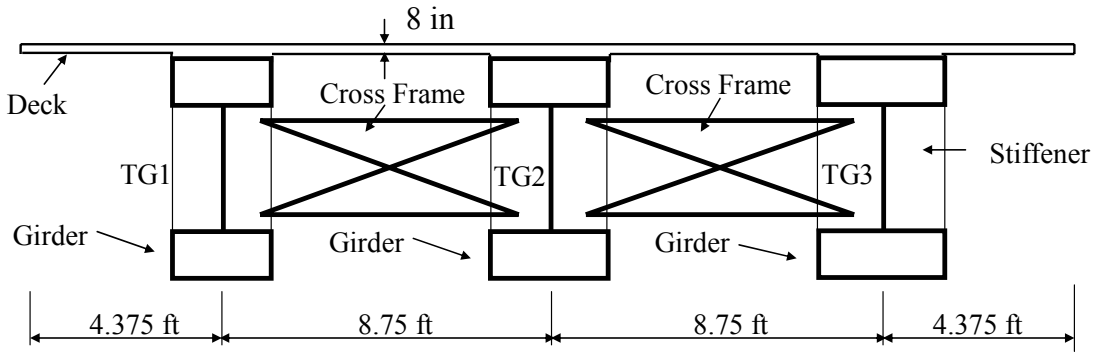

Figure 5.1 Three-Girder Bridge Cross Section Schematic

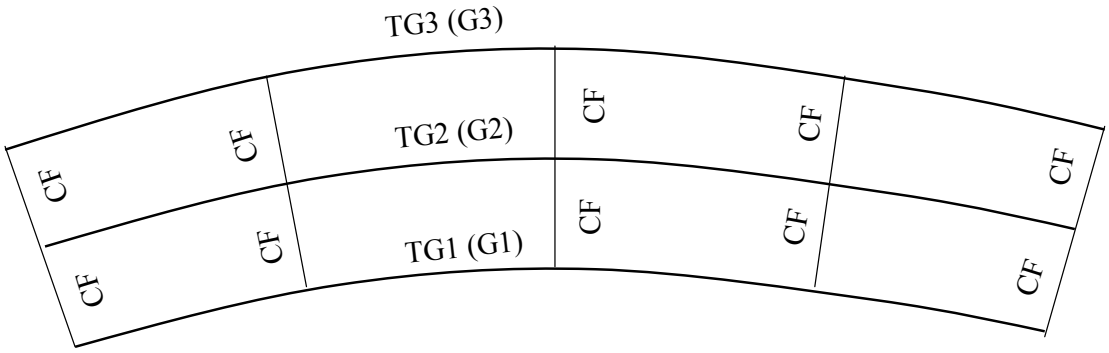

Figure 5.2 Schematic Framing Plan of Three-Girder Bridge

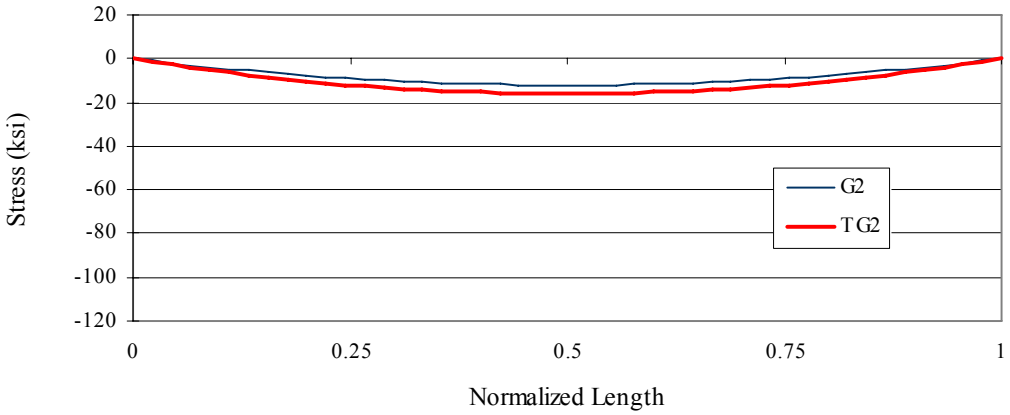

Figure 5.3 Primary Bending Normal Stress at P2 (Single Girder)

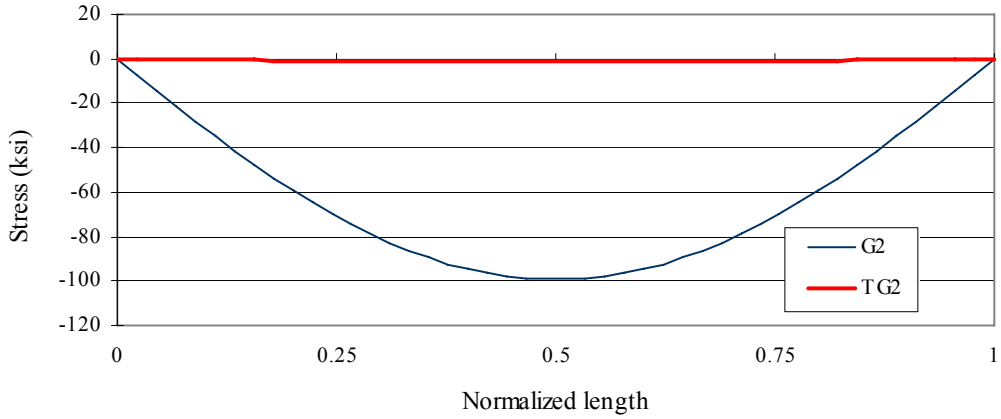

Figure 5.4 Warping Normal Stress at P2 (Single Girder)

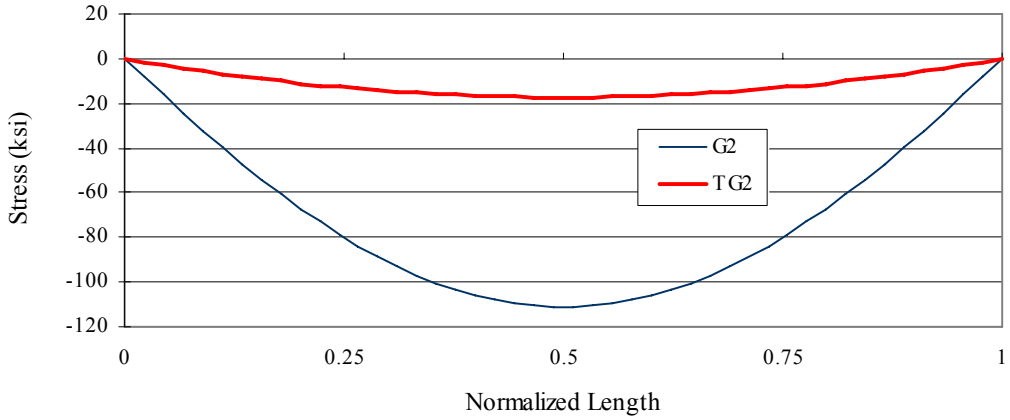

Figure 5.5 Total Normal Stress at P2 (Single Girder)

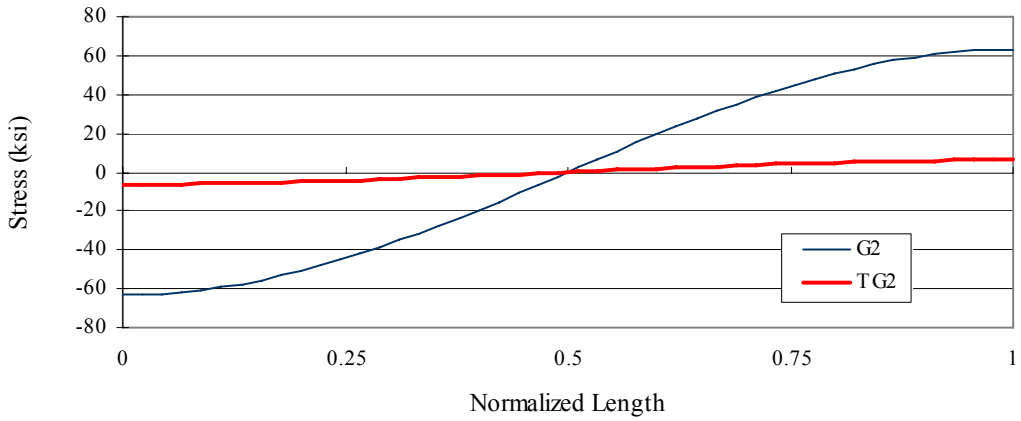

Figure 5.6 St. Venant Shear Stress at P6r (Single Girder)

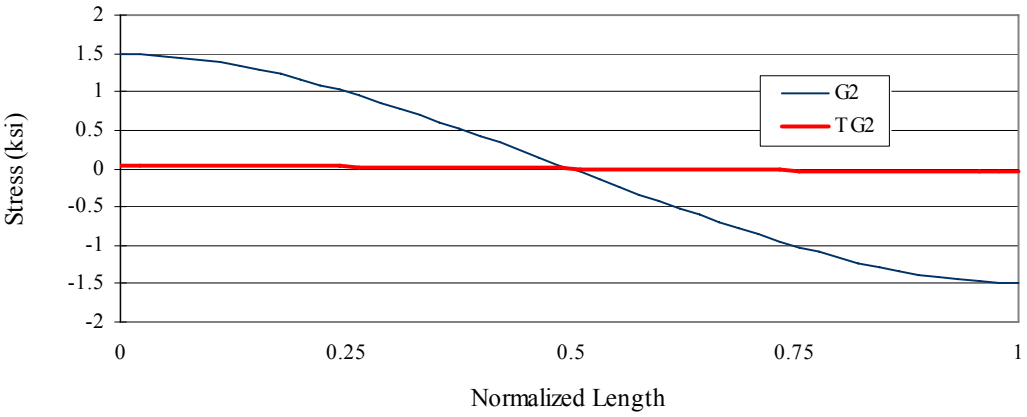

Figure 5.7 Warping Shear Stress at P6r (Single Girder)

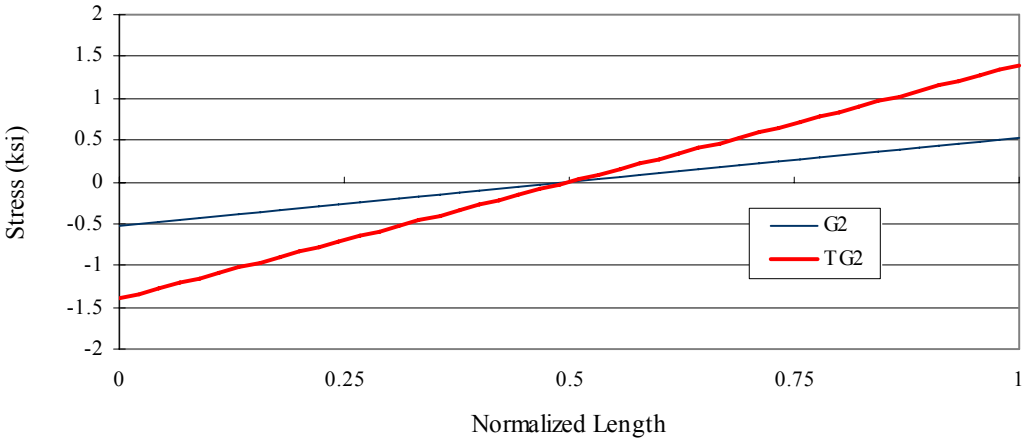

Figure 5.8 Vertical Shear Stress at P6r (Single Girder)

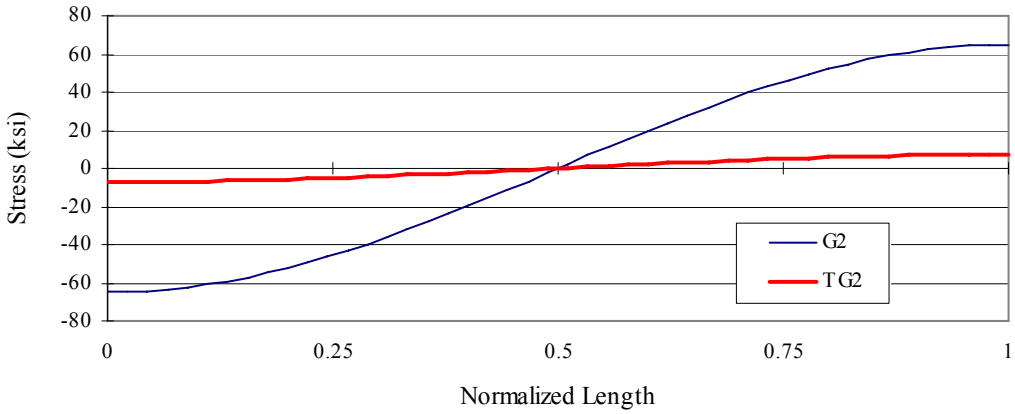

Figure 5.9 Total Shear Stress at P6r (Single Girder)

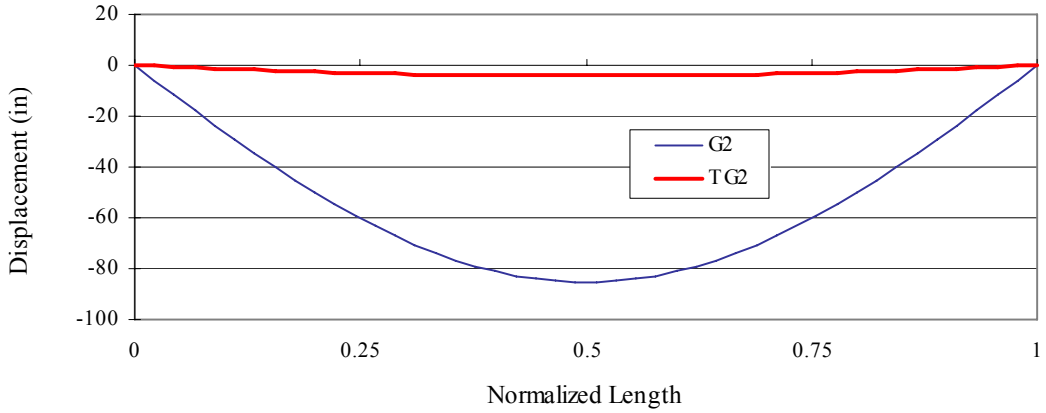

Figure 5.10 Vertical Displacement (Single Girder)

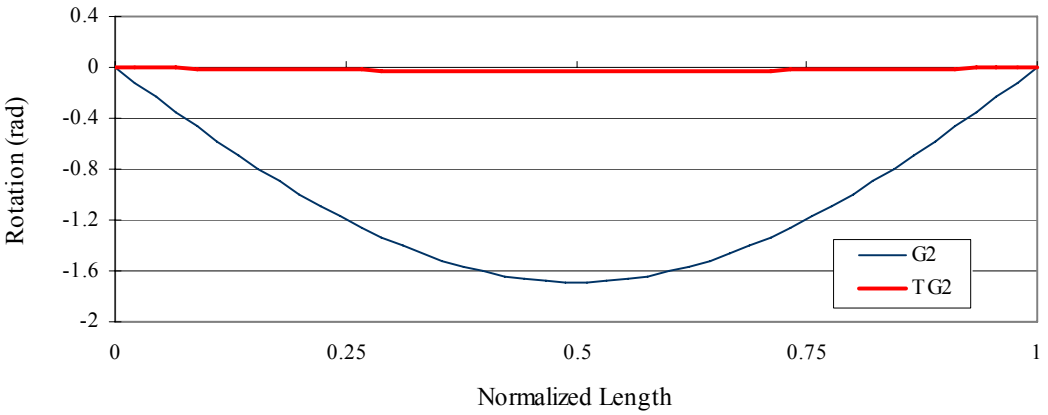

Figure 5.11 Cross Section Rotation (Single Girder)

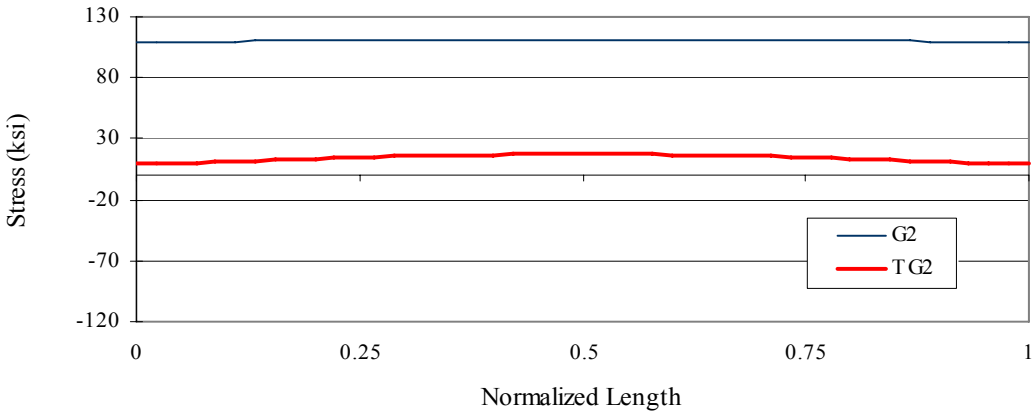

Figure 5.12 Von-Mises Stress at P2 (Single Girder)

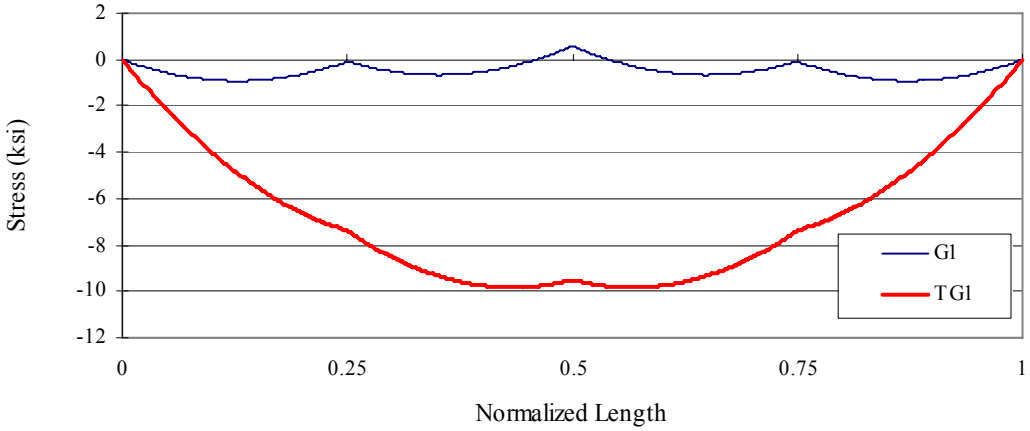

Figure 5.13 Primary Bending Normal Stress of Inner Girder at P2 (Two-Girder Case)

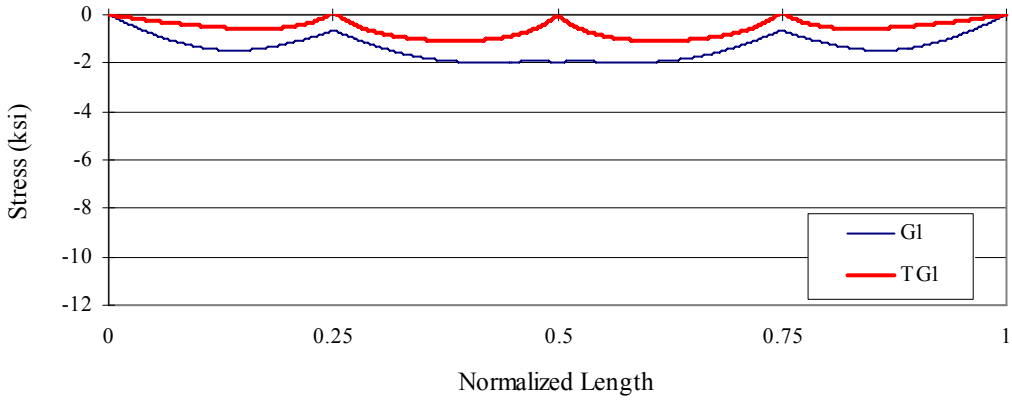

Figure 5.14 Warping Normal Stress of Inner Girder at P2 (Two-Girder Case)

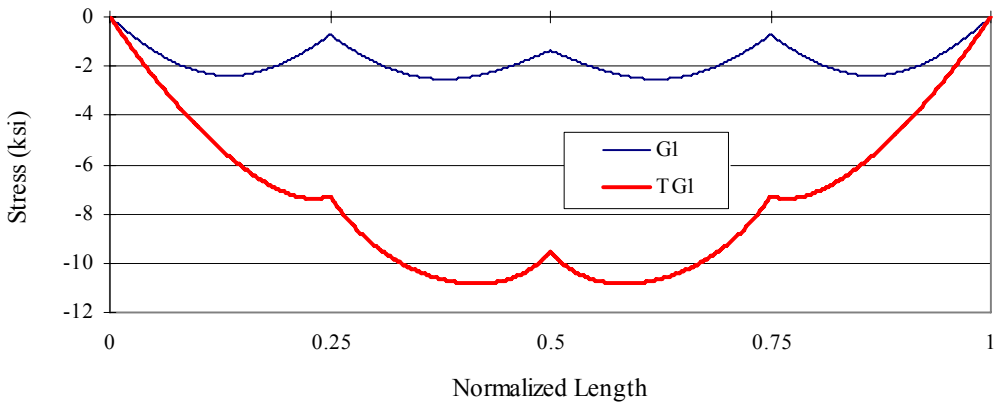

Figure 5.15 Total Normal Stress of Inner Girder at P2 (Two-Girder Case)

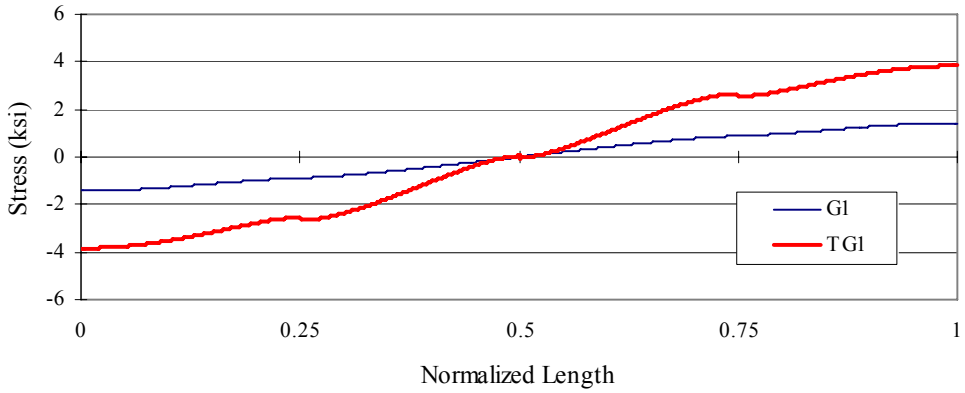

Figure 5.16 St.Venant Shear Stress of Inner Girder at P6r (Two-Girder Case)

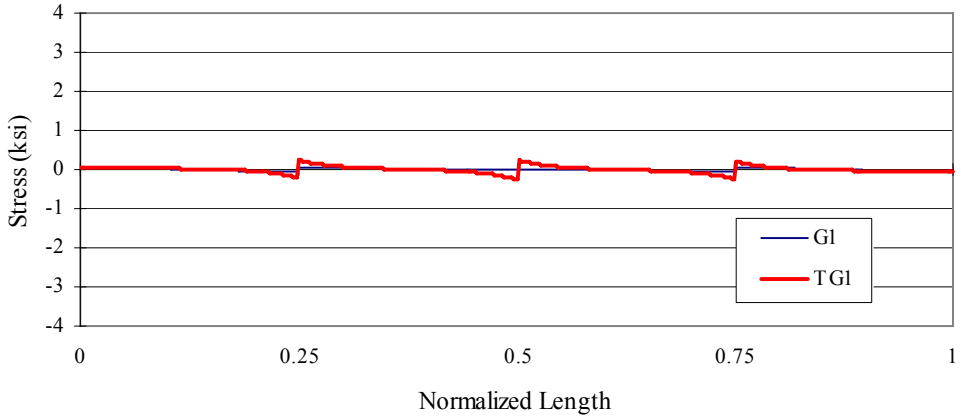

Figure 5.17 Warping Shear Stress of Inner Girder at P6r (Two-Girder Case)

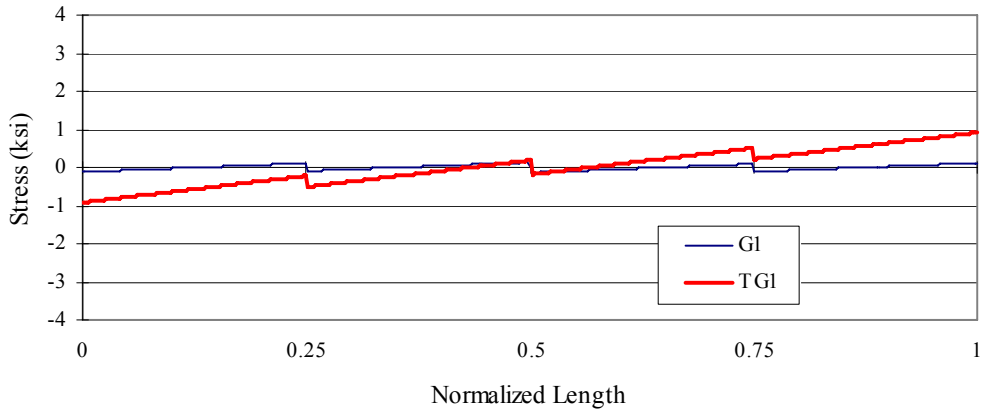

Figure 5.18 Vertical Shear Stress of Inner Girder at P6r (Two-Girder Case)

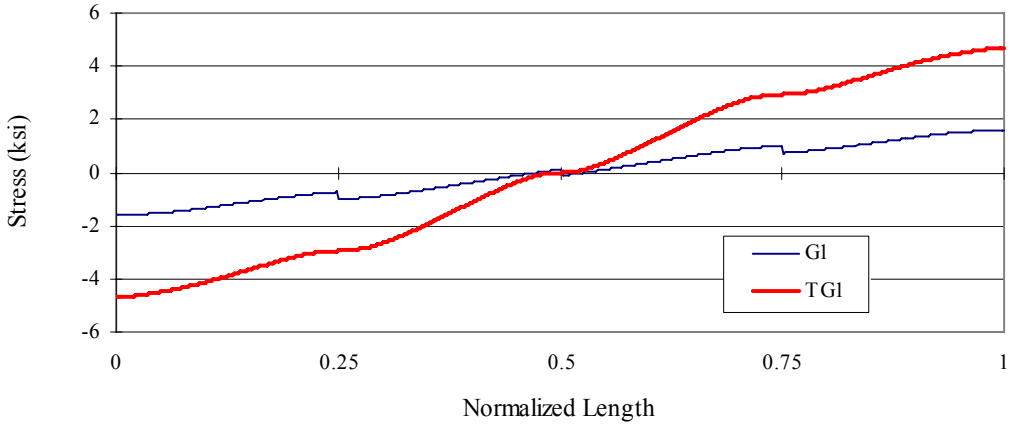

Figure 5.19 Total Shear Stress of Inner Girder at P6r (Two-Girder Case)

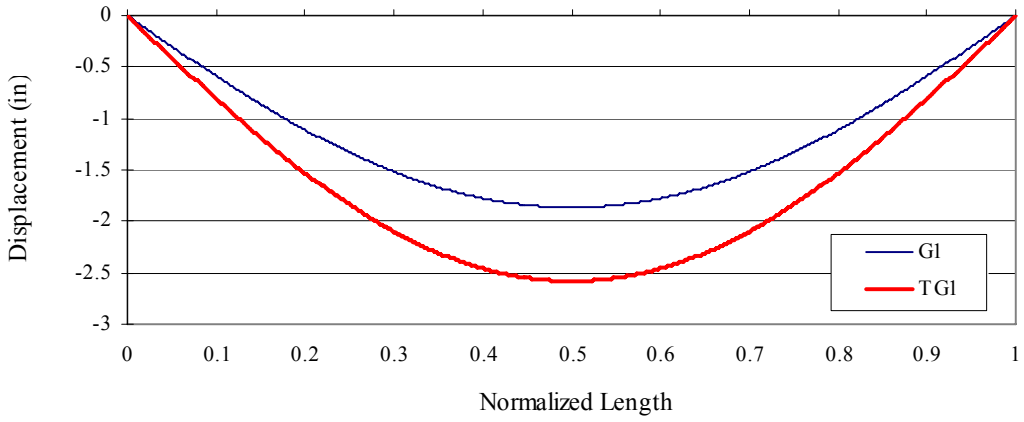

Figure 5.20 Vertical Displacement of Inner Girder (Two-Girder Case)

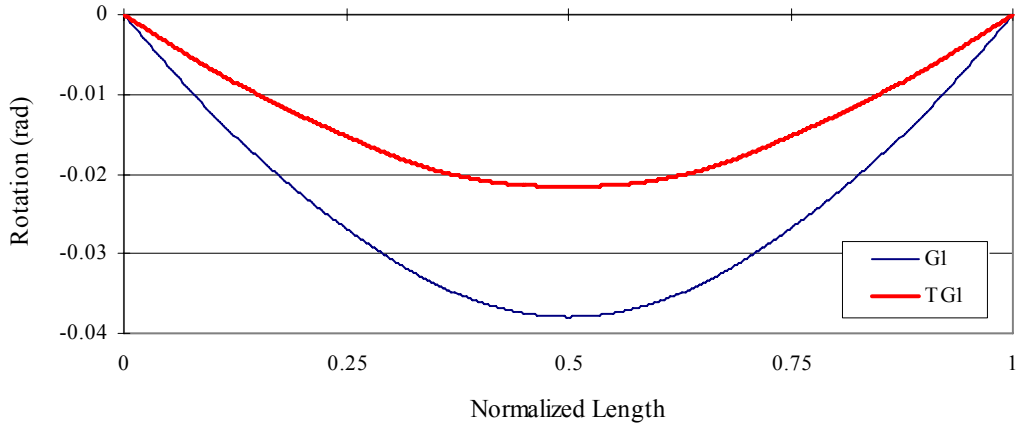

Figure 5.21 Cross Section Rotation of Inner Girder (Two-Girder Case)

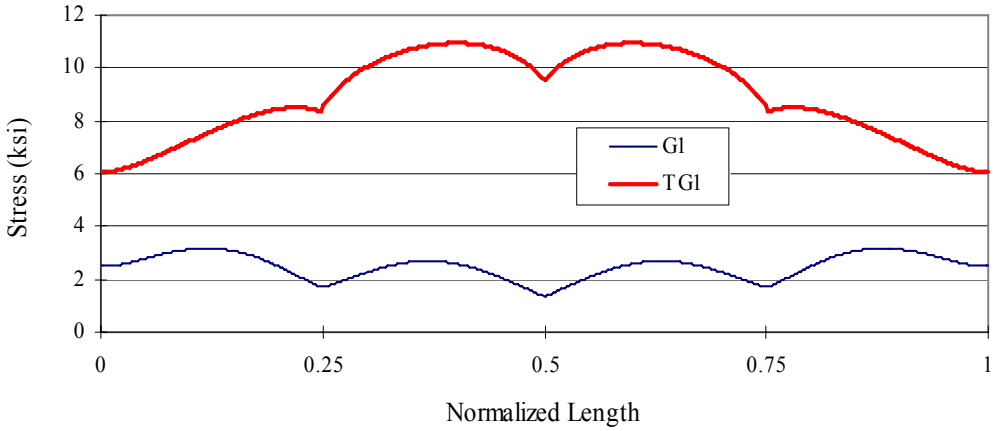

Figure 5.22 Von-Mises Stress of Inner Girder at P2 (Two-Girder Case)

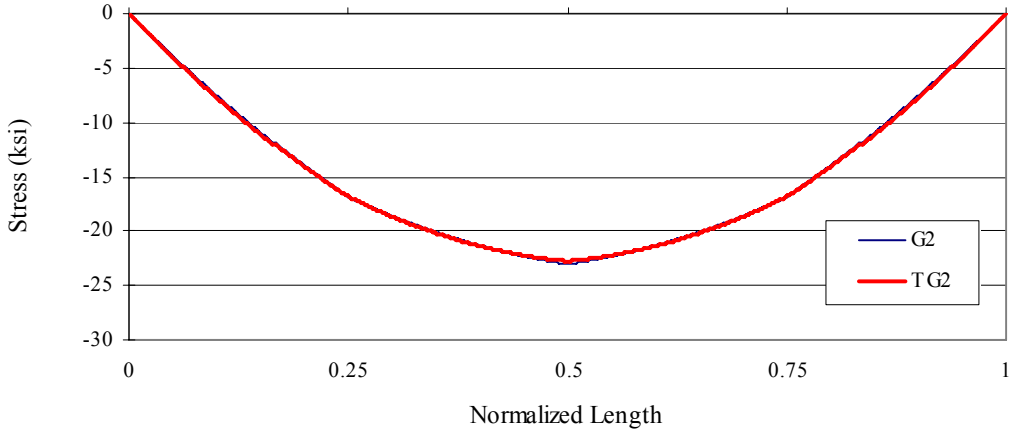

Figure 5.23 Primary Bending Normal Stress of Outer Girder at P3 (Two-Girder Case)

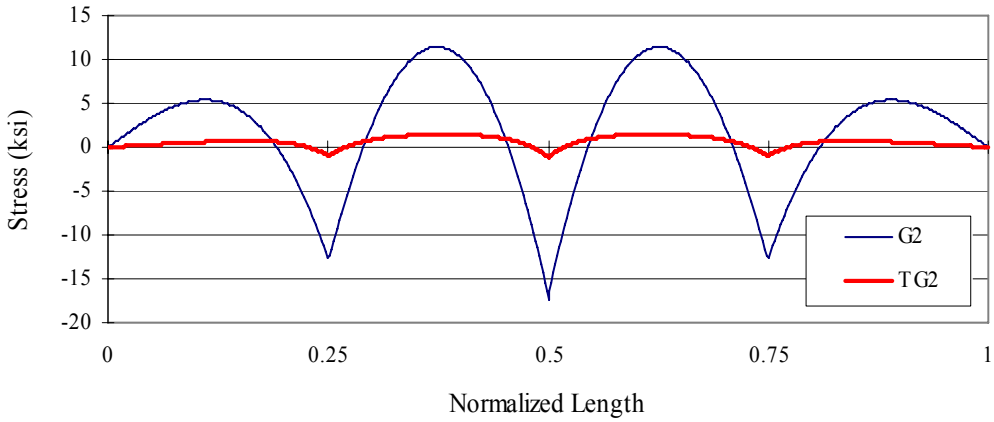

Figure 5.24 Warping Normal Stress of Outer Girder at P3 (Two-Girder Case)

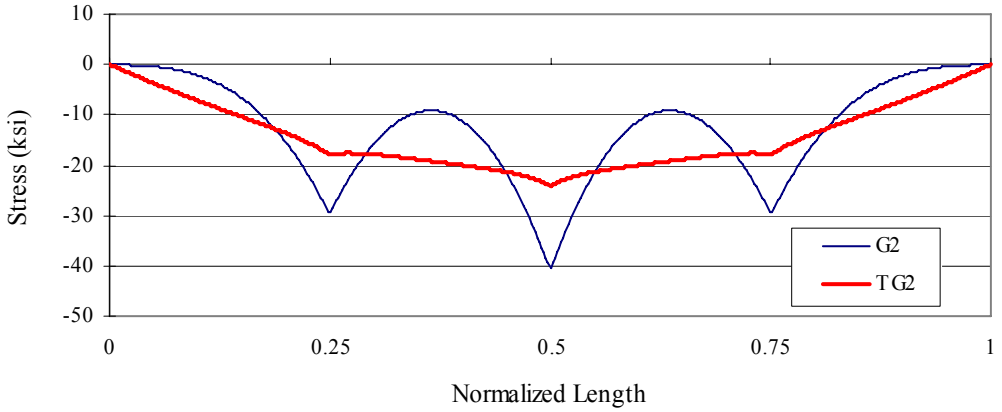

Figure 5.25 Total Normal Stress of Outer Girder at P3 (Two-Girder Case)

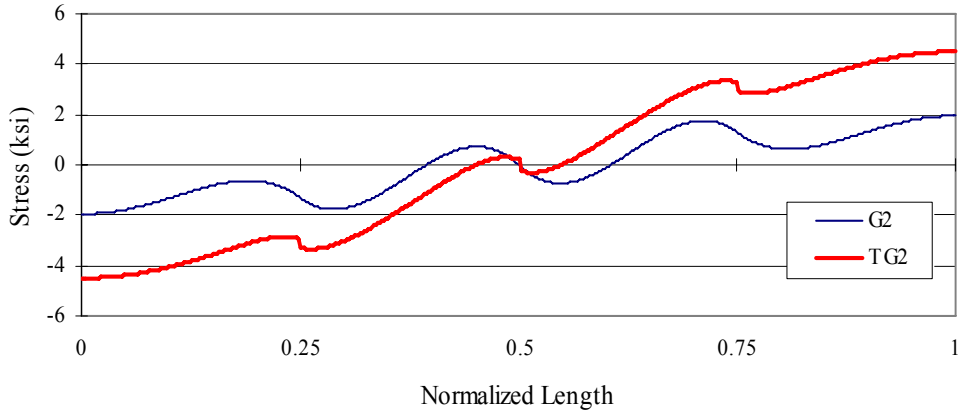

Figure 5.26 St.Venant Shear Stress of Outer Girder at P6r (Two-Girder Case)

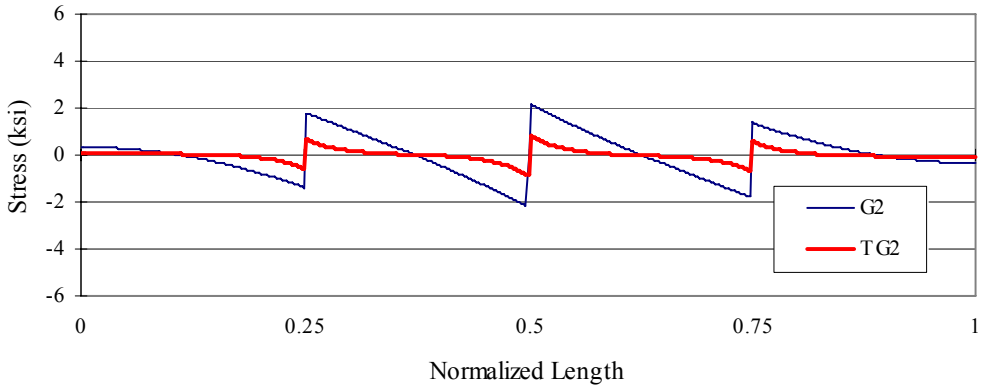

Figure 5.27 Warping Shear Stress of Outer Girder at P6r (Two-Girder Case)

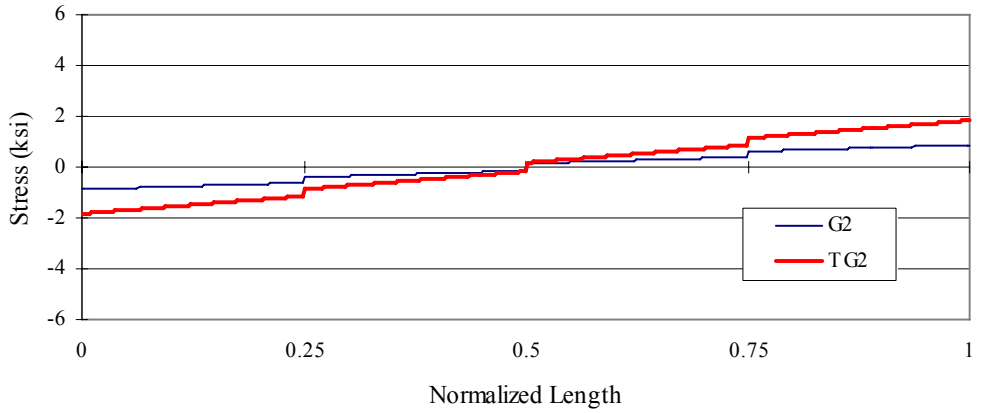

Figure 5.28 Vertical Shear Stress of Outer Girder at P6r (Two-Girder Case)

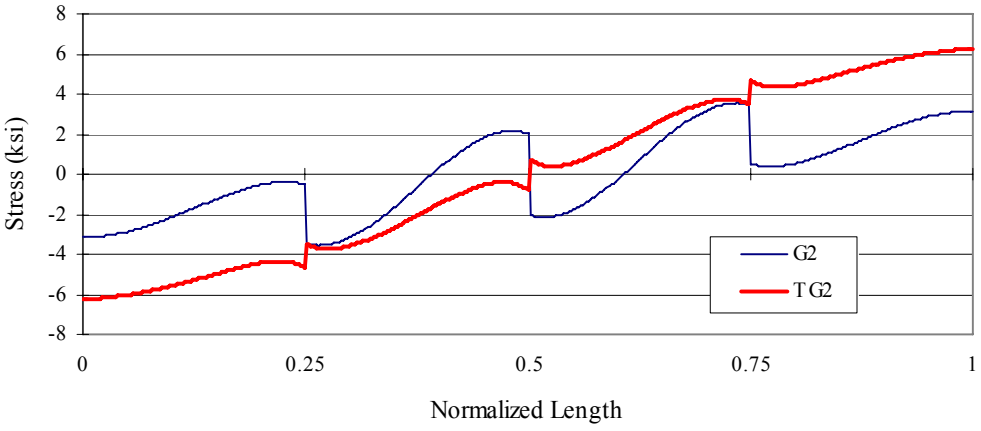

Figure 5.29 Total Shear Stress of Outer Girder at P6r (Two-Girder Case)

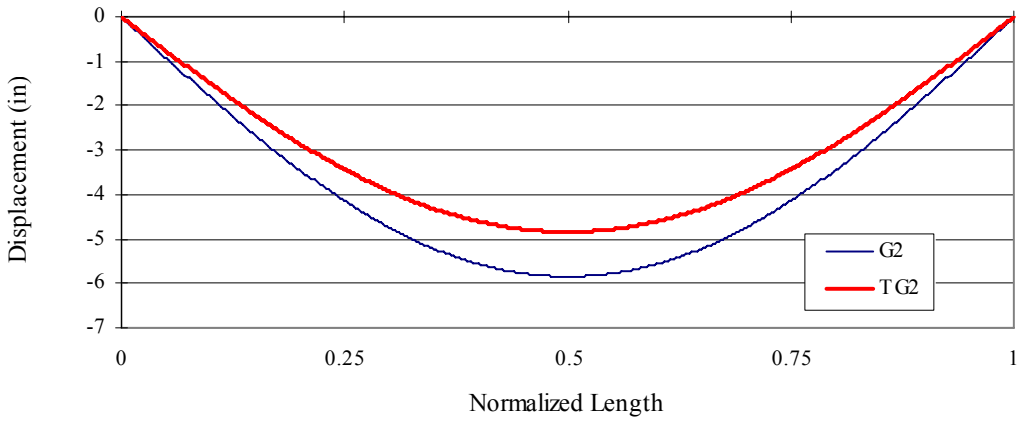

Figure 5.30 Vertical Displacement of Outer Girder (Two-Girder Case)

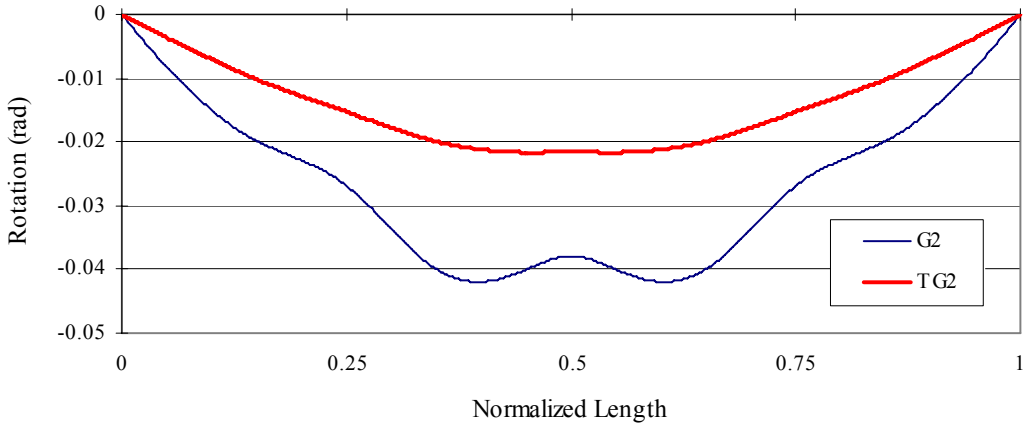

Figure 5.31 Cross Section Rotation of Outer Girder (Two-Girder Case)

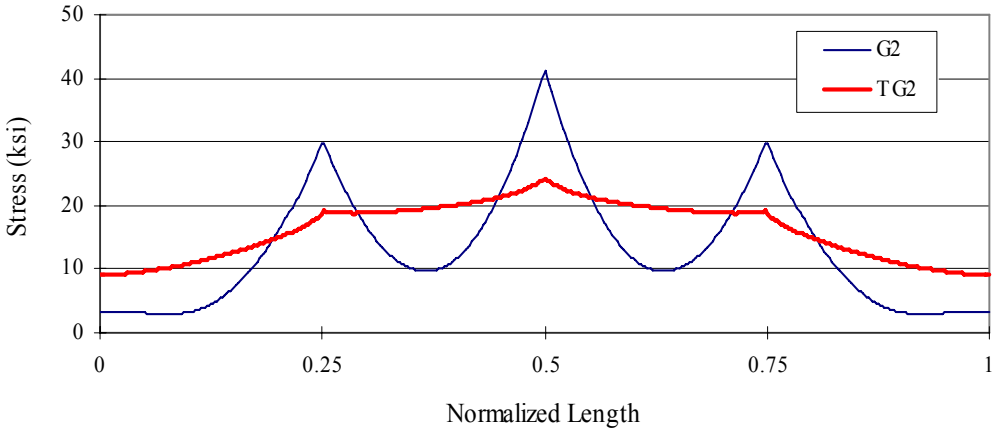

Figure 5.32 Von-Mises Stress of Outer Girder at P3 (Two-Girder Case)

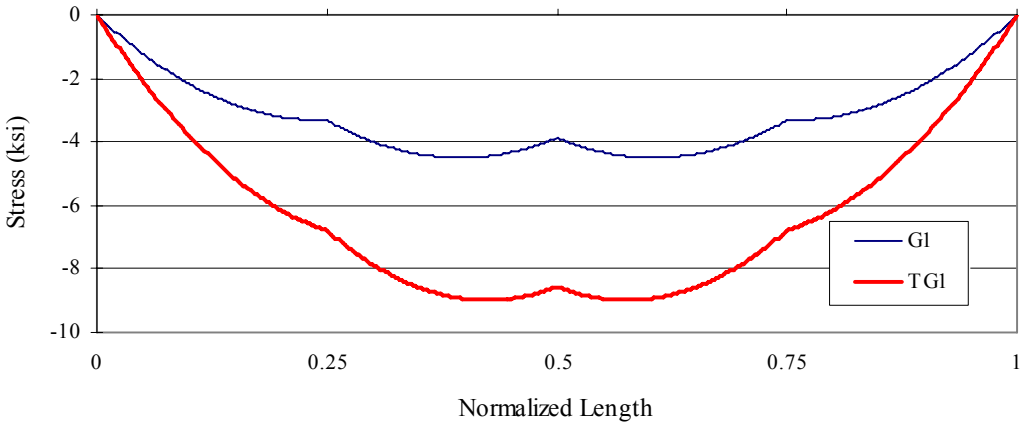

Figure 5.33 Primary Bending Normal Stress of Inner Girder at P3 (Three-Girder Case)

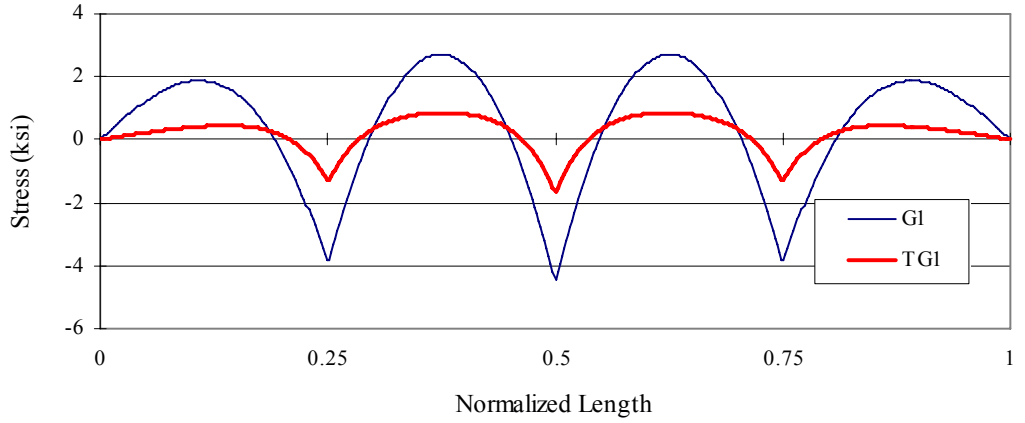

Figure 5.34 Warping Normal Stress of Inner Girder at P3 (Three-Girder Case)

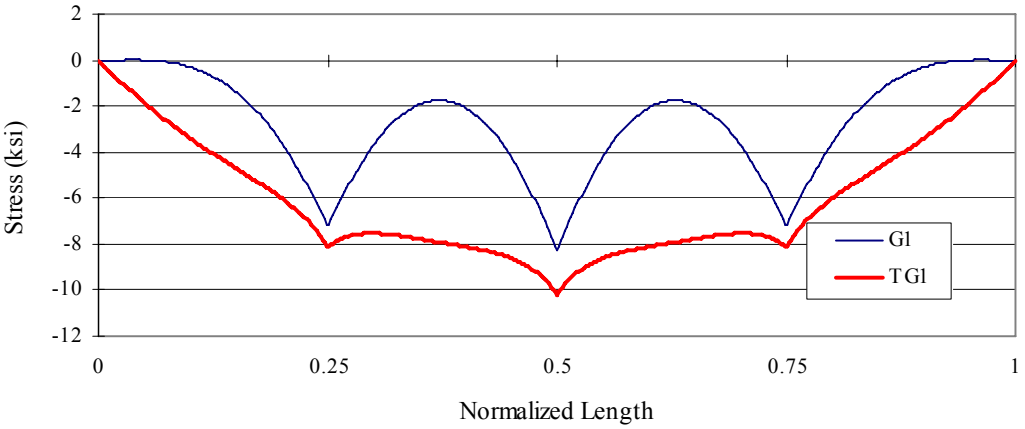

Figure 5.35 Total Normal Stress of Inner Girder at P3 (Three-Girder Case)

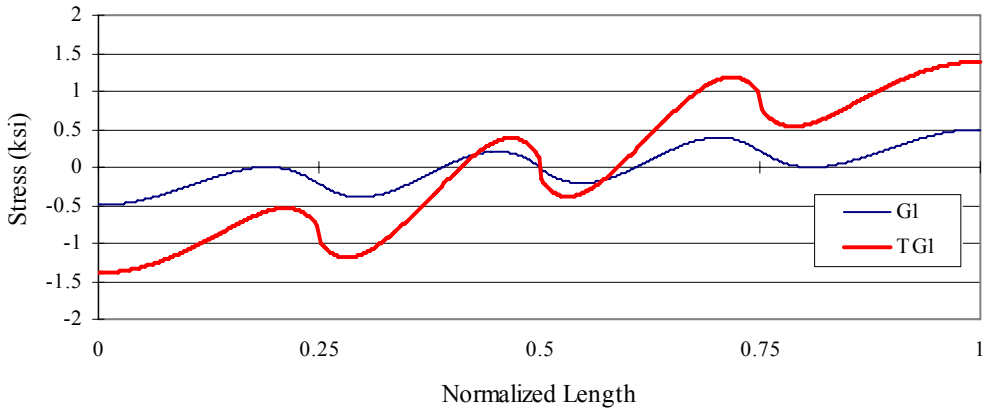

Figure 5.36 St.Venant Shear Stress of Inner Girder at P6r (Three-Girder Case)

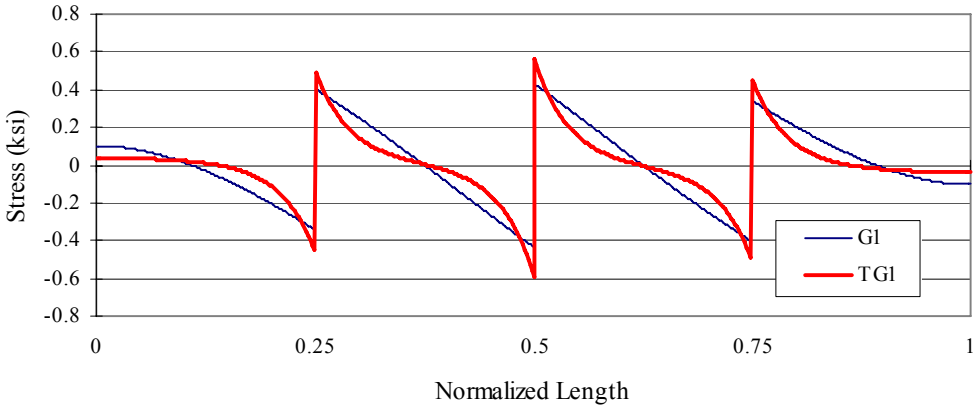

Figure 5.37 Warping Shear Stress of Inner Girder at P6r (Three-Girder Case)

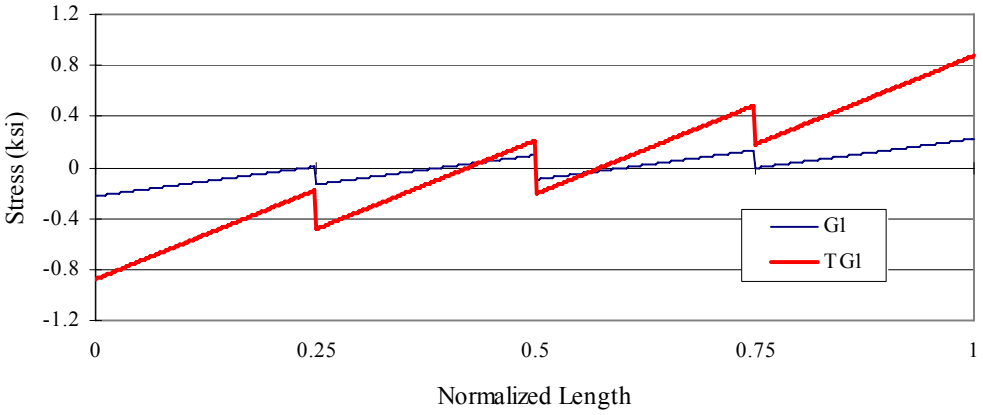

Figure 5.38 Vertical Shear Stress of Inner Girder at P6r (Three-Girder Case)

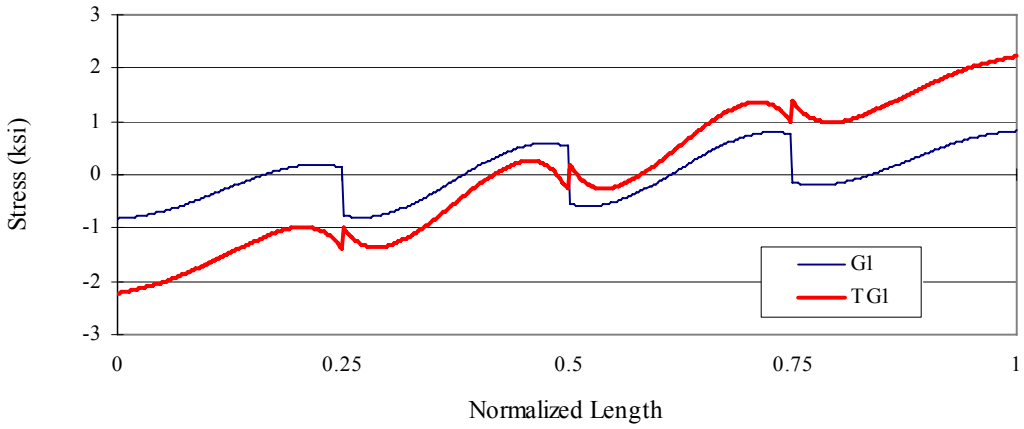

Figure 5.39 Total Shear Stress of Inner Girder at P6r (Three-Girder Case)

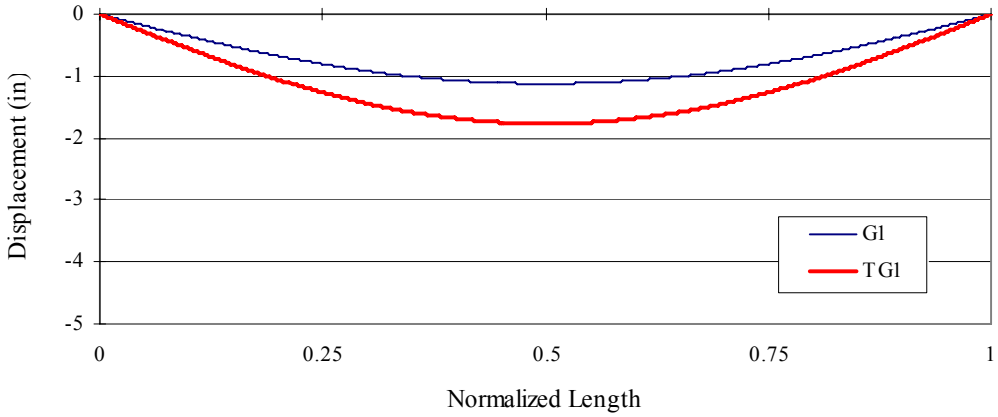

Figure 5.40 Vertical Displacement of Inner Girder (Three-Girder Case)

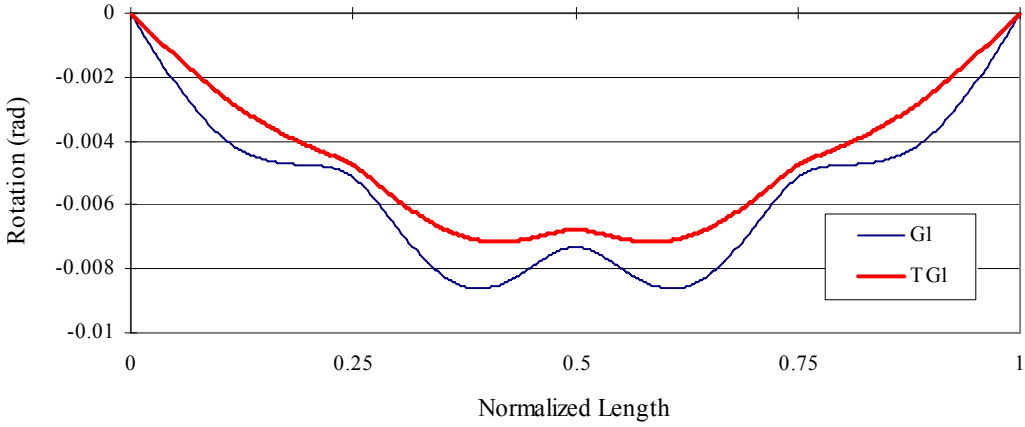

Figure 5.41 Cross Section Rotation of Inner Girder (Three-Girder Case)

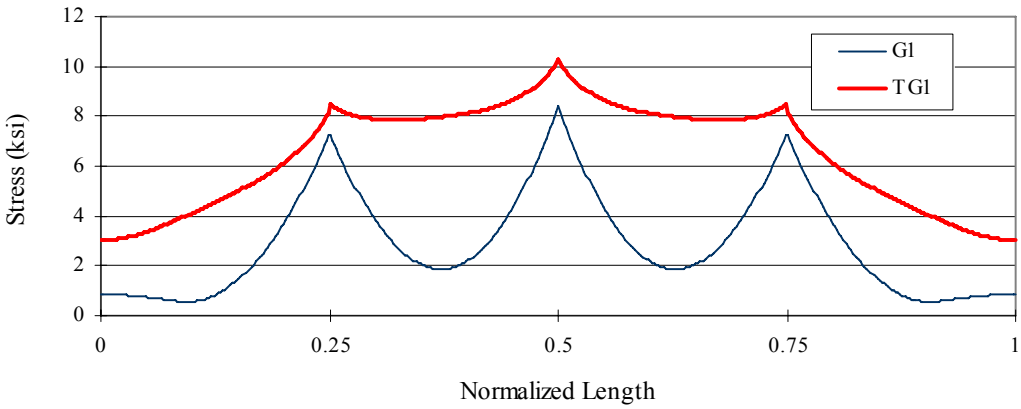

Figure 5.42 Von-Mises Stress of Inner Girder at P3 (Three-Girder Case)

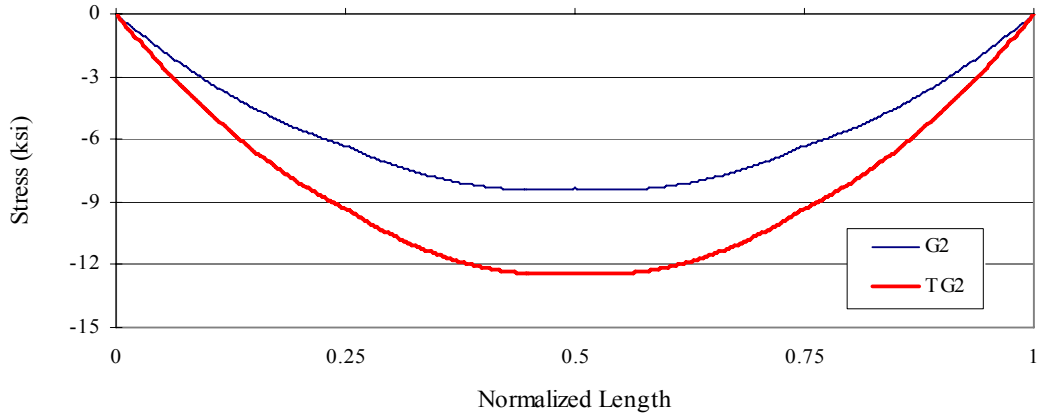

Figure 5.43 Primary Bending Normal Stress of Middle Girder at P3 (Three-Girder Case)

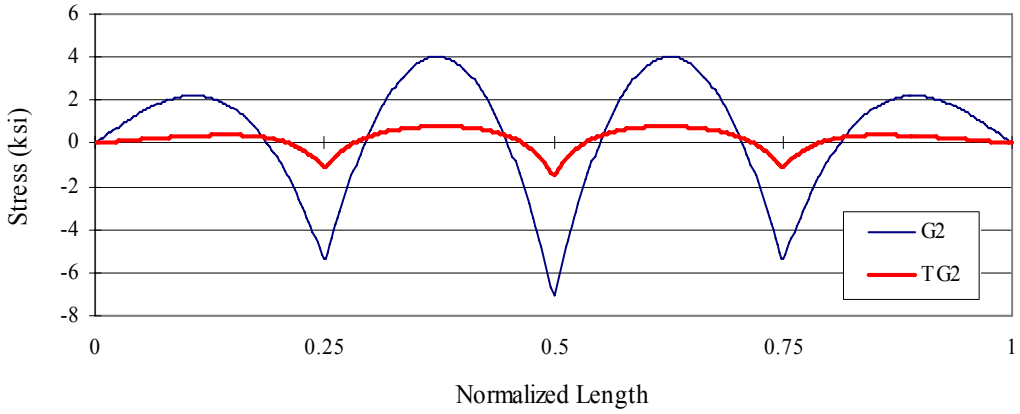

Figure 5.44 Warping Normal Stress of Middle Girder at P3 (Three-Girder Case)

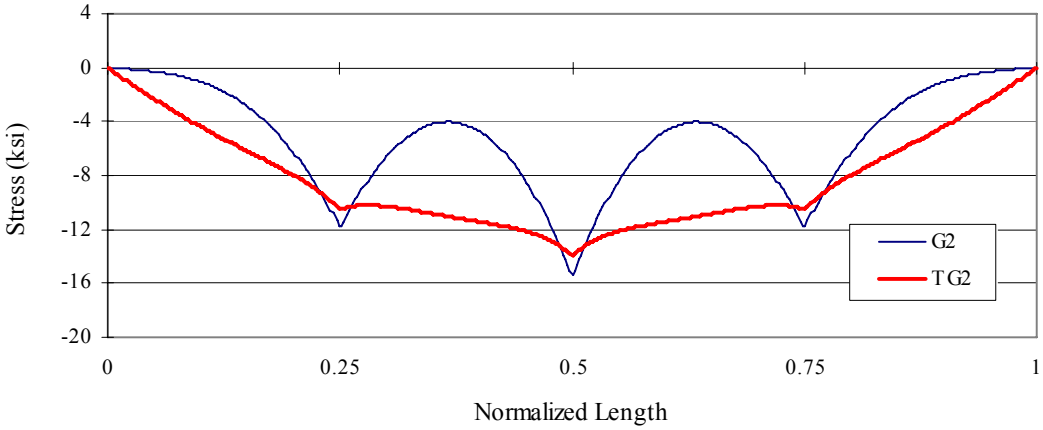

Figure 5.45 Total Normal Stress of Middle Girder at P3 (Three-Girder Case)

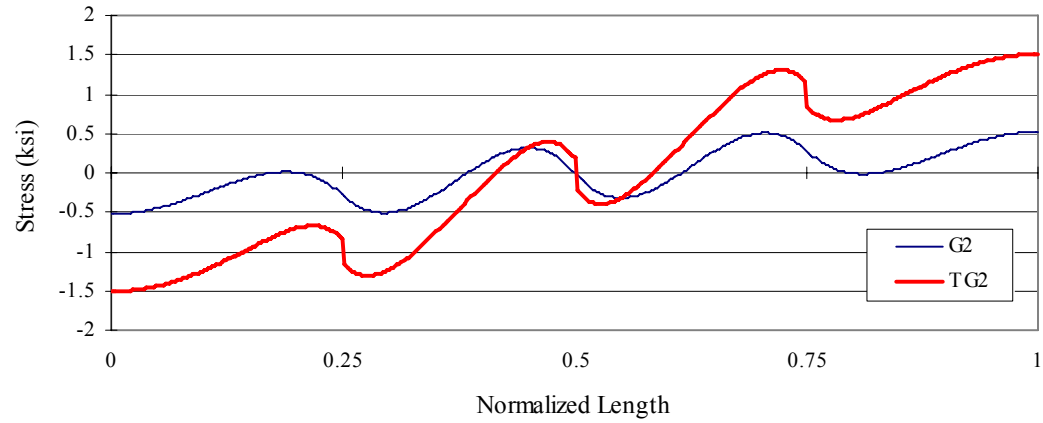

Figure 5.46 St.Venant Shear Stress of Middle Girder at P6r (Three-Girder Case)

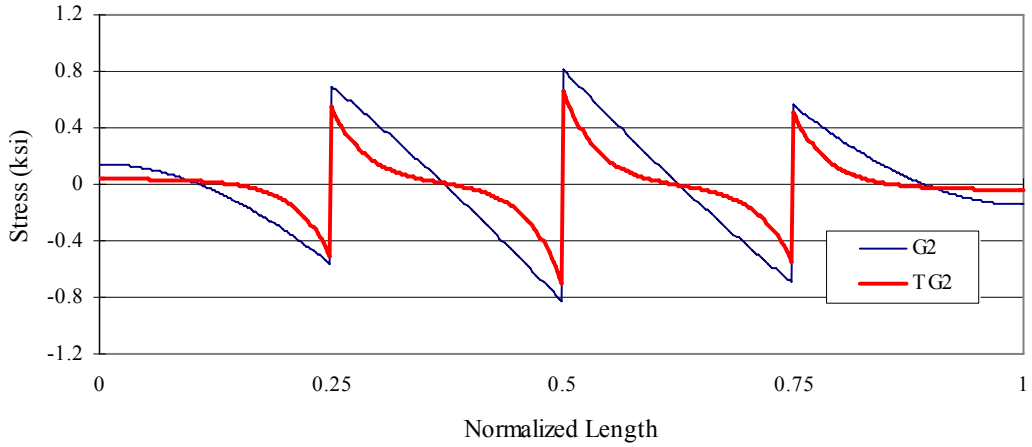

Figure 5.47 Warping Shear Stress of Middle Girder at P6r (Three-Girder Case)

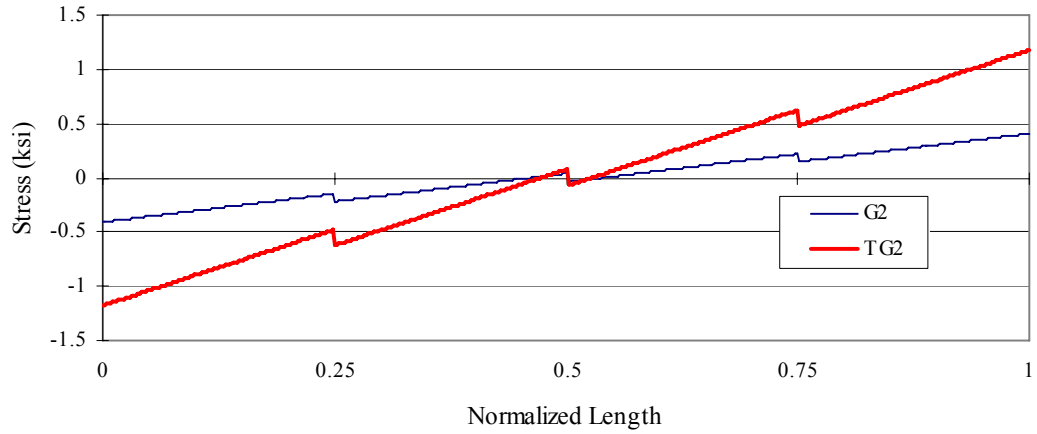

Figure 5.48 Vertical Shear Stress of Middle Girder at P6r (Three-Girder Case)

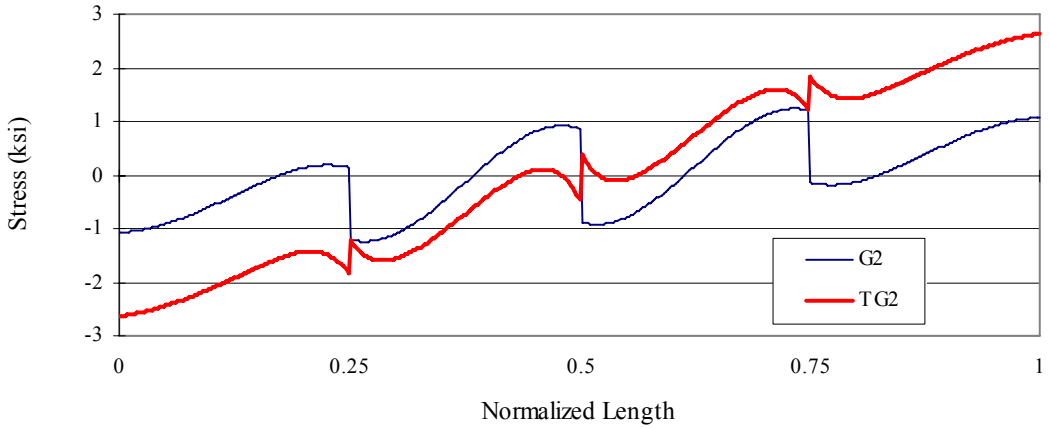

Figure 5.49 Total Shear Stress of Middle Girder at P6r (Three-Girder Case)

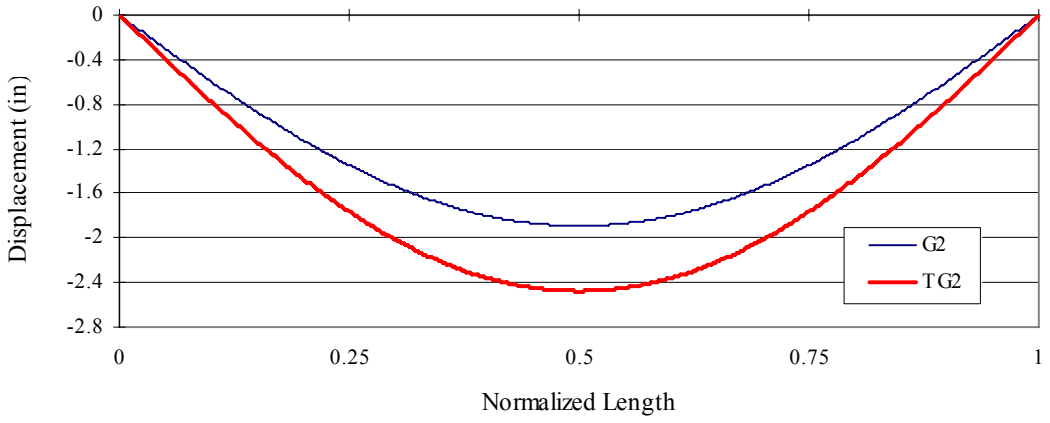

Figure 5.50 Vertical Displacement of Middle Girder (Three-Girder Case)

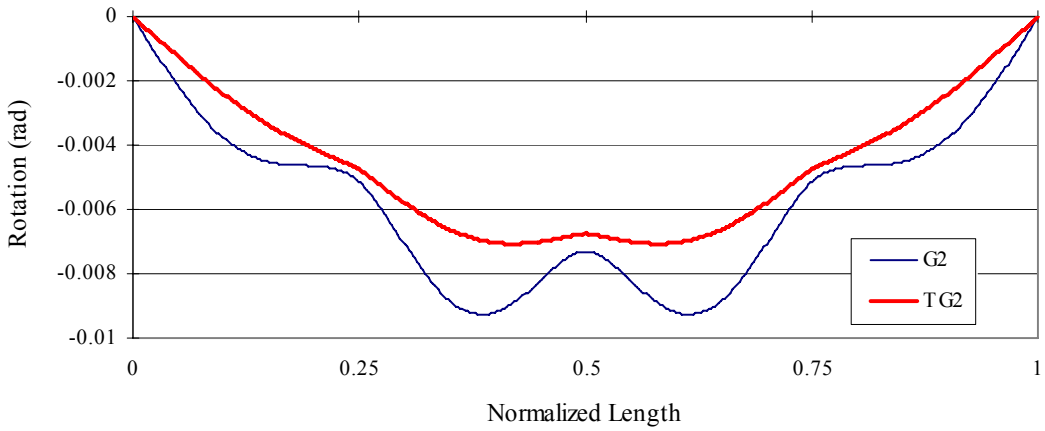

Figure 5.51 Cross Section Rotation of Middle Girder (Three-Girder Case)

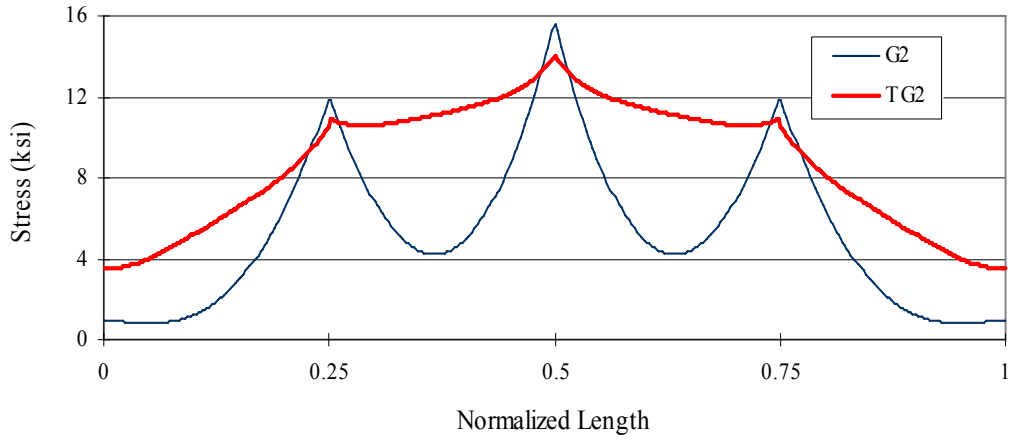

Figure 5.52 Von-Mises Stresses of Middle Girder at P3 (Three-Girder Case)

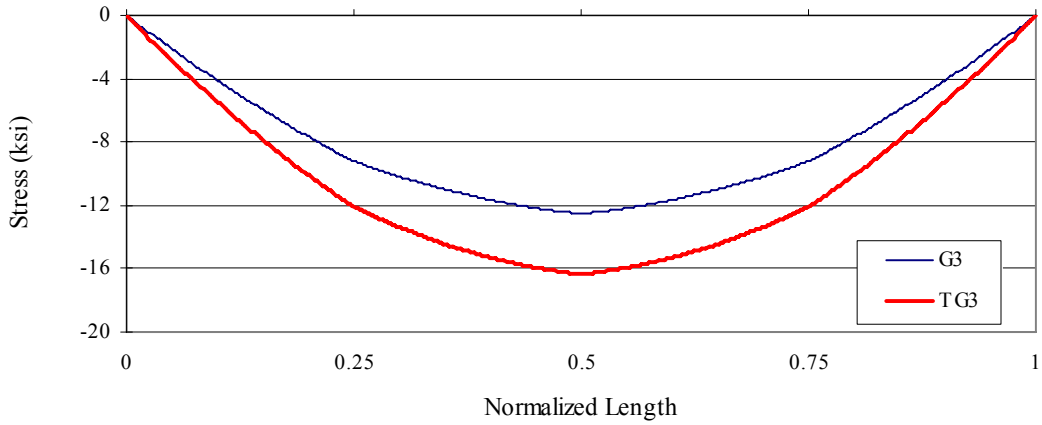

Figure 5.53 Primary Bending Normal Stress of Outer Girder at P3 (Three-Girder Case)

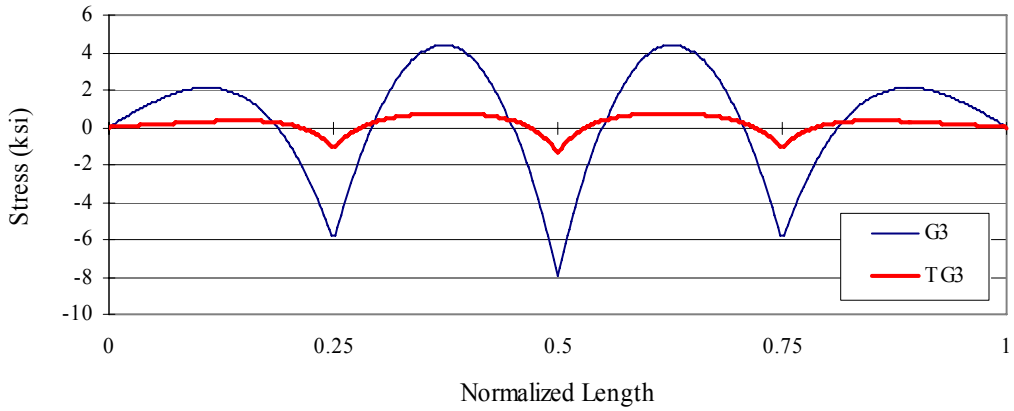

Figure 5.54 Warping Normal Stress of Outer Girder at P3 (Three-Girder Case)

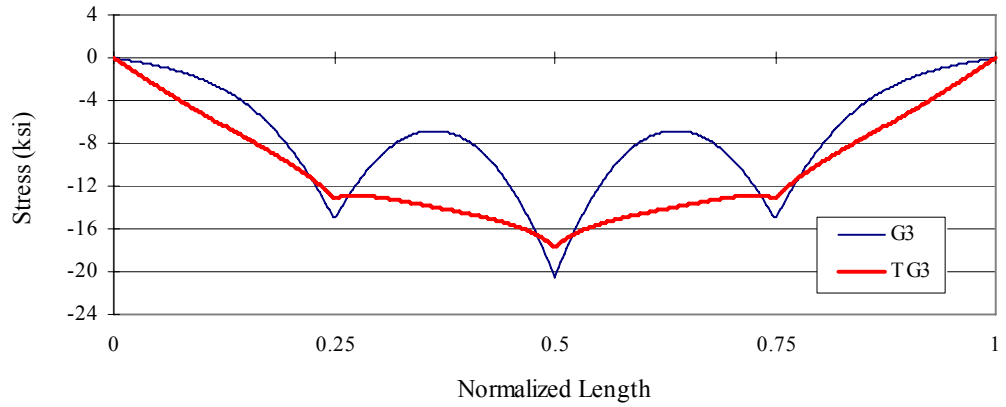

Figure 5.55 Total Normal Stress of Outer Girder at P3 (Three-Girder Case)

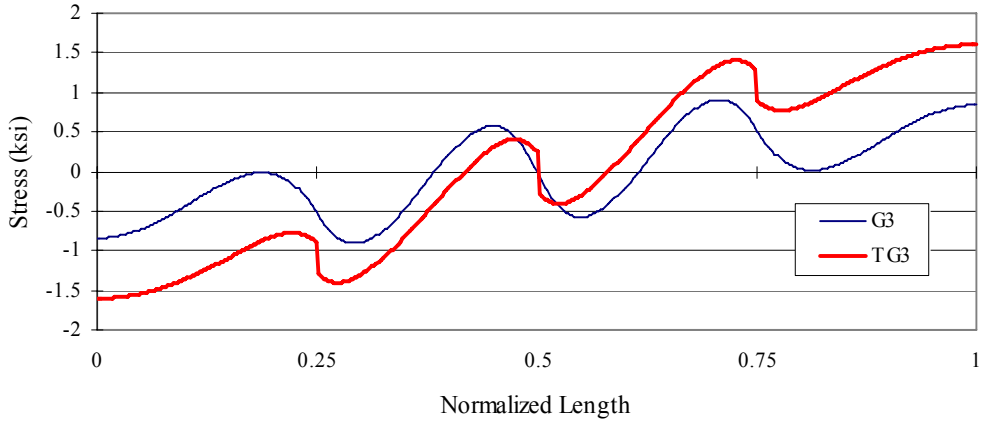

Figure 5.56 St.Venant Shear Stress of Outer Girder at P6r (Three-Girder Case)

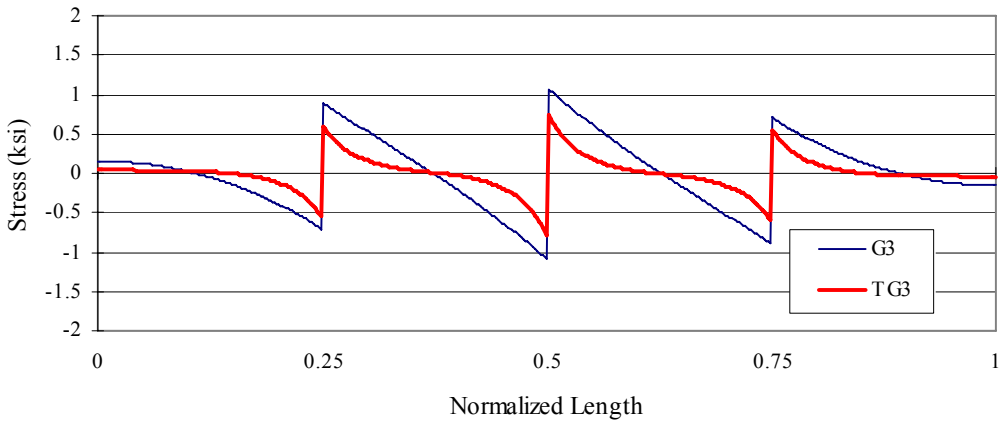

Figure 5.57 Warping Shear Stress of Outer Girder at P6r (Three-Girder Case)

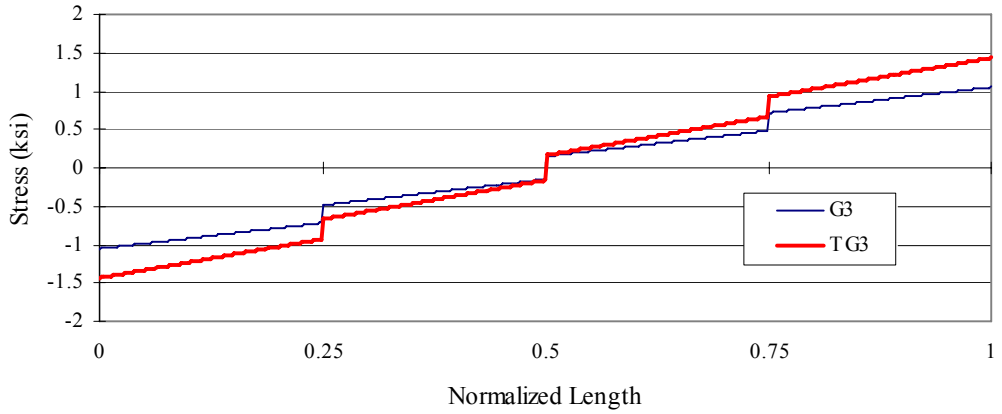

Figure 5.58 Vertical Shear Stress of Outer Girder at P6r (Three-Girder Case)

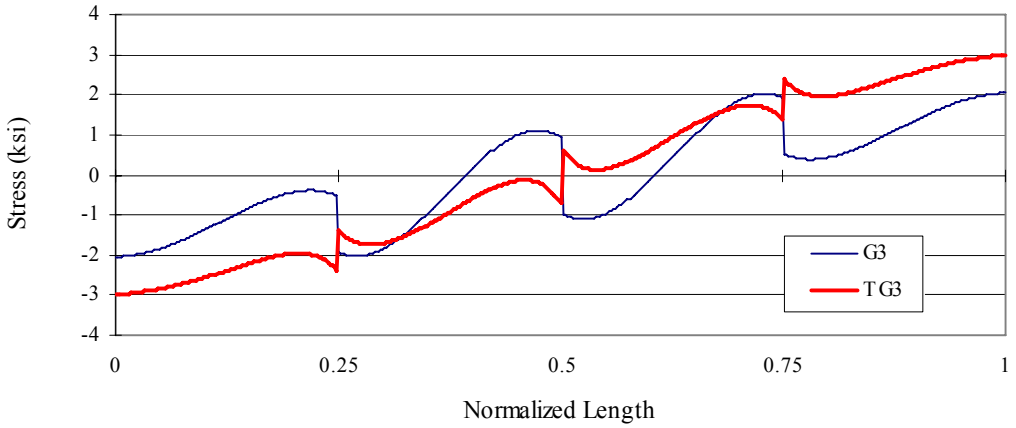

Figure 5.59 Total Shear Stress of Outer Girder at P6r (Three-Girder Case)

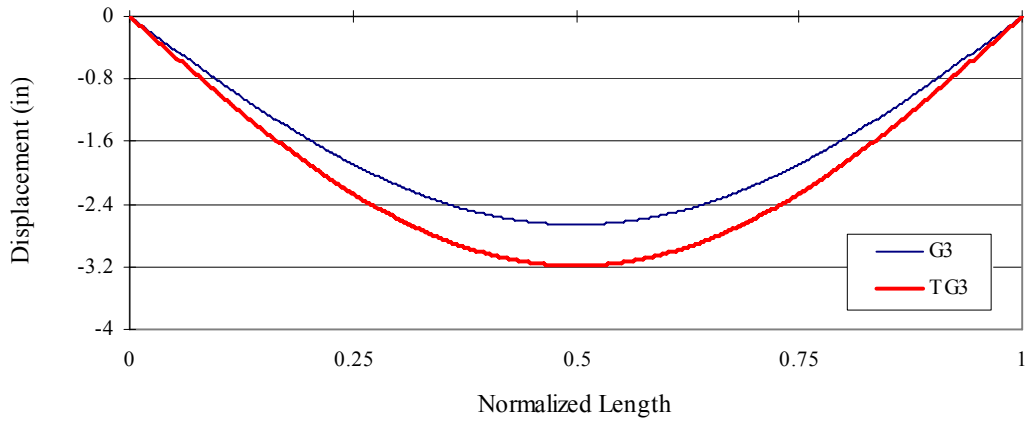

Figure 5.60 Vertical Displacement of Outer Girder (Three-Girder Case)

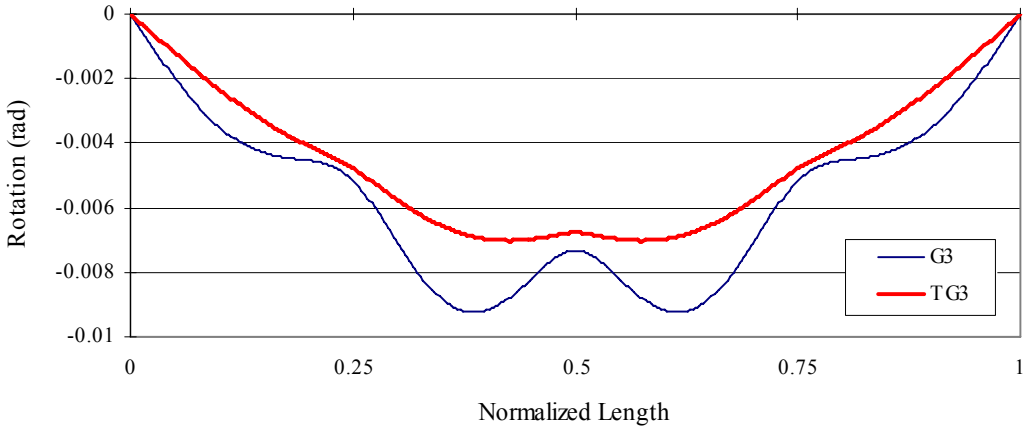

Figure 5.61 Cross Section Rotation of Outer Girder (Three-Girder Case)

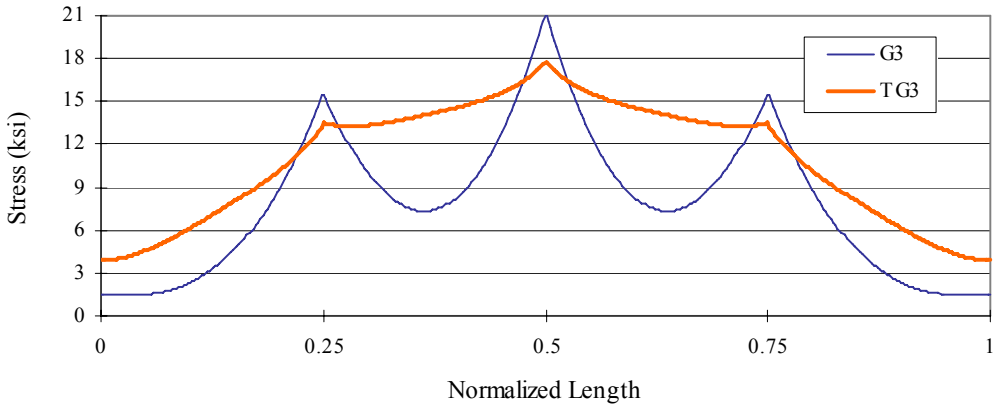

Figure 5.62 Von-Mises Stress of Outer Girder at P3 (Three-Girder Case)

Chapter 6 Finite Element Analysis

Finite element analyses of curved tubular-flange girder systems were conducted to compare with the theoretical analysis results presented in Chapter 5. The general purpose finite element program, ABAQUS v6.5 (ABAQUS 2003) was used for the analyses. The single girder, two-girder, and three-girder systems described in Chapter 5 were modeled and analyzed using the finite element method. The results of the finite element analyses show that cross section distortion develops in a curved tubular-flange girder under load. This distortion is not considered in the theoretical model for the curved tubular-flange girder. In addition, cross frame deflection, also not considered in the theoretical method, was observed. Therefore, multiple finite element models were built to consider these effects, including models with or without cross section distortion, and with or without cross frame deflection. For the models without cross section distortion, linear kinematic constraints were used to restrain the distortion of the cross section. For the models without cross frame deflection, the stiffness of the cross frames was made very large to eliminate the cross frame deflection. Comparisons between the results from these finite element models and those from the theoretical analysis are presented.

6.1 Finite Element Model

The main parameters considered in developing the finite element model include the element type, finite element mesh density, loading, boundary conditions and material properties.

6.1.1 Element Type

The linear, finite-membrane-strain, fully integrated, quadrilateral shell element S4 in ABAQUS v6.5 was used to model the curved tubular-flange girders. This general purpose shell element is valid for analyses of both thin and thick shells. The S4 shell element has four integration points across the element and five section points (integration points) through the thickness of the shell element. Truss element T3D2 was used to model the cross frames.

6.1.2 Mesh Density

For an accurate finite element analysis, a sufficiently refined finite element mesh is necessary. As the mesh density increases, the finite element analysis results will converge. For the finite element models used in this chapter, the web, the top and bottom walls of the tubular flanges have 200 elements along the span length and 12 elements across the plate width. The side walls of the tubular-flanges have 200 elements along the span length and 6 elements across the plate width. Thus, total 16800 elements were used for each curved tubular-flange girder (see **Figure 6.1**).

6.1.3 Boundary Conditions and Loading Conditions

The finite element models include simple support boundary conditions for the girders. The coordinate system and the corresponding degrees of freedom for the finite element models are presented in **Figure 6.2**. The x-axis is in the radial direction. The y-axis is in the circumferential tangential direction. The z-axis is in the vertical direction. The vertical displacements (u_3) are specified as zero at the centroid of the two end cross sections for each girder. The circumferential displacement (u_2) at the centroid of the left end cross section for each girder is restrained. All the nodes on the left and right end cross section of each girder are restrained to prevent displacement in the radial direction (u_1) and rotation about y-axis (u_5). Thus, the end cross sections are restrained against twist, and free to warp. The distributed vertical load is modeled as the pressure load applied to the top flange of each girder.

6.1.4 Linear Constraints

ABAQUS v6.5 defines a linear multiple-point constraint in the form of an equation. That is, $A_1 u_i^P + A_2 u_j^P + \cdots + A_n u_k^R = 0$, where, u_i^P is a nodal variable at node P, degree of freedom i, and the A_n are coefficients that define the relative motion of the nodes. For the curved tubular-flange girder finite element models, the cross section distortion was restrained by imposing the following constraints (see **Figure 6.3**): (1) every node on the cross section has the same rotation about the y-axis (u_5) as that of the cross section centroid, that is, for a node P on the cross section, the linear constraint equation is $u_5^P - u_5^C = 0$; (2) the nodal displacements in the x-axis direction are linearly distributed over the depth of the cross section, that is, for a node P on the cross section, the linear constraint equation is $u_1^P - u_1^C - A_p u_5^C = 0$. These linear constraint equations are written for every node on the cross section.

6.1.5 Material Properties

The steel of the tubular-flange girders was modeled as an elastic isotropic material with an elastic modulus of 29000 ksi, and Poisson's ratio of 0.3. The same material was used for the cross frames, except for the models in which cross frame deflection was restrained, where a large elastic modulus was used.

6.2 Finite Element Analysis Results

6.2.1 Single Curved Tubular-Flange Girder

The girder TG2 described in Chapter 5 was used for the finite element analyses of a single curved tubular-flange girder. Four types of finite element models were built and analyzed. One model, M1, includes kinematic constraints restraining the cross section distortion, making the model consistent with the assumptions of the theoretical analysis. The second model, M2, allows cross section distortion to develop. For the

third model, M3, the cross section distortion was unrestrained, but eleven transverse stiffeners were introduced, evenly spaced along the span. The fourth model, M4, includes linear constraints to restrain the distortion of the web, but does not include constraints on distortion of the tubular flanges. The stresses at the critical points and the deflections at the cross section centroid are shown in plots of the finite element analysis results in **Figure 6.4** through **Figure 6.8**. As discussed in Chapter 5, Point 2 (P2) has the maximum total normal stress and the maximum Von-Mises stress on the cross section in the simply supported single curved tubular-flange girder. The right side of Point 6 (P6r) has the maximum total shear stress on the cross section. Therefore, stresses at these points are shown in the plots.

Figure 6.4 through **Figure 6.8** show that the results from the theoretical analysis are good in agreement with the results from finite element model M1. However, for the Von-Mises stress shown in **Figure 6.8**, the M1 finite element result is smaller than the theoretical result, while, for the other stresses and the displacements, the M1 results are slightly larger than the theoretical results. The Von-Mises stresses in the 3D finite element model, however, also include the contributions from the normal stress in the radial direction, which tend to reduce the Von-Mises stress at P2. The normal stress in the radial direction is small and neglected in the theoretical analysis.

Comparing the theoretical results with the results from finite element model M2 shows that the distortion has a significant effect on the bending normal stress and the deflections. However, the distortion has little influence on the total shear stress (see **Figure 6.5**). As discussed in the previous chapter, most of the total shear stress for the single curved tubular-flange girder is St.Venant shear stress. The vertical shear stress is roughly 20% of the total shear stress and the warping shear stress is negligible. Thus, the cross section distortion has little effect on the St.Venant shear stress for the single curved tubular-flange girder, and the shear stress due to cross section distortion is small enough to be neglected. These findings suggest that the cross section distortion of the single curved tubular-flange girder is mainly from web distortion. To investigate this possibility, eleven evenly spaced transverse web stiffeners were added to model M2 to restrain the web distortion, resulting in model M3.

The results from finite element model M3 show that the total normal stress and the deflections of M3 are very close to the theoretical results. The M3 results show restraint of the web distortion by the stiffeners introduces warping normal and shear stresses which contribute to the total normal stress and the total shear stress. Finite element model M4, with only the web distortion restrained was analyzed. The M4 results show that the total normal stress at P2 is in good agreement with the theoretical results. The M4 displacements are close to the corresponding theoretical results, but M4 cross section rotations are larger than the theoretical results.

These results show that the influence of the cross section distortion on the single curved tubular-flange girder results is mainly from web distortion. This distortion has a significant effect on the normal stress and the displacements, but the effect of web distortion can be reduced by transverse stiffeners.

6.2.2 Two Curved Tubular-Flange Girder System

The girders TG1 and TG2 described in Chapter 5 were used for the finite element analyses of a two-girder system. Four types of finite element models were built and used in the finite element analyses. The first model, denoted M5, restrains the cross section distortion, but allows cross frame deflections to develop. The second model, denoted M6, restrains the cross section distortion, and includes rigid cross frames. For the third model, denoted M7, both the cross section distortion and the cross frame deflections are unrestrained. For the fourth model, denoted M8, web distortion is restrained, but the tubular flange distortion and the cross frame deflections are allowed to develop. The stresses at the girder critical points and the deflections at the cross section centroid are presented in **Figure 6.9** through **Figure 6.18**. Similar to the theoretical results discussed in Chapter 5. P2 has the maximum total normal stress and the maximum Von-Mises stress for the inner girder. P3 has the maximum total normal stress and the maximum Von-Mises stress for the outer girder. The right side of Point 6 (P6r) has the maximum total shear stress for both girders.

The results from the theoretical analyses are in a good agreement with the results from finite element models M5 and M6. The M5 results, which include cross frame deflections, and the M6 results, which do not include cross frame deflections, have little difference. Therefore, the effects of the cross section deflections in the two-girder system may be negligible. For the finite element models including cross section distortion, the results indicate that the cross frames induce the large stresses due to distortion at the cross sections which are braced by the cross frames (see **Figures 6.9**, **6.10**, **6.14** and **6.15**). The cross section distortion also induces greater cross section rotation for both girders. Cross section distortion of the inner girder reduces the total normal stress at the braced cross sections to nearly zero for the model which both web distortion and tube distortion are allowed, M7, (see **Figure 6.9**). Cross section distortion of the outer girder of model M7 increases the total normal stress by about 13% at the braced cross sections (see **Figure 6.14**). Away from the braced cross sections, the total normal stress in both girders of model M7 is close to the theoretical result. The cross section distortion induces a jump in the shear stress at the braced cross sections. As a result, the critical cross section for the total shear stress may change from the end section to the first braced cross section. As shown in the figures, the stresses and displacements from model M8 are close to the results from model M7, which shows that the tubular-flange distortion influences the displacements of model M8. Therefore, the web distortion in the two-girder system may have only a small contribution to the total distortion and a large contribution comes from the tubular-flange distortion.

6.2.3 Three Curved Tubular-Flange Girder System

The girders TG1, TG2 and TG3 described in Chapter 5 were used for the finite element analyses of a three-girder system. Five types of finite element models were built and analyzed to compare with the theoretical results. Four of these finite element models are similar to those used for the two-girder system. The fifth model, denoted

M9, includes nine cross frames evenly spaced to investigate the influence of the number of cross frames on distortion.

It is found that for each of the three girders, the results from the theoretical analyses are in a good agreement with the results from finite element model M6 (without cross section distortion and cross frame deflection). However, the results from finite element model M5 (without cross section distortion, but with cross frame deflection) differ from the theoretical results, especially for the total normal stresses for the inner girder TG1, and the total shear stress and the cross section rotation for the outer girder TG3. A comparison of the model M7 results (with cross section distortion and cross frame deflection) and the model M8 results (with tube distortion and cross frame deflection, but without web distortion) shows that restraining the web distortion reduces some of the cross section rotation and some of the stresses induced by cross section distortion. However, the cross section rotation in model M8 is still much larger than the theoretical results, indicating that significant distortion develops in the tubular flanges. The stresses and cross section rotation for model M9, which includes cross section distortion and cross frame deflection, but has a greater number of cross frames (9) than the other models (5), are smaller than those for models M7 and M8. The model M9 results are closer to the theoretical results than the model M7 and M8 results, indicating that using more cross frames can reduce the effects of cross section distortion.

6.2.4 Summary

The findings of the finite element results can be summarized as follows. When the finite element model includes constraints which are similar to the assumptions of the theoretical method, that is, cross section distortion and cross frame deflection are restrained, the theoretical results are in a good agreement with the finite element results. For a single tubular-flange girder, the effects of the cross section distortion are mainly a result of web distortion. If the web distortion can be restrained, for example, by using transverse stiffeners, the effects of cross section distortion for a single tubular-flange girder can be significantly reduced. For a multiple-girder system, stresses due to cross section distortion develop near the cross sections braced by cross frames which influence the stresses over the unbraced lengths between the cross frames. The cross section distortion results in larger cross section rotations near the middle of the unbraced lengths. Restraining the web distortion in a multiple-girder system produces a modest reduction in stresses and cross section rotation. The tubular flange distortion can have a significant effect on the stresses and cross section rotation. The effect of the cross frame deflections is small for the two-girder system, and somewhat larger for the three-girder system, especially for the inner girder normal stress and the outer girder rotation.

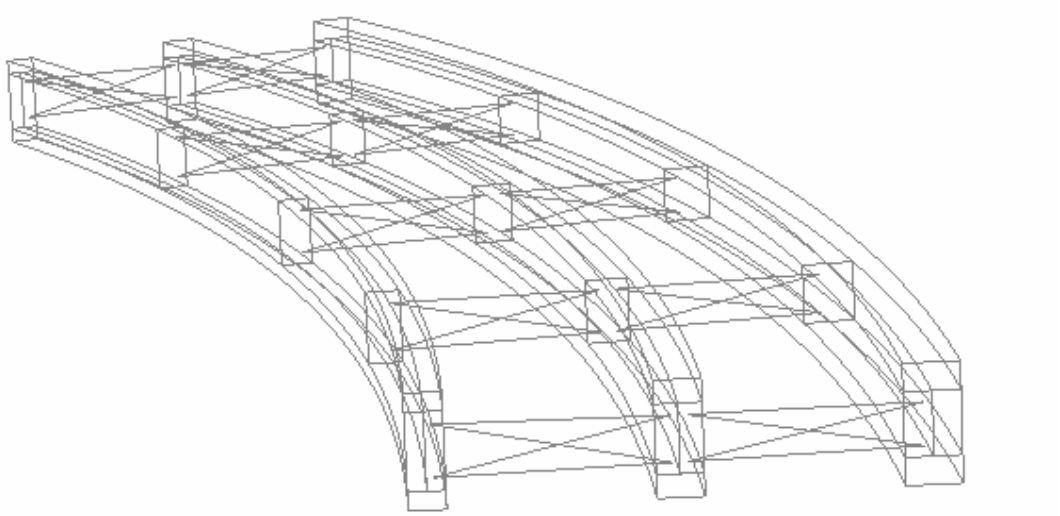

(a) Overview of Three-Girder System

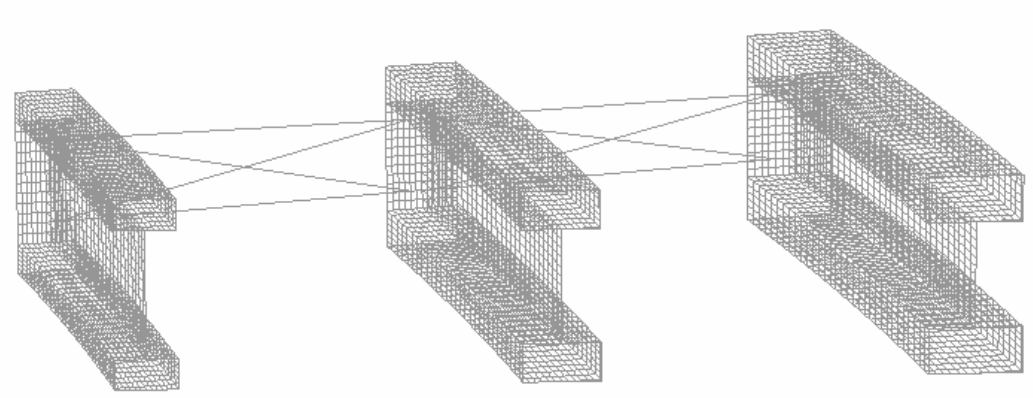

(b) Finite Element Mesh of Three Girder System

Figure 6.1 Finite Element Model of Three-Girder System

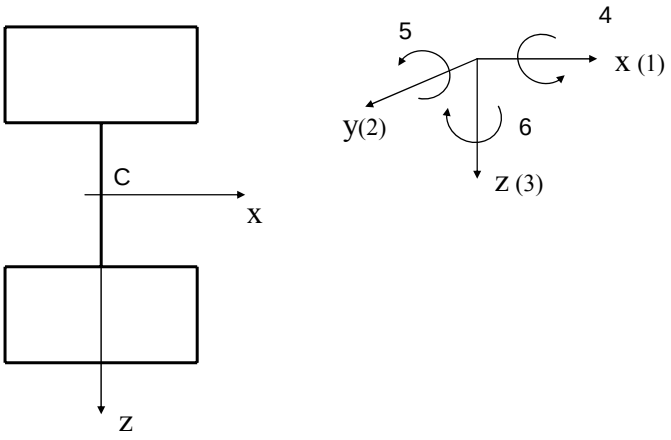

Left End Section:

Centroid (C):

$u_1^C = 0, \quad u_2^C = 0, \quad u_3^C = 0$

Other Nodes:

$u_1 = 0, \quad u_5 = 0$

Right End Section:

Centroid (C):

$u_1^C = 0, \quad u_3^C = 0$

Other Nodes:

$u_1 = 0, \quad u_5 = 0$

Figure 6.2 Boundary Condition

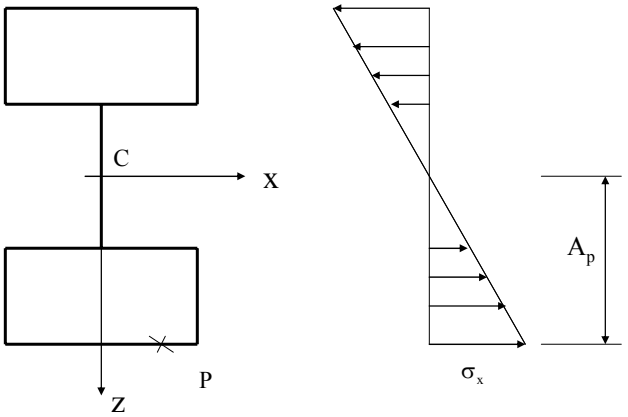

(1) $u_5^P - u_5^C = 0$

(2) $u_1^P - u_1^C - A_p u_5^C = 0$

Figure 6.3 Linear Constraints

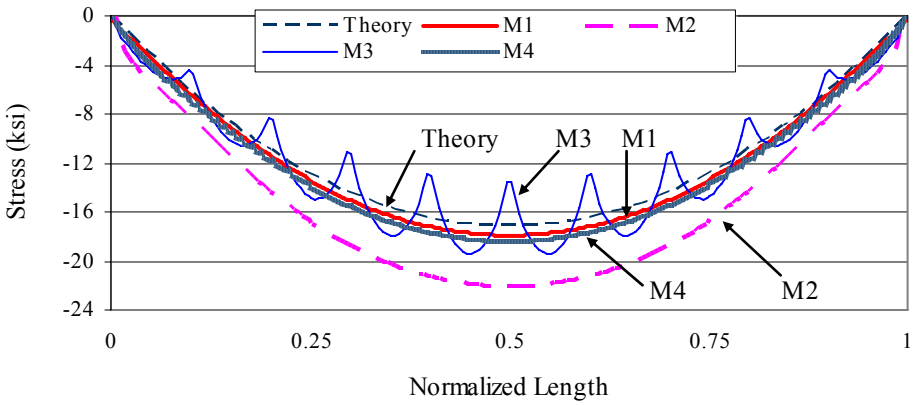

Figure 6.4 Total Normal Stress at P2 (Single Girder)

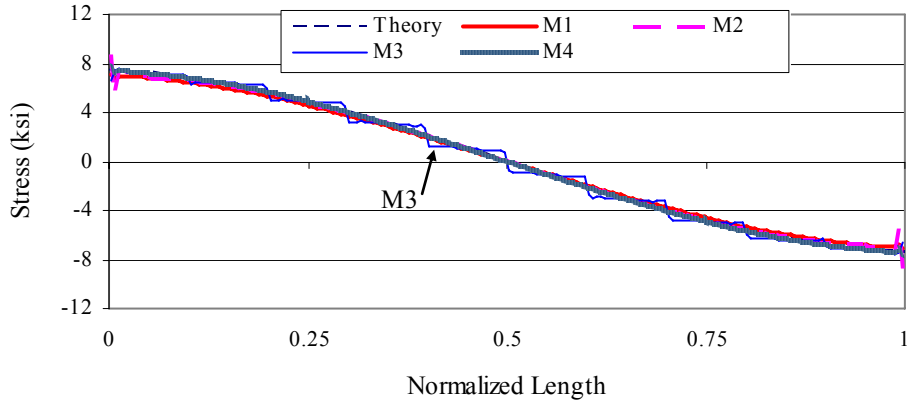

Figure 6.5 Total Shear Stress at P6r (Single Girder)

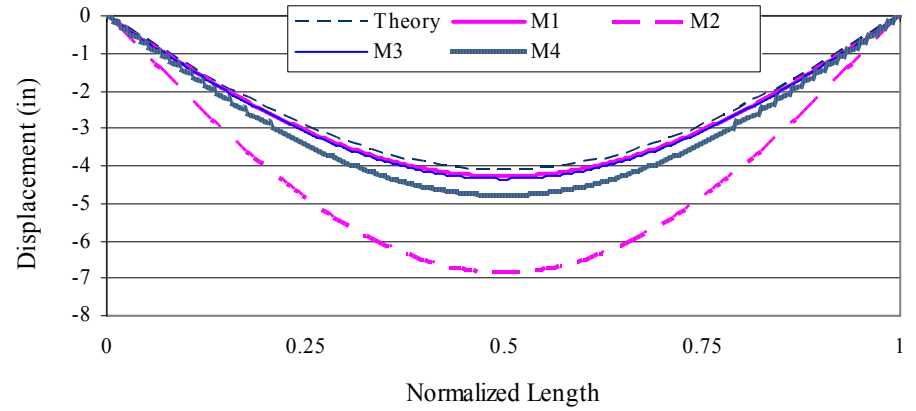

Figure 6.6 Vertical Displacement (Single Girder)

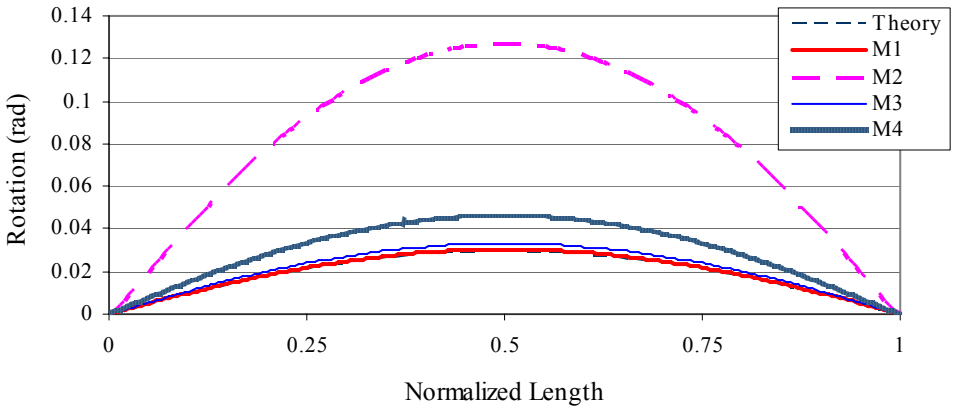

Figure 6.7 Cross Section Rotation (Single Girder)

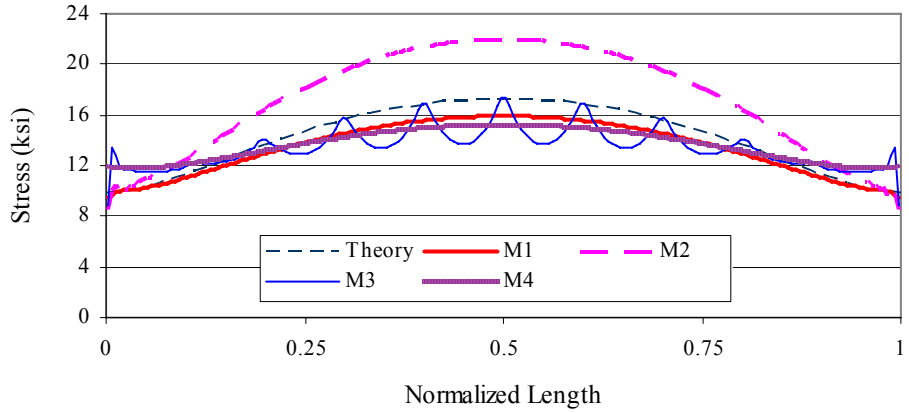

Figure 6.8 Von-Mises Stress at P2 (Single Girder)

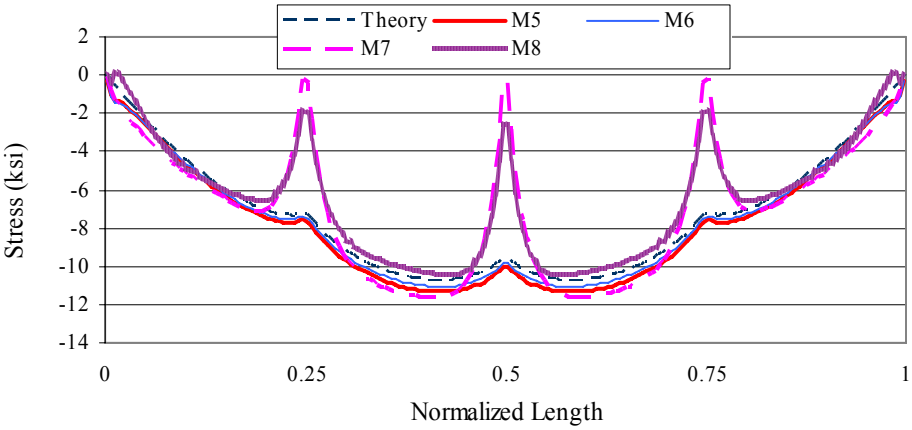

Figure 6.9 Total Normal Stress of Inner Girder at P2 (Two-Girder Case)

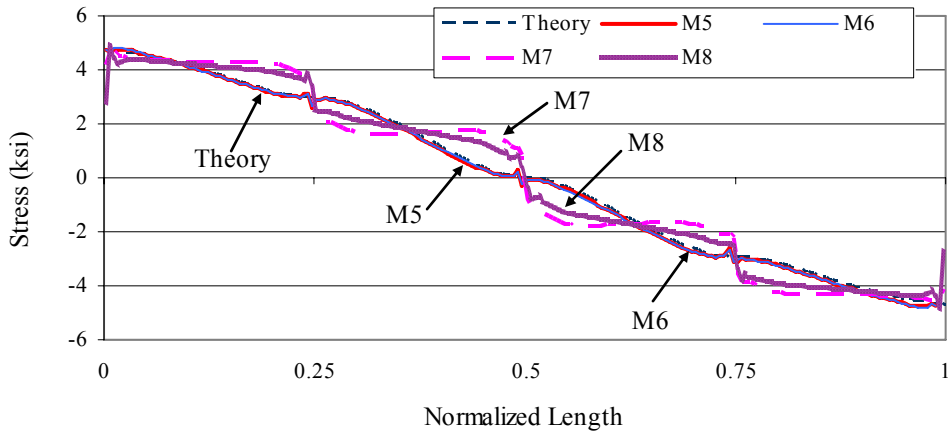

Figure 6.10 Total Shear Stress of Inner Girder at P6r (Two-Girder Case)

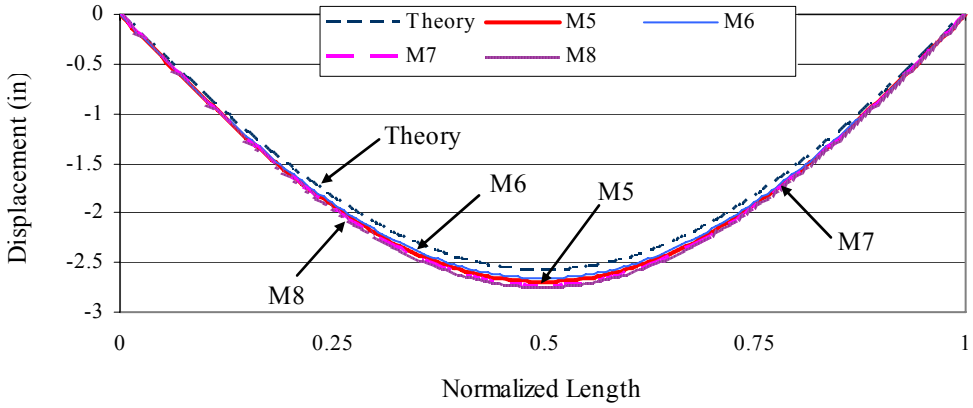

Figure 6.11 Vertical Displacement of Inner Girder (Two-Girder Case)

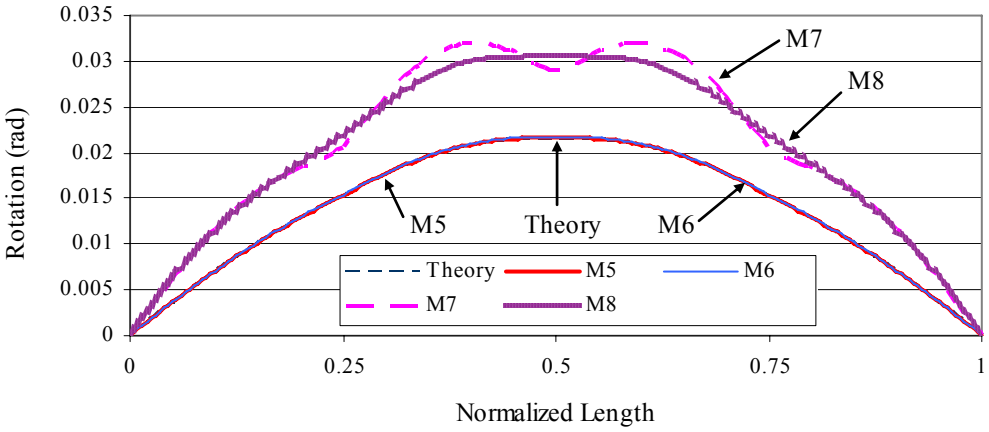

Figure 6.12 Cross Section Rotation of Inner Girder (Two-Girder Case)

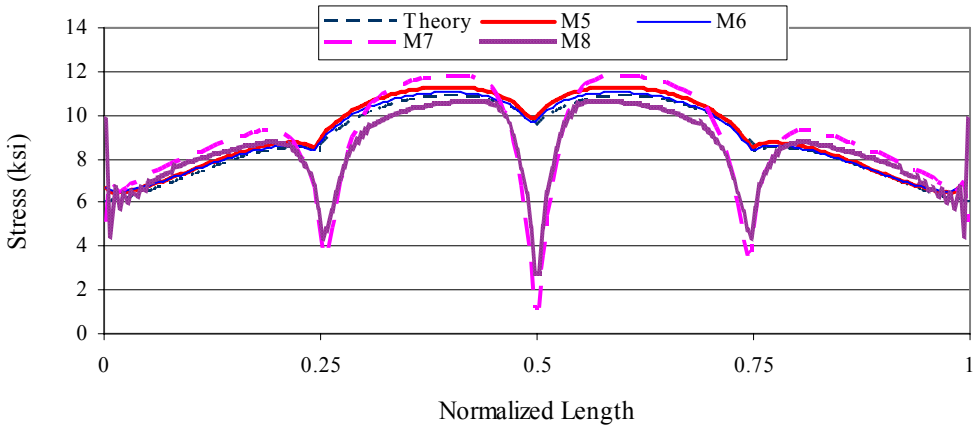

Figure 6.13 Von-Mises Stress of Inner Girder at P2 (Two-Girder Case)

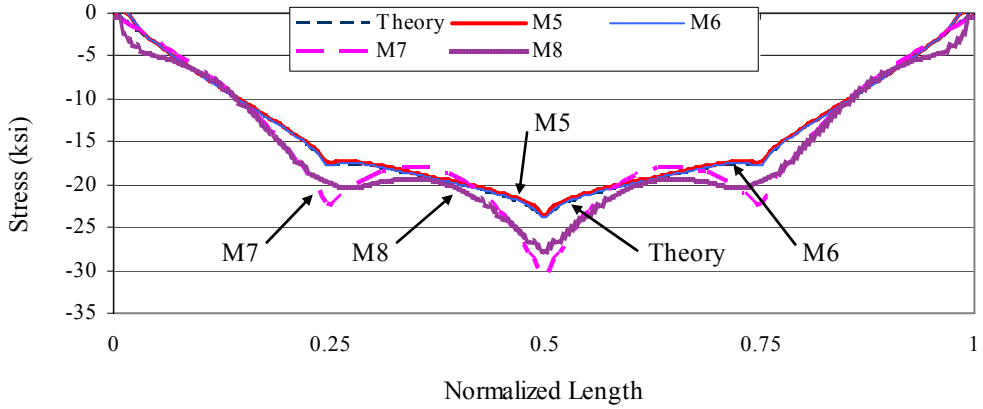

Figure 6.14 Total Normal Stress of Outer Girder at P3 (Two-Girder Case)

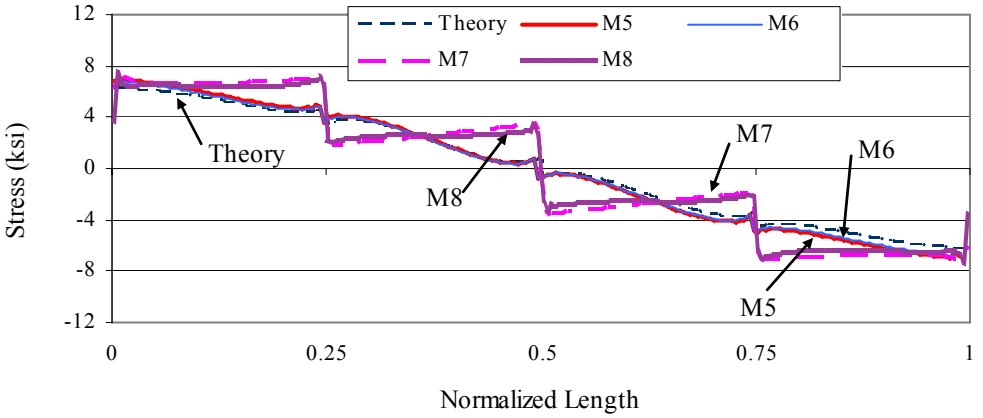

Figure 6.15 Total Shear Stress of Outer Girder at P6r (Two-Girder Case)

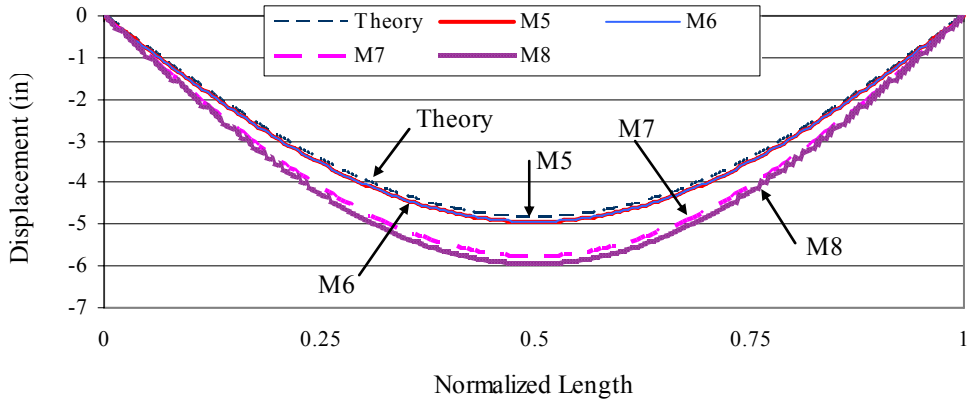

Figure 6.16 Vertical Displacement of Outer Girder (Two-Girder Case)

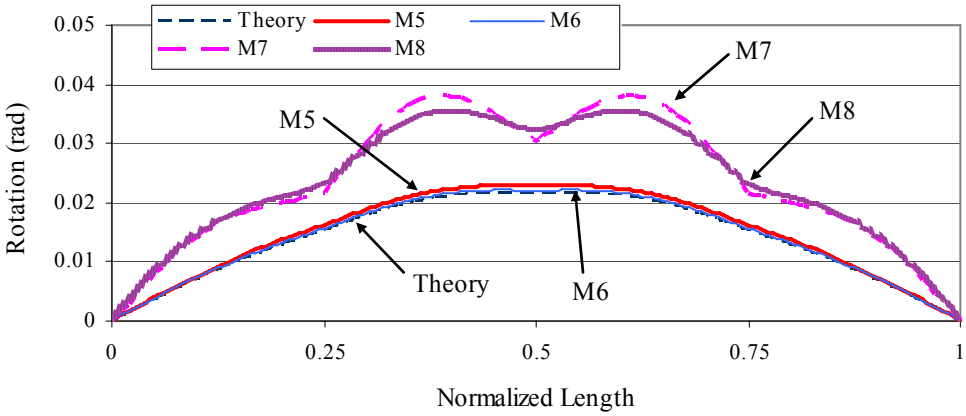

Figure 6.17 Cross Section Rotation of Outer Girder (Two-Girder Case)

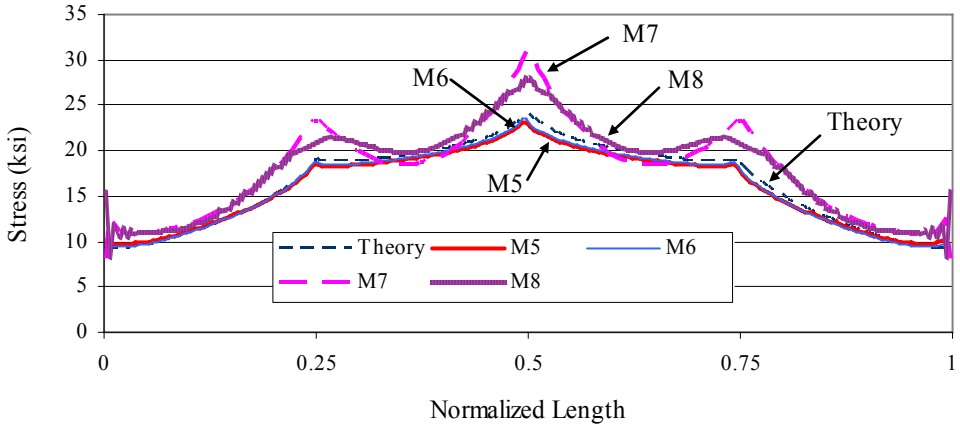

Figure 6.18 Von-Mises Stress of Outer Girder at P3 (Two-Girder Case)

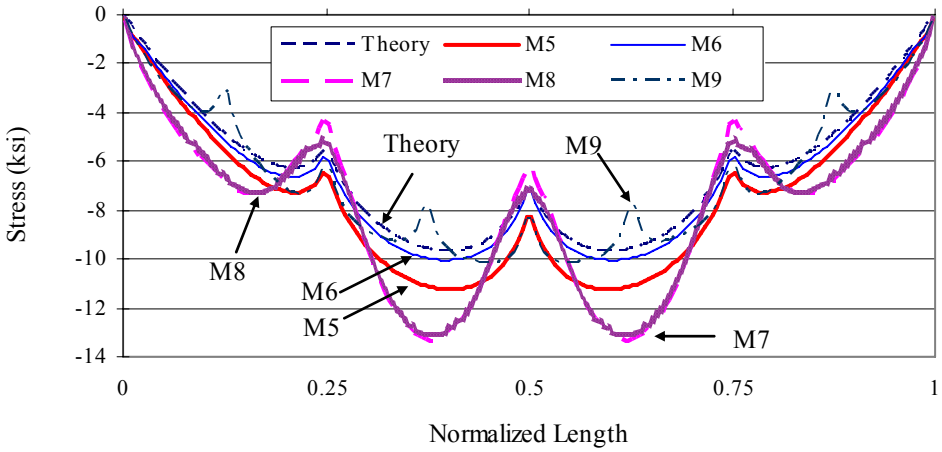

Figure 6.19 Total Normal Stress of Inner Girder at P2 (Three-Girder Case)

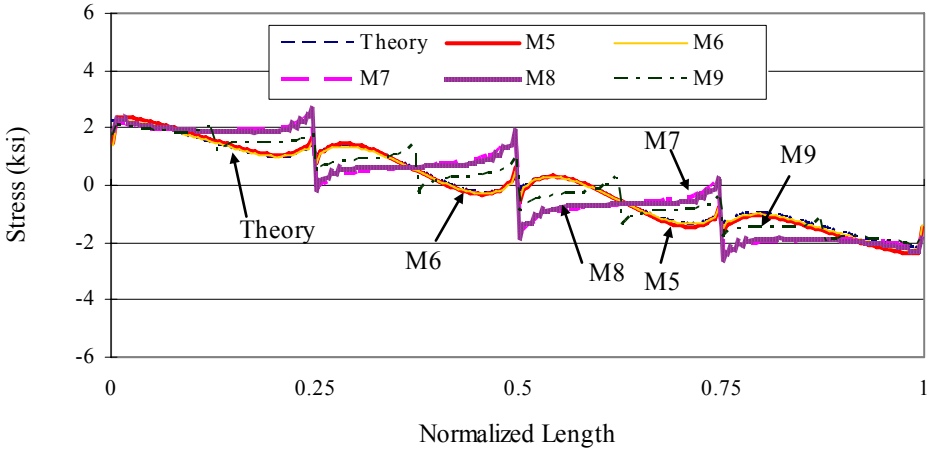

Figure 6.20 Total Shear Stress of Inner Girder at P6r (Three-Girder Case)

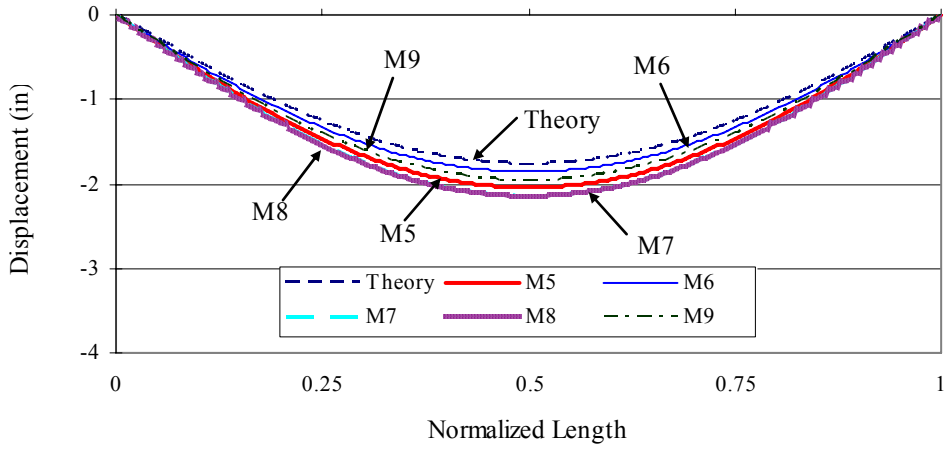

Figure 6.21 Vertical Displacement of Inner Girder (Three-Girder Case)

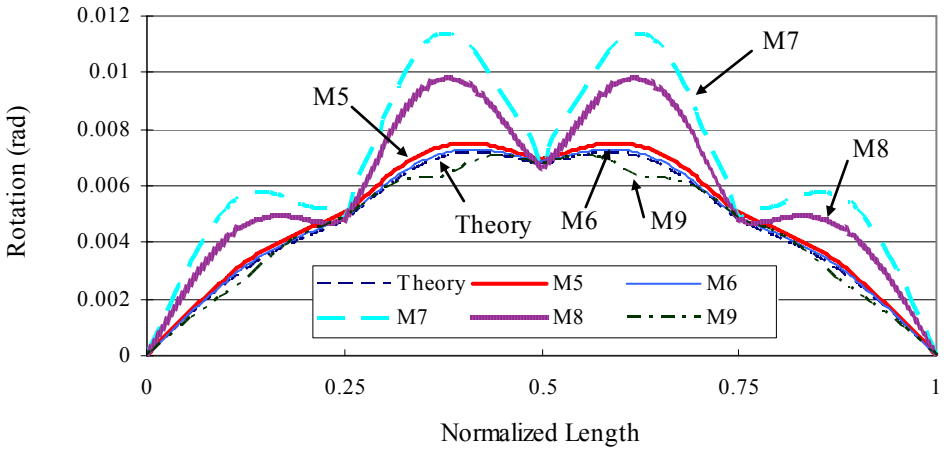

Figure 6.22 Cross Section Rotation of Inner Girder (Three-Girder Case)

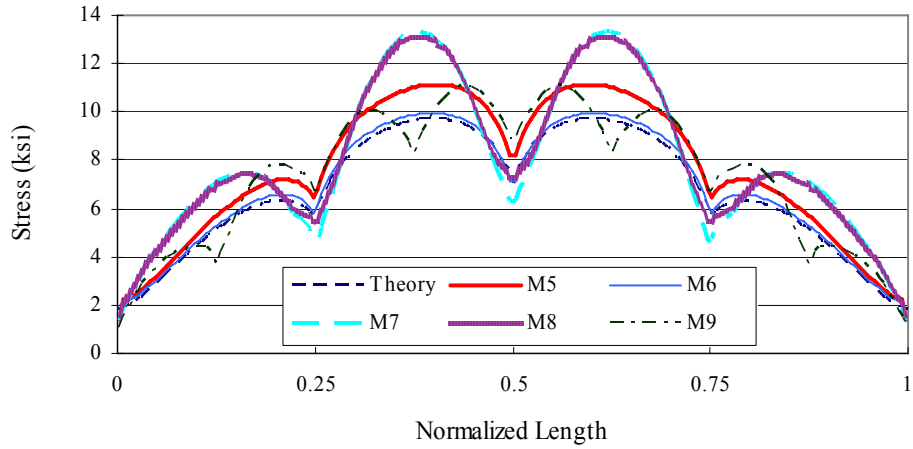

Figure 6.23 Von-Mises Stress of Inner Girder at P2 (Three-Girder Case)

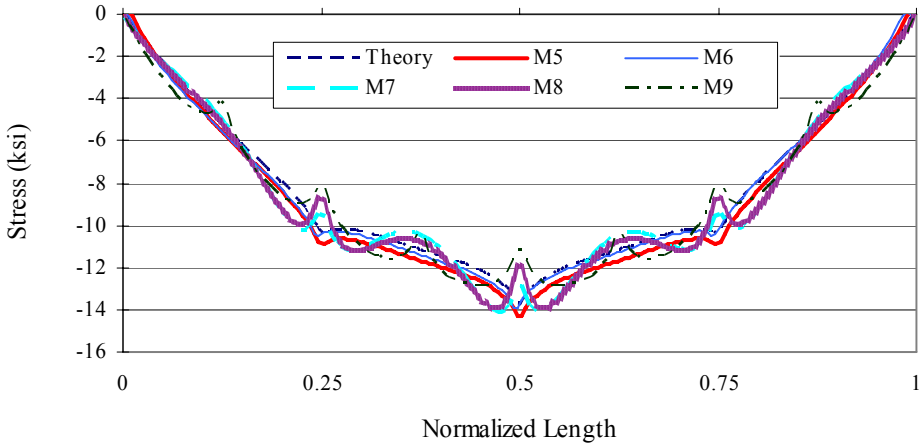

Figure 6.24 Total Normal Stress of Middle Girder at P3 (Three-Girder Case)

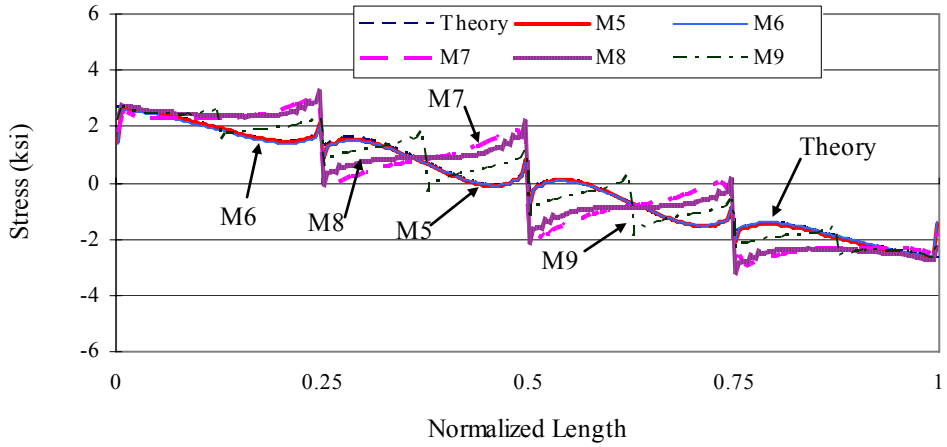

Figure 6.25 Total Shear Stress of Middle Girder at P6r (Three-Girder Case)

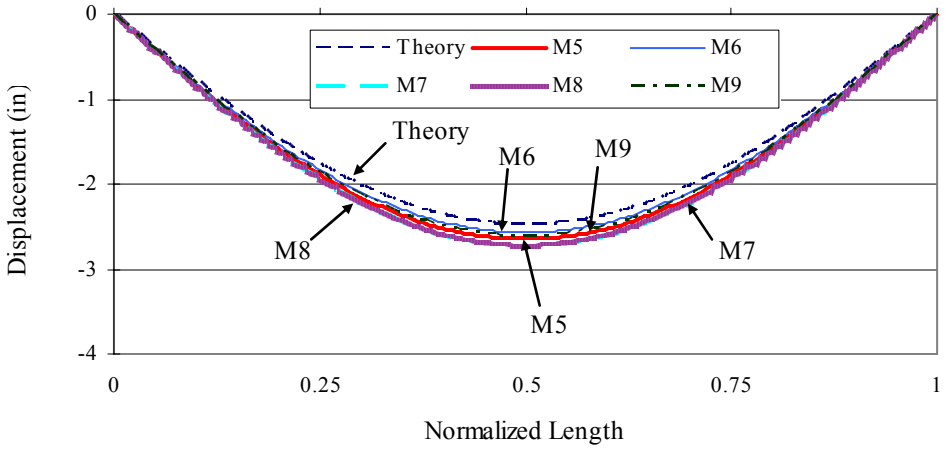

Figure 6.26 Vertical Displacement of Middle Girder (Three-Girder Case)

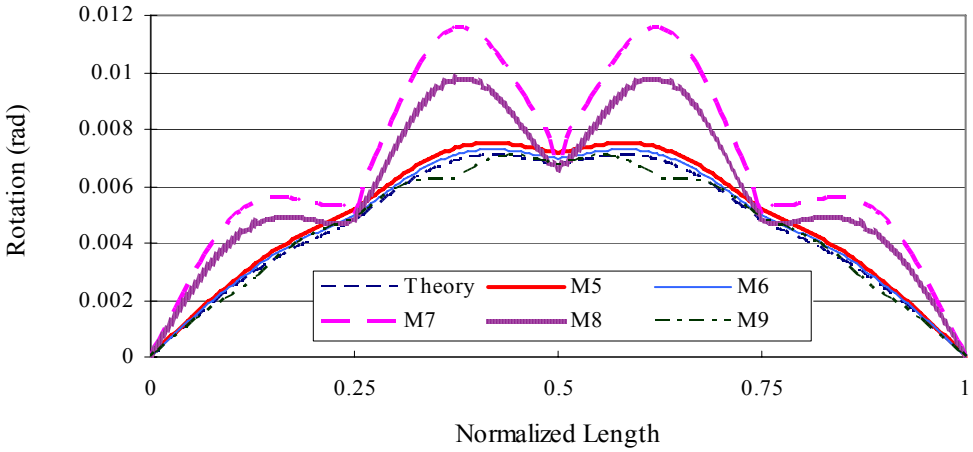

Figure 6.27 Cross Section Rotation of Middle Girder (Three-Girder Case)

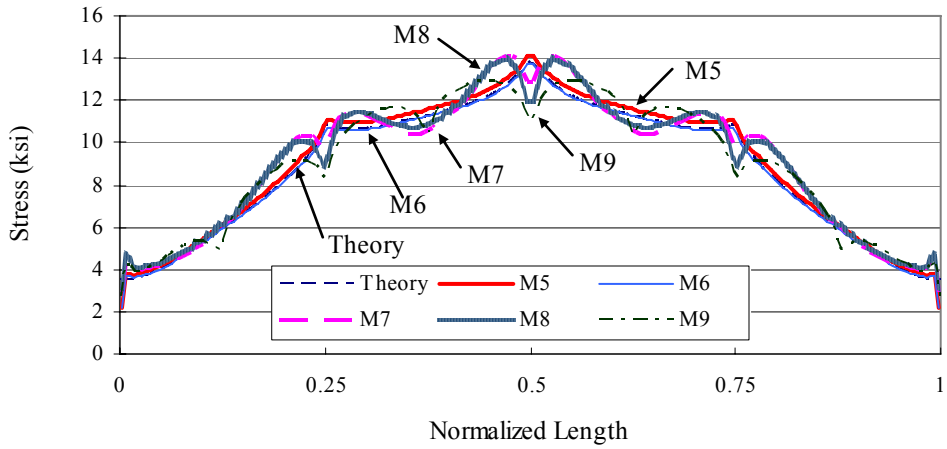

Figure 6.28 Von-Mises Stress of Middle Girder at P3 (Three-Girder Case)

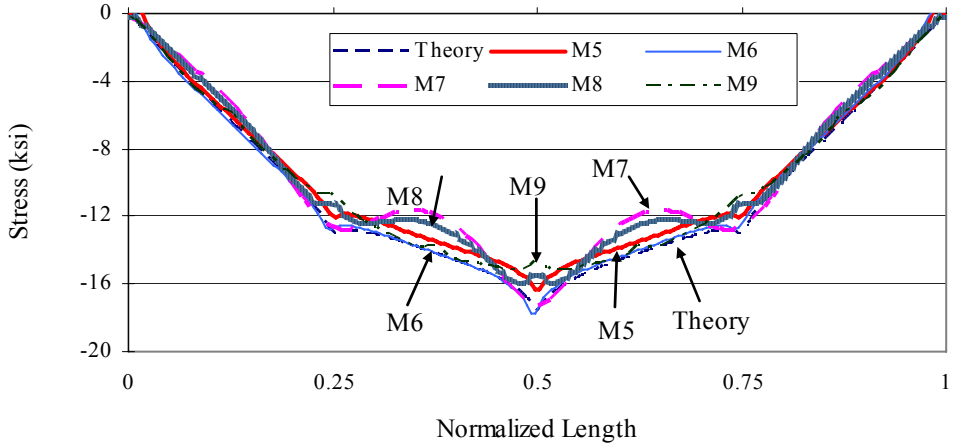

Figure 6.29 Total Normal Stress of Outer Girder at P3 (Three-Girder Case)

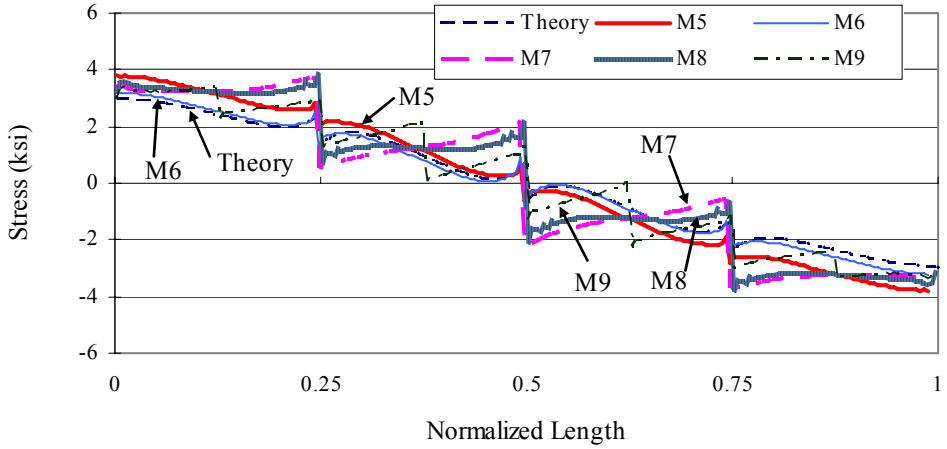

Figure 6.30 Total Shear Stress of Outer Girder at P6r (Three-Girder Case)

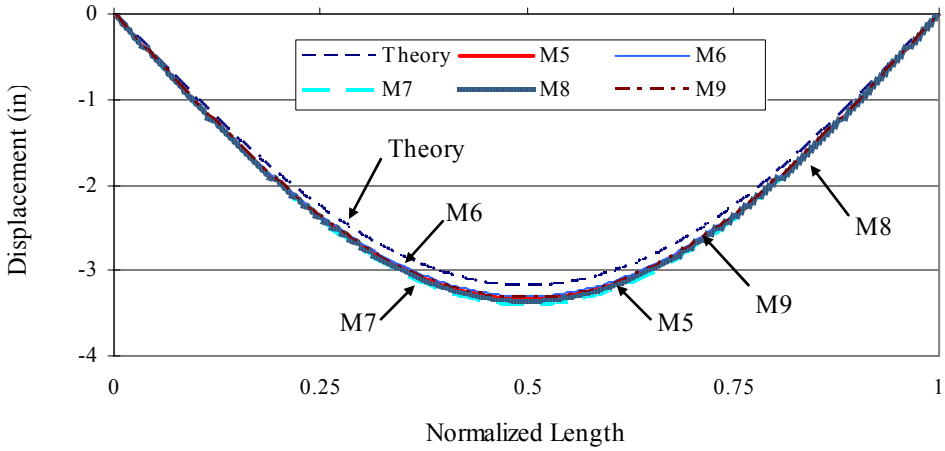

Figure 6.31 Vertical Displacement of Outer Girder (Three-Girder Case)

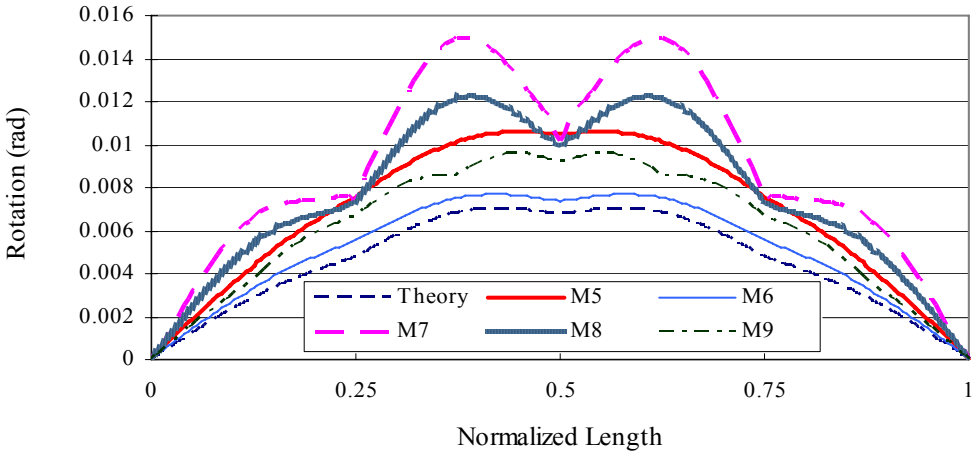

Figure 6.32 Cross Section Rotation of Outer Girder (Three-Girder Case)

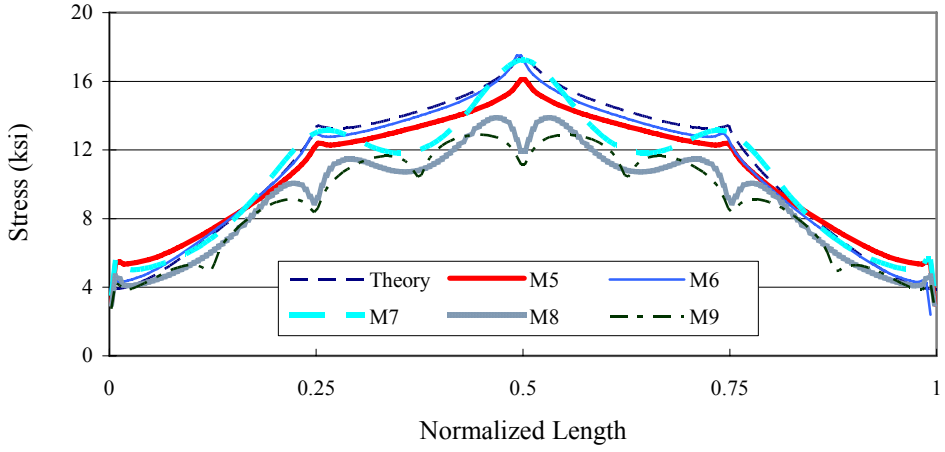

Figure 6.33 Von-Mises Stress of Outer Girder at P3 (Three-Girder Case)

Chapter 7 Parametric Study

This chapter presents the results of a parametric study of the effect of different curved tubular-flange girder cross section parameters on the stresses and displacements. The parametric study is carried out for the single curved tubular-flange girder and the three curved tubular-flange girder system described previously. For this parametric study, as each parameter is varied, the cross section area (the girder self-weight) and the other cross section dimensions are kept constant, except the web thickness which are adjusted to keep the cross section area constant.

7.1 Single Tubular-Flange Girder

The parameters included in this study are the tubular flange width, b_f, tubular flange depth, d_f, web thickness, t_w, cross section depth, d, and the girder curvature parameter, L/R. For each single tubular-flange girder considered in this study, the arc span length, L, the radius of curvature, R, and the cross section area are equal to those of the single tubular-flange girders described in Chapter 5, except when the study focuses on the girder curvature parameter, L/R. For the study of the girder curvature, L is constant and R varies. For the study of the effect of tubular flange width, the tubular-flange depth and the cross section depth, the applied load is the full dead load described in Chapter 5. Thus, the results of the parametric study can be compared with the results presented in Chapter 5 and Chapter 6. For the study of the girder curvature i.e., L/R, the applied load is the girder self-weight.

7.1.1 Effect of Tubular Flange Width

The cross section dimensions for the girders considered in this study are given in **Table 7.1**. As the tubular flange width, b_f, varies, the cross section depth, d, the tubular flange depth, d_f, the tubular flange thickness, t_f, are constant, but the web thickness, t_w, is varied to keep the cross section area constant.

The analysis results are shown in **Figure 7.1** through **Figure 7.9**. As b_f increases, I_x, I_{yf}, I_w, J, and A_e also increase. The bending normal stress, σ_b, is inversely proportional to I_x and the St.Venant shear stress, τ_{st}, is inversely proportional to A_e, therefore, σ_b and τ_{st} decrease with the increase in b_f. The warping normal stress, σ_w, has a slight decrease with the increae in b_f, since I_w increases. The vertical displacement, v, and the cross section rotation, θ, are related to both bending and torsion. v and θ decrease with the increase in b_f, since I_x and J both increase. σ_b dominates the total normal stress, σ_x, so σ_x has the same trend as σ_b. τ_{st} dominates the total shear stress, τ_t, so τ_t has the same trend as τ_{st}. Since the increase in b_f

significantly increases J, increasing b_f is an effective method to reduce τ_{st}, τ_t, v and θ. b_f has a relatively larger influence on σ_b than σ_w.

7.1.2 Effect of Cross Section Depth

The dimensions of the girders used to study the effect of total cross section depth, d, are given in **Table 7.2**. The girders have the same b_f, d_f, and t_f, but t_w is adjusted to keep the cross section area constant, as d varies. Since d_f is constant, a change in the cross section depth, d, is equivalent to a change in the web depth.

The results are presented in **Figures 7.10** through **Figure 7.18**. Since the tube dimensions are constant for each girder, A_e, J, and I_{yf} are constant. Thus, the variation in d influences only the vertical bending and the warping behavior for the girders. The St.Venant shear stress, τ_{st}, and the cross section rotation, θ, of the girders have negligible change with increasing d. A greater cross section depth significantly increases I_x. As a result, the bending normal stress, σ_b, the total normal stress, σ_x, the vertical shear stress, τ_v, and the vertical displacement, v, decrease with increasing d. Eq. (2.25) shows that the warping normal stress, σ_w, is proportional to the normalized unit warping, ω_n. When b_f, and the tube aspect ratio, d_f/b_f, are constant, ω_n is proportional to the tubular flange centroid distance, h_0, (see **Figure 4.6**). As d increases, h_0 increases. Therefore, σ_w increases as d increases.

For the girders considered in this study, σ_b dominates σ_x and τ_{st} dominates τ_t. So σ_x and τ_t follow the trends in σ_b and τ_{st}, respectively. Except for the case with the largest value of d ($b_f/h = 0.25$), the maximum Von-Mises stress, σ_{mises}, occurs at midspan and the contribution is only from σ_x. When d is large, σ_b is significantly reduced, and the magnitude of τ_t is close to that of σ_x. As a result, the maximum σ_{mises} occurs at the ends of the girder where τ_t is the only contribution to σ_{mises}.

The above discussion indicates that a change in the cross section depth, d, has no significant effect on the St.Venant shear stress, τ_{st}, and the cross section rotation, θ. However, an increased cross section depth decreases the bending normal stress, σ_b, the vertical shear stress, τ_v, and the vertical displacement, v. The penalty is an increase in the warping normal stress, σ_w. Since the warping normal stress is usually small for a single curved tubular-flange girder, this disadvantage may be small.

7.1.3 Effect of Tubular Flange Depth

The cross section dimensions of the girders considered in this study are given in **Table 7.3**. For these girders, the tubular flange depth, d_f, is varied, while the cross section depth, d, the tube centerline distance, h, the tubular flange width, b_f, and the

tubular flange thickness, t_f, are constant. The web thickness, t_w, is varied to keep the cross section area constant.

The analysis results are presented in **Figure 7.19** through **Figure 7.27**. As d_f, decreases, I_x, I_w and h_0 increase, but I_{yf} and A_e are significantly decreased. J is proportional to A_e, so J decreases as d_f decreases, Since the St. Venant shear stress, τ_{st}, is inversely proportional to A_e, τ_{st} increases, as d_f decreases. The bending normal stress, σ_b, decreases as d_f decreases, since I_x increases. The warping normal stress, σ_w, increases as d_f decreases, since I_w increases.

The cross section rotation, θ, and the vertical displacement, v, are influenced by both bending and torsion. The contribution from bending reduces as d_f decreases, since I_x increases. The contribution from torsion increases as d_f decreases, since J decreases. The decrease in d_f results in a significant decrease in J and only a slight increase in I_x. Therefore, the contribution from torsion dominates the change in θ and v. As a result, θ and v increase as d_f decreases.

As d_f varies, the change in the bending normal stress and the warping normal stress have different trends. Since the warping normal stress has a more significant change than the bending normal stress, the total normal stress follows the trend of the warping normal stress, that is, the total normal stress for the girders increases as d_f decreases. This result suggests that d_f has more influence on the warping normal stress than the bending normal stress. Since the St.Venant shear stress, τ_{st}, dominates the total shear stress, τ_t, the total shear stress has the same trend as the St.Venant shear stress. For the girders with the smallest values of d_f, (d_f/b_f equal to 0.25 and 0.3), the maximum Von-Mises stress, σ_{mises}, occurs at the girder ends, where only the shear stress contributes to the Von-Mises stress. For the other girders, the maximum Von-Mises stress occurs at midspan, where only the normal stress contributes.

Hence, based on the above discussion, it is observed that the tubular flange depth, d_f, is a significant parameter to reduce the warping normal stress, σ_w, the St. Venant shear stress, τ_{st}, and the displacements, θ and v. For the studied girders, an increase in d_f reduces the warping normal stress, the St.Venant shear stress, and the displacements.

7.1.4 Effect of Curvature

The curved tubular-flange girder TG2 and the curved I-girder G2, described in Chapter 5, are used to study the effect of girder curvature. **Table 5.2** and **Table 5.3** give the dimensions of these girders. The cross section dimensions and the girder arc span length, L, are kept constant, but the radius of curvature, R, is varied so that the ratio, L/R, is varied from 0.1 to 0.6. As noted earlier, unlike the other parameter studies described previously, which used the full dead load as the applied load, for this study of girder curvature, the girder self-weight is used as the applied load.

Figure 7.28 through **Figure 7.37** plot the maximum stresses and displacements for the single tubular-flange girder and the single I-girder as the girder curvature varies. The plots show that the maximum total normal stress, total shear stress, and the displacements for the single curved tubular-flange girder and the single curved I-girder increase with an increase in the curvature. The maximum bending normal stress and the maximum vertical shear stress for both types of girders are almost constant as the girder curvature is varied. The curvature has more influence on the warping normal stress, warping shear stress, St. Venant shear stress, vertical displacement, and cross section rotation.

The results show that the single curved I-girder develops much larger stresses and displacements than the single curved tubular-flange girder for the same L/R. As shown in **Figure 7.28** through **Figure 7.37**, the slope of the curve at each point for the single I-girder is much larger than that for the single tubular-flange girder. Therefore, as L/R increases, the rate of increase in the stresses and displacements for the single curved I-girder is significantly larger than for the single curved tubular-flange girder.

7.2 Three Curved Tubular-Flange Girder System

A parametric study of a three-girder system is presented in this section. The three girders in the system have different cross section dimensions. Five cases are included in the parametric study and the girder cross section dimensions for each case are given, respectively, in **Table 7.4** through **Table 7.8**. Each case has three cross frames, except for the study of the effect of cross frames. The applied load is the full dead load described in Chapter 5.

7.2.1 Effect of Tubular Flange Width

The cross section dimensions of the three-girder systems used to study the effect of the tubular flange width are given in **Tables 7.4**, **7.5**, and **7.6**. The three girders in each system have different cross section dimensions. In each case, as the tubular-flange width, b_f, is varied, the tubular-flange depth, d_f, the tubular-flange thickness, t_f, and the total cross section depth, d, are kept constant for each girder. The web thickness, t_w, is varied to keep the cross section area constant.

The effect of tubular flange width is discussed for the inner girder, TG1, the middle girder, TG2, and the outer girder, TG3, respectively. The results are presented in **Figure 7.38** through **Figure 7.47**. The results show that the stresses and displacements for TG1, TG2 and TG3 have similar trends and decrease with the increase in b_f. As b_f increases, J, I_x, I_w, and A_e increase. Therefore, the bending normal stress decreases due to the increase of I_x; the warping normal stress decreases due to the increase of I_w; the St.Venant shear stress decreases due to the increase of A_e. The cross section rotation and the vertical displacement are influenced by both bending and torsion, and the cross section rotation and the vertical displacement decrease, since J and I_x increase. The results show that the increase in b_f significantly decreases the warping normal stress.

Hence, the tubular flange width, b_f, is an important parameter to reduce the stresses and displacements, especially the warping normal stress.

7.2.2 Effect of Tubular Flange Depth

The three cases that were studied are presented in **Tables 7.6**, **7.7**, and **7.8**. The three girders in each case have different cross section dimensions. The analysis results are given in **Figure 7.48** through **Figure 7.57**. In each case, the tubular-flange depth, d_f, is varied, while the tubular-flange width, b_f, the tubular-flange thickness, t_f, and the total cross section depth, d, are kept constant for each girder. The web thickness, t_w, is varied to keep the cross section area constant.

The stresses and displacements for the inner girder, TG1, the middle girder, TG2, and the outer girder, TG3, have similar trends as d_f varies. The results show that the bending normal stress, the vertical shear stress, and the vertical displacements increase as d_f increases, but the warping normal stress and the cross section rotation decrease as d_f increases. d_f has little influence on the St.Venant shear stress, the bending normal stress in the outer girder, and the vertical displacement of the outer girder.

As d_f increases, A_e, J, and I_w also increase, but I_x slightly decreases. Since the bending normal stress, the vertical shear stress, and the vertical displacement are inversely proportional to I_x, the bending normal stress, the vertical shear stress, and the vertical displacement increase with the increase in d_f. The twist angle is inversely proportional to J and the cross section rotation is dominated by the twist angle, so the cross section rotation decreases with the increase in d_f. The warping normal stress also decreases as d_f increases, since I_w increases. As discussed in Chapter 5, the cross frames restrain the rotation of the girders, but increase the vertical load on the outside girder and decrease the vertical load on the inside girder. Since the torsional constant, J, increases as d_f increases, the increment of the vertical load decrease on the inner girder and vertical load increase on the outer girder is decreased. Thus, the vertical loads applied on the inner girder become larger and the vertical loads applied on the outer girder become smaller with the increase in d_f. Therefore, the bending moment, M_x, increases in the inner girder and decreases in the outer girder as d_f increases. For the inner girder, as d_f increases, the changes in both M_x and I_x have the same influence on the bending normal stress. That is, M_x is increasing and I_x is decreasing, so the bending normal stress increases as d_f increases. For the outer girder, both M_x and I_x decrease as d_f increases, but I_x is dominant, and the bending normal stress increases as d_f increases. However, as shown in **Figure 7.48**, the increase in the bending normal stress is small. For a similar reason, d_f has little influence on the St.Venant shear stress. The increase in J and the decrease in I_x decreases the cross frame restraint of the cross section rotation, so the total St.Venant torque, M_{st}, carried by each girder increases as d_f increases. The St. Venant shear stress is proportional to M_{st}, but inversely proportional to A_e. The influence on the St. Venant shear stress from M_{st} and A_e counteract each other and the St.Venant shear stress remains relatively constant. Based on the previous discussion, it is concluded that the tubular flange depth, d_f, is a significant parameter to reduce the

warping normal stress and the cross section rotation of the curved tubular-flange girder system.

7.2.3. Effect of Curvature

7.2.3.1 Curved Tubular-Flange Girder System

Case 3 for the three-girder system, shown in **Table 7.6**, was used to study the effect of curvature on the stresses and displacements for curved tubular-flange girder systems. The curvature parameter, L/R, was varied from 0.1 to 0.6, while the girder spacing and the arc span length for the middle girder, TG2, were kept constant. To maintain the overall geometry of the curved girder system, the arc span length for the inner girder, TG1, and the outer girder, TG3, was varied slightly. The analysis results are presented in **Figure 7.58** through **Figure 7.67**.

The results show that the total shear stress and cross section rotation for each girder in the system increases as L/R increases. The total normal stress and the vertical displacement of the middle and outer girder increase as L/R increases, but the total normal stress and the vertical displacement for the inner girder decrease. Since the cross section dimensions were kept constant as L/R varied, only the internal forces are influencing the stresses and displacements. As discussed in Chapter 5, the cross frames increase the vertical load on the outer girder and decrease the vertical load on the inner girder. As L/R increases, the increment of vertical load on the outer girder and the decrement of vertical load on the inner girder also increase. Therefore, the bending moment and the vertical shear force increase in the outer girder and decrease in the inner girder, as L/R increases. As a result, the bending normal stress, the vertical shear stress, and the vertical displacement increase for the outer girder, and decrease for the inner girder as L/R increases.

Since there are two cross frames connected to the middle girder, only a small increase in vertical load on the middle girder occurs as L/R increases. Compared to the inner and outer girder, the bending normal stress and the vertical shear stress in the middle girder increase slightly as L/R increases. The decrease in vertical load on the inner girder also results in a decrease in bimoment for the inner girder as L/R increases. As shown in **Figure 7.59**, the warping normal stress in the inner girder starts to decrease as L/R increases, after L/R is greater 0.3.

The St.Venant torque in the three girders increases as L/R increases. So the St.Venant shear stress and the cross section rotation also increase as L/R increases. The total normal stress is dominated by the bending normal stress and if has the same trend as the bending normal stress. The total shear stress is dominated by the St.Venant shear stress and it has the same trend as the St.Venant shear stress.

The plots show that the total normal stress, the total shear stress, the vertical displacement for the inner girder, TG1, is larger than the outer girder, TG3, when L/R is less than 0.2. These results indicate that when the curvature is very small, there is not much load transferred from TG1 to TG3. Since the dimensions of TG1 are smaller than

the dimensions of TG3 and they carry similar load, TG1 develops larger stresses and displacements than TG3. Hence, when L/R is less than 0.2 for the studied tubular-flange girder system, the curvature has only a small effect on the tubular-flange girder system.

7.2.3.2 Comparison with Curved I-Girder System

The curved I-girder system, given in **Table 5.2**, was used for the comparative study. **Figure 7.68** through **Figure 7.77** present the analysis results of the curvature effect for the I-girder system. The plots show that the stresses and displacements for the three girders in the I-girder system have trends similar to those for the corresponding girder in the tubular-flange girder system as the curvature parameter, L/R, varies.

Figure 7.78 through **Figure 7.87** present the results from both the tubular-flange girder and I-girder system for comparison. Since the I-girder is more efficient under bending and less efficient under torsion, the bending normal stress and the vertical displacement for each I-girder is smaller than that for the corresponding tubular-flange girder, but the warping normal stress for each I-girder is larger than that for the corresponding tubular-flange girder. As L/R increases, the rate of increase in the bending normal stress and the vertical displacement for each girder in both systems is similar, but the rate of increase in the warping normal stress for each I-girder is significantly greater than that for the corresponding tubular-flange girder. When L/R is larger than 0.35, the total normal stress for the inner I-girder, G1, is smaller than for the corresponding tubular-flange girder, TG1, but the total normal stress for the outer I-girder, G3, is larger than for the corresponding tubular-flange girder TG3, since the warping normal stress is large for the I-girder. The rate of increase in the total normal stress for each I-girder is faster than for the corresponding tubular-flange girder as L/R increases. For the total shear stress, the St.Venant shear stress and the vertical shear stress for each I-girder is smaller than for the corresponding tubular-flange girder, so the total shear stress for each girder in the I-girder system is smaller than for the corresponding tubular-flange girder, except for TG3, when L/R is less than 0.3. The rate of increase in the total shear stress for the I-girder system is slower than for the tubular-flange system as L/R increases. The cross section rotation for each I-girder is larger than for the corresponding tubular-flange girder, since the tubular-flange girder system has higher torsional stiffness. The Von-Mises stress has a trend similar to the trend in bending normal stress, since the bending normal stress is dominant in the Von-Mises stress.

Based on the above discussion, the following findings are obtained: (1) when L/R is greater than 0.3 (see **Figure 7.85**), the tubular-flange girder system has less Von-Mises stress than the I-girder system and the stress in the I-girder is more sensitive to the curvature increase; (2) for any curvature, the bending normal stress and the vertical displacement for the I-girder system is smaller than for the tubular-flange girder system, but the cross section rotation for the I-girder system is larger than for the tubular-flange girder system.

7.2.4 Effect of Number of Cross Frames

7.2.4.1 Curved Tubular-Flange Girder System

This section presents a study of the effect of the number of intermediate cross frames on the stresses and displacements in a tubular-flange girder system. As in the previous study, the three-girder system described in **Table 7.6** was used for the study. The maximum stresses and displacements from the theoretical and finite element analyses are shown in **Figure 7.88** through **Figure 7.117**. The theoretical results for a curved I-girder bridge system with the dimensions given in **Table 5.2** are also presented in the plots for comparison. The number of cross frames given in the plots denotes only the intermediate cross frames and does not include the end cross frames at the bearings.

The results show that increasing the number of cross-frames has little effect on the bending normal stress for the inner girder, TG1, the middle girder, TG2, and the outer girder, TG3, but reduces the warping normal stress for the three girders, TG1, TG2, and TG3. The total normal stress for the inner girder, TG1, the middle girder, TG2, and the outer girder, TG3, gradually decreases with the increase in the number of cross frames. The further decrease in the total normal stress as cross frames are added is negligible after four intermediate cross-frames are used in the system. The St.Venant shear stress and the warping shear stress for the three girders decrease with the increase in the number of cross-frames, but the reduction in the warping shear stress is larger than the reduction in St.Venant shear stress. Similar to the bending normal stress, the number of cross frames has little influence on the vertical shear stress. The total shear stress gradually decreases with the increase in the number of cross-frames. The vertical displacement for TG1 becomes smaller when the number of the cross-frames increases. The further decrease in the vertical displacement as cross frames are added is negligible after three cross frames are used in the system. The vertical displacement of TG2 and TG3 has little change with the increase in the number of cross frames. After the system has three cross frames, increasing the number of cross frames has a small influence on the cross section rotation for the three girders. Since only the total normal stress contributes to the maximum Von-Mises stress, the trend of the Von-Mises stress is similar to that of the total normal stress.

Overall, an increase in the number of cross frames reduces the warping normal stress, warping shear stress, the St.Venant shear stress. Based on the above discussion, the following findings are obtained: (1) increasing the number of cross frames reduces the stresses and displacements for the curved tubular-flange girder system; (2) the number of cross frames has more influence on the warping normal stress, the warping shear stress, and the St.Venant shear stress for a curved tubular-flange girder system; (3) only three cross frames are needed, since more than three cross frames produces very limited reductions in stresses and displacements. Therefore, three cross-frames are recommended for the curved tubular-flange girder system that was studied.

7.2.4.2 Comparison with Curved I-Girder System

Theoretical analysis results for the curved I-girder system with multiple cross frames are also presented in **Figure 7.88** through **Figure 7.117**. The results show that the increase in the number of cross frames has a negligible effect on the bending normal stress and the vertical shear stress for the I-girder system. This result is similar to the result for the tubular-flange girder system. The bending normal stress and the vertical shear stress in the I-girder system with any number of cross frames is smaller than in the corresponding tubular-flange girders, since the I-section is more efficient in bending and shear.

The warping normal stress and warping shear stress in the I-girder system are much larger than in the corresponding tubular-flange girder for any number of cross frames. The warping normal stress is especially large for the I-girder. The increase in the number of cross frames provides a more significant reduction in the warping normal and the warping shear stress for the I-girder system than for the tubular-flange girder system. The St.Venant shear stress in the I-girder system with one cross frame is much larger than that in the tubular-flange girder system. However, the St.Venant shear stress in the I-girder system is significantly reduced by using two or three cross frames. When three or more cross frames are used, the St.Venant shear stress in the I-girder system slightly decreases with the increase in the number of the cross frames, and becomes smaller than the St.Venant shear stress in the tubular-flange girder system.

The total normal stress for a girder in the I-girder system with one cross frame is significantly larger than for the corresponding girder in the tubular-flange girder system. With an increase in the number of cross frames, the total normal stress in the I-girder system decreases and becomes smaller than that of the corresponding girder in the tubular-flange girder system when enough cross frames are used. The results show that to make the total normal stress in the I-girder system less than that in the tubular-flange system, at least three cross frames are needed for the inner girder, four cross frames are needed for the middle girder and six cross frames are needed for the outer girder. Thus, when the recommended three cross frames are used for each system, the total normal stress in the middle and outer girder in the tubular-flange girder system is smaller than in the corresponding girder in the I-girder system.

The total shear stress in the I-girder system is less than in the tubular-flange girder, except for the case with one cross frame. The cross section rotation for the I-girder system is significantly larger than for the tubular-flange girder system for the cases with one or two cross frames. When three or more cross frames are used, the cross section rotations in the I-girder system are similar to or slightly larger than those in the tubular-flange girder system.

As discussed in Chapter 5, compared to the curved tubular-flange girder, the curved I-girder has a much smaller torsional stiffness, and significant stresses and displacements, especially the warping normal stress and the St.Venant shear stress, develop in a single curved I-girder. These stresses and displacements are large enough

so that the single curved I-girder can not carry its self-weight when supported at the ends. However, a curved tubular-flange girder has large torsional stiffness and develops much smaller stresses and displacements under self-weight when supported at the ends. A single curved tubular-flange girder carries its self-weight easily. For the three-girder system, the cross frames effectively restrain the torsion in each I-girder, and thus, significantly reduce the warping normal stress, St.Venant shear stress, and cross section rotation. Since the curved tubular-flange girder develops the much smaller warping normal stress, St.Venant shear stress, and cross section rotation, the cross frames have less effect on it. Only a few cross frames are needed for the tubular-flange girder to sufficiently reduce the stresses and displacements.

Based on the above discussion, the following findings are obtained: (1) increasing the number of cross frames has more influence on the curved I-girder system behavior than the curved tubular-flange girder system behavior; (2) only a few cross frames are needed in a tubular-flange girder system; (3) a curved tubular-flange system has smaller stresses and displacements than a curved I-girder system when three or less cross frames are used.

7.3. Comparison with Finite Element Results

Finite element analyses of the three-girder systems used to study the effect of tubular-flange width were conducted. Cases 3, 4 and 5, as given in **Tables 7.6**, **7.7**, and **7.8**, were analyzed. The purpose of these analyses was to verify the theoretical analysis results. As mentioned in Chapter 4, the cross frames are assumed to be rigid in the theoretical analysis model, which may not fully reflect the actual situation. The finite element model, M5, described in Chapter 6, was used to conduct the finite element analysis. Model M5 does not include the cross section distortion, but includes cross frame deflections.

7.3.1 Three Curved Girder System with Three Cross Frames

Only the total normal stress, the total shear stress, the vertical displacement and the cross section rotation from the finite element (FE) analysis are presented in **Figures 7.40**, **7.44**, **7.46**, and **7.47**. The results show the differences between the finite element results and the theoretical results for stresses and displacements are largest for the inner girder and the outer girder, but the differences for the middle girder are small. The maximum difference is for the cross section rotation of the outer girder and this difference is about 35%. Since the cross frame deflections greatly influence the cross section rotation, as well as the vertical loads on the inner girder and the outer girder, these differences between the finite element results and the theoretical results are understandable.

7.3.2 Three Curved Girder System with Multiple Cross Frames

The results from the finite element analyses for the cases with multiple cross frames are presented together with the theoretical results. The finite element results are given for only the total normal stress, the total shear stress, the Von-Mises stress, the vertical displacement and the cross section rotation.

Similar to the case with three cross frames, the stresses and the displacements from the finite element analyses and theoretical analyses for the middle girder are relatives close to each other. The maximum difference occurs in the cross section rotation of the outer girder (**Figure 7.117**), which shows more than 30% difference between the finite element and theoretical analysis results. The results show that the differences between the finite element results and the theoretical results become slightly smaller with the increase in the number of cross frames. The total normal stress in the inner girder, TG1, the vertical displacement of the inner girder, TG1, the total shear stress in the outer girder, TG3, and the cross section rotation of the outer girder,TG3, have larger differences. When the number of cross frames increases from three to seven, the difference in the total normal stress and the vertical displacement of TG1 changes from 13% to 10%, and the difference in the total shear stress and the cross section rotation of TG3 changes from 21% to 17% and from 34% to 27% respectively. For the other stresses and displacements, most of the differences are less than 5%. Despite the differences between the theoretical results and the finite element results, the plots show that the stresses and displacements have the same trends as the theoretical results with an increasing number of cross frames.

Based on the above discussion, the following findings are obtained: (1) neglecting the cross frame deflections introduces errors in the theoretical analysis results, especially for the cross section rotation of the outer girder; (2) the errors for the three-girder system with different cross section dimensions do not influence findings of the parameter study, regarding the variations in stresses and displacements as parameters change, but the actual values of the stresses and displacements may not be accurate.

Table 7.1 Cross Section Dimensions for Study of Tubular Flange Width

Girders	b_f/h	d (in)	h (in)	b_f (in)	d_f (in)	d_f/b_f	t_f (in)	t_w (in)
PG1	0.24	50.3863	49.8863	12	6	0.500	0.5	0.9496
PG2	0.30	50.3863	49.8863	16	6	0.375	0.5	0.7356
PG3	0.36	50.3863	49.8863	20	6	0.300	0.5	0.5216

Table 7.2 Cross Section Dimensions for Study of Cross Section Depth

Girders	b_f/h	d (in)	h (in)	b_f (in)	d_f (in)	d_f/b_f	t_f (in)	t_w (in)
PG8	0.25	72.535	72	18	9	0.5	0.535	0.2565
PG9	0.30	60.535	60	18	9	0.5	0.535	0.3308
PG7	0.36	50.420	49.886	18	9	0.5	0.535	0.4375
PG10	0.40	45.535	45	18	9	0.5	0.535	0.5183
PG11	0.45	40.535	40	18	9	0.5	0.535	0.6390

Table 7.3 Cross Section Dimensions for Study of Tubular Flange Depth

Girders	b_f/h	d (in)	h (in)	b_f (in)	d_f (in)	d_f/b_f	t_f (in)	t_w (in)
PG16	0.40	50.375	49.886	20	5	0.25	0.4887	0.5745
PG17	0.40	50.375	49.886	20	6	0.30	0.4887	0.5530
PG18	0.40	50.375	49.886	20	7	0.35	0.4887	0.5290
PG19	0.40	50.375	49.886	20	8	0.40	0.4887	0.5021
PG20	0.40	50.375	49.886	20	9	0.45	0.4887	0.4719
PG4	0.40	50.375	49.886	20	10	0.50	0.4887	0.4375

Table 7.4 Case 1 for Three-Girder System

Girders	b_f/h	d (in)	h (in)	b_f (in)	d_f (in)	d_f/b_f	t_f (in)	t_w (in)
TG1	0.241	50.125	49.704	12	8	0.667	0.4212	0.4375
TG2	0.321	50.375	49.886	16	10	0.625	0.4887	0.4375
TG3	0.387	52.500	51.677	20	12	0.600	0.8234	0.500

Table 7.5 Case 2 for Three-Girder System

Girders	b_f/h	d (in)	h (in)	b_f (in)	d_f (in)	d_f/b_f	t_f (in)	t_w (in)
TG1	0.282	50.125	49.704	14	8	0.571	0.4212	0.6401
TG2	0.361	50.375	49.886	18	10	0.556	0.4887	0.7033
TG3	0.426	52.500	51.677	22	12	0.545	0.8234	0.9908

Table 7.6 Case 3 for Three-Girder System

Girders	b_f/h	d (in)	h (in)	b_f (in)	d_f (in)	d_f/b_f	t_f (in)	t_w (in)
TG1	0.322	50.125	49.704	16	8	0.5	0.4212	0.4375
TG2	0.401	50.375	49.886	20	10	0.5	0.4887	0.4375
TG3	0.465	52.500	51.677	24	12	0.5	0.8234	0.500

Table 7.7 Case 4 for Three-Girder System

Girders	b_f/h	d (in)	h (in)	b_f (in)	d_f (in)	d_f/b_f	t_f (in)	t_w (in)
TG1	0.322	50.125	49.704	16	6.4	0.4	0.4212	0.4732
TG2	0.401	50.375	49.886	20	8	0.4	0.4887	0.502
TG3	0.464	52.500	51.677	24	9.6	0.4	0.8234	0.674

Table 7.8 Case 5 for Three-Girder System

Girders	b_f/h	d (in)	h (in)	b_f (in)	d_f (in)	d_f/b_f	t_f (in)	t_w (in)
TG1	0.322	50.125	49.704	16	4.8	0.3	0.4212	0.5029
TG2	0.401	50.375	49.886	20	6	0.3	0.4887	0.5529
TG3	0.464	52.500	51.677	24	7.2	0.3	0.8234	0.8021

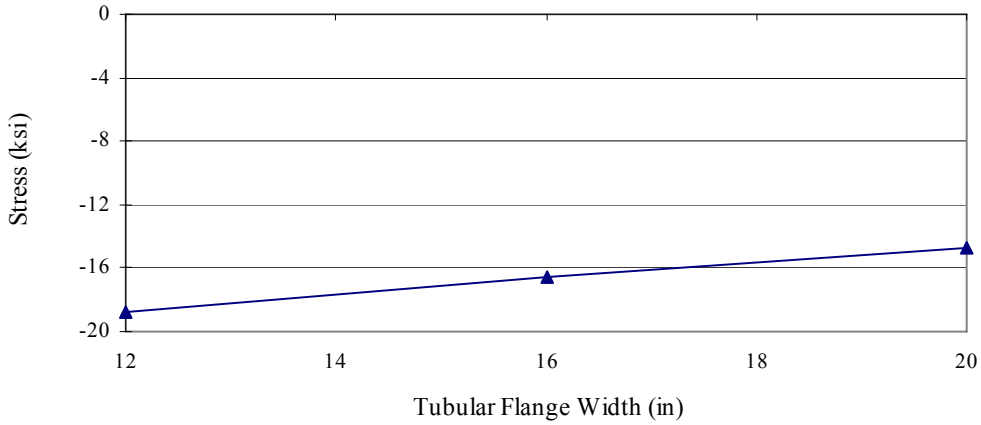

Figure 7.1 Maximum Bending Normal Stress vs. Tubular Flange Width

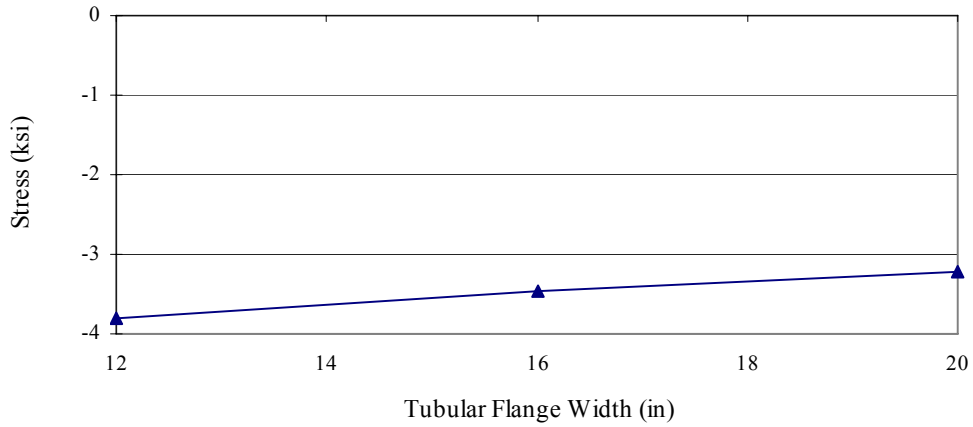

Figure 7.2 Maximum Warping Normal Stress vs. Tubular Flange Width

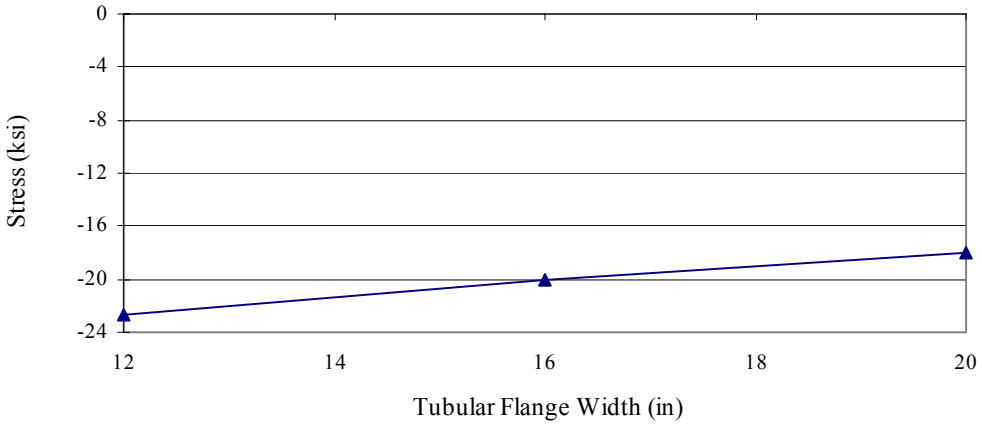

Figure 7.3 Maximum Total Normal Stress vs. Tubular Flange Width

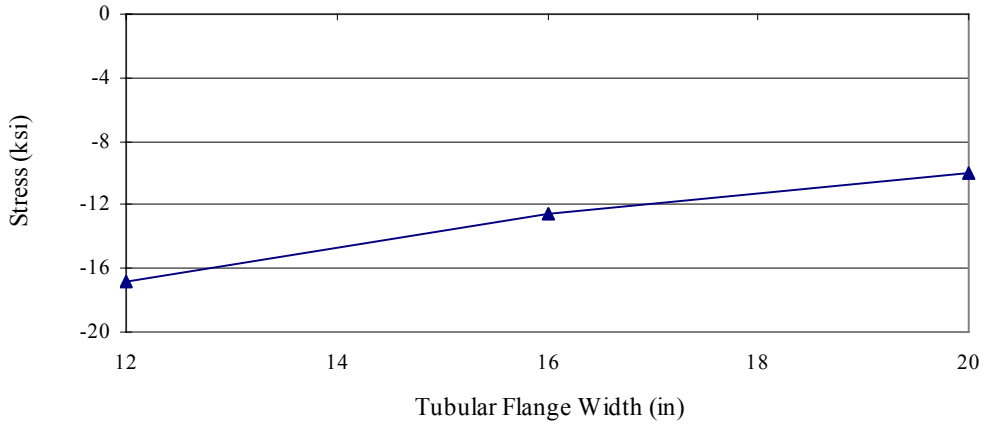

Figure 7.4 Maximum St.Venant Shear Stress vs. Tubular Flange Width

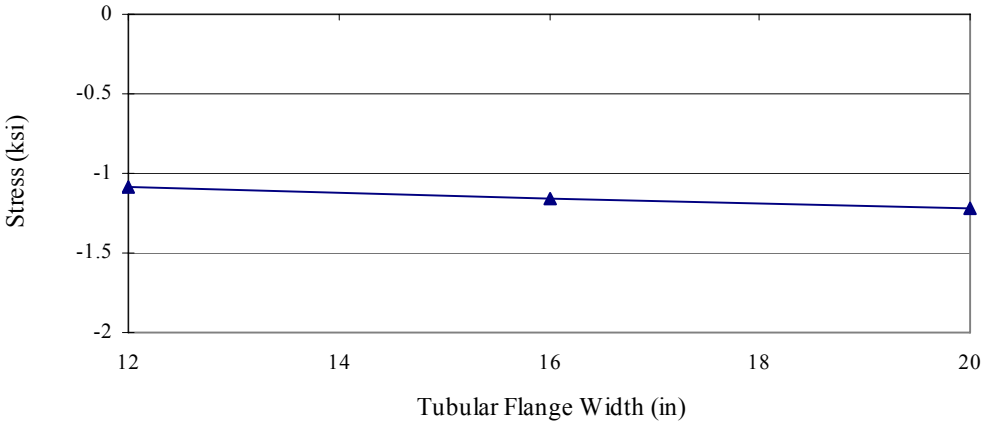

Figure 7.5 Maximum Vertical Shear Stress vs. Tubular Flange Width

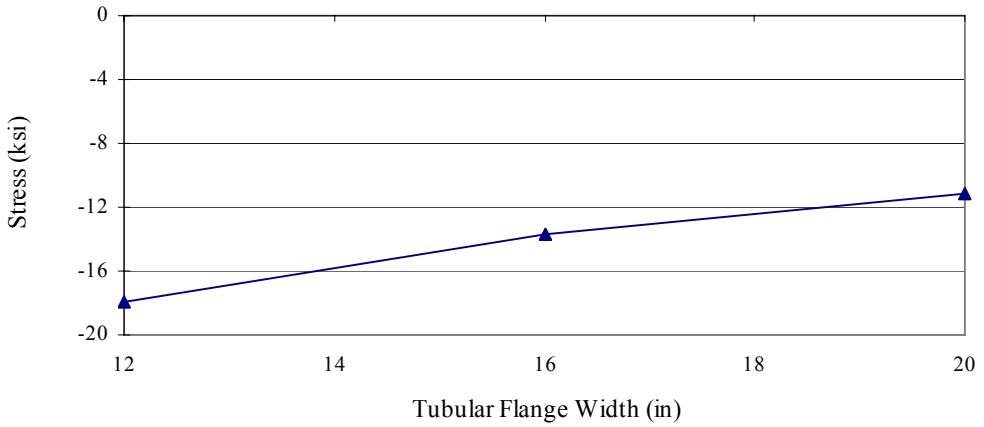

Figure 7.6 Maximum Total Shear Stress vs. Tubular Flange Width

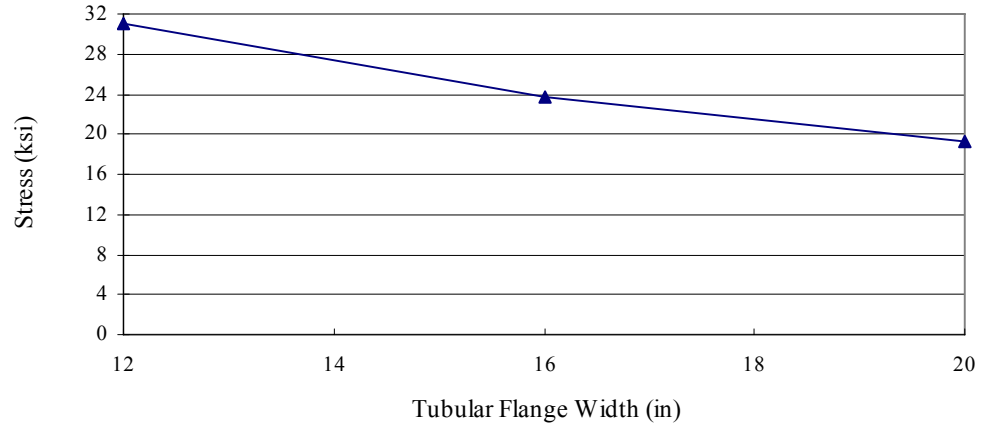

Figure 7.7 Maximum Von-Mises Stress vs. Tubular Flange Width

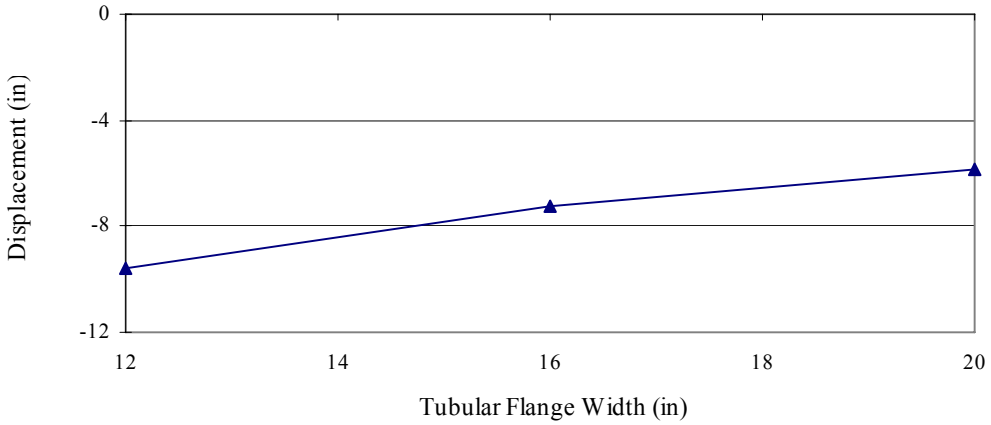

Figure 7.8 Maximum Vertical Displacement vs. Tubular Flange Width

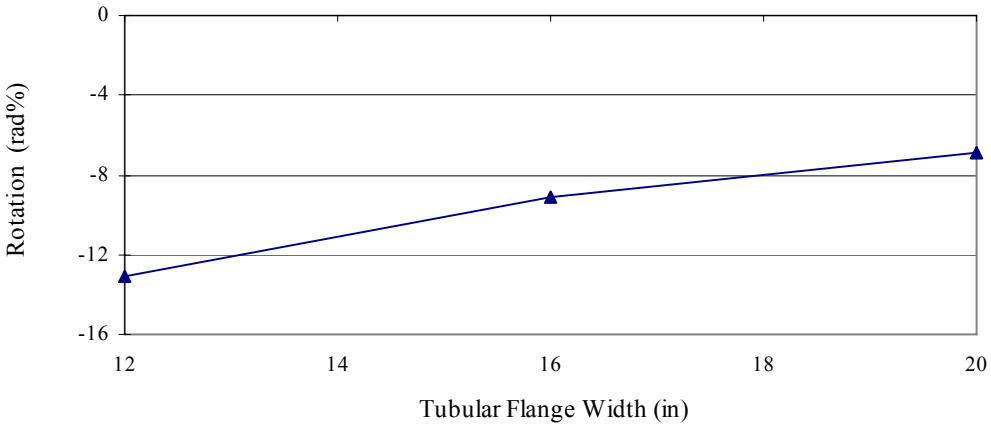

Figure 7.9 Maximum Cross Section Rotation vs. Tubular Flange Width

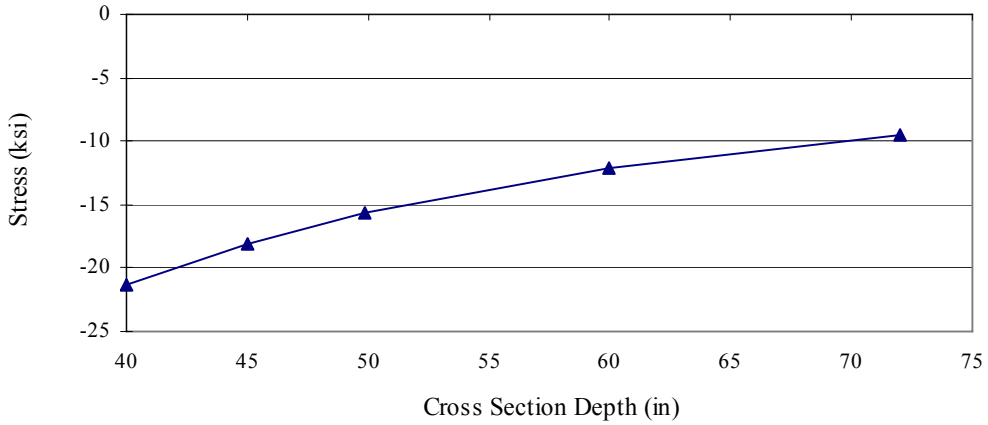

Figure 7.10 Maximum Bending Normal Stress vs. Cross Section Depth

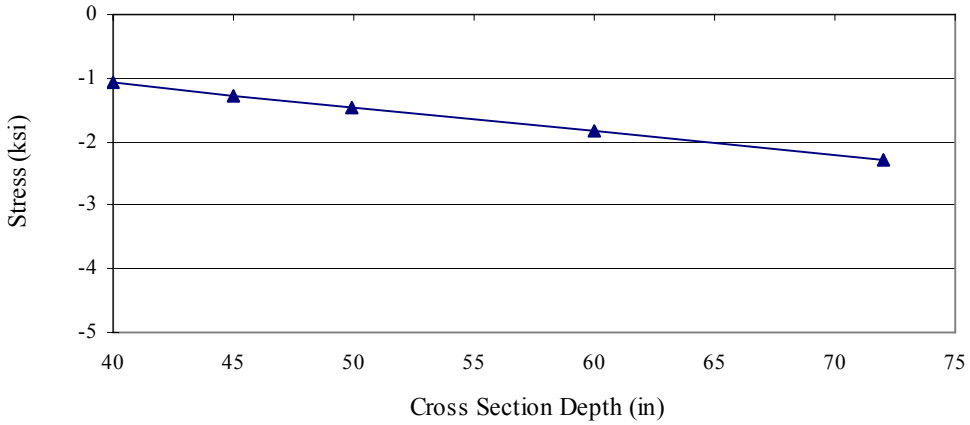

Figure 7.11 Maximum Warping Normal Stress vs. Cross Section Depth

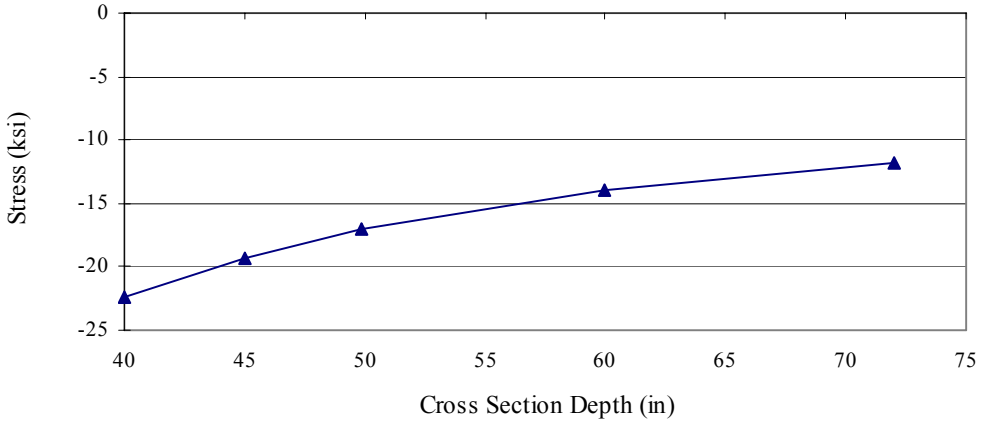

Figure 7.12 Maximum Total Normal Stress vs. Cross Section Depth

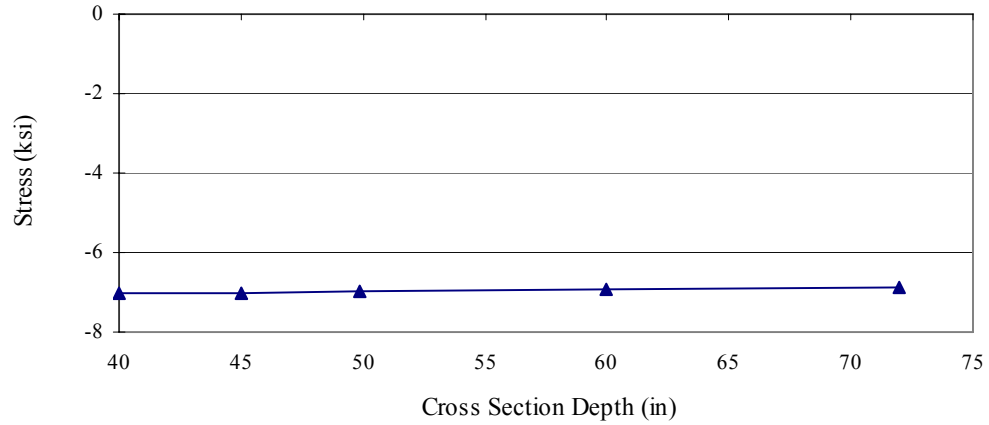

Figure 7.13 Maximum St. Venant Shear Stress vs. Cross Section Depth

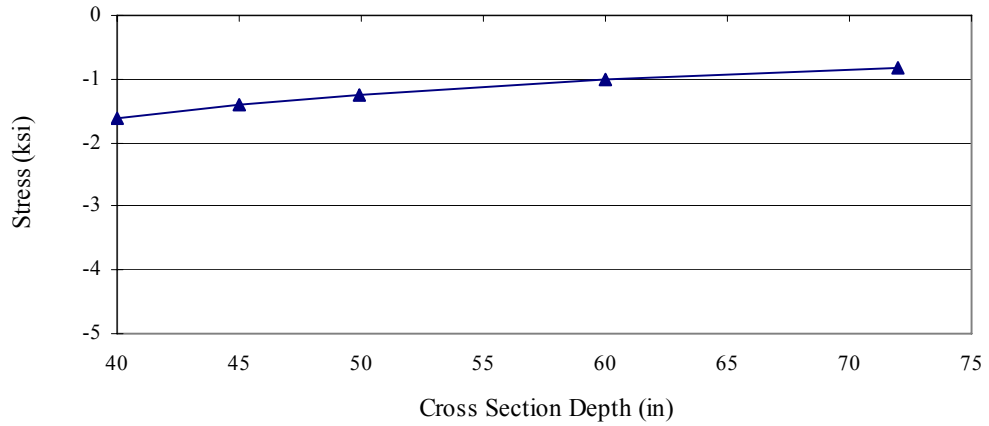

Figure 7.14 Maximum Vertical Shear Stress vs. Cross Section Depth

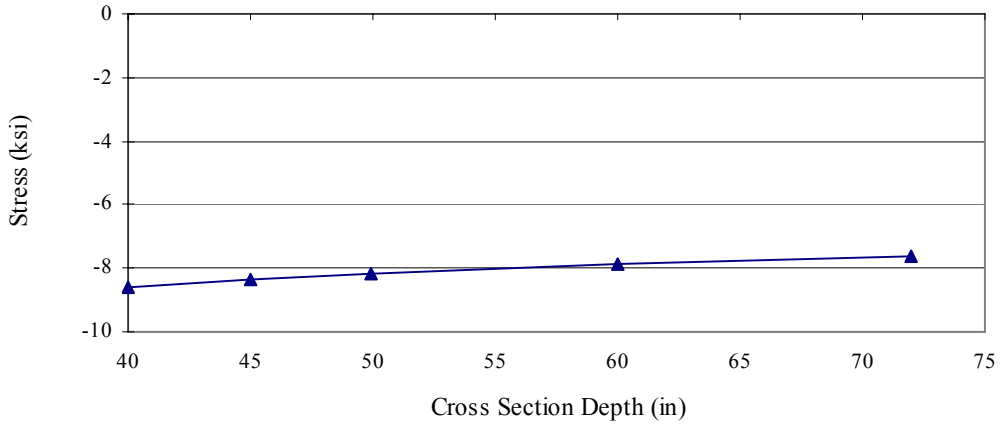

Figure 7.15 Maximum Total Shear Stress vs. Cross Section Depth

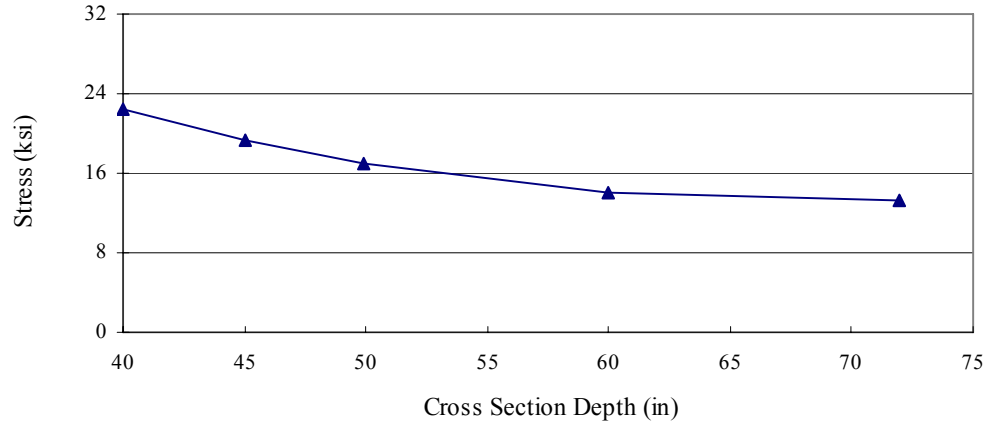

Figure 7.16 Maximum Von-Mises Stress vs. Cross Section Depth

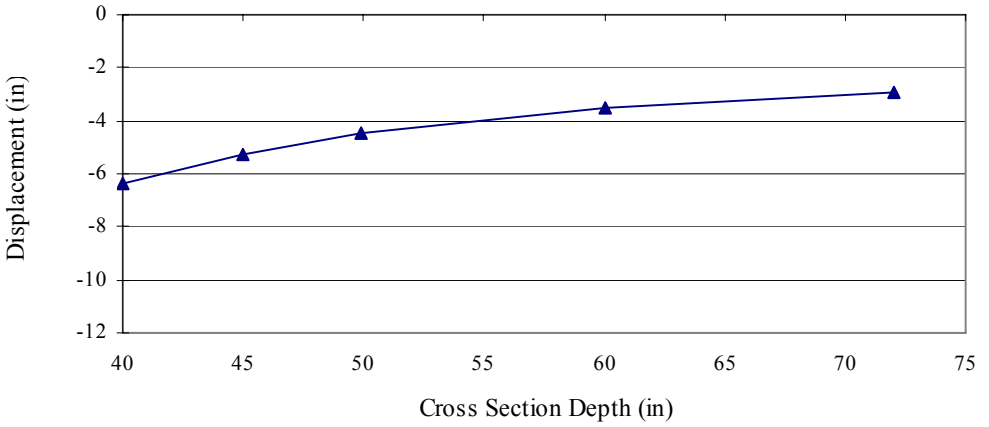

Figure 7.17 Maximum Vertical Displacement vs. Cross Section Depth

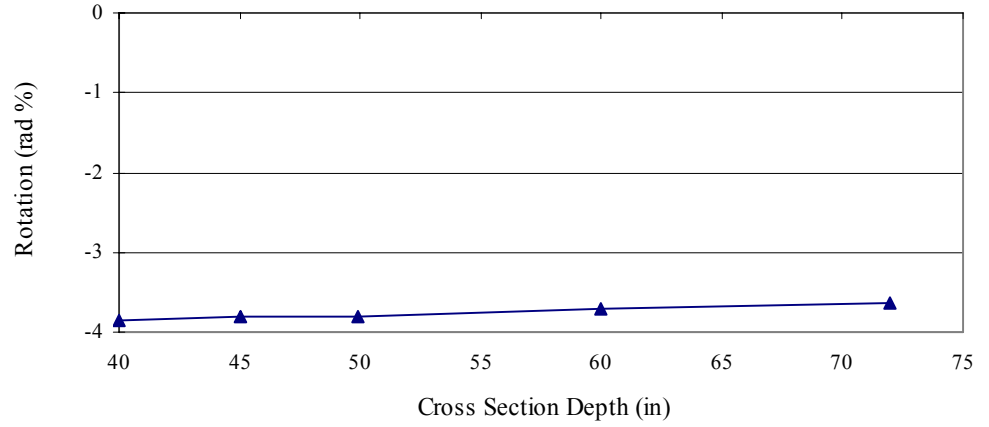

Figure 7.18 Maximum Cross Section Rotation vs. Cross Section Depth

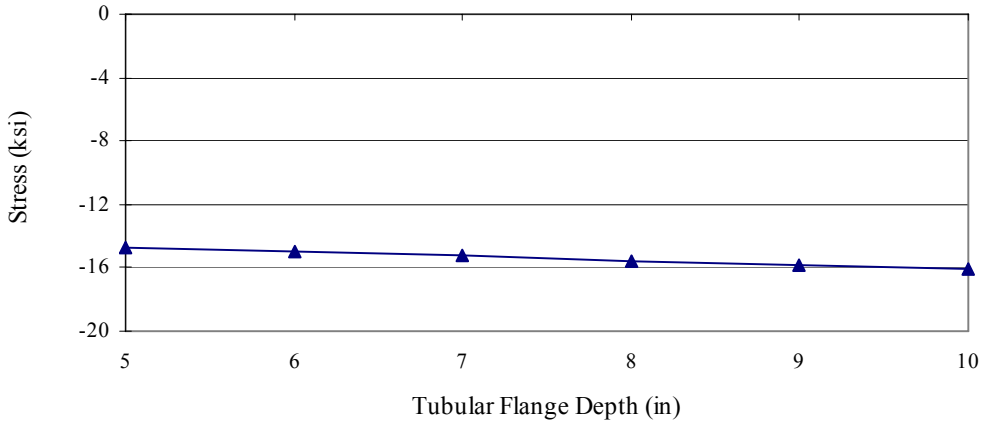

Figure 7.19 Maximum Bending Normal Stress vs. Tubular Flange Depth

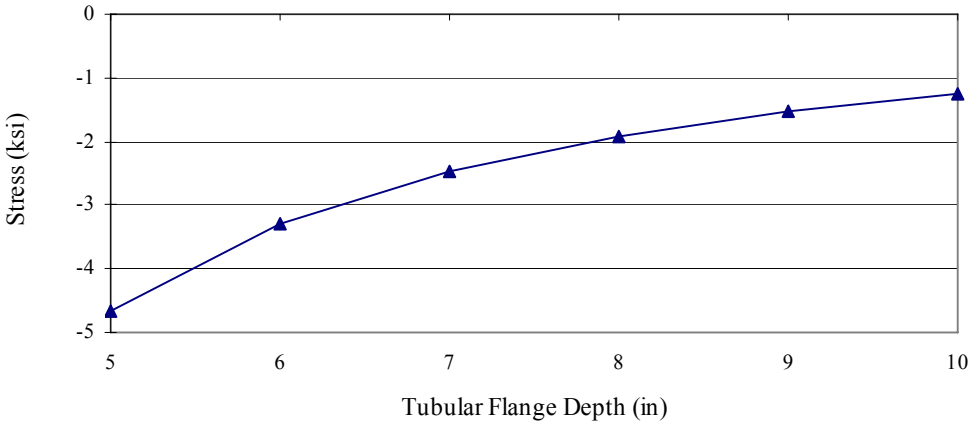

Figure 7.20 Maximum Warping Normal Stress vs. Tubular Flange Depth

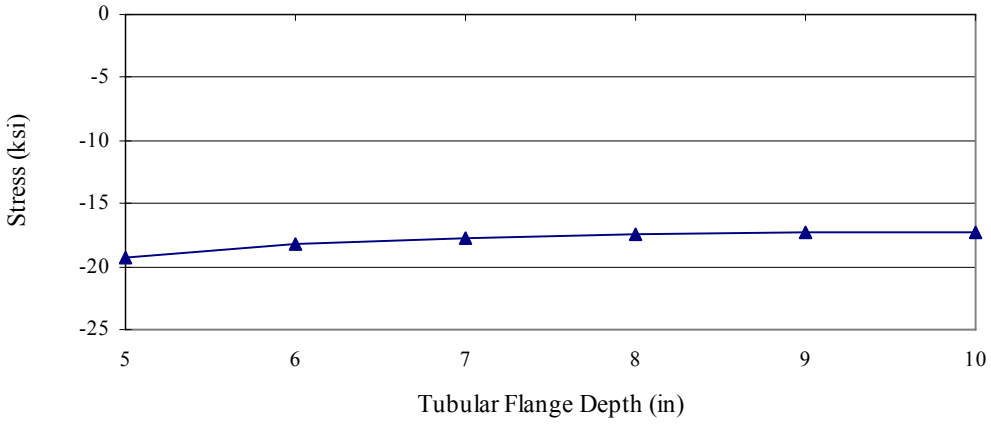

Figure 7.21 Maximum Total Normal Stress vs. Tubular Flange Depth

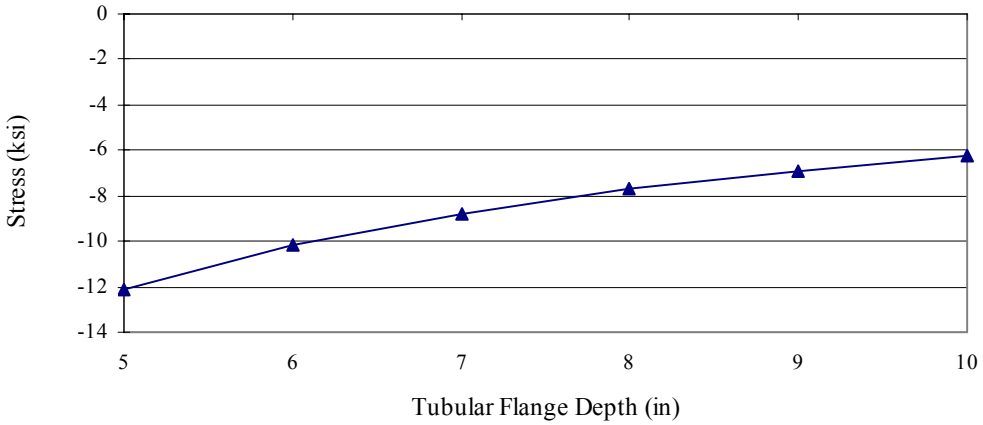

Figure 7.22 Maximum St. Venant Shear Stress vs. Tubular Flange Depth

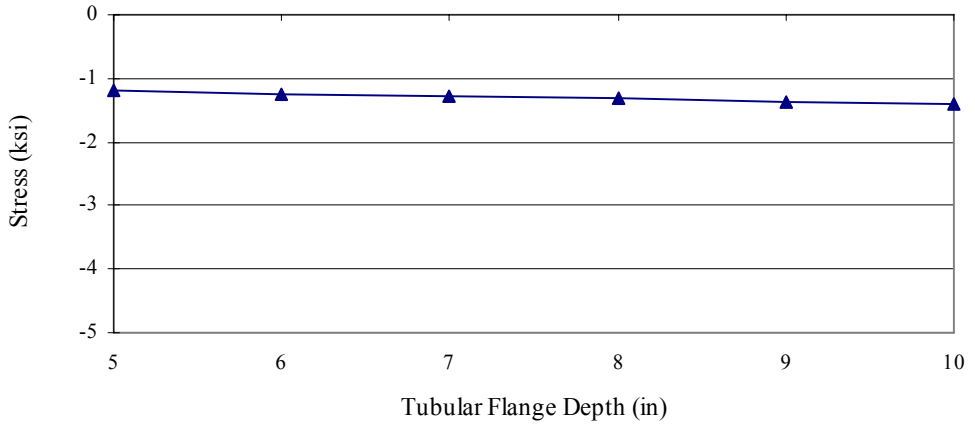

Figure 7.23 Maximum Vertical Shear Stress vs. Tubular Flange Depth

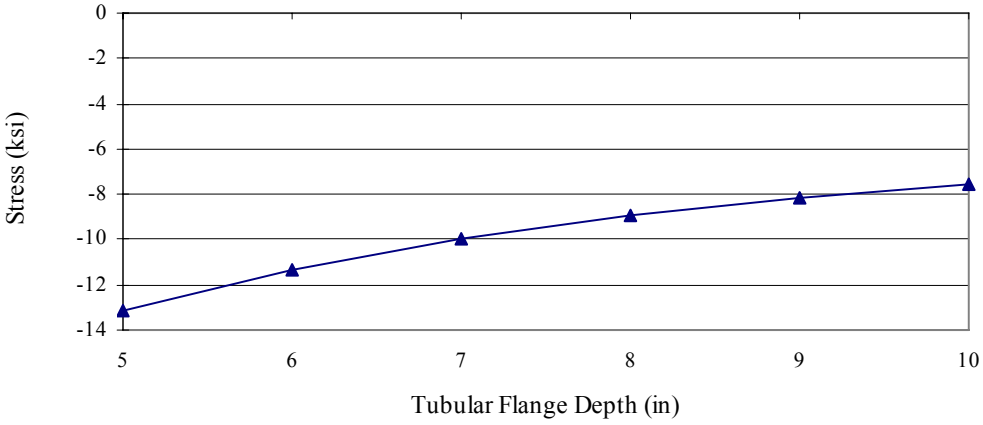

Figure 7.24 Maximum Total Shear Stress vs. Tubular Flange Depth

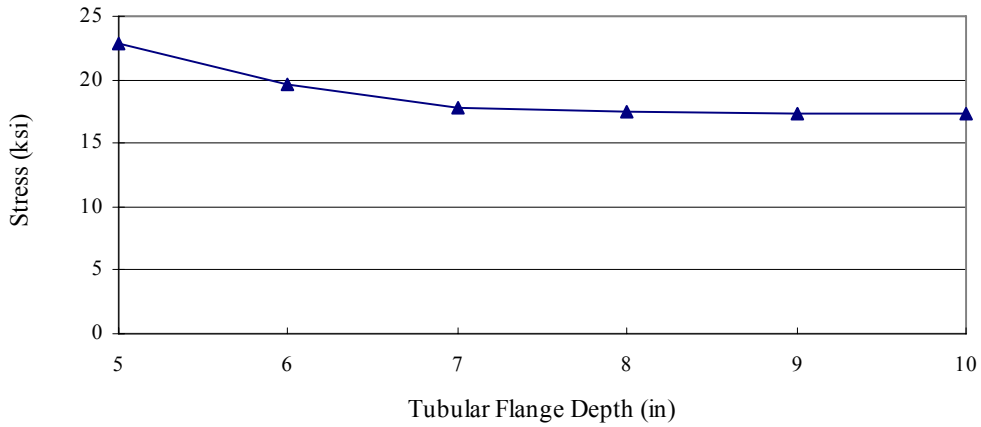

Figure 7.25 Maximum Von-Mises Stress vs. Tubular Flange Depth

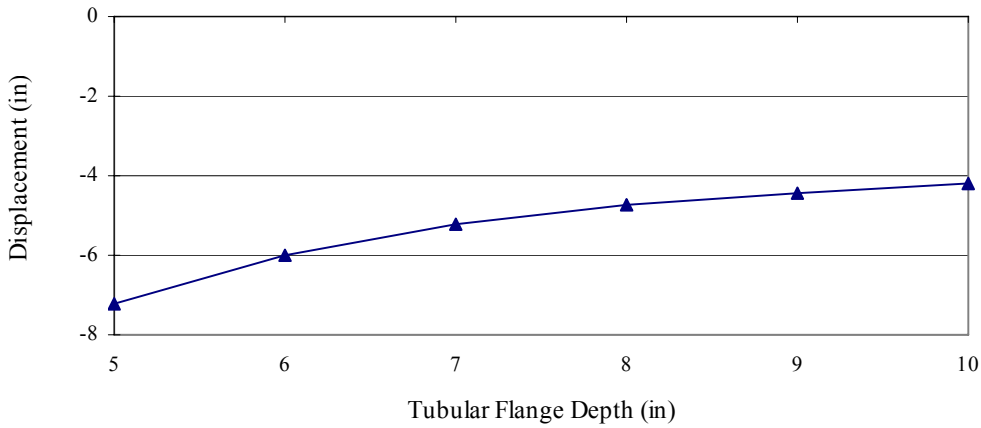

Figure 7.26 Maximum Vertical Displacement vs. Tubular Flange Depth

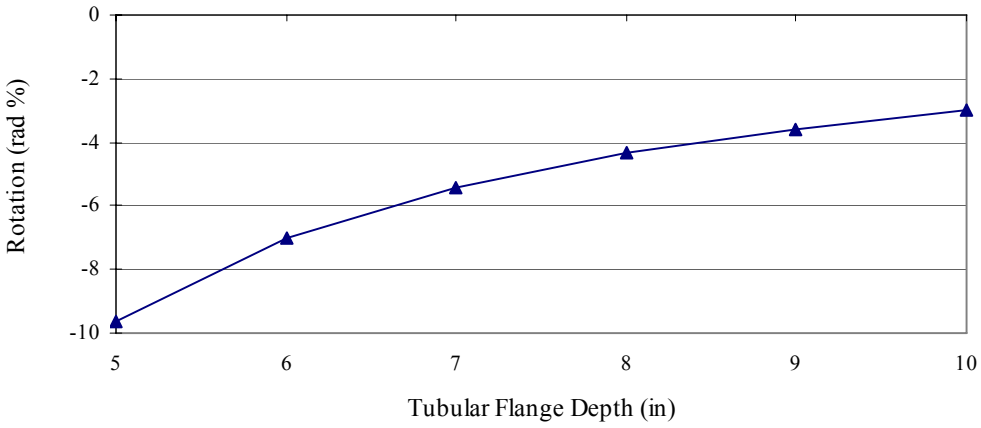

Figure 7.27 Maximum Cross Section Rotation vs. Tubular Flange Depth

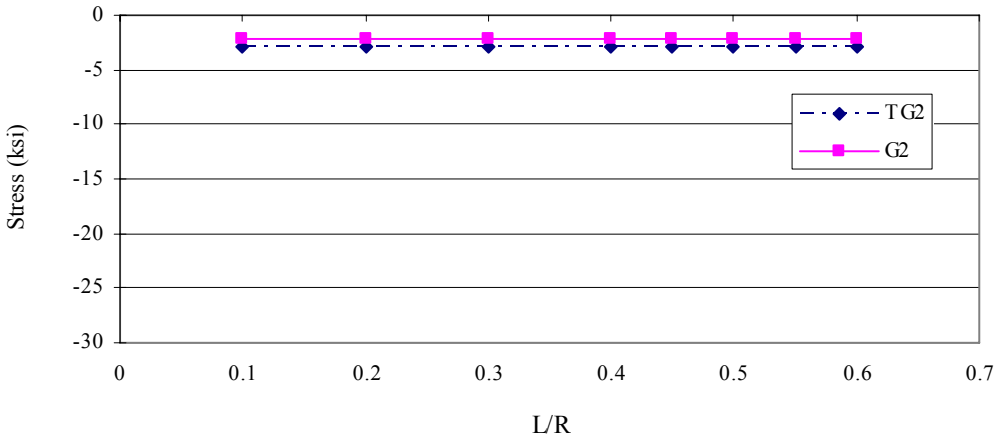

Figure 7.28 Maximum Bending Normal Stress vs. Girder Curvature

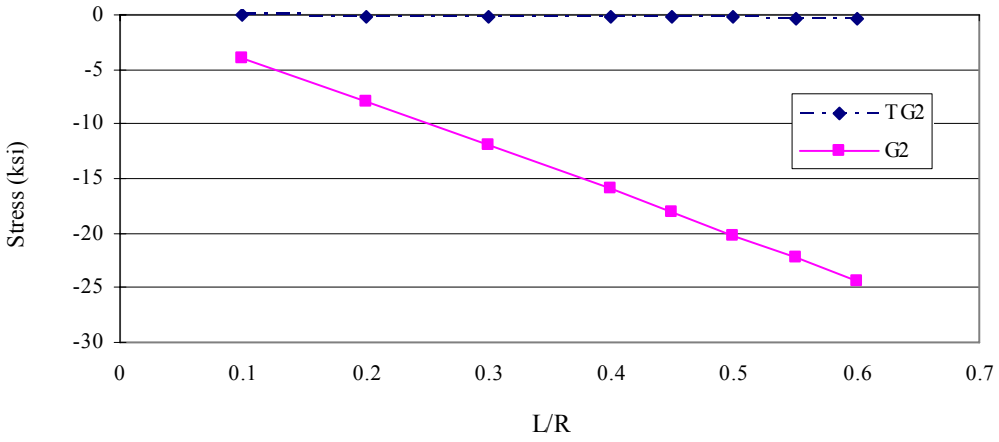

Figure 7.29 Maximum Warping Normal Stress vs. Girder Curvature

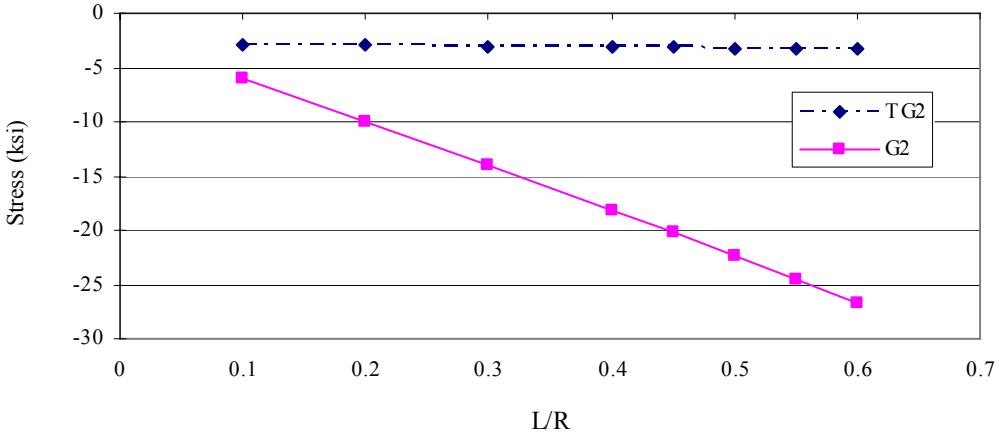

Figure 7.30 Maximum Total Normal Stress vs. Girder Curvature

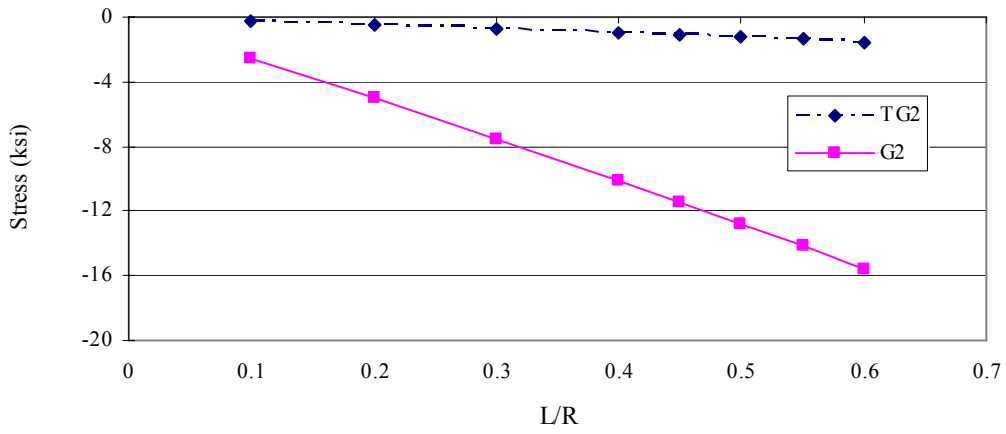

Figure 7.31 Maximum St.Venant Shear Stress vs. Girder Curvature

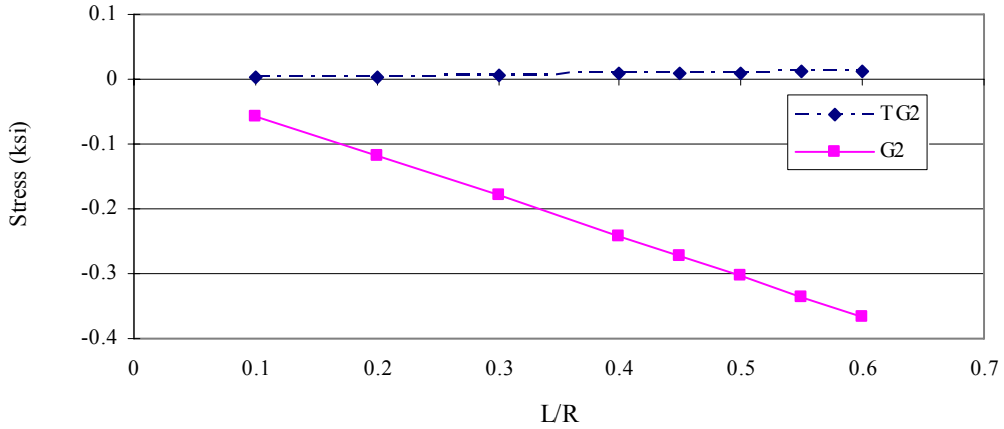

Figure 7.32 Maximum Warping Shear Stress vs. Girder Curvature

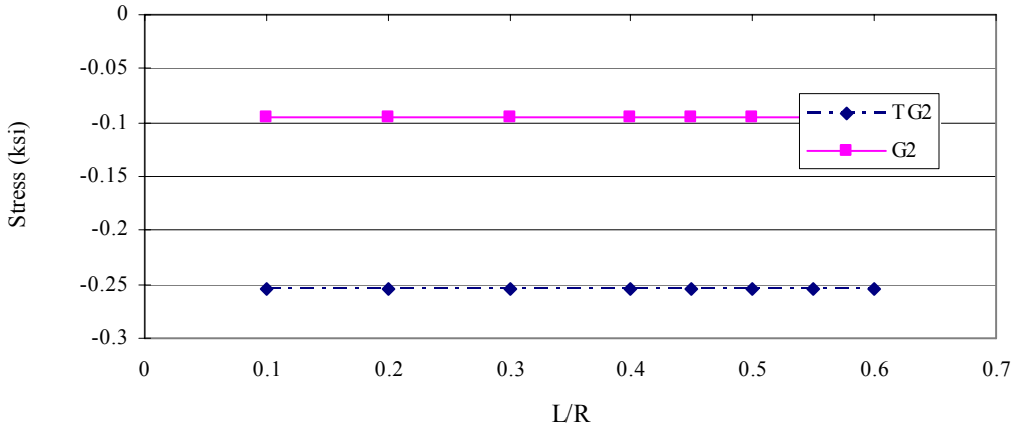

Figure 7.33 Maximum Vertical Shear Stress vs. Girder Curvature

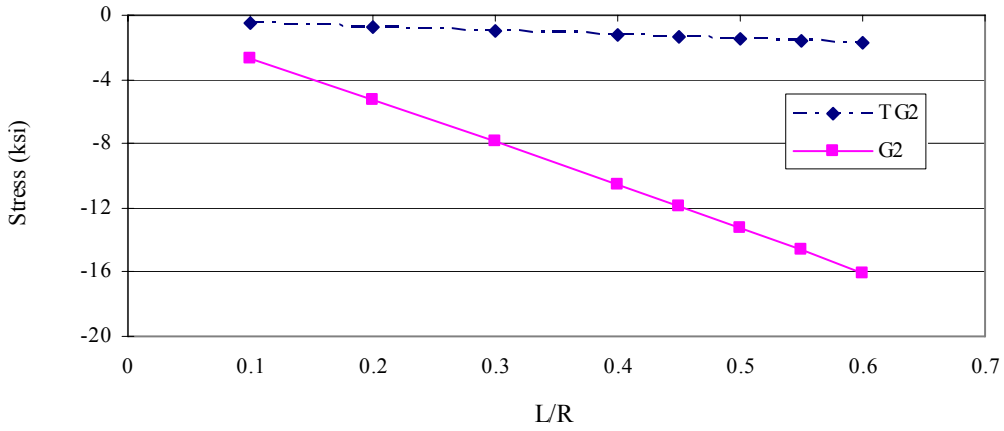

Figure 7.34 Maximum Total Shear Stress vs. Girder Curvature

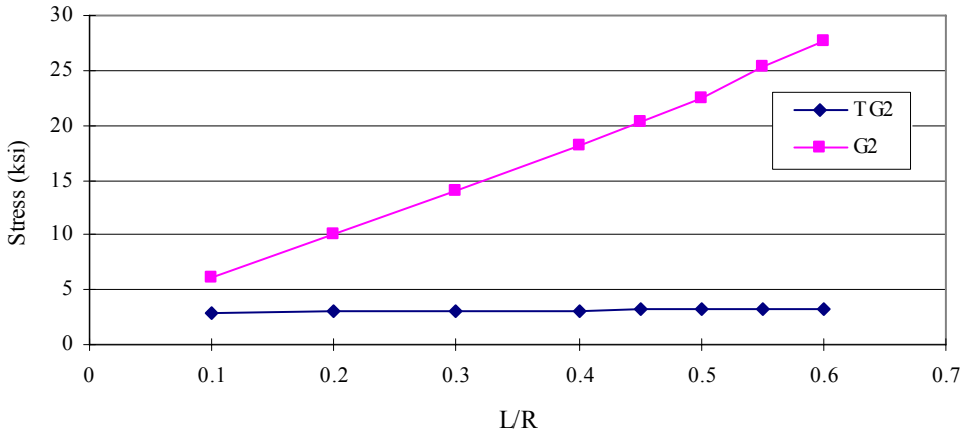

Figure 7.35 Maximum Von-Mises Stress vs. Girder Curvature

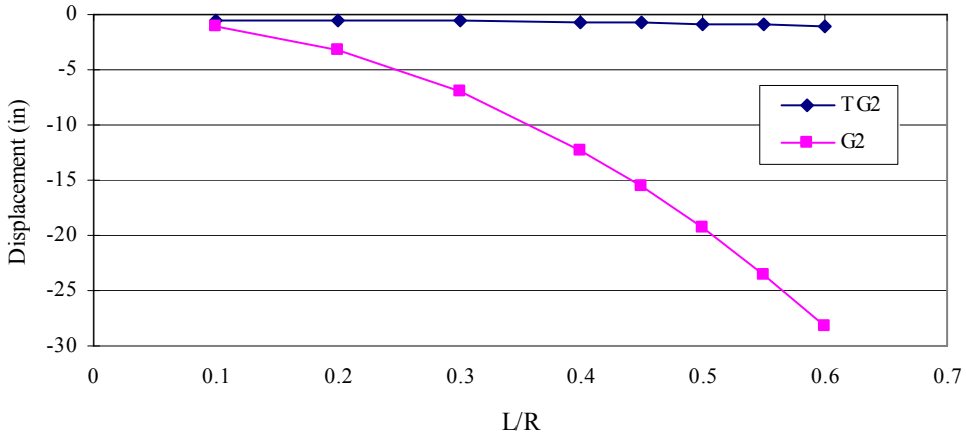

Figure 7.36 Maximum Vertical Displacement vs. Girder Curvature

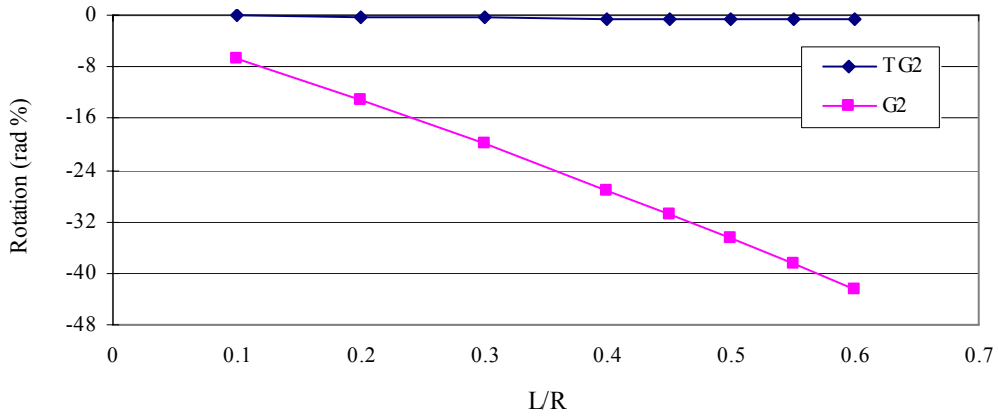

Figure 7.37 Maximum Cross Section Rotaion vs. Girder Curvature

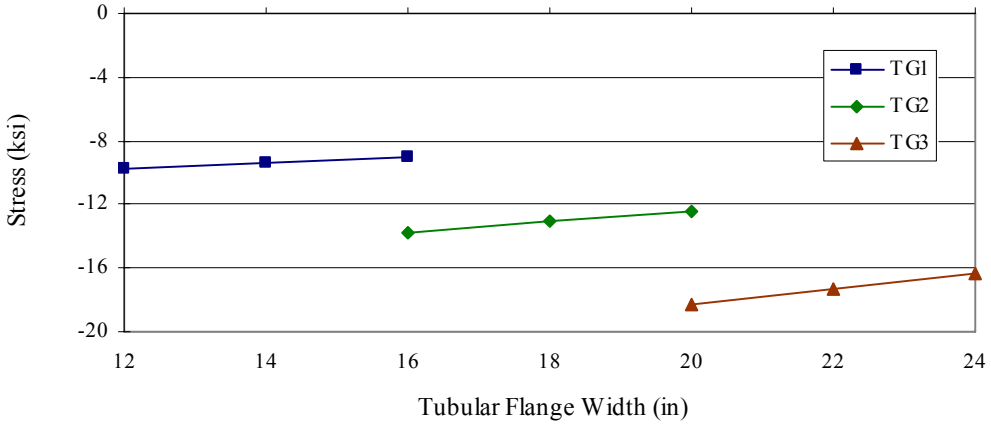

Figure 7.38 Maximum Bending Normal Stress vs. Tubular Flange Width

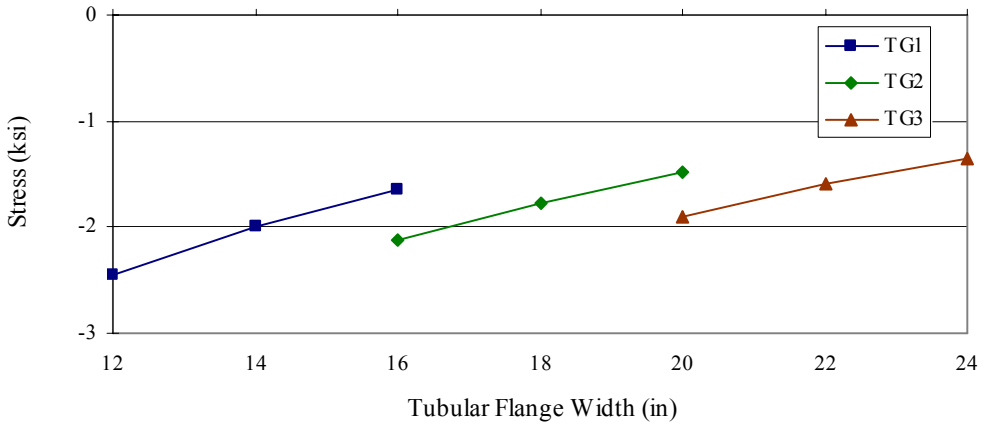

Figure 7.39 Maximum Warping Normal Stress vs. Tubular Flange Width

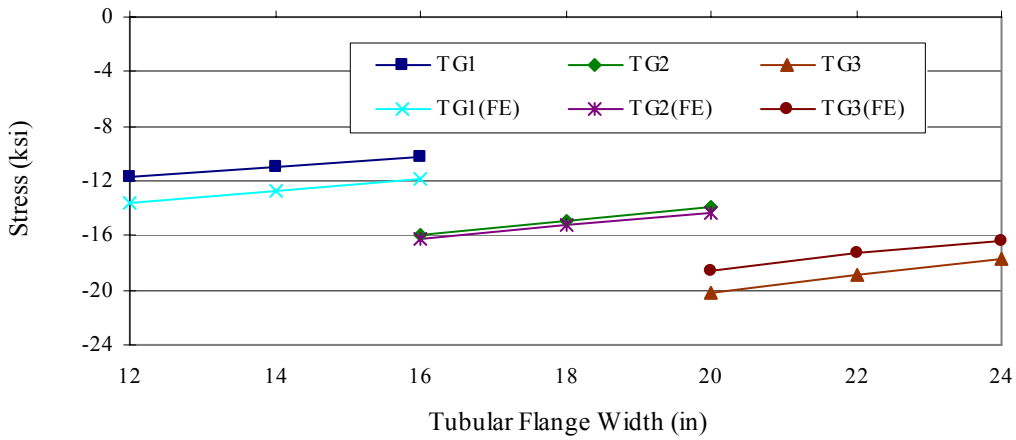

Figure 7.40 Maximum Total Normal Stress vs. Tubular Flange Width

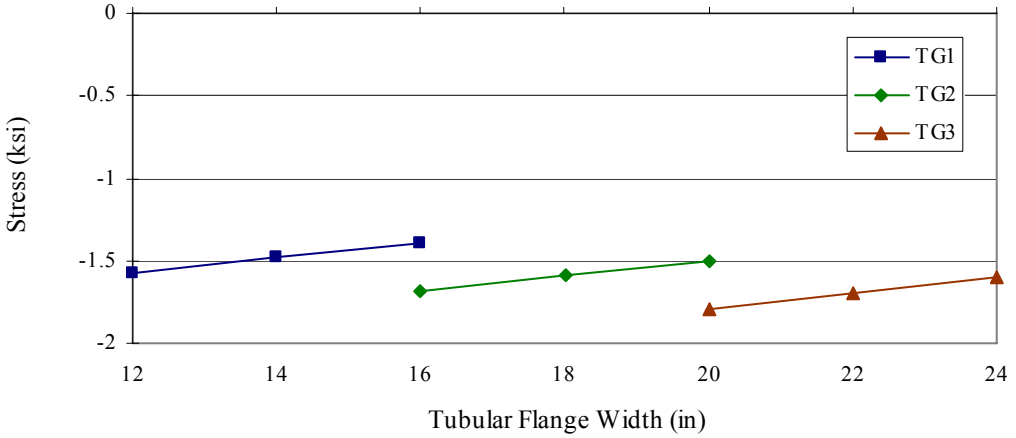

Figure 7.41 Maximum St.Venant Shear Stress vs. Tubular Flange Width

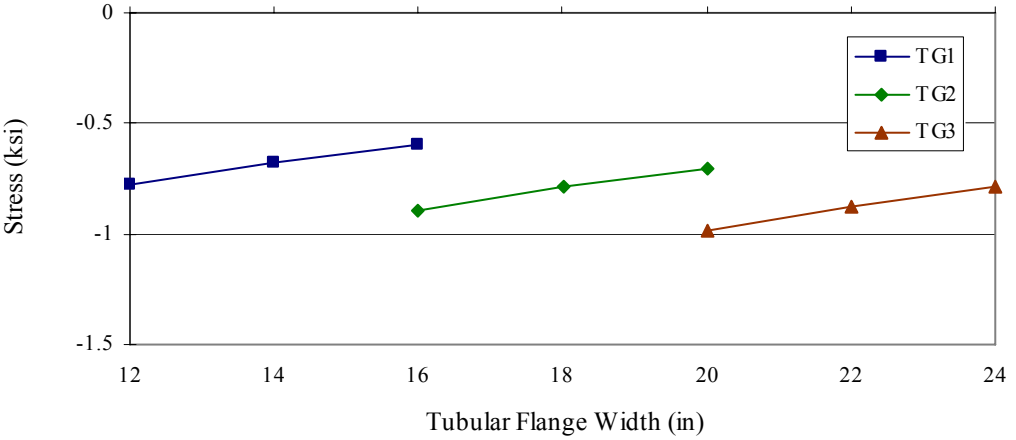

Figure 7.42 Maximum Warping Shear Stress vs. Tubular Flange Width

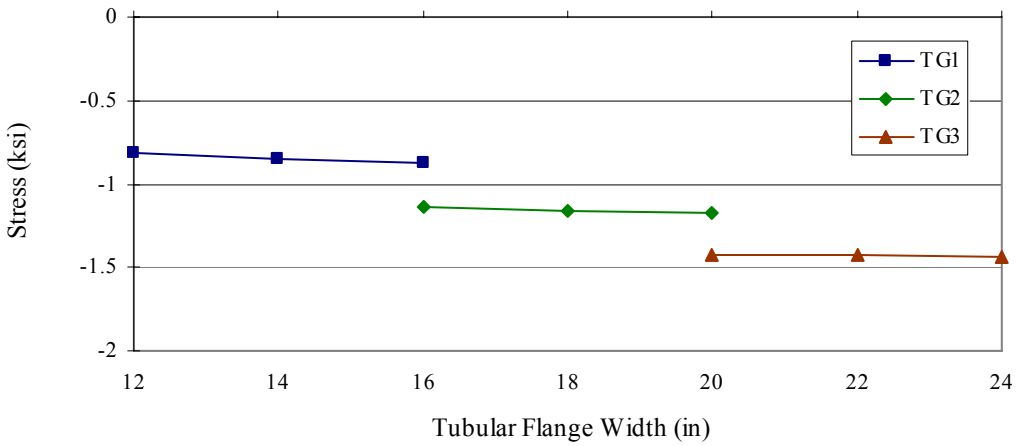

Figure 7.43 Maximum Vertical Shear Stress vs. Tubular Flange Width

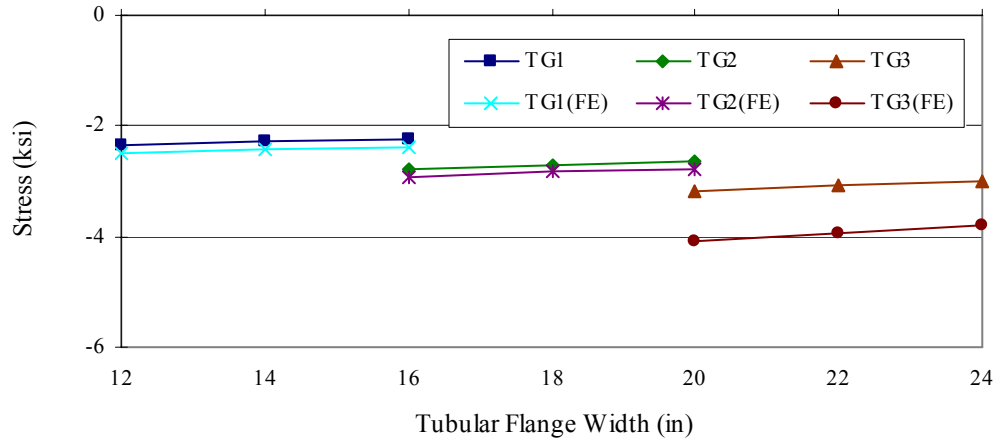

Figure 7.44 Maximum Total Shear Stress vs. Tubular Flange Width

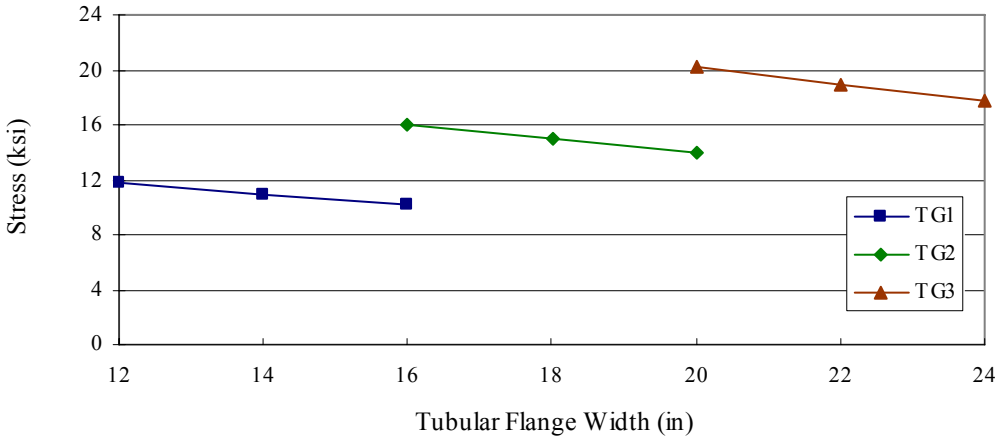

Figure 7.45 Maximum Von Mises Stress vs. Tubular Flange Width

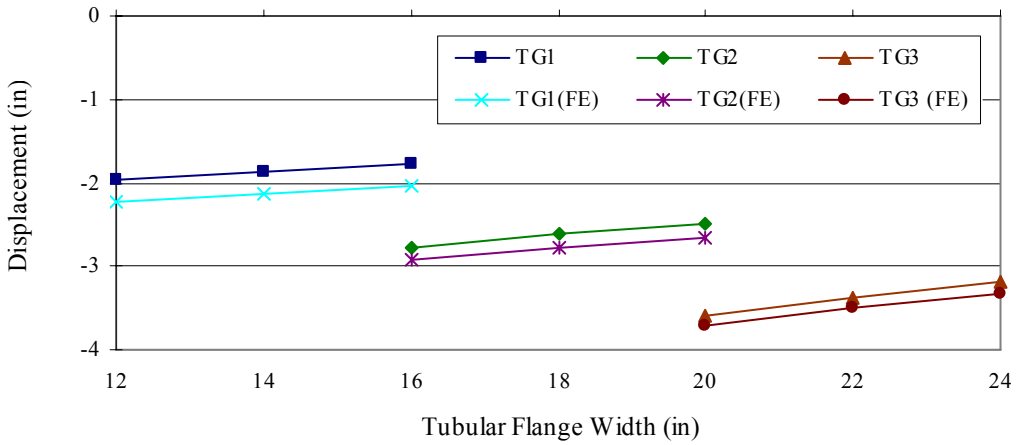

Figure 7.46 Maximum Vertical Displacement vs. Tubular Flange Width

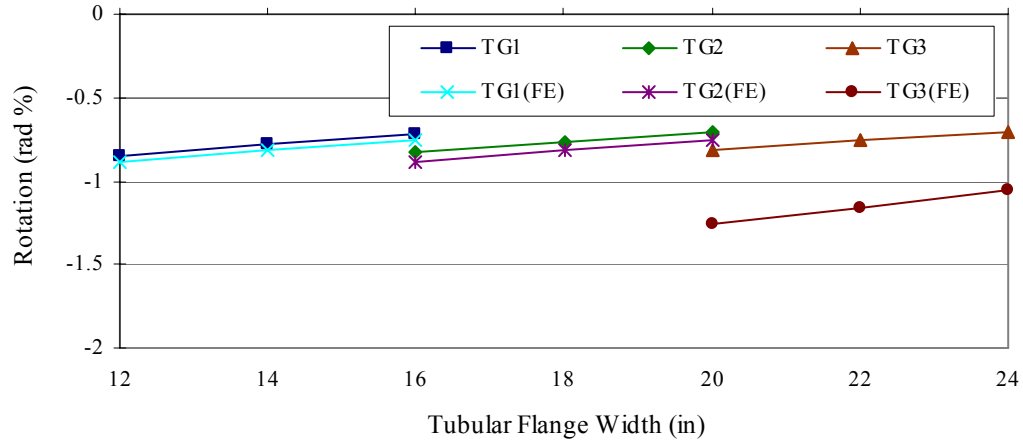

Figure 7.47 Maximum Cross Section Rotation vs. Tubular Flange Width

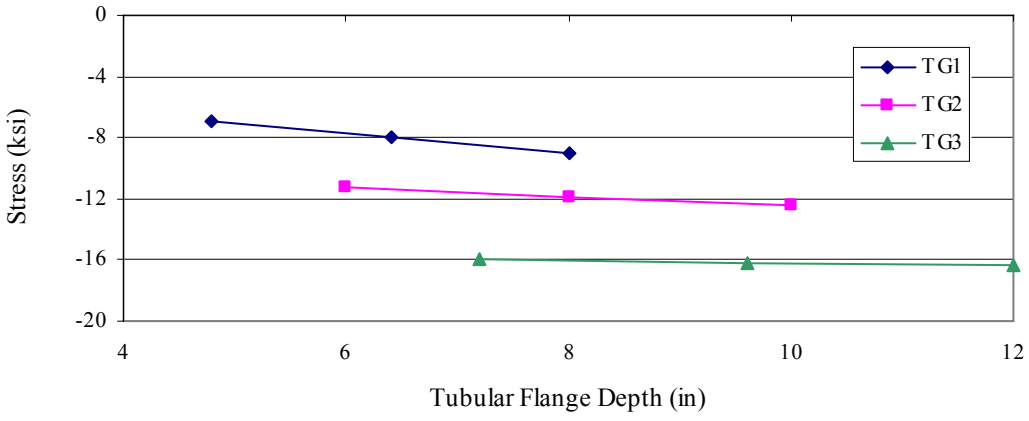

Figure 7.48 Maximum Bending Normal Stress vs. Tubular Flange Depth

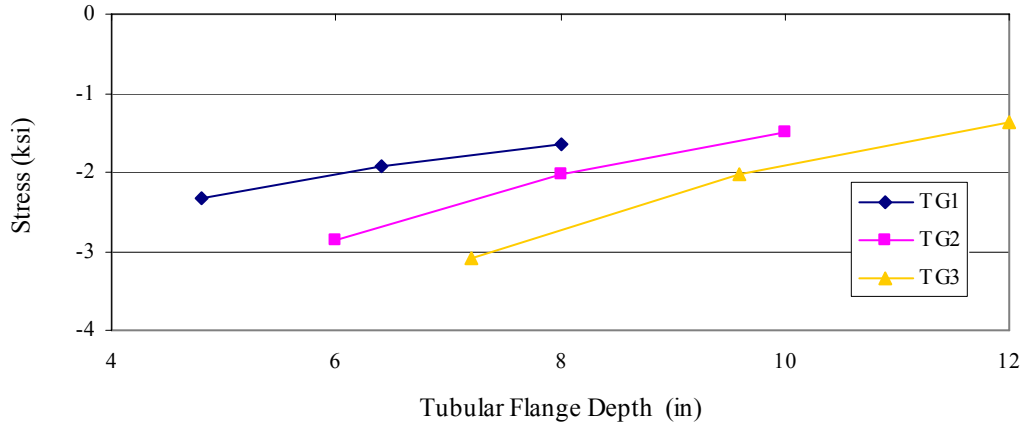

Figure 7.49 Maximum Warping Normal Stress vs. Tubular Flange Depth

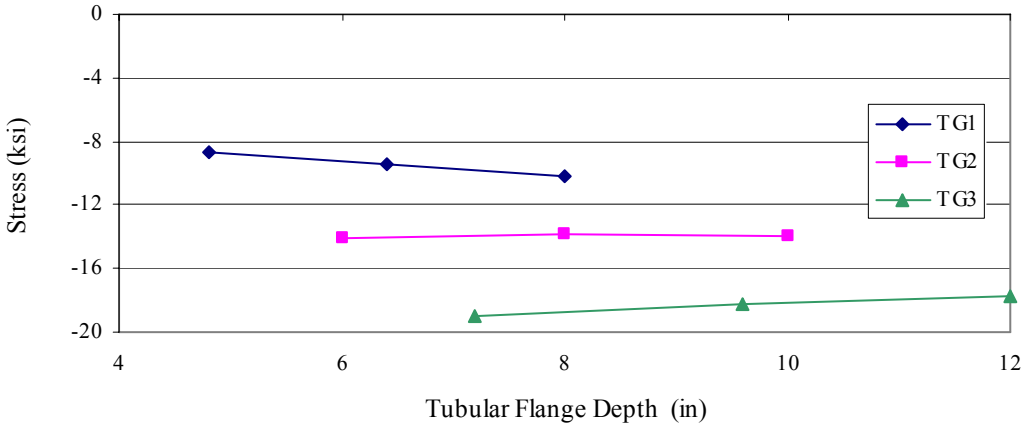

Figure 7.50 Maximum Total Normal Stress vs. Tubular Flange Depth

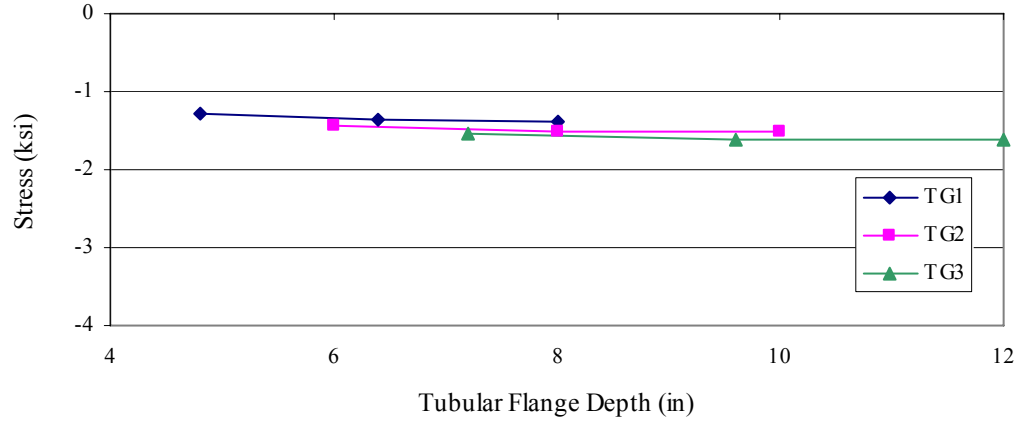

Figure 7.51 Maximum St.Venant Shear Stress vs. Tubular Flange Depth

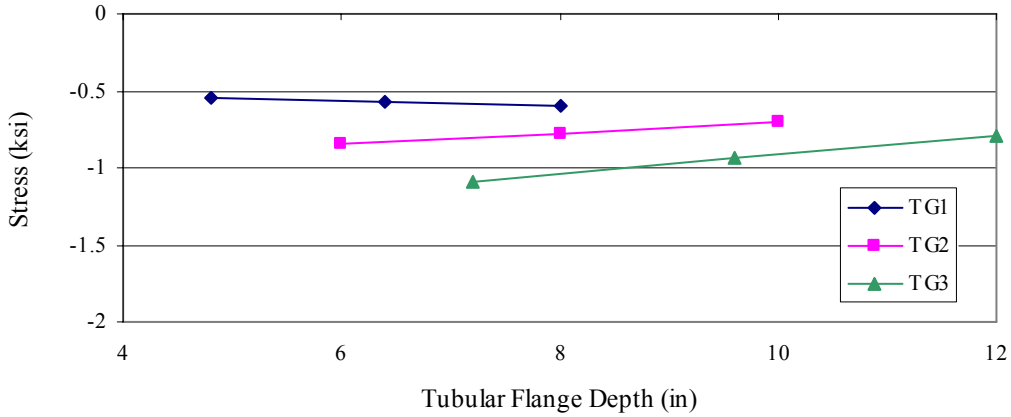

Figure 7.52 Maximum Warping Shear Stress vs. Tubular Flange Depth

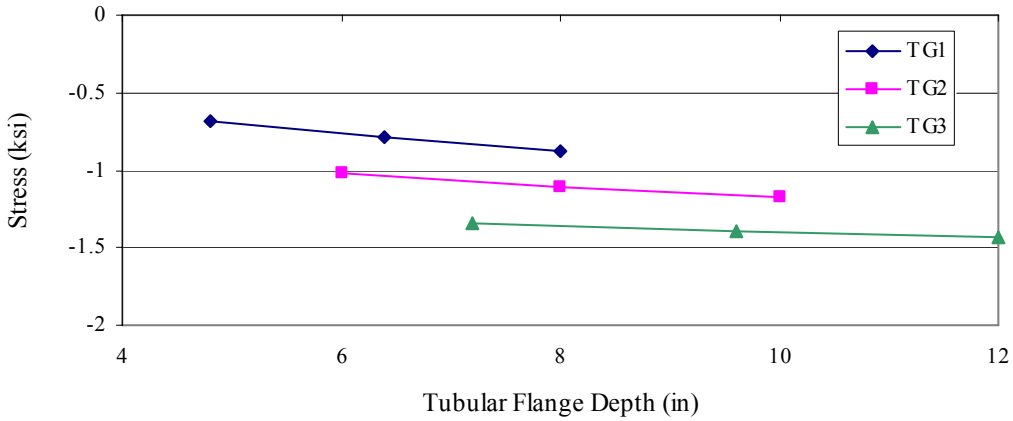

Figure 7.53 Maximum Vertical Shear Stress vs. Tubular Flange Depth

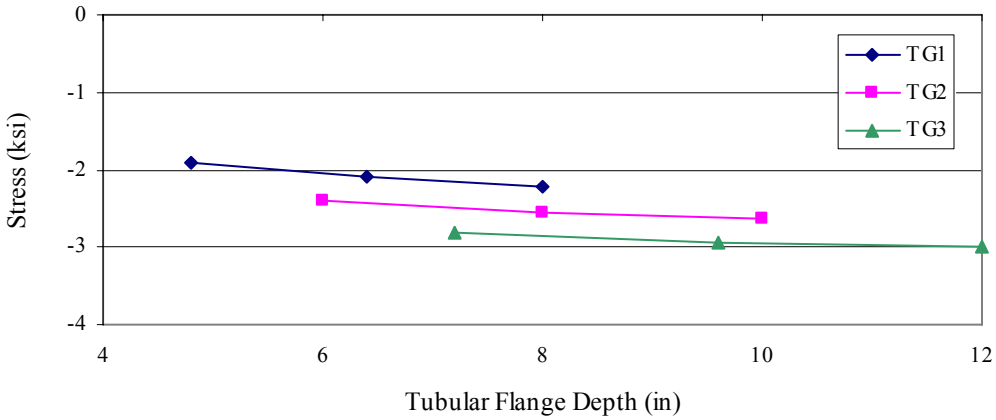

Figure 7.54 Maximum Total Shear Stress vs. Tubular Flange Depth

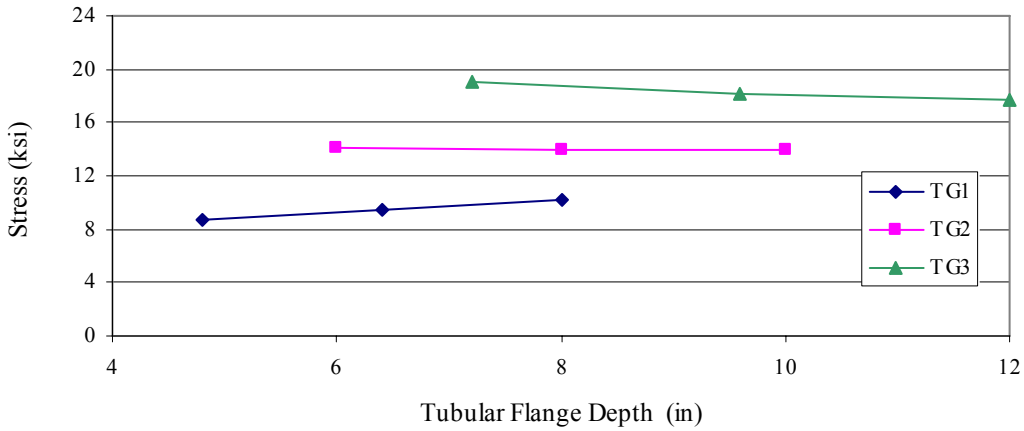

Figure 7.55 Maximum Von-Mises Stress vs. Tubular Flange Depth

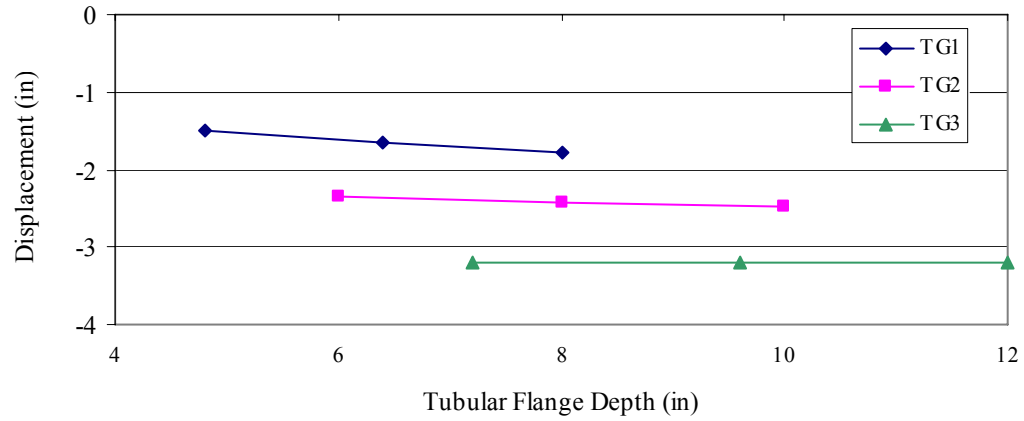

Figure 7.56 Maximum Vertical Displacement vs. Tubular Flange Depth

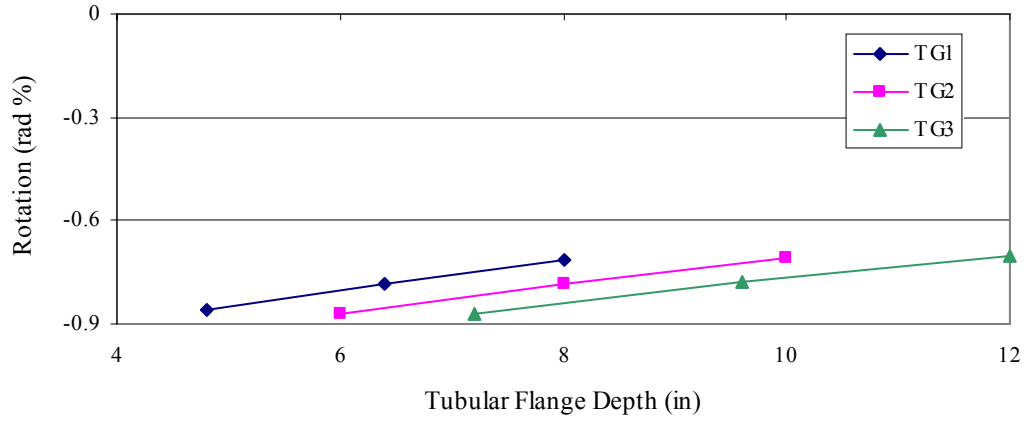

Figure 7.57 Maximum Cross Section Rotation vs. Tubular Flange Depth

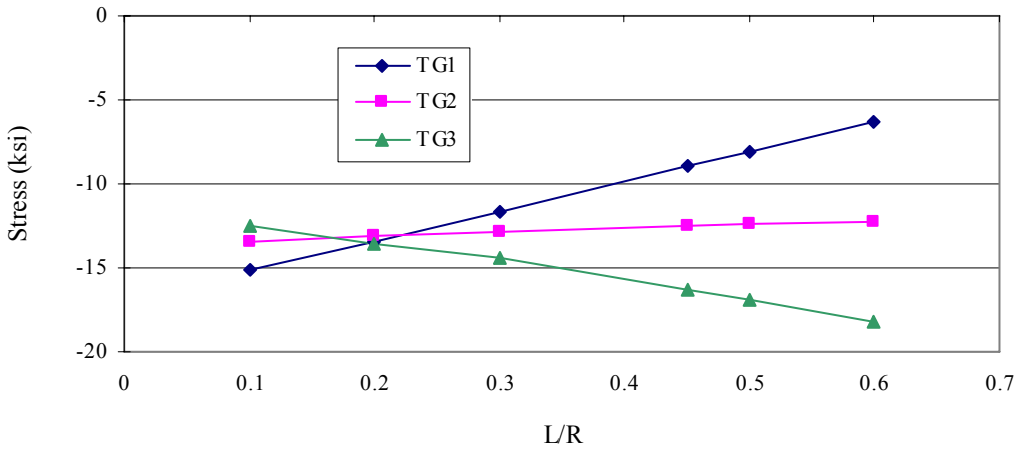

Figure 7.58 Maximum Bending Normal Stress vs. Girder Curvature for TFG System

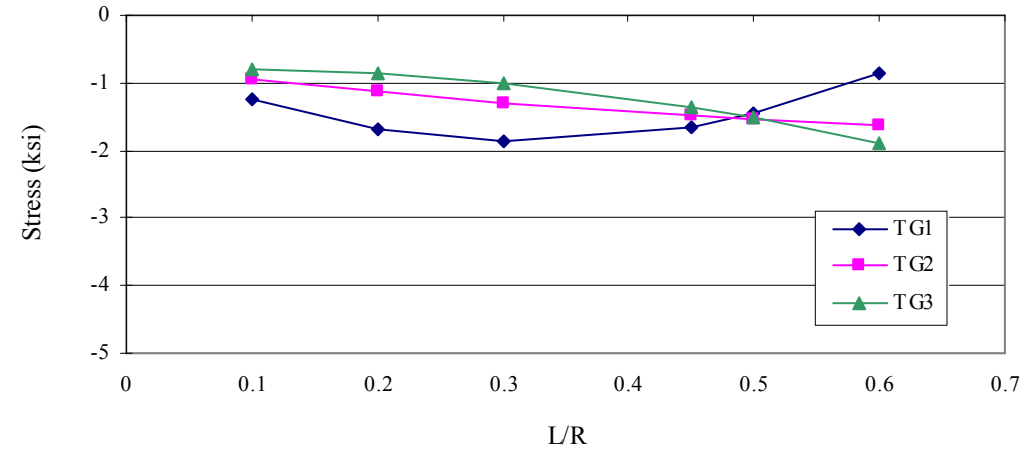

Figure 7.59 Maximum Warping Normal Stress vs. Girder Curvature for TFG System

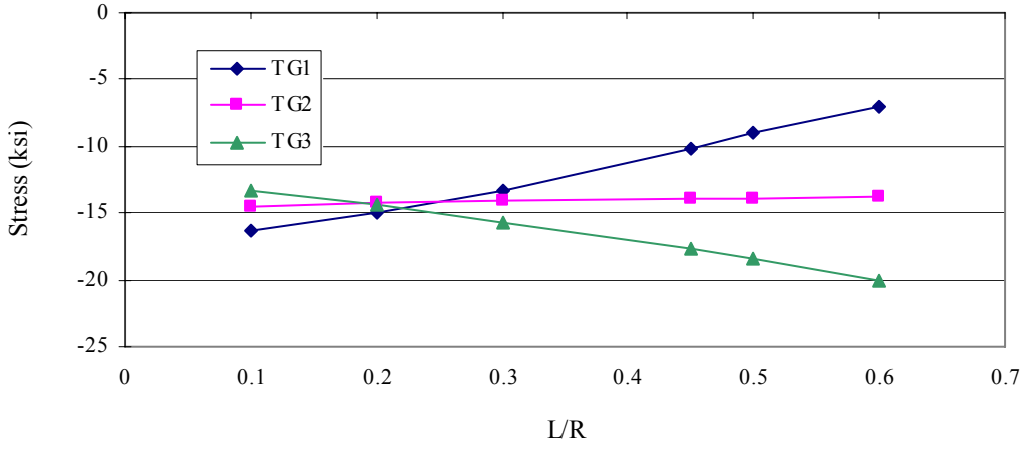

Figure 7.60 Maximum Total Normal Stress vs. Girder Curvature for TFG System

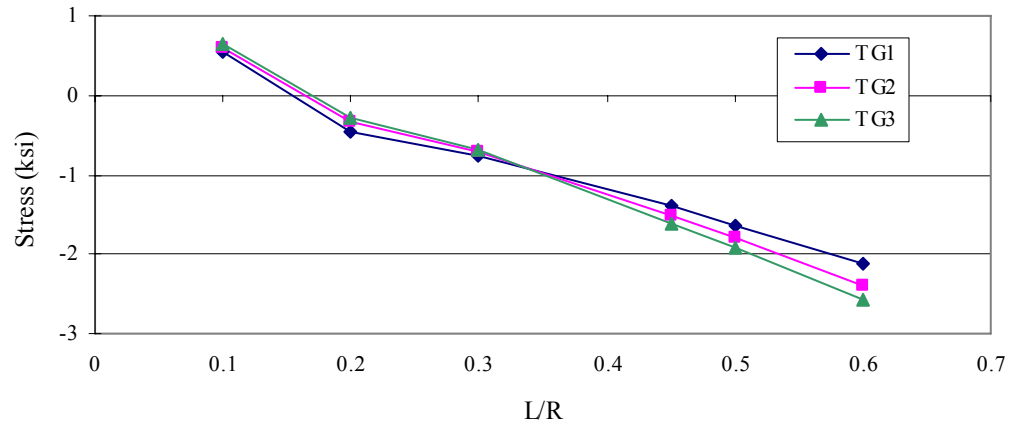

Figure 7.61 Maximum St. Venant Shear Stress vs. Girder Curvature for TFG System

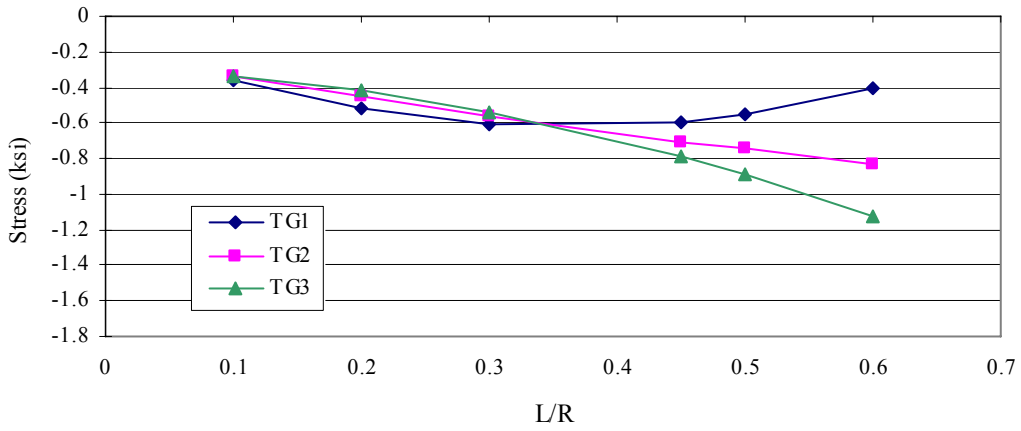

Figure 7.62 Maximum Warping Shear Stress vs. Girder Curvature for TFG System

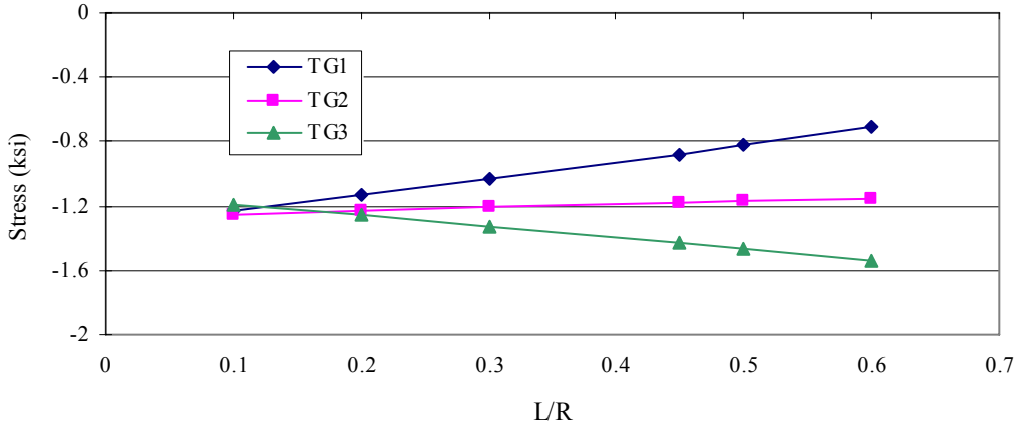

Figure 7.63 Maximum Vertical Shear Stress vs. Girder Curvature for TFG System

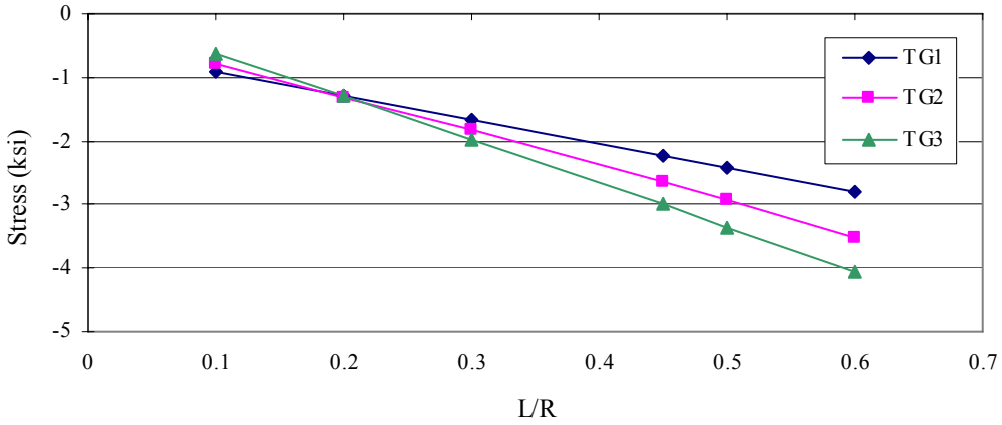

Figure 7.64 Maximum Total Shear Stress vs. Girder Curvature for TFG System

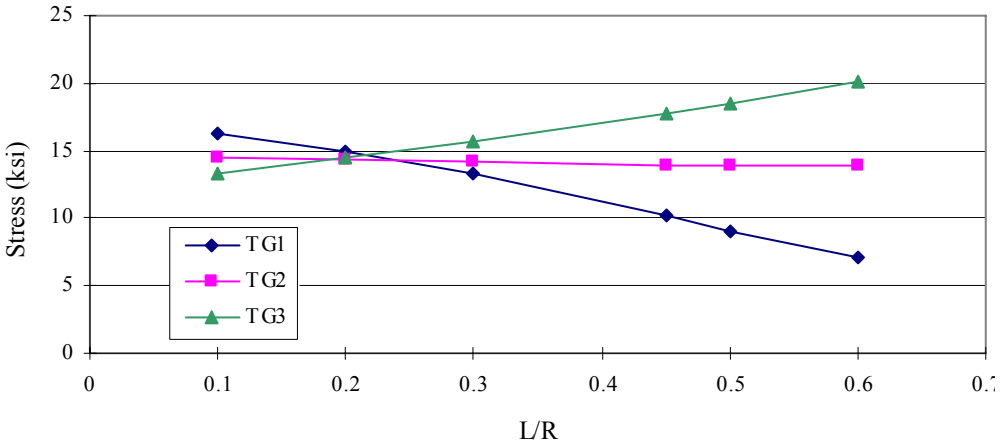

Figure 7.65 Maximum Von-Mises Stress vs. Girder Curvature for TFG System

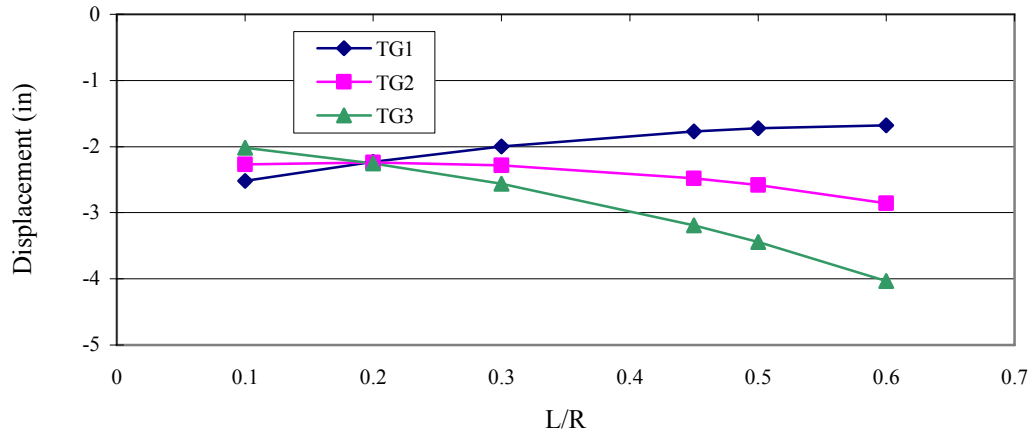

Figure 7.66 Maximum Vertical Displacement vs. Girder Curvature for TFG System

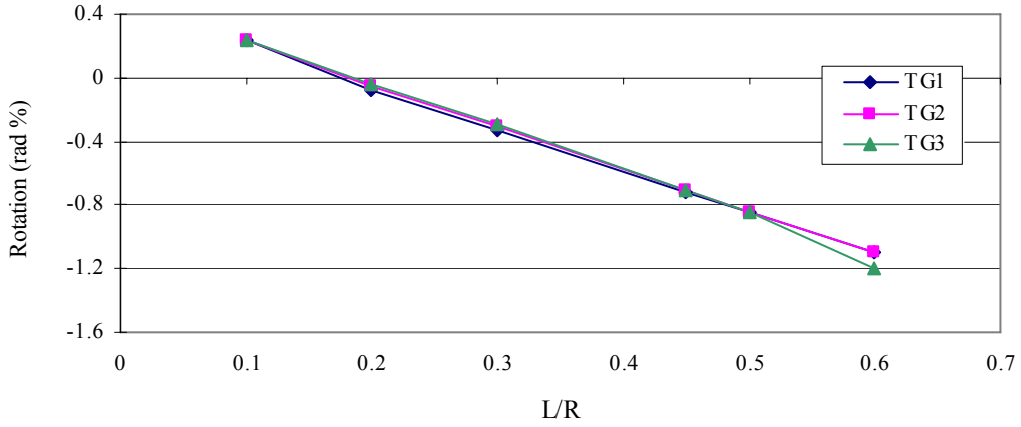

Figure 7.67 Maximum Cross Section Rotation vs. Girder Curvature for TFG System

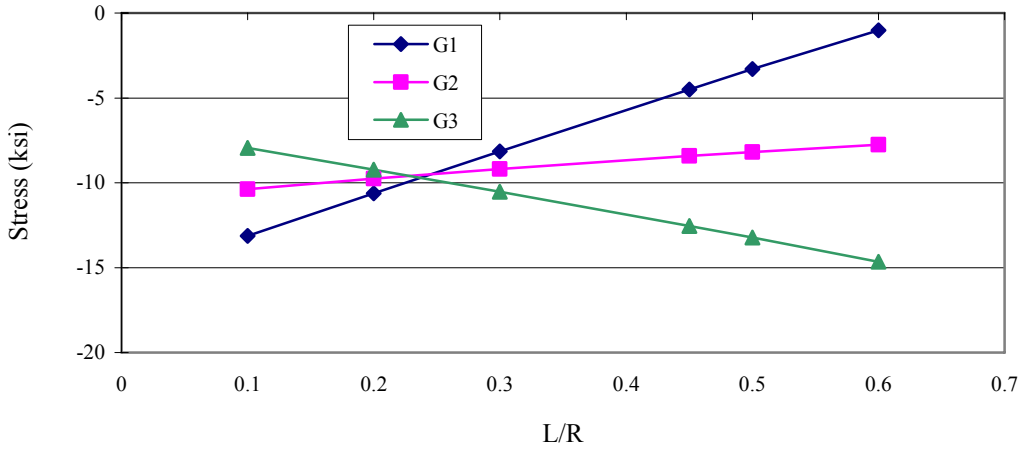

Figure 7.68 Maximum Bending Normal Stress vs. Girder Curvature for I-Girder System

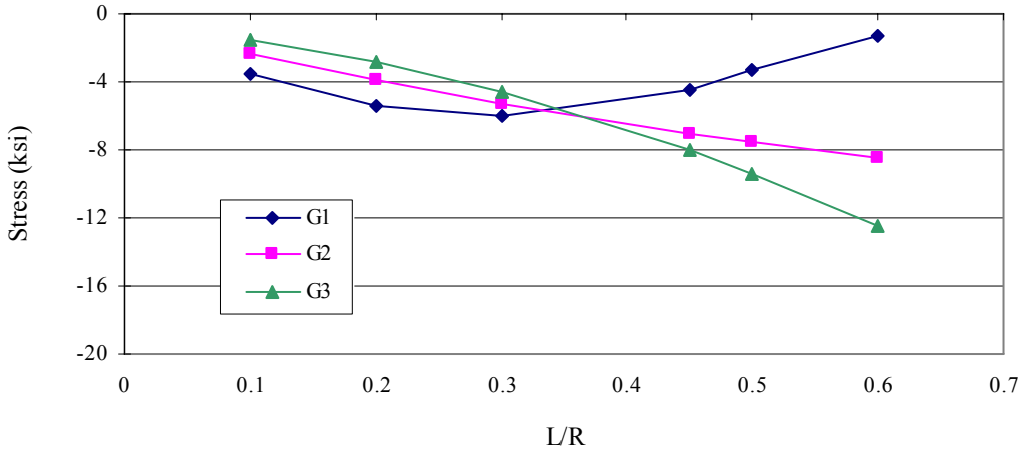

Figure 7.69 Maximum Warping Normal Stress vs. Girder Curvature for I-Girder System

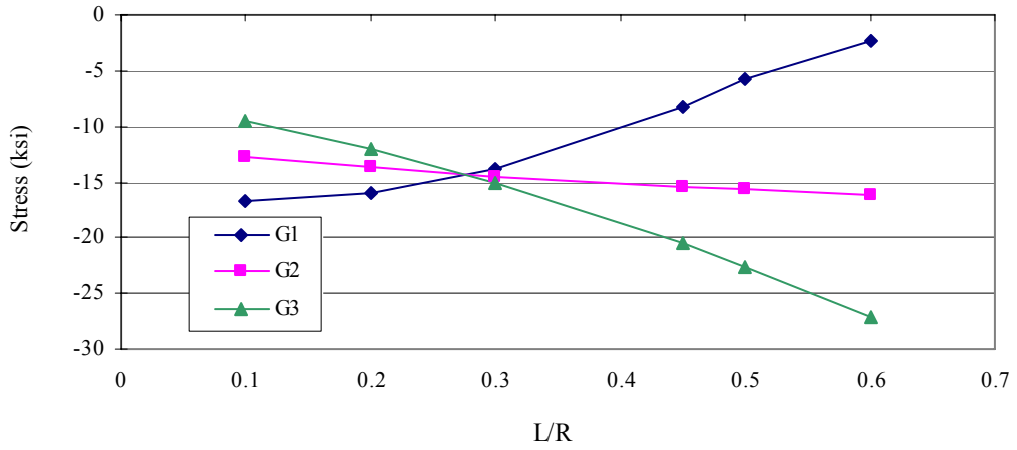

Figure 7.70 Maximum Total Normal Stress vs. Girder Curvature for I-Girder System

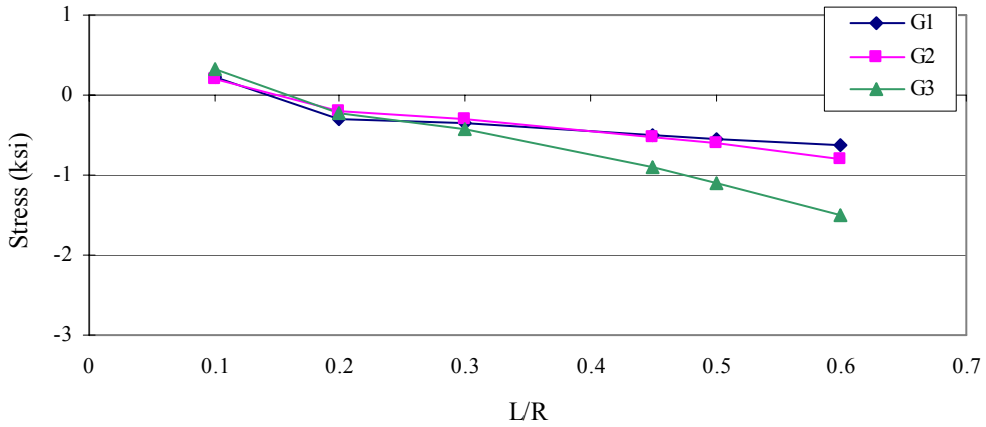

Figure 7.71 Maximum St.Venant Shear Stress vs. Girder Curvature for I-Girder System

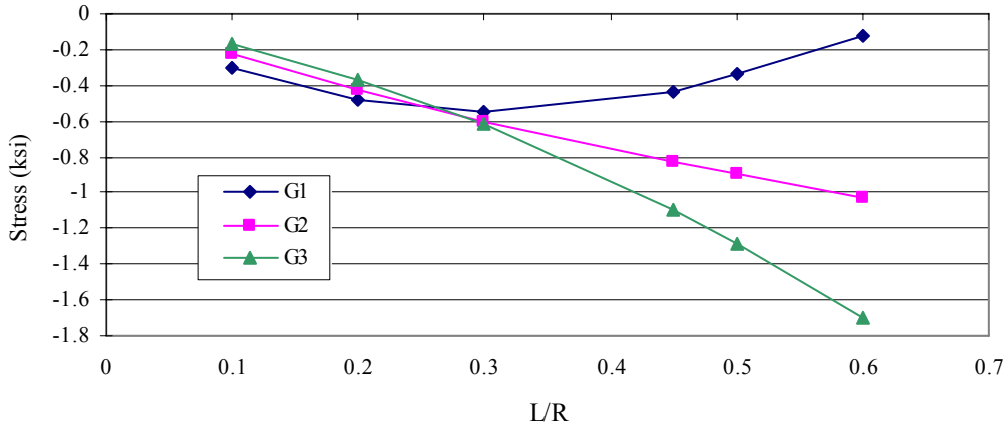

Figure 7.72 Maximum Warping Shear Stress vs. Girder Curvature for I-Girder System

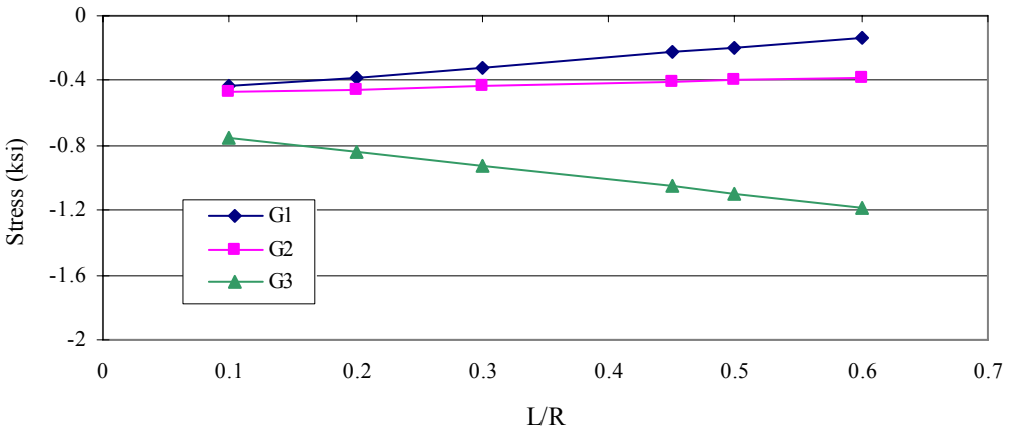

Figure 7.73 Maximum Vertical Shear Stress vs. Girder Curvature for I-Girder System

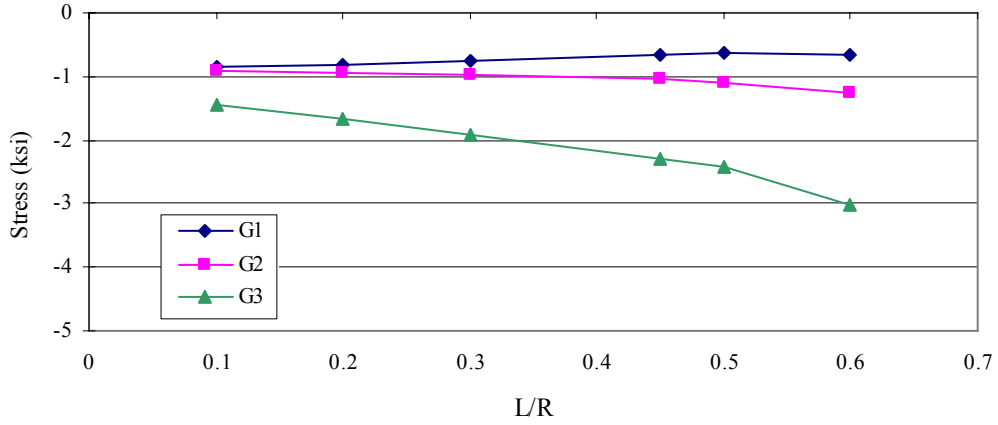

Figure 7.74 Maximum Total Shear Stress vs. Girder Curvature for I-Girder System

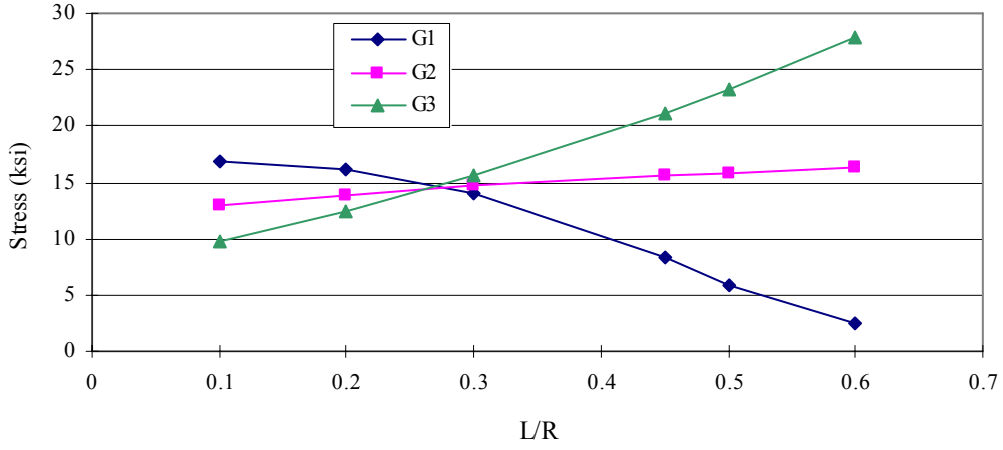

Figure 7.75 Maximum Von-Mises Stress vs. Girder Curvature for I-Girder System

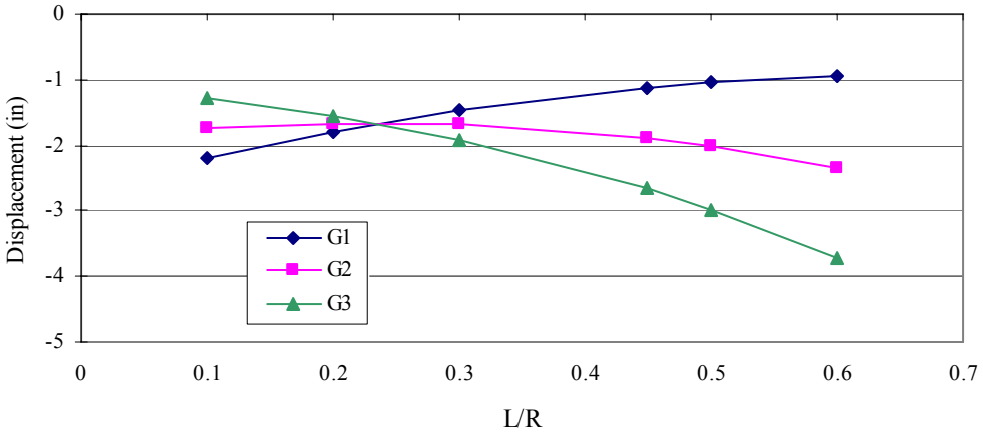

Figure 7.76 Maximum Vertical Displacement vs. Girder Curvature for I-Girder System

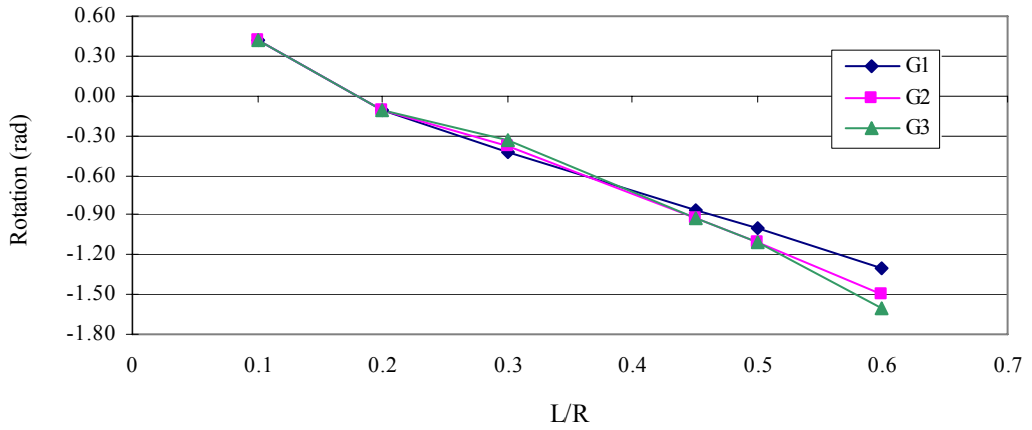

Figure 7.77 Maximum Cross Section Rotation vs. Girder Curvature for I-Girder System

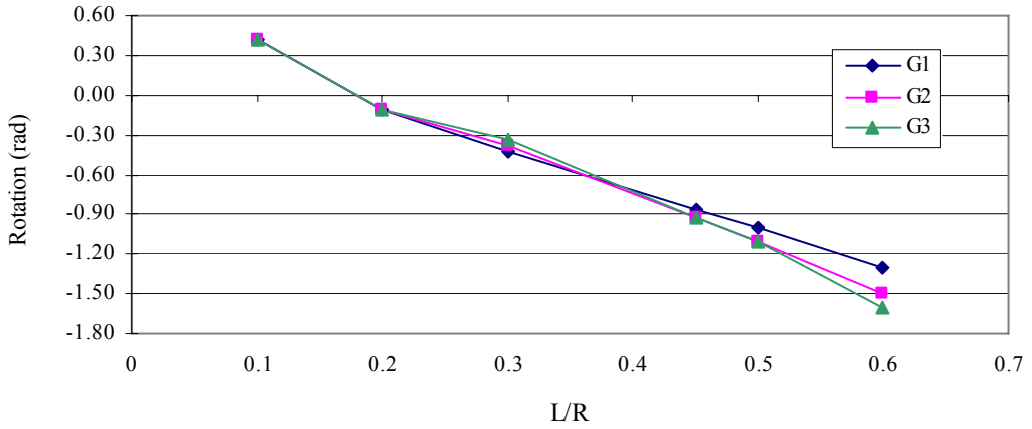

Figure 7.78 Maximum Bending Normal Stress vs. Girder Curvature

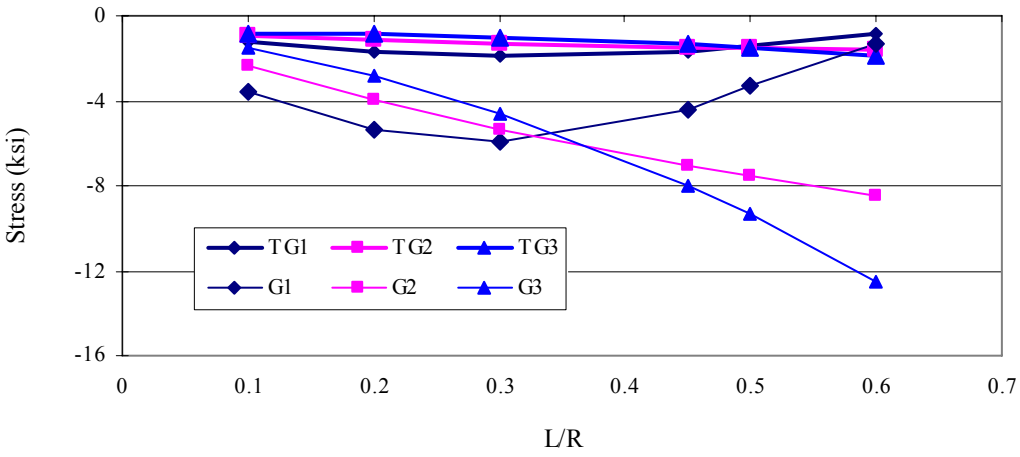

Figure 7.79 Maximum Warping Normal Stress vs. Girder Curvature

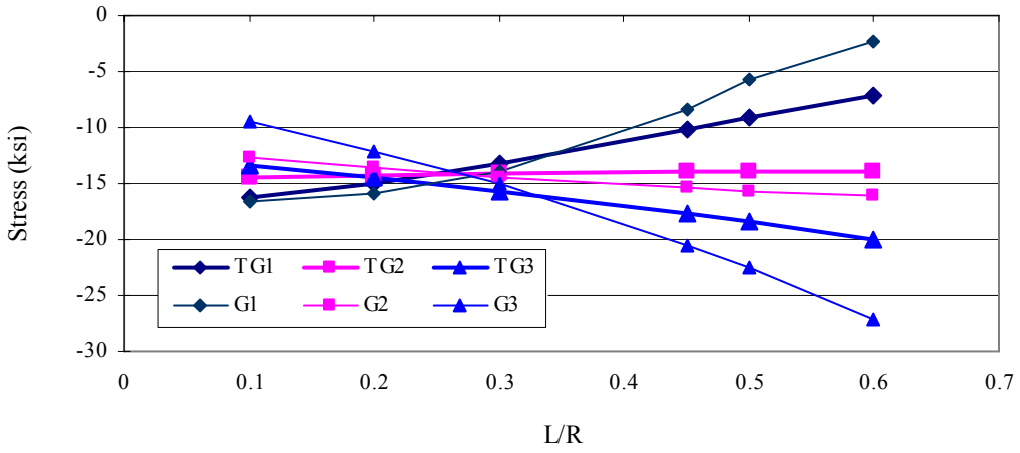

Figure 7.80 Maximum Total Normal Stress vs. Girder Curvature

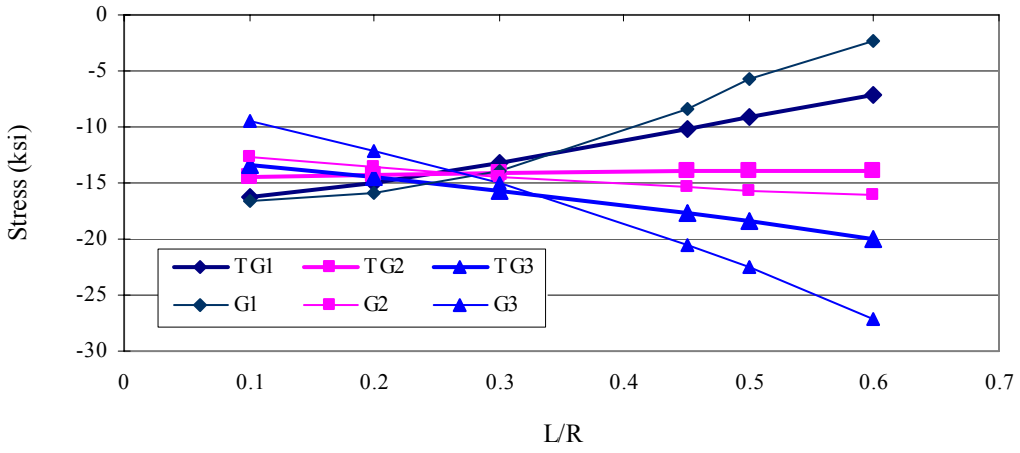

Figure 7.81 Maximum St.Venant Shear Stress vs. Girder Curvature

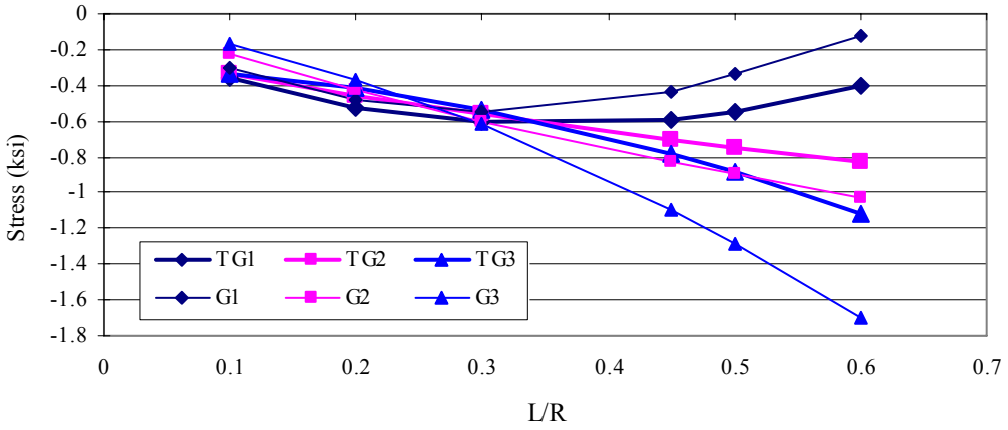

Figure 7.82 Maximum Warping Shear Stress vs. Girder Curvature

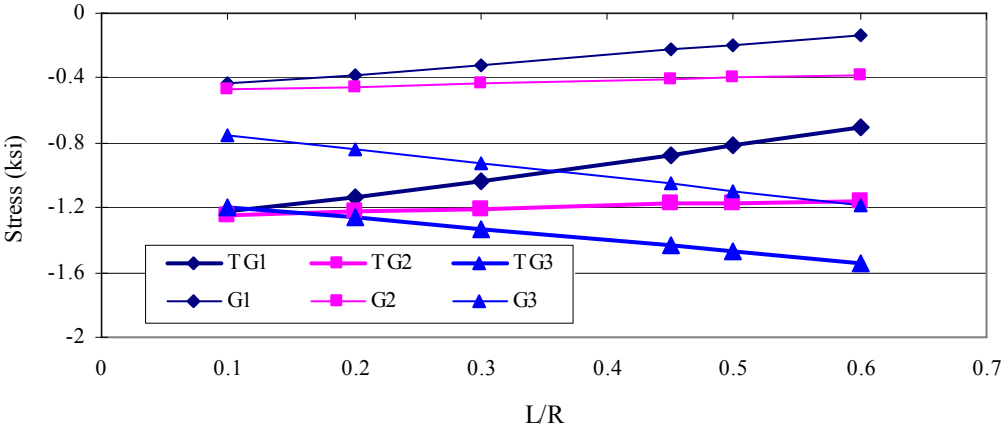

Figure 7.83 Maximum Vertical Shear Stress vs. Girder Curvature

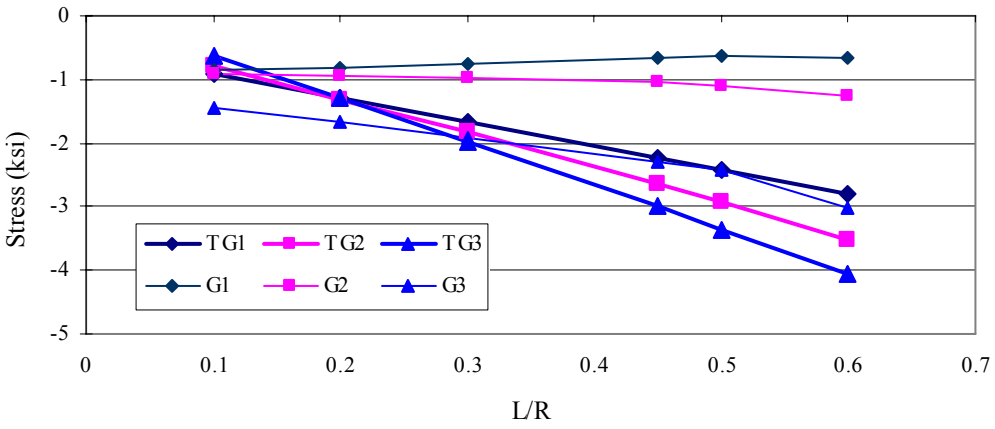

Figure 7.84 Maximum Total Shear Stress vs. Girder Curvature

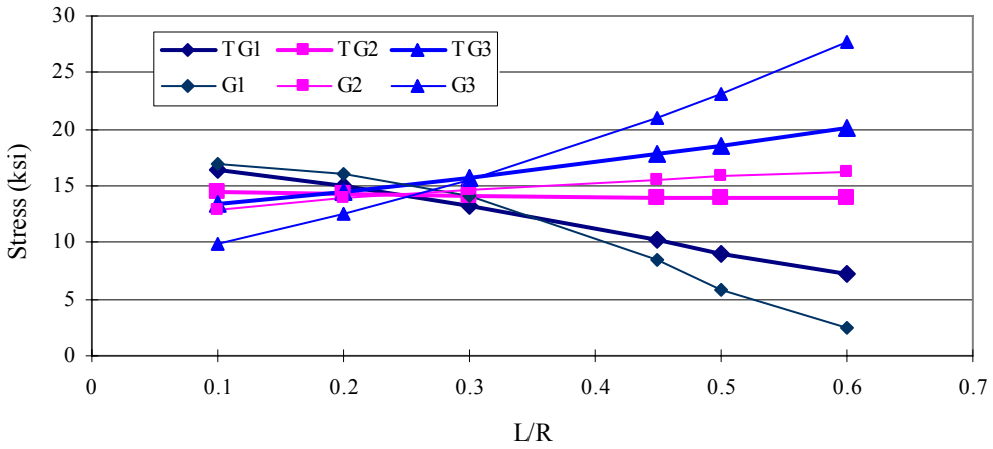

Figure 7.85 Maximum Von-Mises Stress vs. Girder Curvature

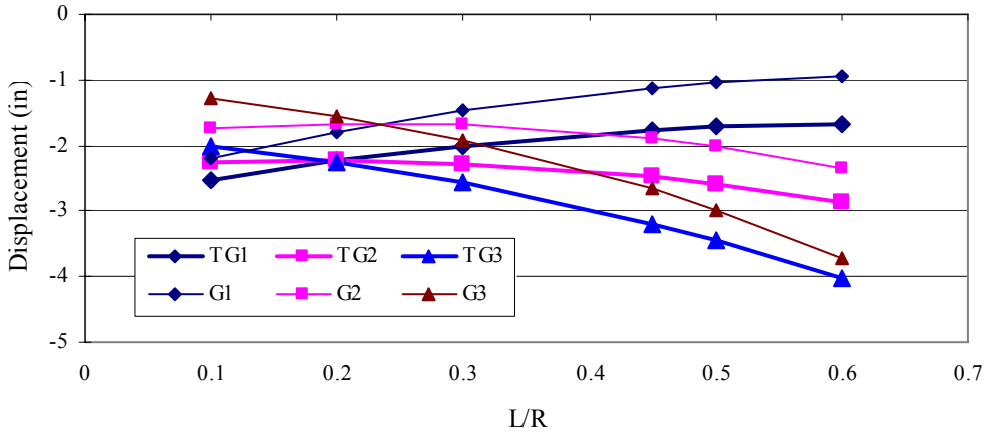

Figure 7.86 Maximum Vertical Displacement vs. Girder Curvature

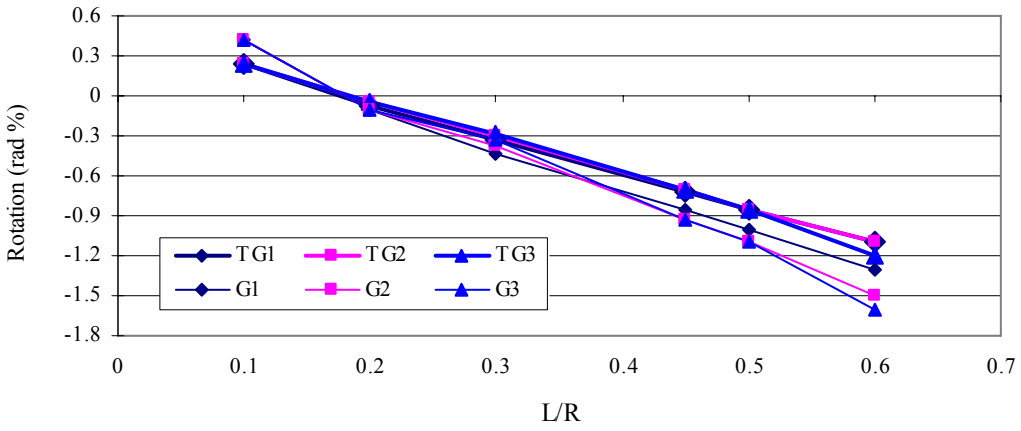

Figure 7.87 Maximum Cross Section Rotation vs. Girder Curvature

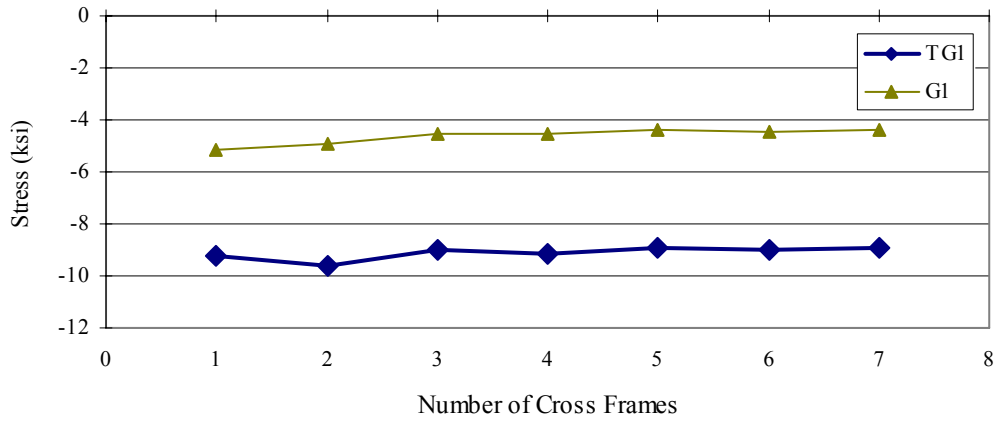

Figure 7.88 Maximum Bending Normal Stress of Inner Girder vs. Number of Cross Frames

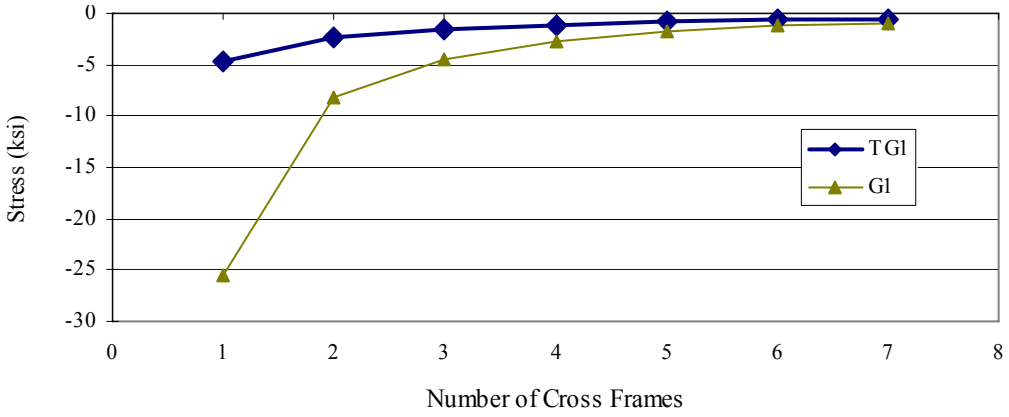

Figure 7.89 Maximum Warping Normal Stress of Inner Girder vs. Number of Cross Frames

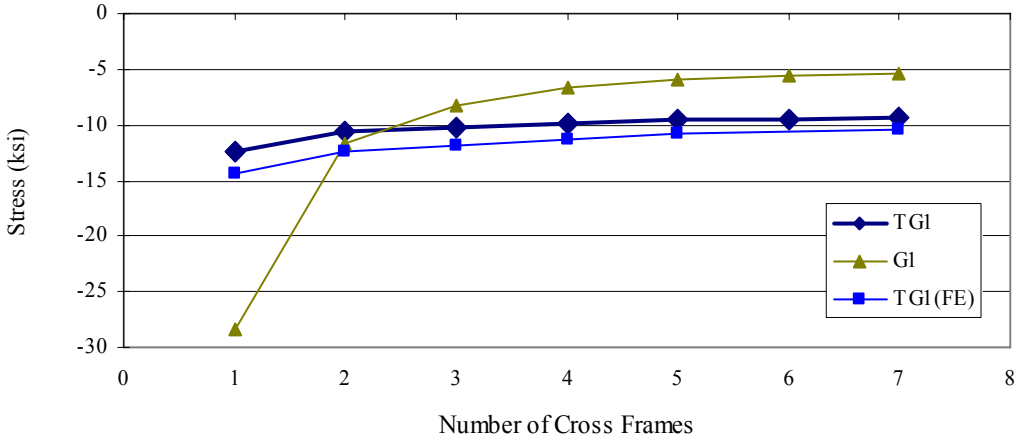

Figure 7.90 Maximum Total Normal Stress of Inner Girder vs. Number of Cross Frames

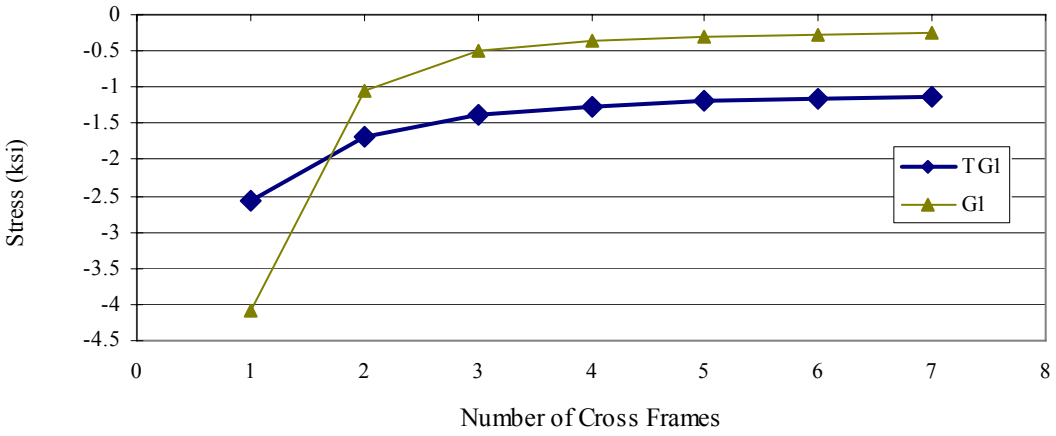

Figure 7.91 Maximum St.Venant Shear Stress of Inner Girder vs. Number of Cross Frames

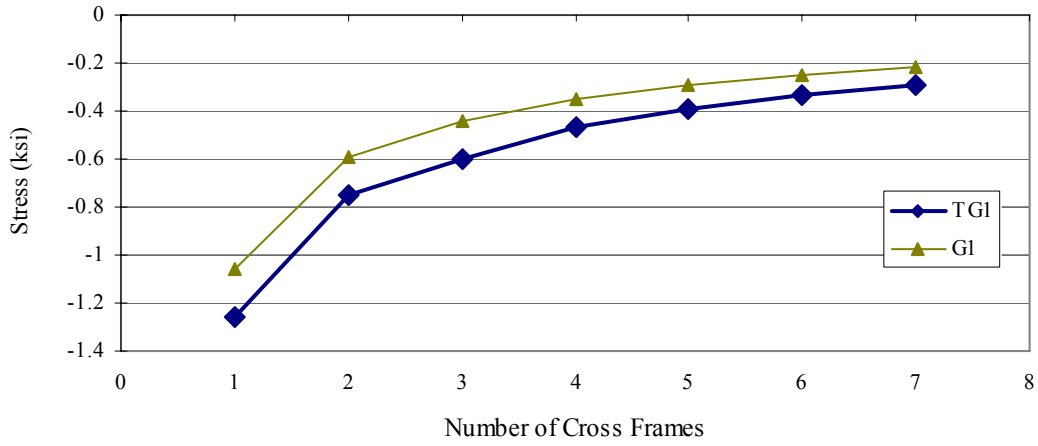

Figure 7.92 Maximum Warping Shear Stress of Inner Girder vs. Number of Cross Frames

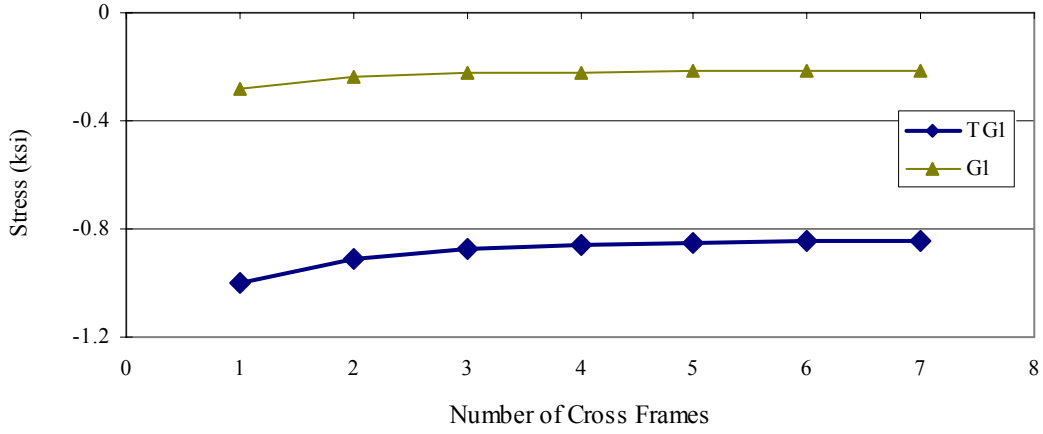

Figure 7.93 Maximum Vertical Shear Stress of Inner Girder vs. Number of Cross Frames

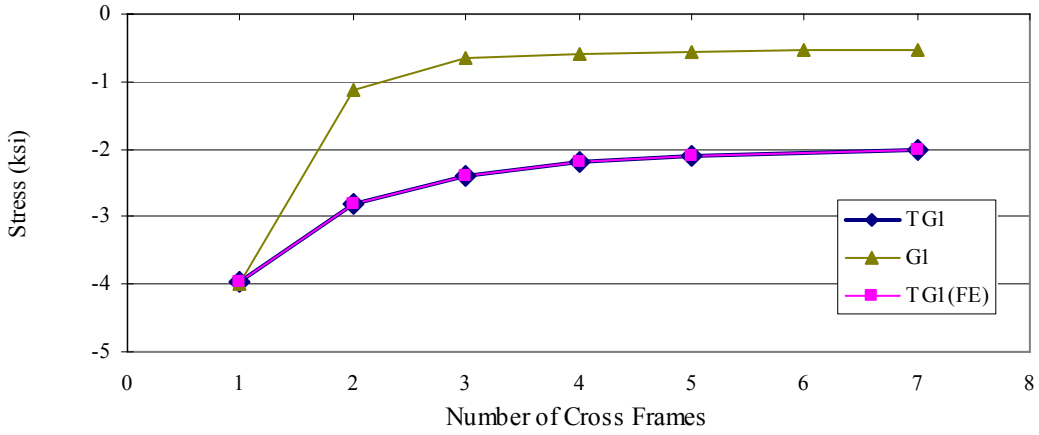

Figure 7.94 Maximum Total Shear Stress of Inner Girder vs. Number of Cross Frames

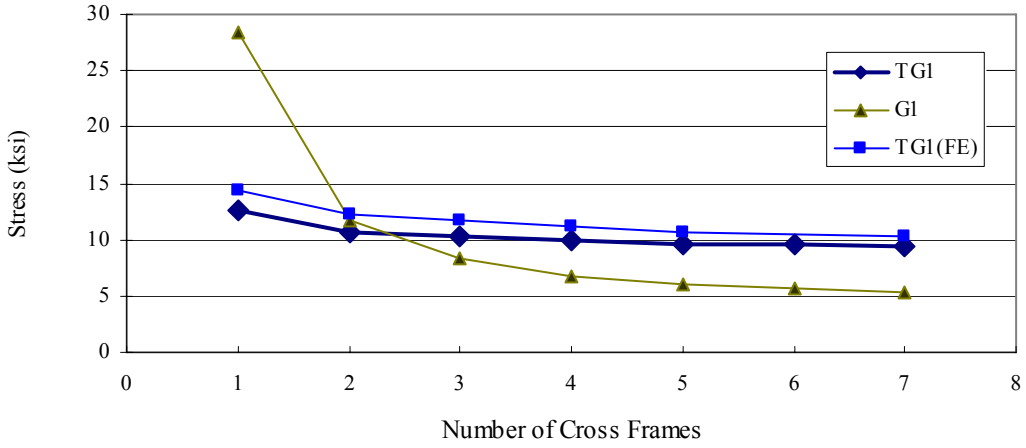

Figure 7.95 Maximum Von-Mises Stress of Inner Girder vs. Number of Cross Frames

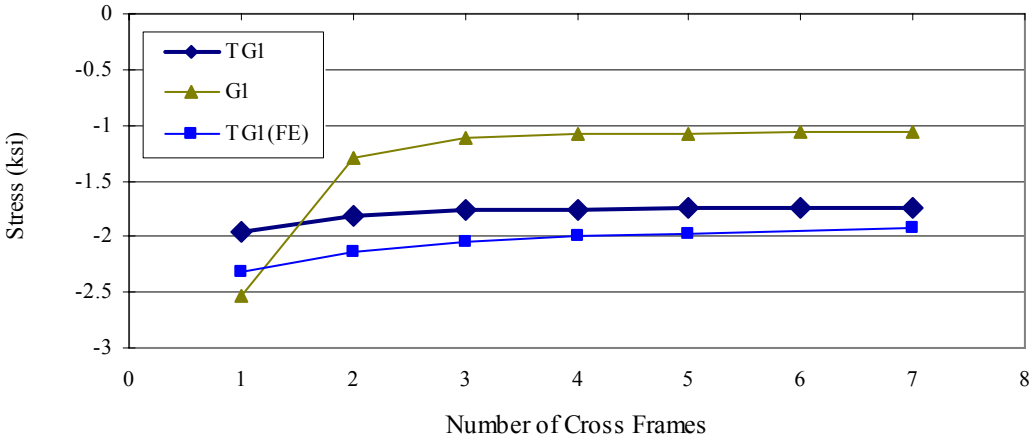

Figure 7.96 Maximum Vertical Displacement of Inner Girder vs. Number of Cross Frames

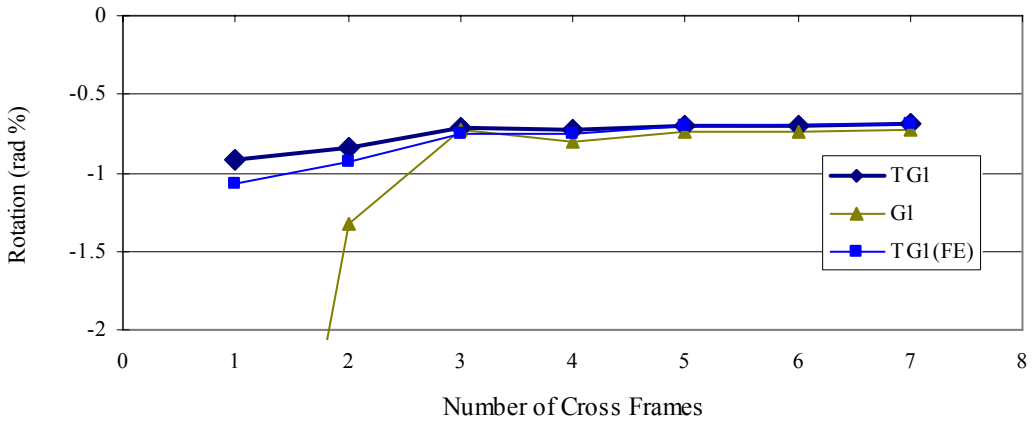

Figure 7.97 Maximum Cross Section Rotation of Inner Girder vs. Number of Cross Frames

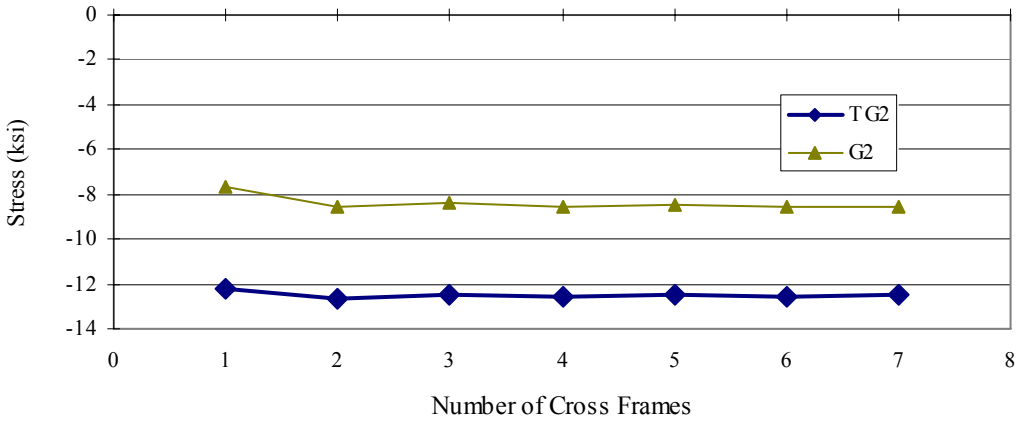

Figure 7.98 Maximum Bending Normal Stress of Middle Girder vs. Number of Cross Frames

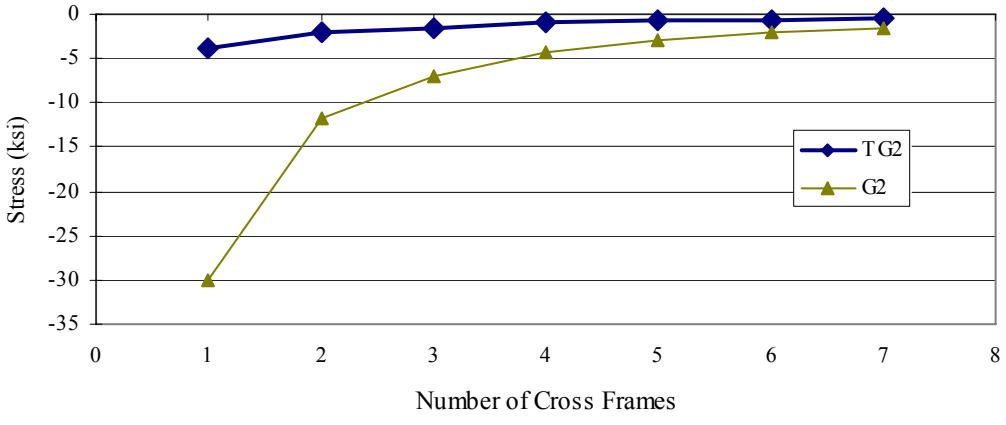

Figure 7.99 Maximum Warping Normal Stress of Middle Girder vs. Number of Cross Frames

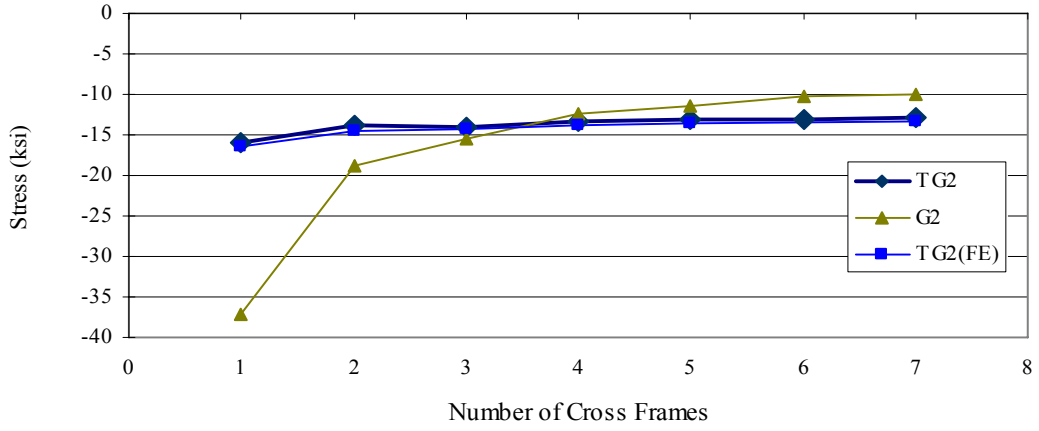

Figure 7.100 Maximum Total Normal Stress of Middle Girder vs. Number of Cross Frames

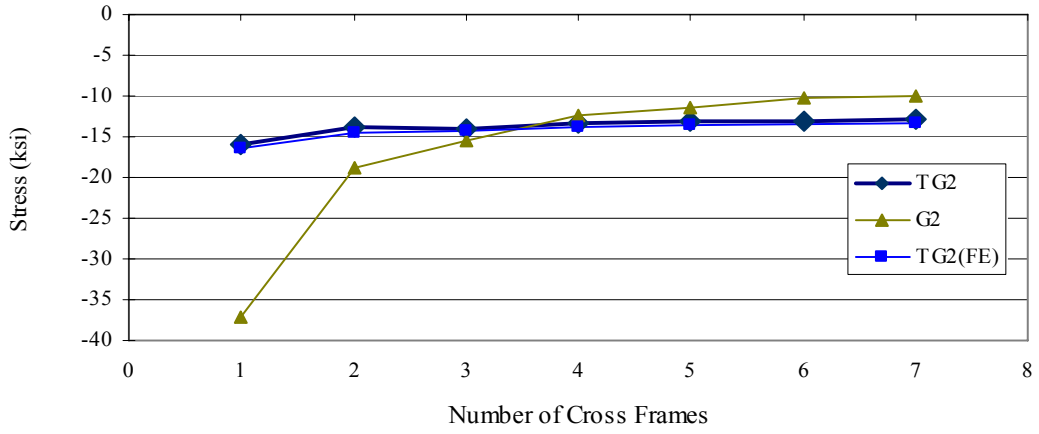

Figure 7.101 Maximum St.Venant Shear Stress of Middle Girder vs. Number of Cross Frames

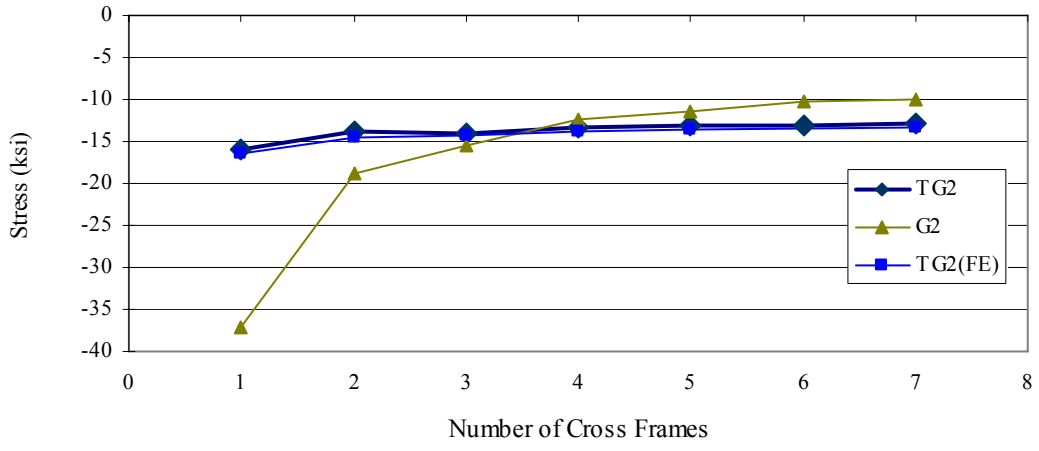

Figure 7.102 Maximum Warping Shear Stress of Middle Girder vs. Number of Cross Frames

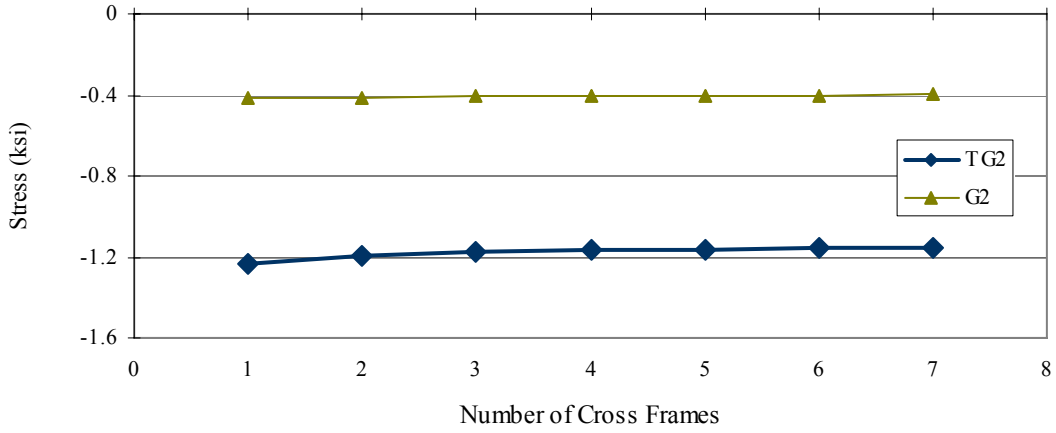

Figure 7.103 Maximum Vertical Shear Stress of Middle Girder vs. Number of Cross Frames

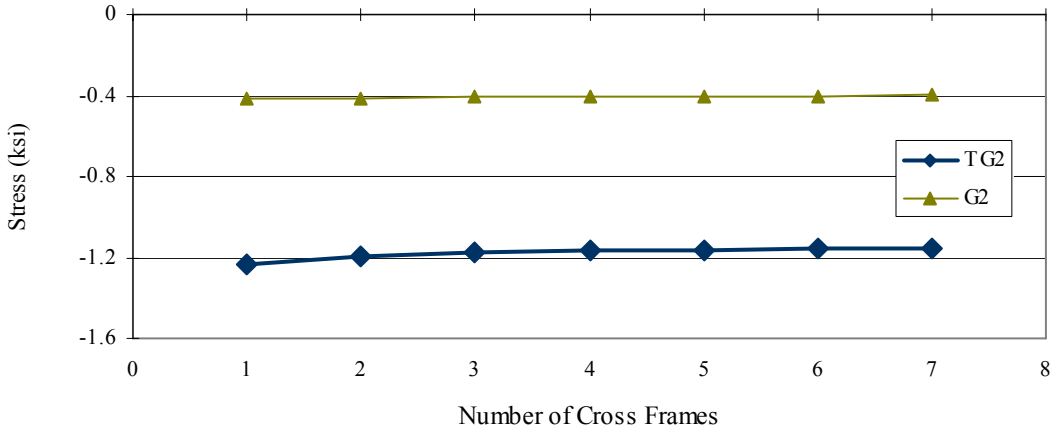

Figure 7.104 Maximum Total Shear Stress of Middle Girder vs. Number of Cross Frames

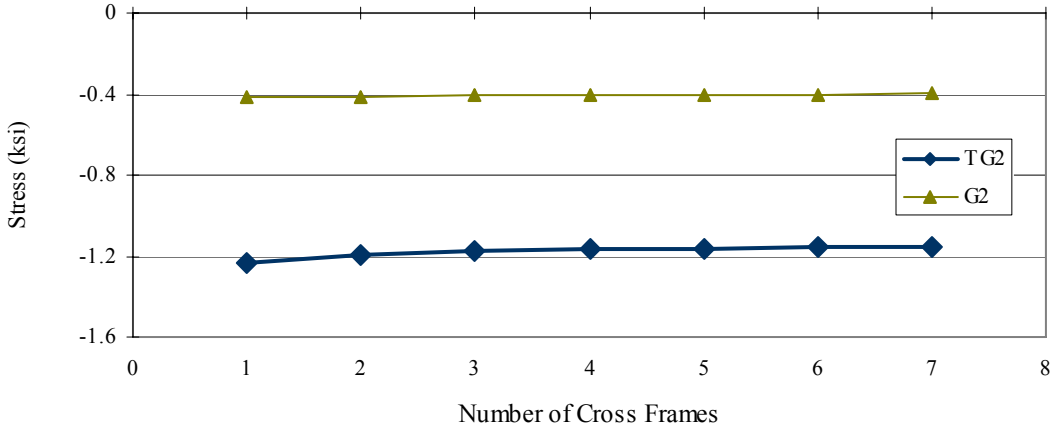

Figure 7.105 Maximum Von-Mises Stress of Middle Girder vs. Number of Cross Frames

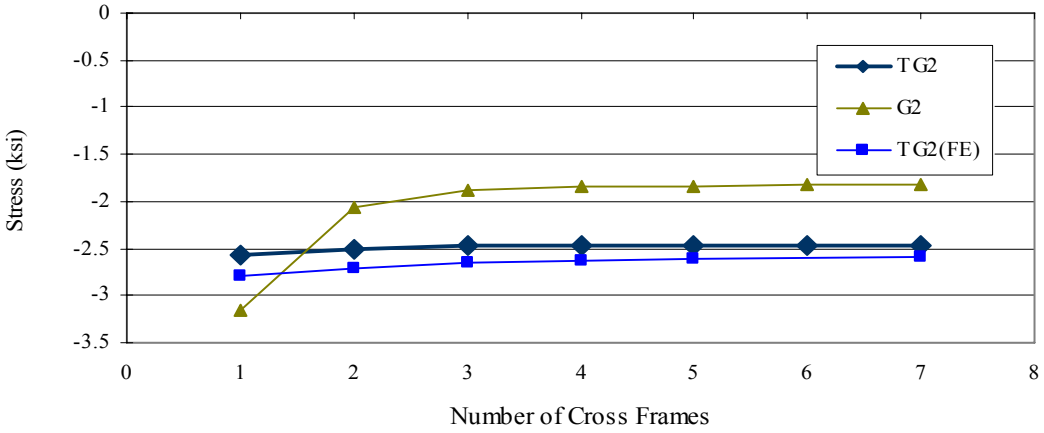

Figure 7.106 Maximum Vertical Displacement of Middle Girder vs. Number of Cross Frames

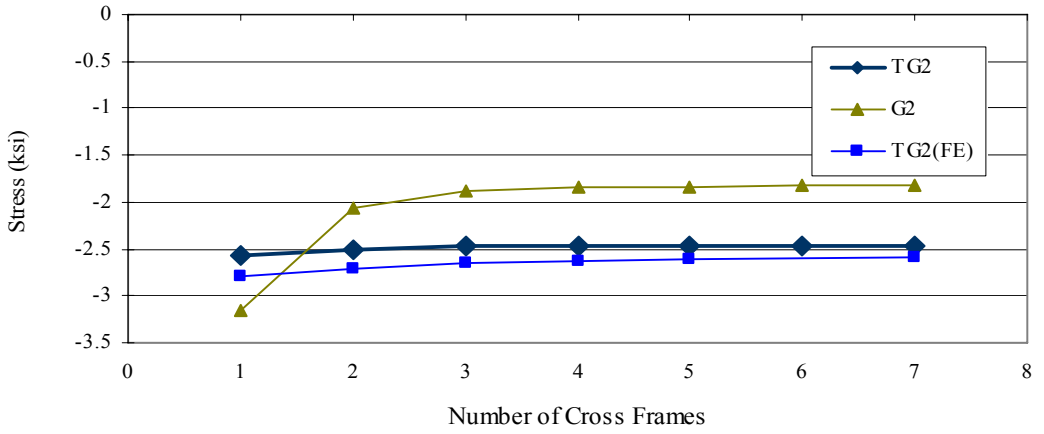

Figure 7.107 Maximum Cross Section Rotation of Middle Girder vs. Number of Cross Frames

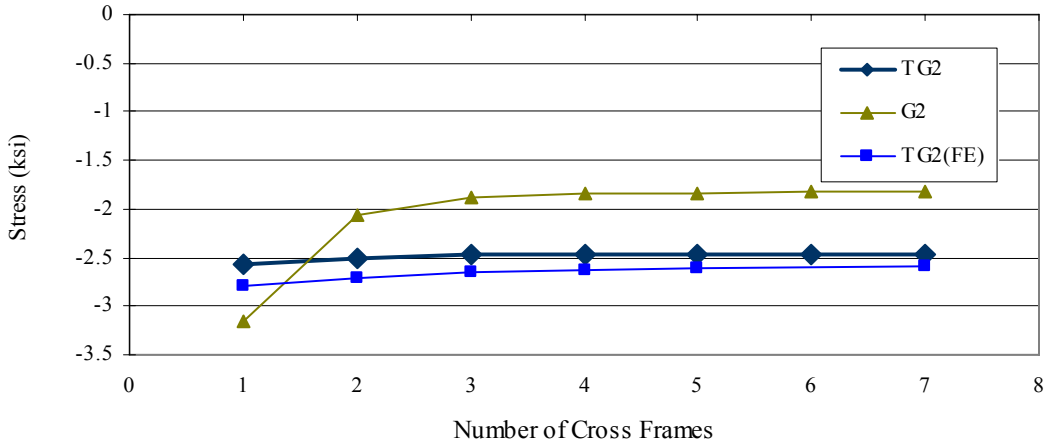

Figure 7.108 Maximum Bending Normal Stress of Outer Girder vs. Number of Cross Frames

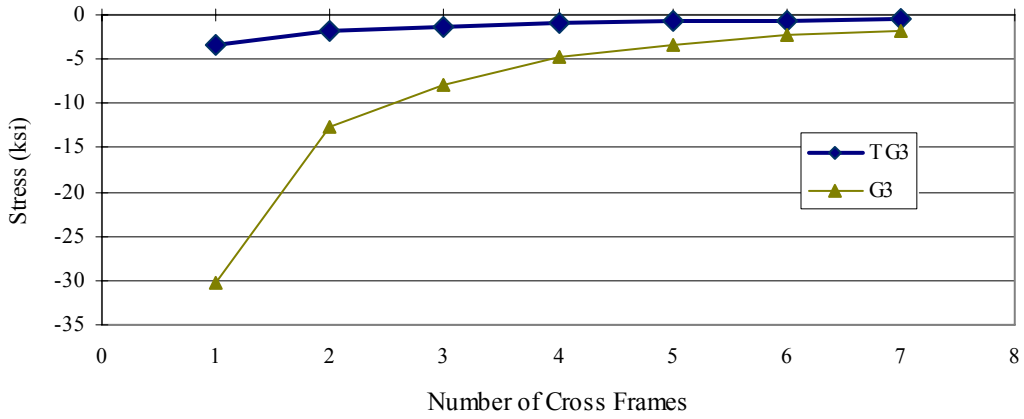

Figure 7.109 Maximum Warping Normal Stress of Outer Girder vs. Number of Cross Frames

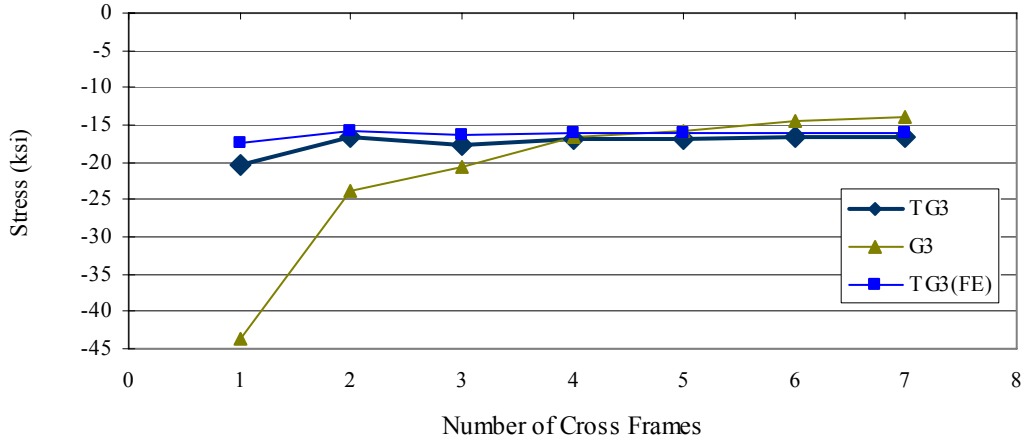

Figure 7.110 Maximum Total Normal Stress of Outer Girder vs. Number of Cross Frames

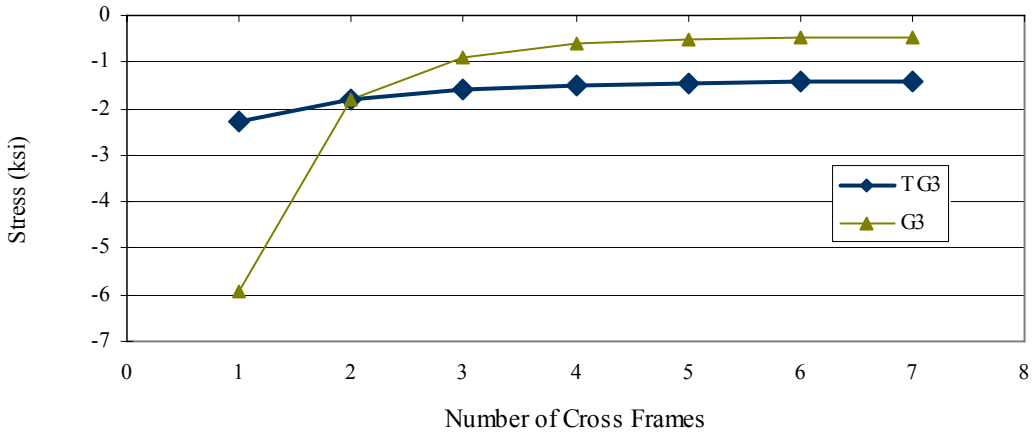

Figure 7.111 Maximum St.Venant Shear Stress of Outer Girder vs. Number of Cross Frames

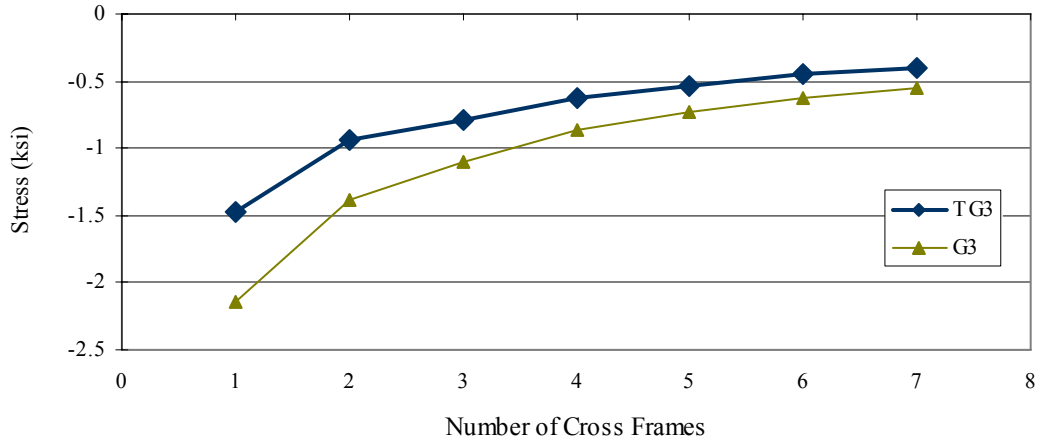

Figure 7.112 Maximum Warping Shear Stress of Outer Girder vs. Number of Cross Frames

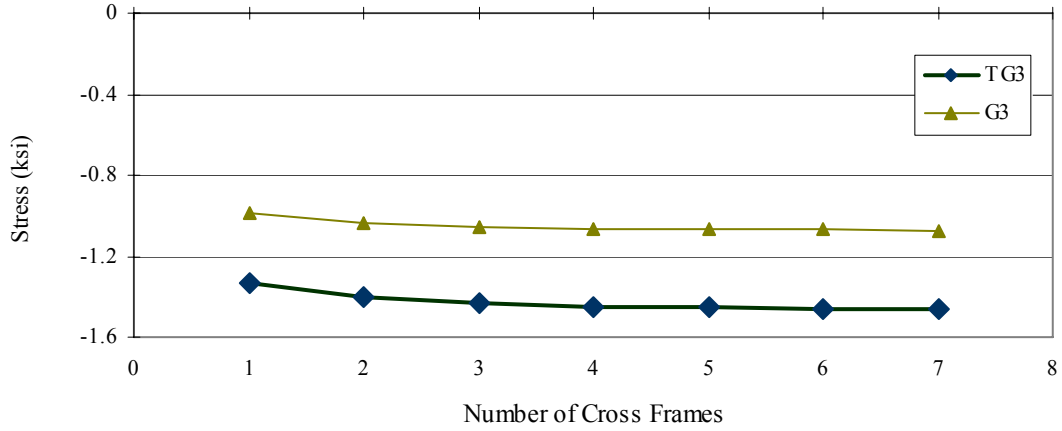

Figure 7.113 Maximum Vertical Shear Stress of Outer Girder vs. Number of Cross Frames

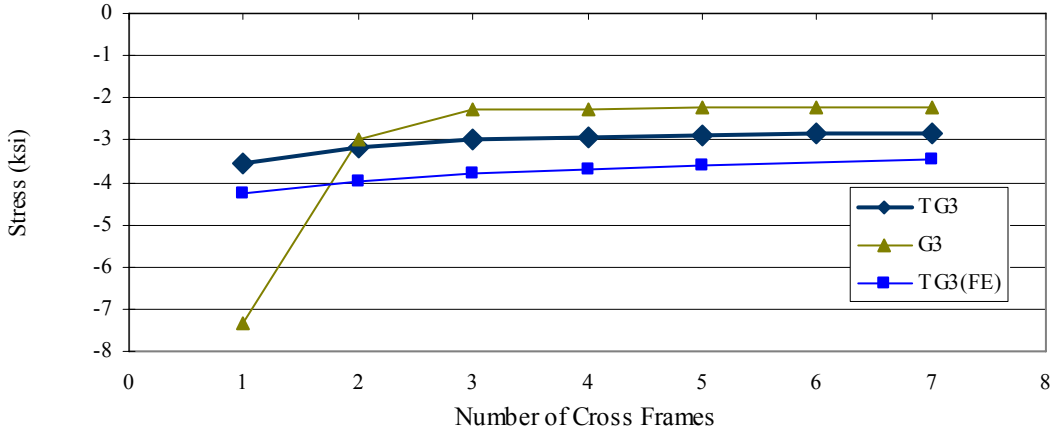

Figure 7.114 Maximum Total Shear Stress of Outer Girder vs. Number of Cross Frames

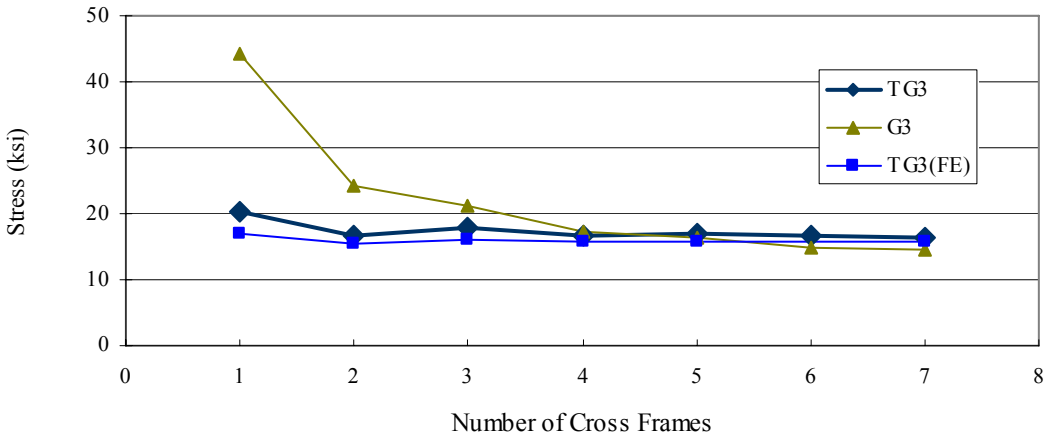

Figure 7.115 Maximum Von-Mises Stress of Outer Girder vs. Number of Cross Frames

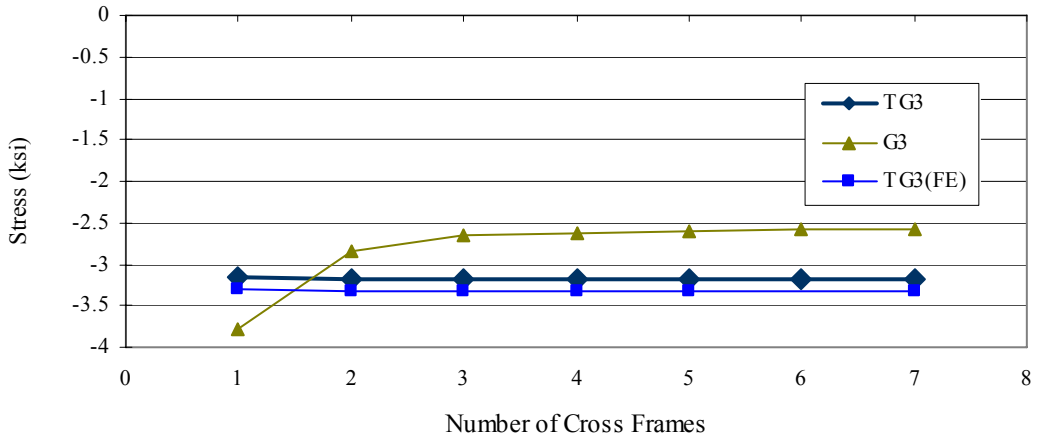

Figure 7.116 Maximum Vertical Displacement of Outer Girder vs. Number of Cross Frames

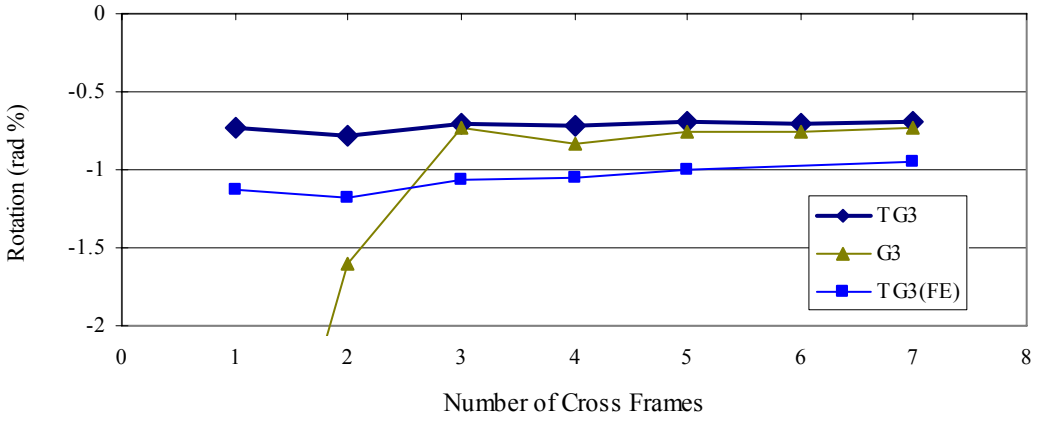

Figure 7.117 Maximum Cross Section Rotation of Outer Girder vs. Number of Cross Frames

Chapter 8 Girder Systems with Deck and Live Load

The studies presented in the previous chapters focus on curved tubular-flange girder bridge systems under construction conditions before the deck is placed on the bridge. These previous studies focus on individual girders or systems of girders with cross frames under dead load. This chapter presents studies on the behavior of a curved tubular-flange girder bridge system after the concrete deck is composite with the girders. First, the effect of the concrete deck on curved tubular-flange girder bridge system behavior is investigated. Then, a study of a curved tubular-flange girder bridge with a composite concrete deck under live load is presented. The live load considered in this study consists of the design truck and design lane loads from the AASHTO LRFD bridge design specification (AASHTO 2004). Finite element models are utilized to analyze the curved tubular-flange girder bridge with a composite concrete deck.

8.1 Finite Element Model

ABAQUS v6.5 (2003) was used to model the curved tubular-flange girder bridge system with a composite concrete deck. The element type, mesh density, boundary and loading conditions for the girders and the cross frames are the same as those described in Chapter 6. An 8-in thick concrete slab was added to the finite element model for the curved tubular-flange girder system without a concrete deck, described in Chapter 6. The concrete was modeled as an elastic isotropic material with an elastic modulus of 3860 ksi and a Poisson's ratio of 0.11. The concrete deck was modeled using shell element S4 in ABAQUS (2003). The mesh for the concrete deck has 200 elements along the span length and 94 elements across the deck width. Thus, a total of 18800 elements were used for the concrete deck model (see **Figure 8.1**). The nodes at the left corner, midpoint and right corner of the top surface of the top tubular-flange are connected to the concrete deck. The connection between the concrete deck and the top flange of the girders was modeled as a rigid beam (see **Figure 8.1**).

When the top flange of the girder is composite with the concrete deck, the stresses in the top flange are very small. So the studies presented in this chapter focus on the stresses in the bottom flange.

8.2 Effect of Concrete Deck

To study the effect of the concrete deck, the finite element results for a curved tubular-flange girder with a composite concrete deck are compared to the results for a girder with non-composite concrete deck. The finite element models for a girder with non-composite concrete deck were described in Chapter 6. The non-composite deck is treated as dead load applied on the girders. The curved tubular-flange girder system with a composite concrete deck is studied under the same loading applied to the curved tubular-flange girder with a non-composite concrete deck, which is described in Chapter 5 and includes the dead load of the girders, cross frames, deck forms, concrete haunch,

and deck. The girders in both systems are given in **Table 5.3**. Two types of finite element models are considered to study the effect of the composite concrete deck. One model is the model M5, described in Chapter 6, which restrains cross section distortion, but allows cross frame deflection; the other model is the model M7, described in Chapter 6, which allows cross section distortion and cross frame deflection. In models M5 and M7, five lines of cross frames and five sets of transverse stiffeners per girder are included.

The analysis results from model M5 are presented in **Figure 8.2** through **Figure 8.16**. The results show that the stresses and displacements in the system with a composite concrete deck (Composite TG1, TG2, TG3) are smaller than those in the system with a non-composite deck (non-composite TG1, TG2, TG3). For the composite case, the concrete deck is integrated with the curved tubular-flange girders and the structure stiffness is significantly increased. As a result, the stresses and displacements are reduced in the system with a composite concrete deck. In particular, the warping normal and shear stress in the cross section with cross frames is significantly reduced. For the system with the composite concrete deck, the total normal stress of each girder at P3 and P2 are close and the difference is less than 8%. That indicates that most of the normal stress in the girder is bending normal stress and the warping normal stress is negligible in the system with composite deck (and without distortion). **Figures 8.4, 8.9** and **8.14** show that the total shear stress in the system with the composite concrete deck (and without distortion) has no jump in shear stress at the cross sections attached to the cross frames, which indicates that the warping shear stress is small. As discussed in Chapter 5, the cross frames induce the significant warping normal stress and warping shear stress near the cross sections attached to the cross frames. It appears that the concrete deck produces a continuous restraint against girder torsion (rather than the discrete restraint produced by cross frames), and, as a result, the warping normal stress and the warping shear stress are significantly reduced. Hence, it is concluded that the composite concrete deck effectively increases the system stiffness and reduces the stress and displacements, especially, the warping normal and shear stress.

The results from the model M7 are shown in **Figure 8.17** through **Figure 8.31**. Comparing the results from M7 with the corresponding results from M5 indicates that considerable additional stress and displacement occur due to girder distortion in both the system with the composite concrete deck and the system with the non-composite deck. The results from M7 also show that the stresses and displacements in the system with the composite concrete deck are smaller than those in the system with the non-composite concrete deck. Comparing the results for TG1 with the results for TG2 and TG3, it shows that the composite concrete deck reduces the effect of cross section distortion on the girders and this influence is gradually increasing from TG1 to TG3. However, the distribution of stresses and displacements along the length of the girders are similar for the non-composite and composite cases. The results suggest that the composite concrete deck does not prevent the cross section distortion from developing in the girder system, but reduces the effect of cross section distortion on the stresses and displacements.

Based on the discussion given above, the following findings are summarized: (1) the composite concrete deck increases the structure system stiffness and reduces stresses and displacements, especially the warping normal stress; (2) the composite deck reduces the effect of the cross section distortion on the stresses and displacements, especially for the outer girder TG3; (3) for a curved tubular-flange girder system with a composite concrete deck and without cross section distortion, the primary bending normal stress is dominant in the total normal stress and the warping normal stress is very small and may be negligible.

8.3 Live Load Analysis

Live load analyses were conducted for both a curved tubular-flange girder system and a curved I-girder system, and the results were compared. Both systems had a composite concrete deck. The lane load and design truck load given in AASHTO (2004) are considered separately in the live load analysis for the curved girder bridge in this study. A new finite element model, denoted model M10, was built for the live load analyses. The model M10 allows cross section distortion and cross frame deflection, but nine equally spaced transverse stiffeners were added to reduce the cross section distortion. The live load distributions for the maximum load effect on each girder are shown in **Figure 8.17** through **Figure 8.19.**

8.3.1 Design Lane and Design Loads

The design lane is the lane designation used by the bridge engineer for live-load placement. The width and location of the design lanes may or may not be the same as the traffic lanes. For the curved tubular-flange girder bridge considered in this report (see **Figure 5.1**), the total bridge deck width is 26.25 ft. The curb is assumed to be located 2.375 ft. inside the edge of the deck. Two design lanes were assumed, and labeled Design Lane I and Design Lane II, as shown in **Figure 8.17** through **Figure 8.19**. The design lane width is 10.75 ft.

The design truck load and the design lane load are both used to model the live load. The AASHTO HS20 truck given in AASHTO (2004) is used as the design truck load and the design lane load is a uniform pressure of 0.64 kips/ft per design lane applied over a 10-ft width in each design lane (AASHTO 2004).

8.3.2 Live Load Distribution

Live load analyses should produce the maximum load effect on each girder. Hence, the design truck and the design load are placed in a position within the design lanes on the deck to produce the maximum flexural effect on each girder. The location of the design truck and the design lane load for each girder are described as follows.

To obtain the maximum flexural effect on girder TG3, two trucks are positioned side by side with the middle axles on the midspan of the bridge (see **Figure 8.17**). Both

axle spacings of the AASHTO HS20 truck are 14 ft. The wheel transverse spacing is 6 ft. The front and back outside wheel of the truck in Design Lane I (Truck I) are positioned on the top of TG3, which is 2 ft. radially inside the curb. The resulting position of the middle outside wheel of Truck I is 2.47 ft. radially inside the curb. The front and back outside wheel of the truck in Design Lane II (Truck II) are positioned 2 ft. radially inside the outside edge of the Design Lane II, which is centered on girder TG2. The resulting position of the middle outside wheel of Truck II is 2.50 ft. radially inside the edge of Design Lane II. The design lane loads (0.64 kips/ft) in each design lane are uniformly distributed over the 10-ft radial width from the outside edge of each design lane.

The live load distribution to maximize the flexural effect on girder TG2 (see **Figure 8.18**) is similar to that on girder TG3. However, for girder TG2, Design Truck I is moved 0.28 ft. towards the center line of the bridge and the design lane load in Design Lane I is moved 0.75 ft. towards the center line. The middle inside wheel of Design Truck I is then 2 ft. away from girder TG2, which is also the inside edge of the design lane. The design lane load starts from the inside edge of Design Lane I and is uniformly distributed over the 10-ft width.

For the inside girder TG1 (see **Figure 8.19**), one design truck is used and the middle inside wheel is positioned on top of the midspan of girder TG1, which is 2 ft. inside the curb. The design lane load is uniformly distributed from the inside edge of the design lane outward 10-ft radially.

8.3.3 Analysis Results

The live load analysis results for each tubular-flange girder and the corresponding I-girder are presented in **Figure 8.20** through **Figure 8.67**.

The results from model M7 under the lane load, presented from **Figure 8.20** through **Figure 8.31,** and under the truck load, presented in **Figure 8.32** through **Figure 8.43**, show that the maximum total normal stress and the cross section rotation for the curved tubular-flange girder system with the composite deck are smaller than those for the corresponding curved I-girder system with the composite deck. However, the vertical displacement for the curved tubular-flange girder system with the composite deck is similar to or slightly larger than that for the curved I-girder system with the composite deck. The I-girder system has much larger variation in total normal stress along the span length than the tubular-flange girder system. This variation shows that significant warping normal stress is developed in the I-girder system.

The results from model M10 are shown in **Figure 8.44** through **Figure 8.55** for the lane load and **Figure 8.56** through **Figure 8.67** for the truck load. The results show that using more stiffeners significantly reduces effects of cross section distortion in the tubular-flange girder system under live load, especially for the middle girder TG2 and the outer girder TG3. The variation of the total normal stress along the span length for TG2 and TG3 are similar to that shown in the previous section for TG2 and TG3 (with a

composite deck) under uniform load when cross section distortion was restrained (model M5). That is, the sharp changes in normal stress due to distortion absence.

Hence, based on the above discussion, the following findings are obtained: (1) For a curved tubular-flange girder system with a composite concrete deck under the action of live load, using more stiffeners (greater than five) significantly reduces the cross section distortion, and as a result, the primary bending normal stress dominates the total normal stress and the warping normal stress is small; (2) compared to a curved tubular-flange girder system, a curved I-girder system with a composite deck under live load develops larger warping normal stress and cross section rotation.

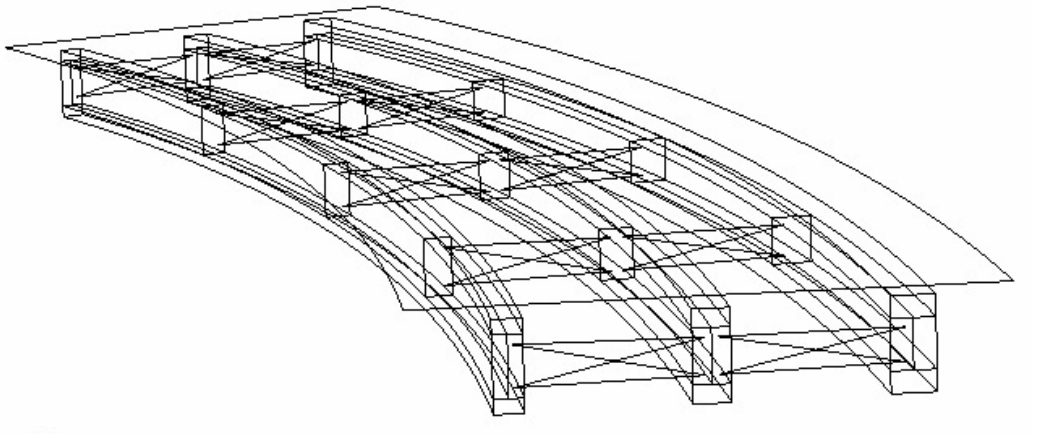

a. Overview of Girder System with Composite Concrete Deck

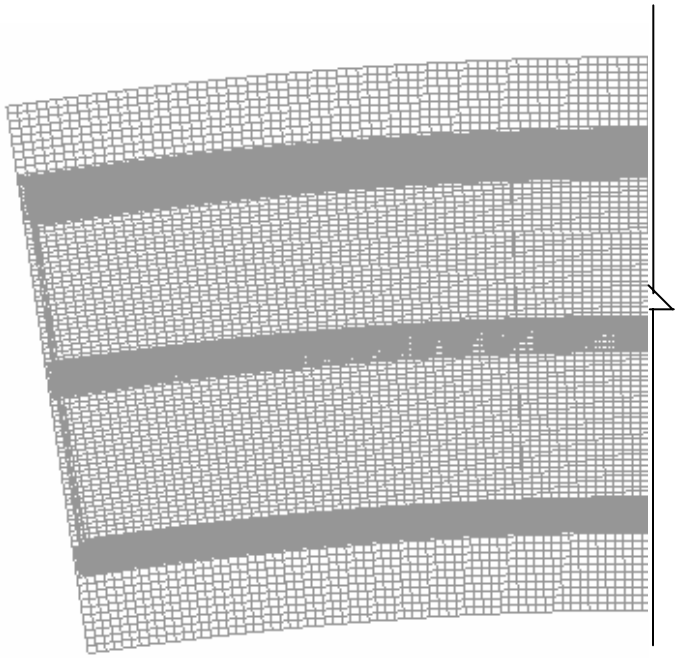

(b) Mesh of Concrete Slab (Part of Span Length)

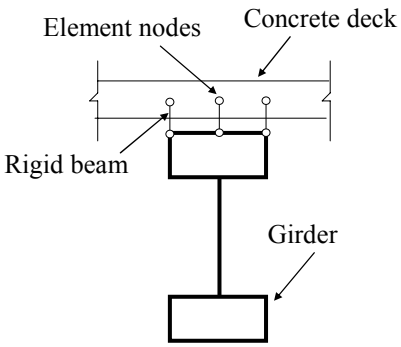

(c) Connection of Concrete Slab to Girder

Figure 8.1 Finite Element Model for Girder System with Composite Concrete Deck

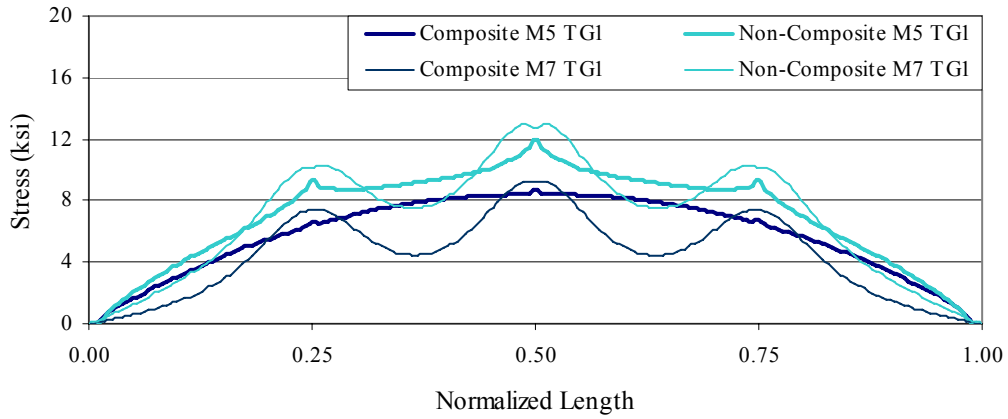

Figure 8.2 Total Normal Stress at P3 for TG1

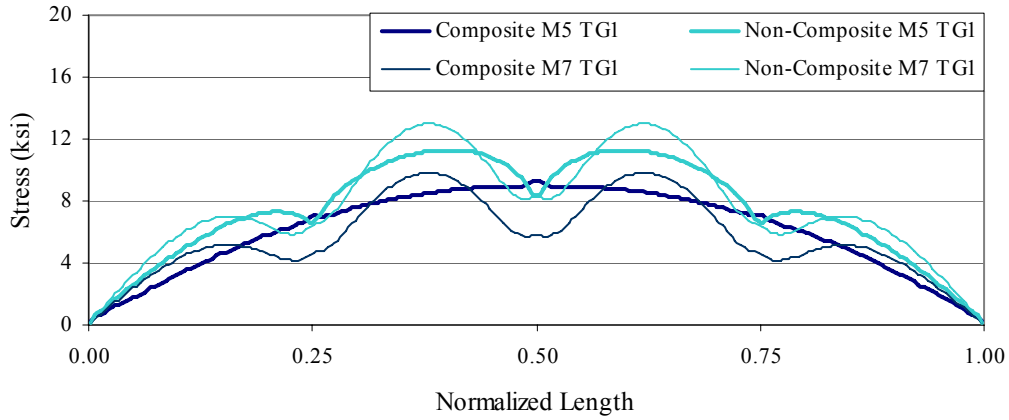

Figure 8.3 Total Normal Stress at P2 for TG1

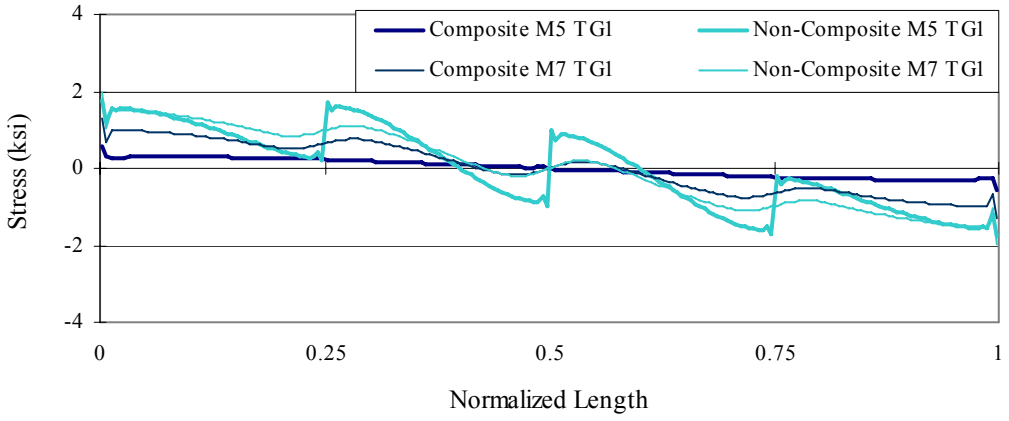

Figure 8.4 Total Shear Stress at P6r for TG1

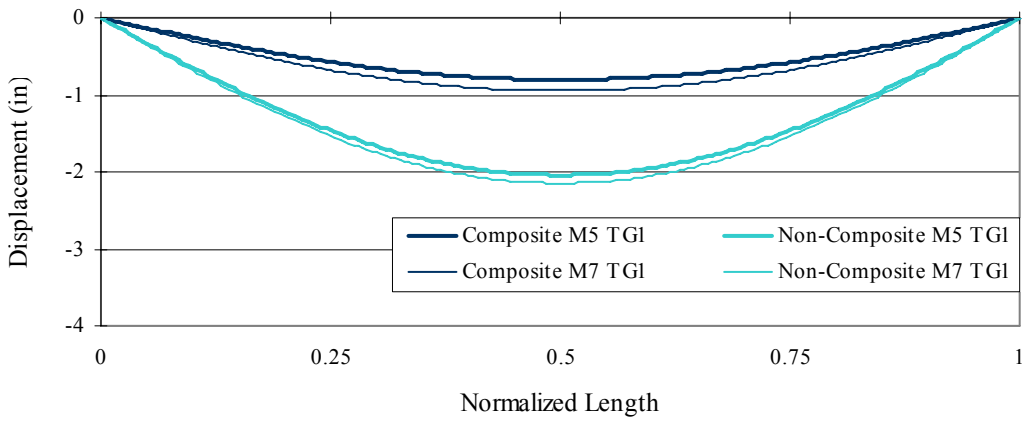

Figure 8.5 Vertical Displacement for TG1

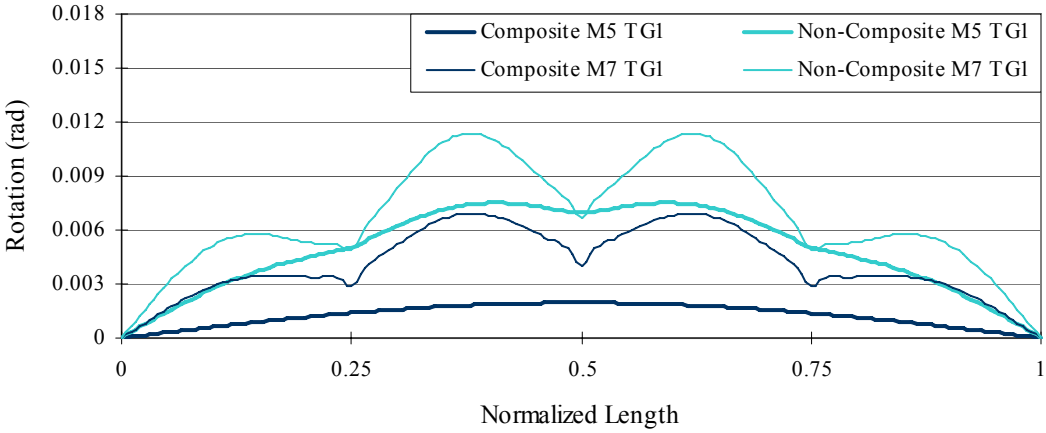

Figure 8.6 Cross Section Rotation for TG1

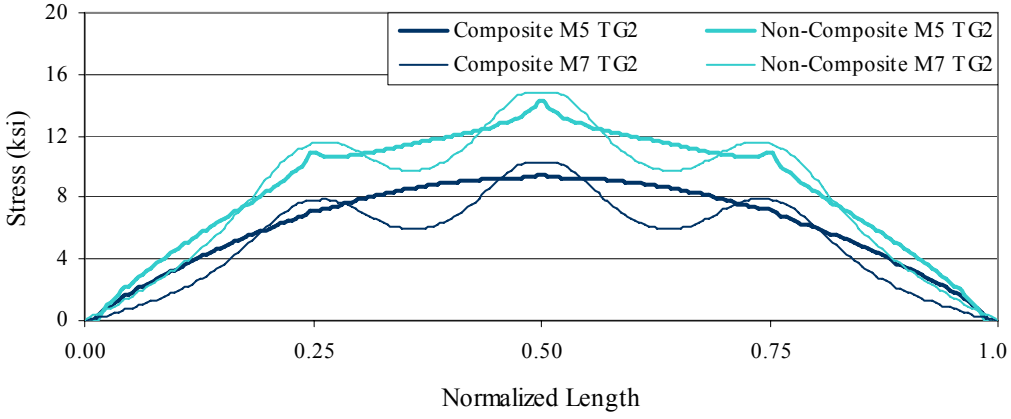

Figure 8.7 Total Normal Stress at P3 for TG2

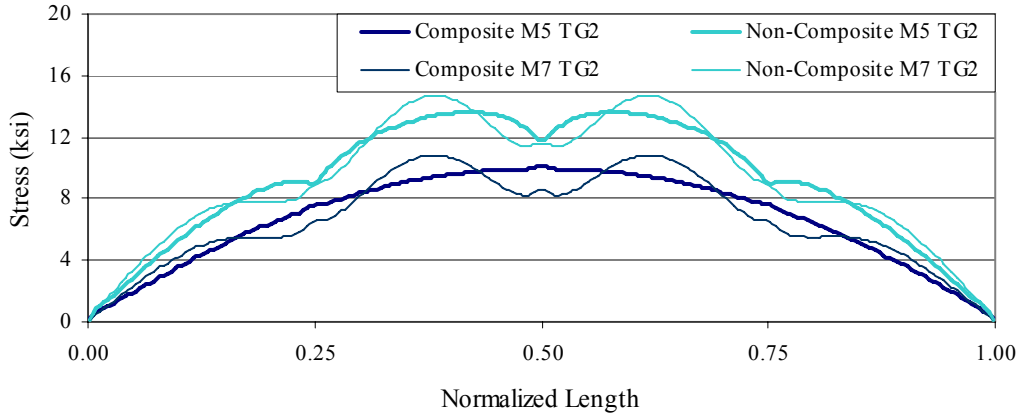

Figure 8.8 Total Normal Stress at P2 for TG2

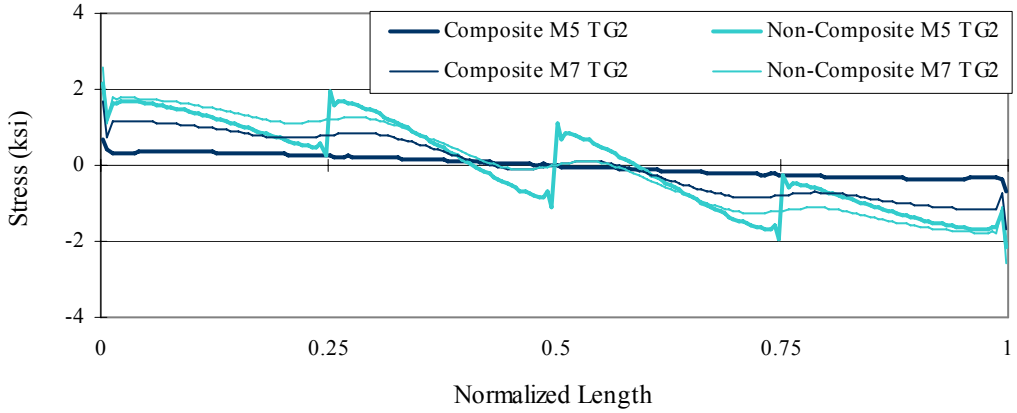

Figure 8.9 Total Shear Stress at P6r for TG2

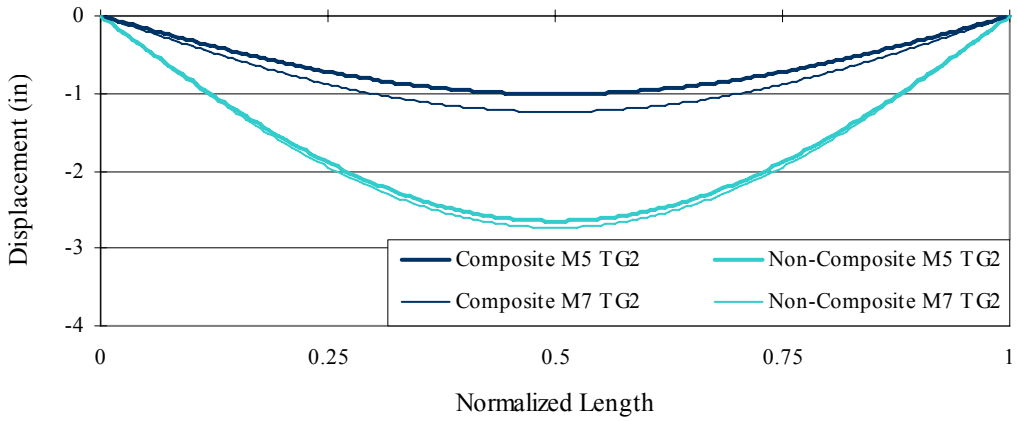

Figure 8.10 Vertical Displacement for TG2

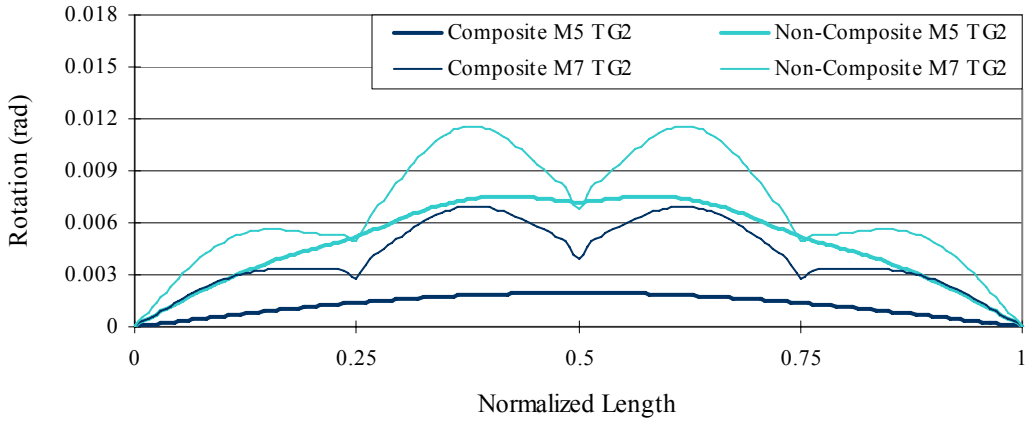

Figure 8.11 Cross Section Rotation for TG2

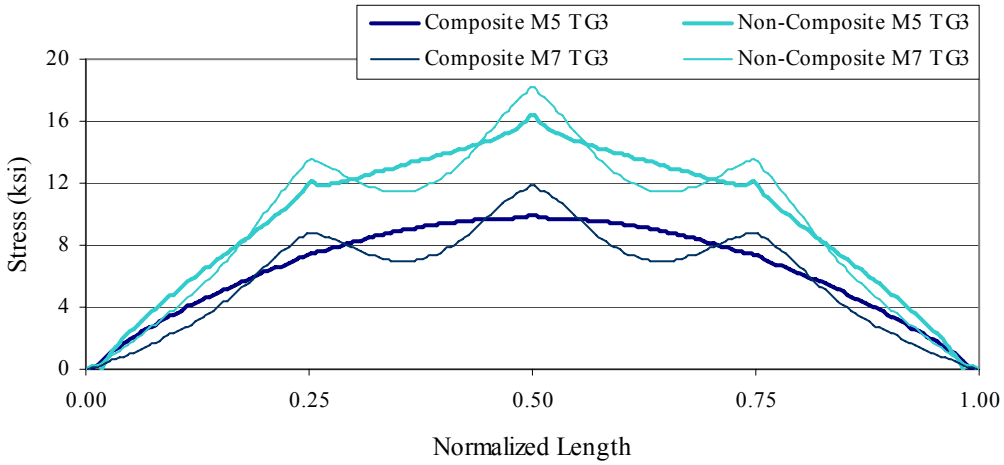

Figure 8.12 Total Normal Stress at P3 for TG3

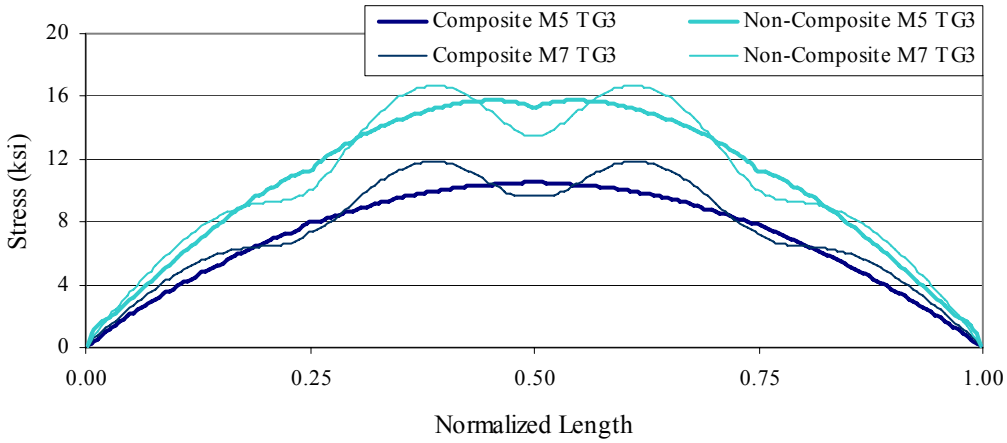

Figure 8.13 Total Normal Stress at P2 for TG3

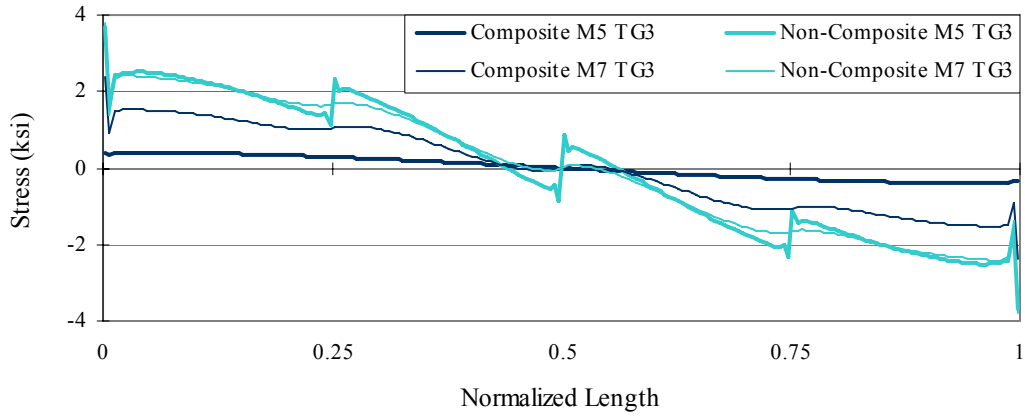

Figure 8.14 Total Shear Stress at P6r for TG3

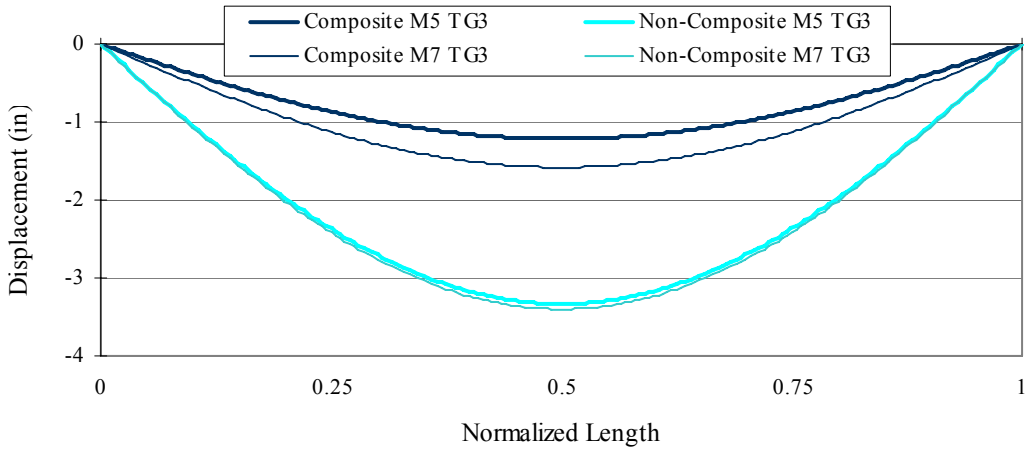

Figure 8.15 Vertical Displacement for TG3

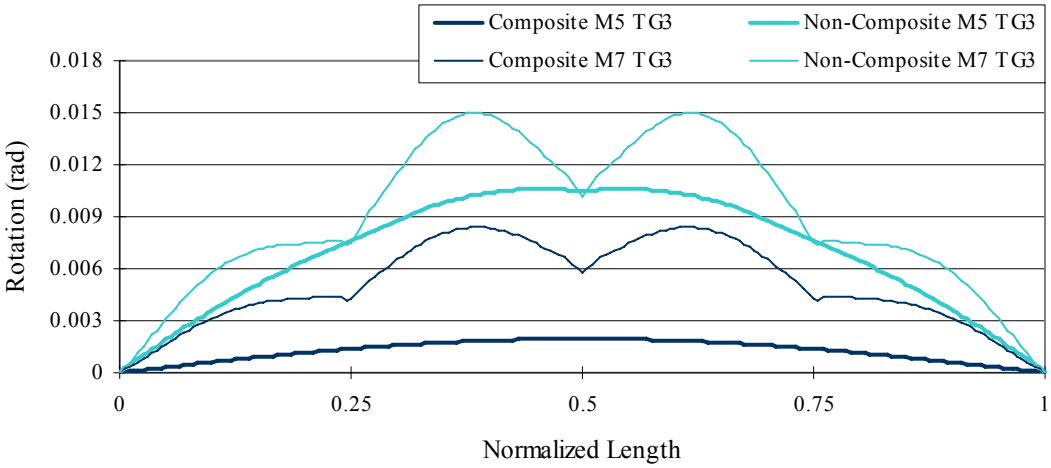

Figure 8.16 Cross Section Rotation for TG3

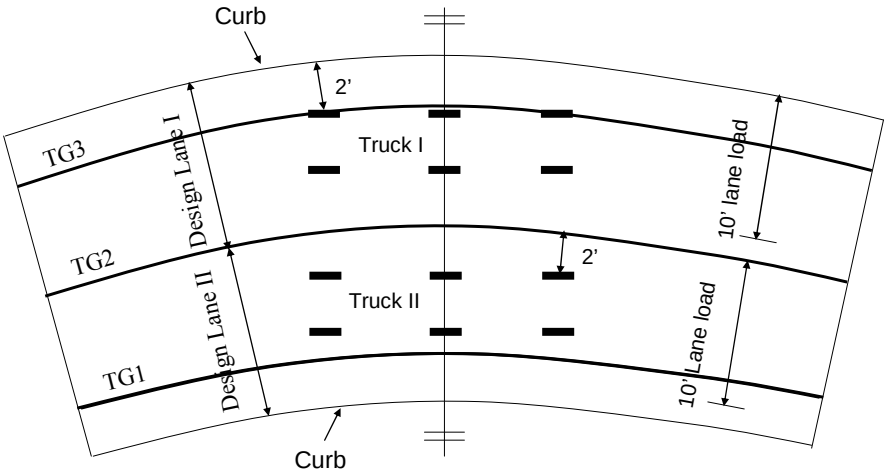

Figure 8.17 Live Load Distribution for Maximum Effect on TG3

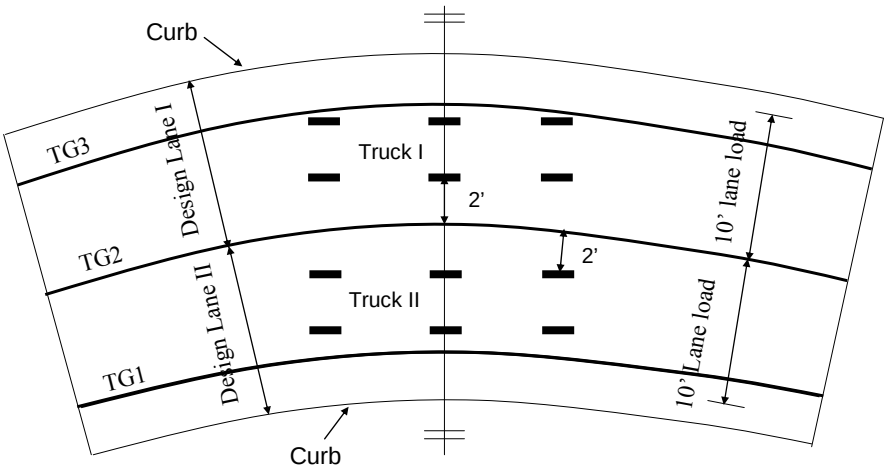

Figure 8.18 Live Load Distribution for Maximum Effect on TG2

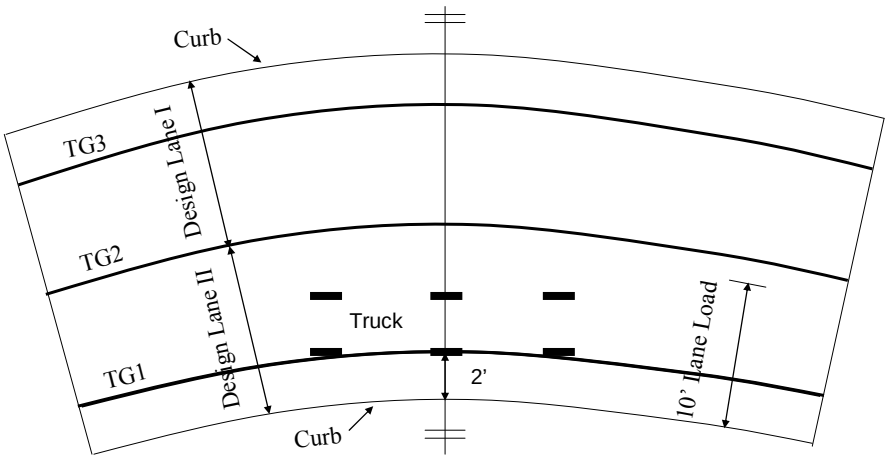

Figure 8.19 Live Load Distribution for Maximum Effect on TG1

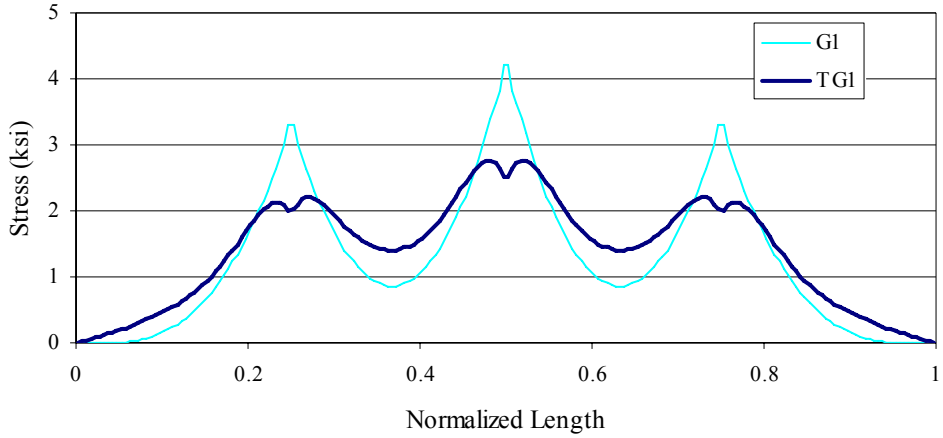

Figure 8.20 Total Normal Stress at P3 for G1 and TG1 with 5 stiffeners (Lane Load)

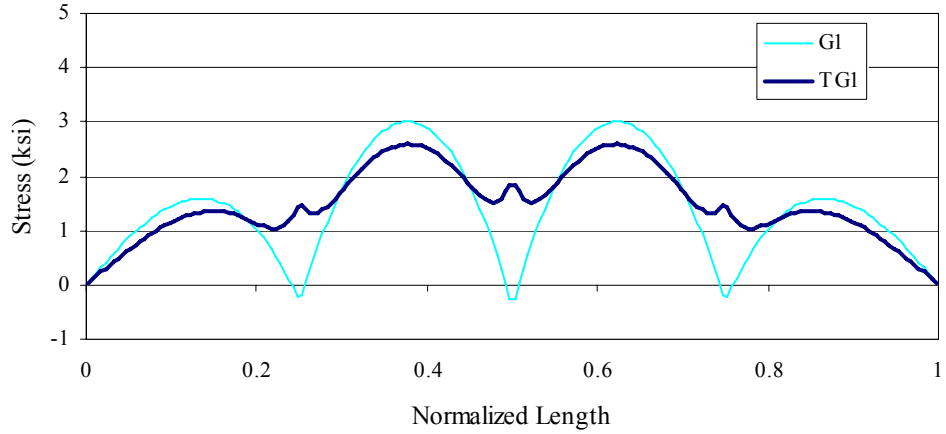

Figure 8.21 Total Normal Stress at P2 for G1 and TG1 with 5 stiffeners (Lane Load)

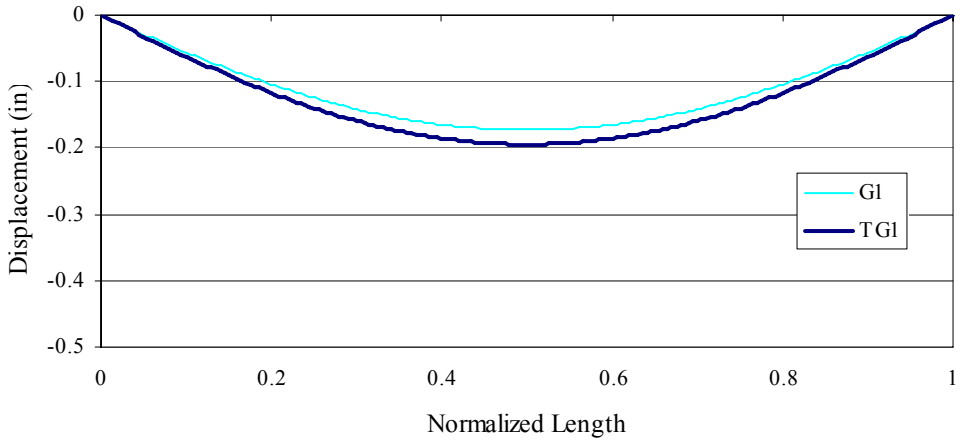

Figure 8.22 Vertical Displacement for G1 and TG1 with 5 stiffeners (Lane Load)

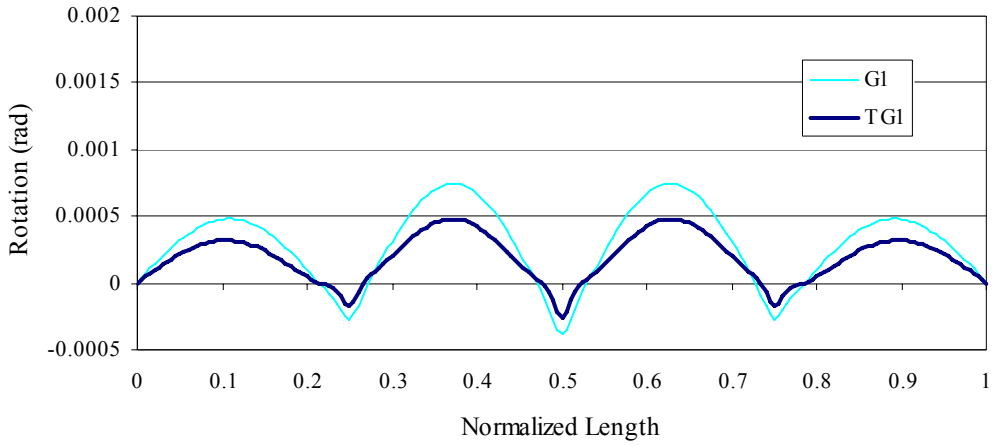

Figure 8.23 Cross Section Rotation for G1 and TG1 with 5 Stiffeners (Lane Load)

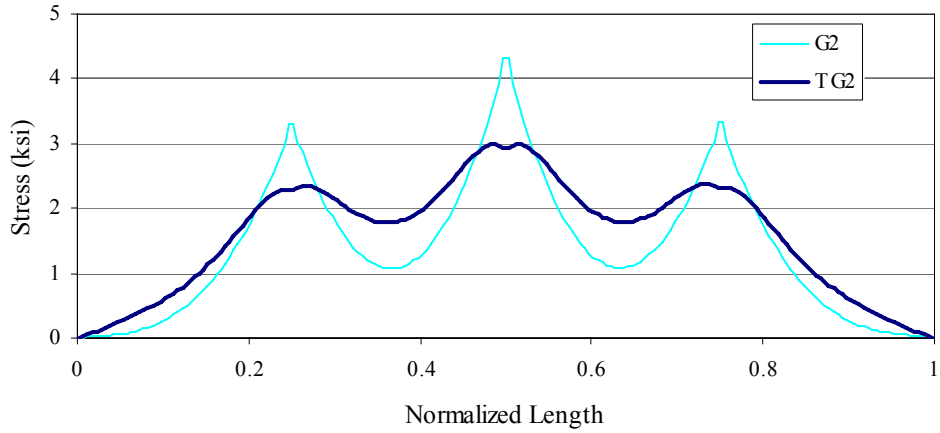

Figure 8.24 Total Normal Stress at P3 for G2 and TG2 with 5 Stiffeners (Lane Load)

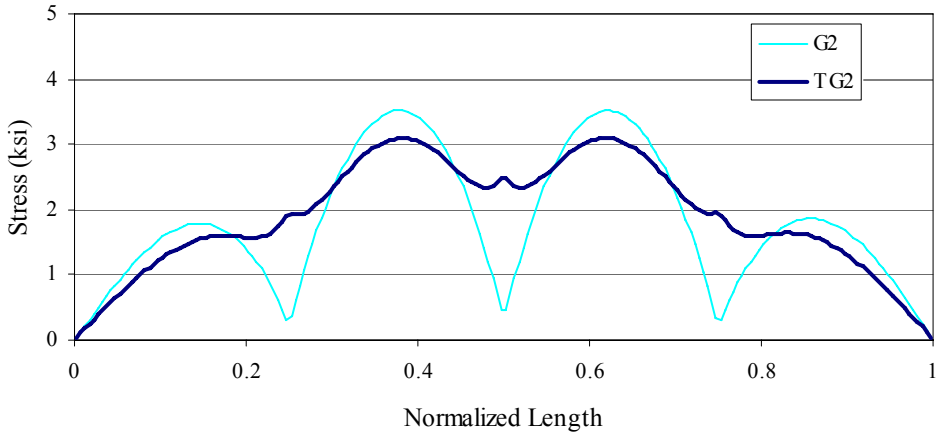

Figure 8.25 Total Normal Stress at P2 for G2 and TG2 with 5 Stiffeners (Lane Load)

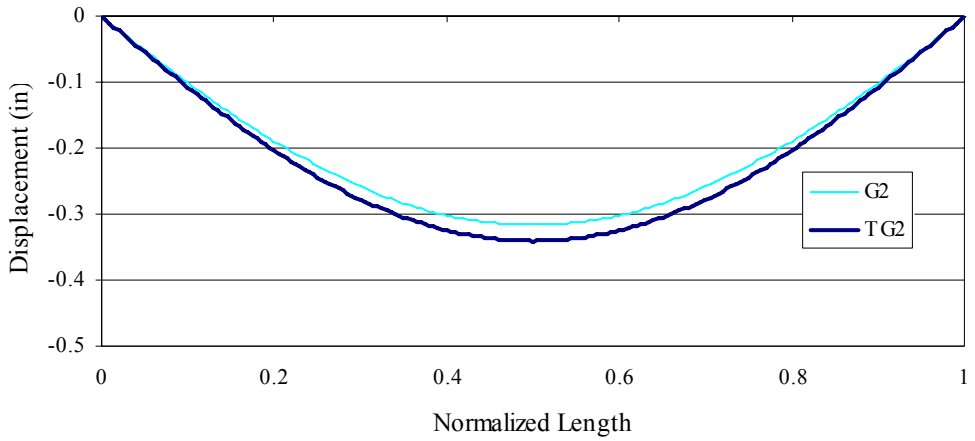

Figure 8.26 Vertical Displacement for G2 and TG2 with 5 Stiffeners (Lane Load)

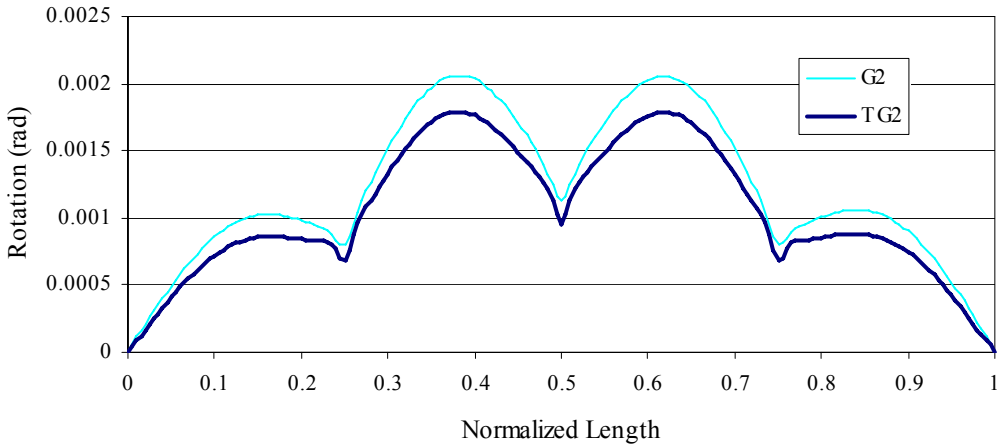

Figure 8.27 Cross Section Rotation for G2 and TG2 with 5 Stiffeners (Lane Load)

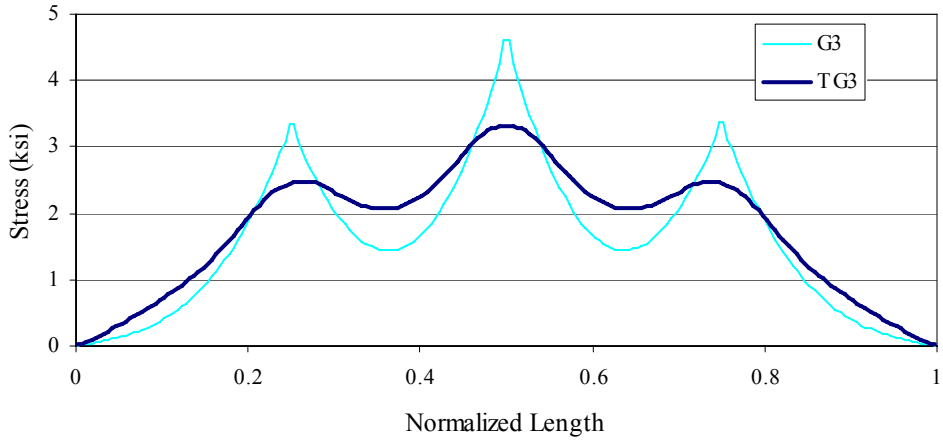

Figure 8.28 Total Normal Stress at P3 for G3 and TG3 with 5 Stiffeners (Lane Load)

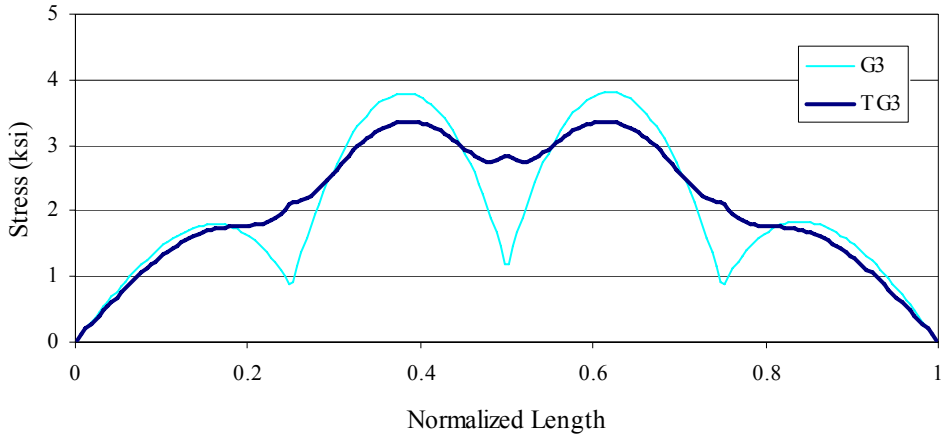

Figure 8.29 Total Normal Stress at P2 for G3 and TG3 with 5 Stiffeners (Lane Load)

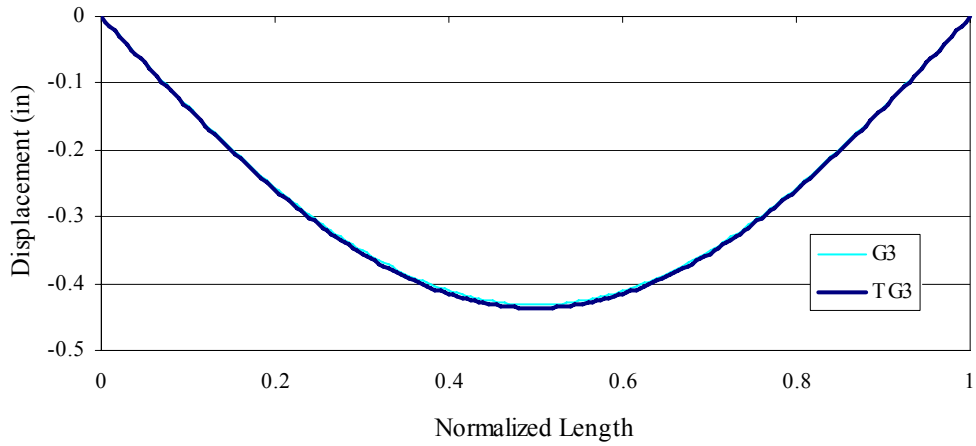

Figure 8.30 Vertical Displacement for G3 and TG3 with 5 Stiffeners (Lane Load)

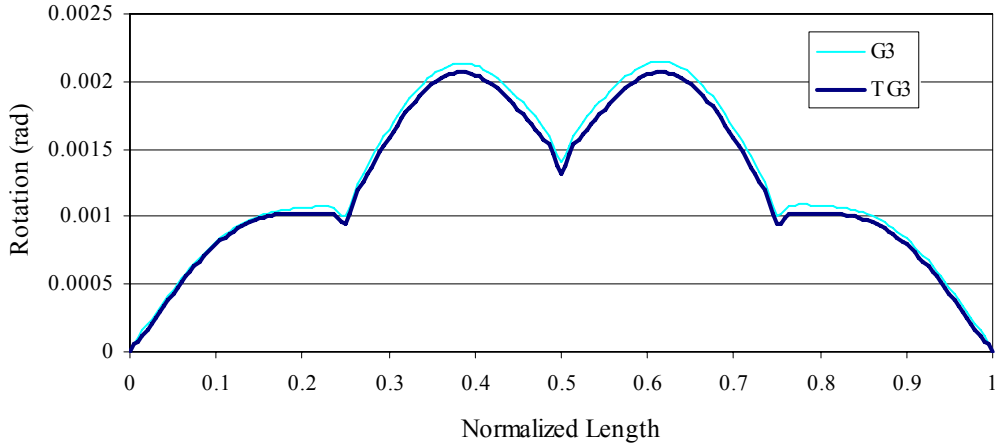

Figure 8.31 Cross Section Rotation for G3 and TG3 with 5 Stiffeners (Lane Load)

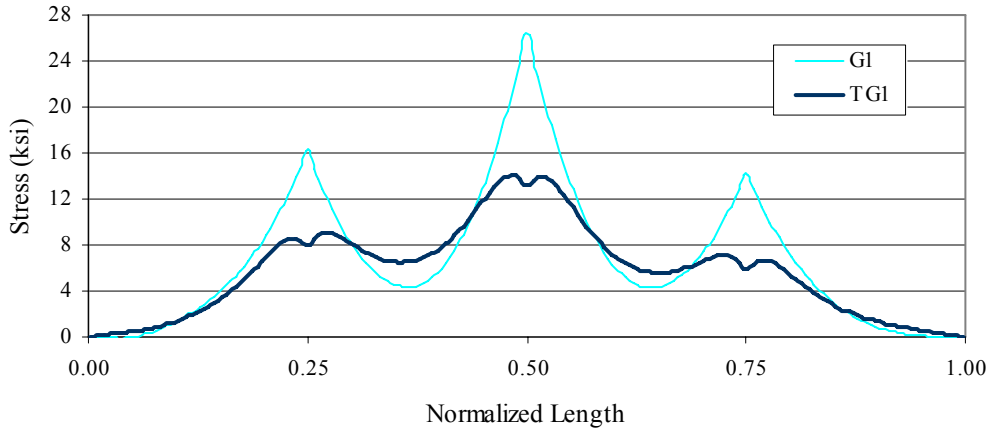

Figure 8.32 Total Normal Stress at P3 for G1 and TG1 with 5 Stiffeners (Truck Load)

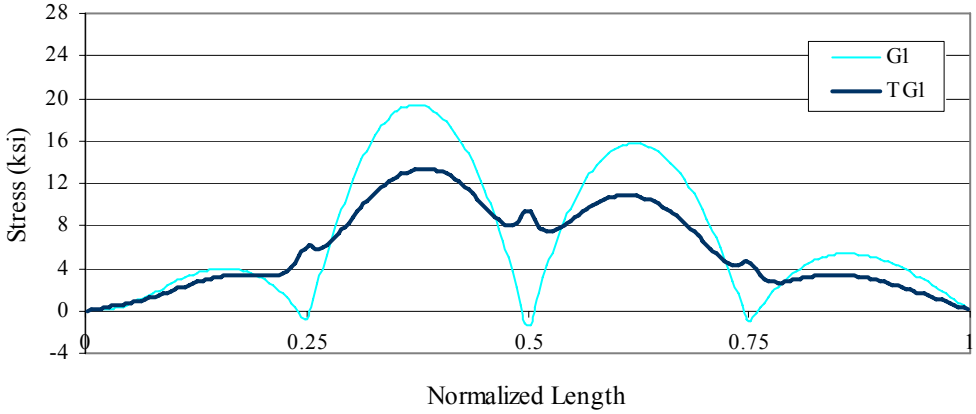

Figure 8.33 Total Normal Stress at P2 for G1 and TG1 with 5 Stiffeners (Truck Load)

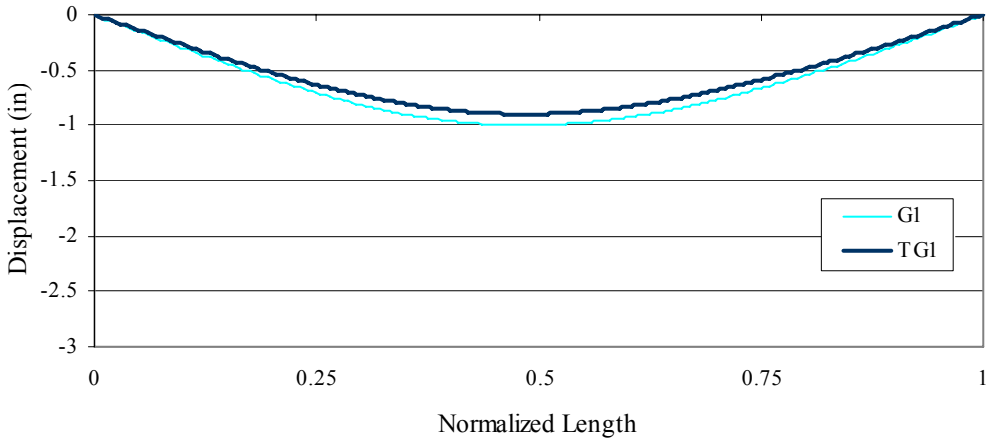

Figure 8.34 Vertical Displacement for G1 and TG1 with 5 Stiffeners (Truck Load)

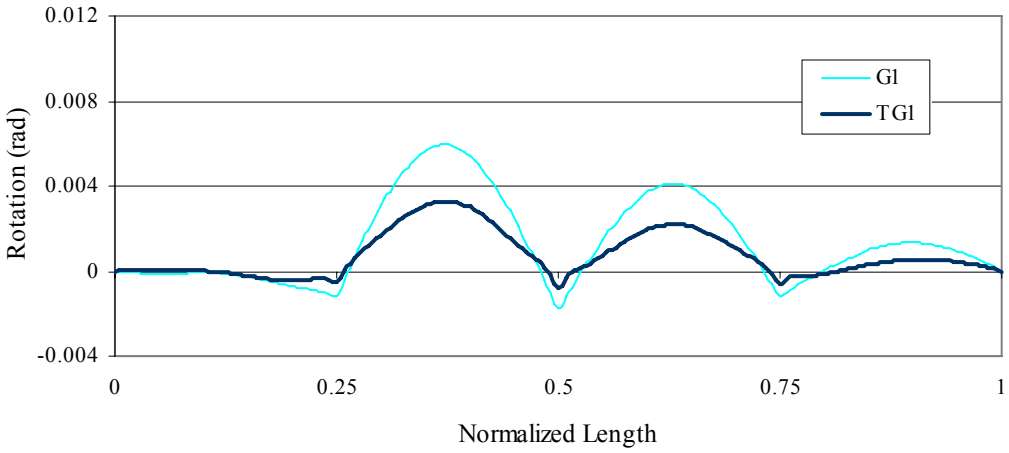

Figure 8.35 Cross Section Rotation for G1 and TG1 with 5 Stiffeners (Truck Load)

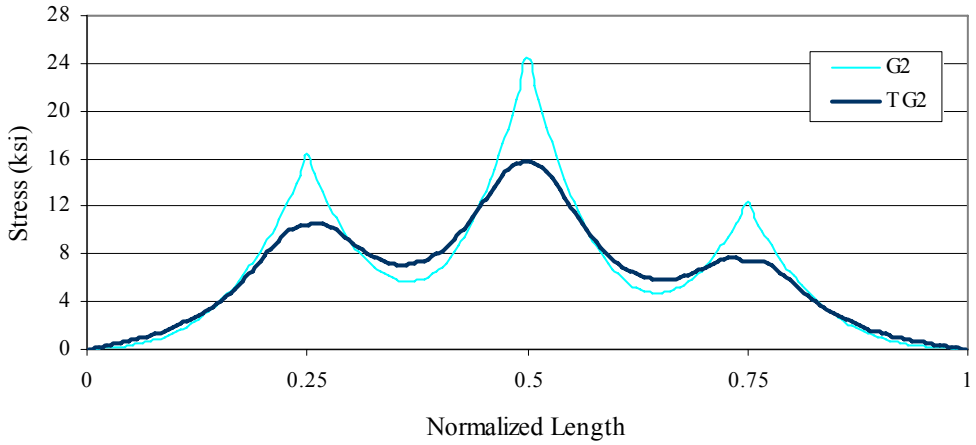

Figure 8.36 Total Normal Stress at P3 for G1 and TG2 with 5 Stiffeners (Truck Load)

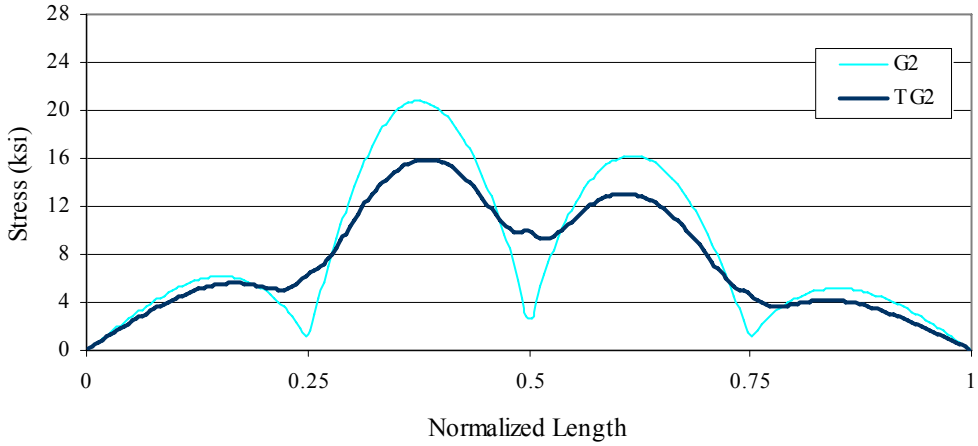

Figure 8.37 Total Normal Stress at P2 for G2 and TG2 with 5 Stiffeners (Truck Load)

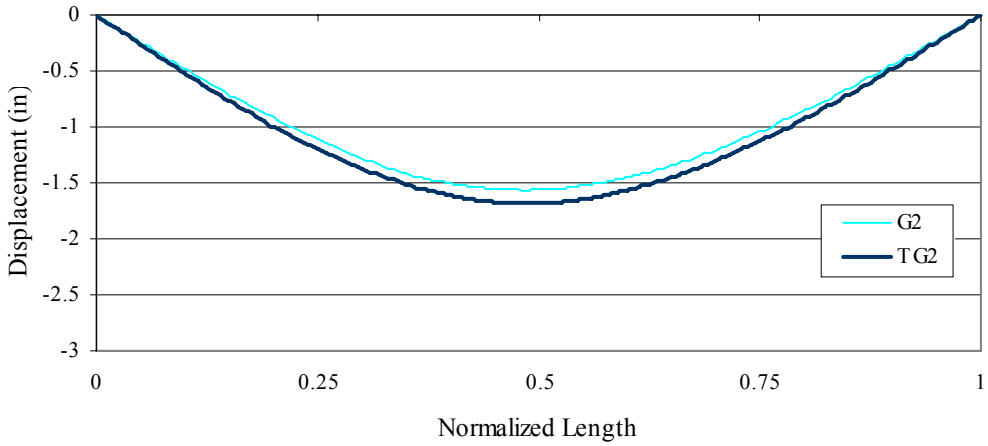

Figure 8.38 Vertical Displacement for G2 and TG2 with 5 Stiffeners (Truck Load)

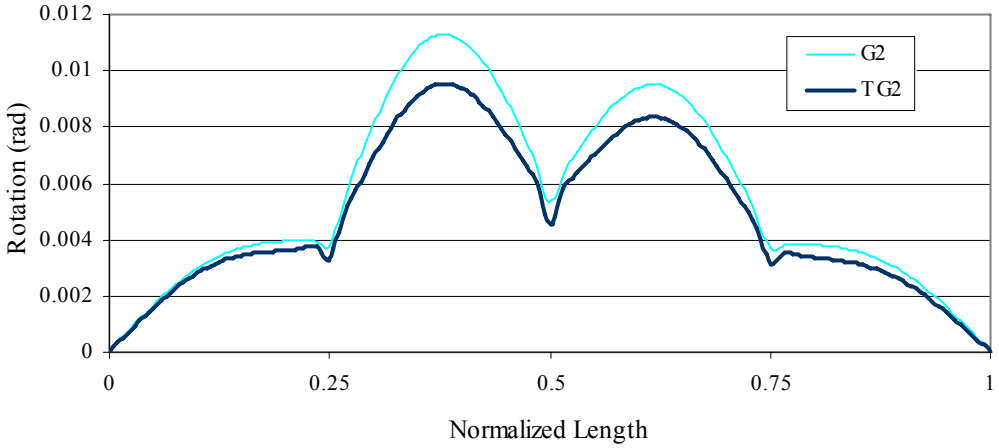

Figure 8.39 Cross Section Rotation for G2 and TG2 with 5 Stiffeners (Truck Load)

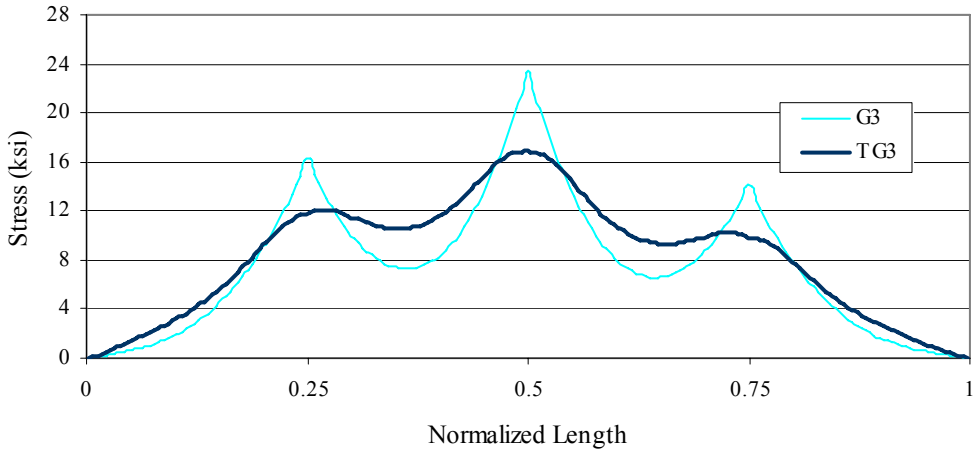

Figure 8.40 Total Normal Stress at P3 for G3 and TG3 with 5 Stiffeners (Truck Load)

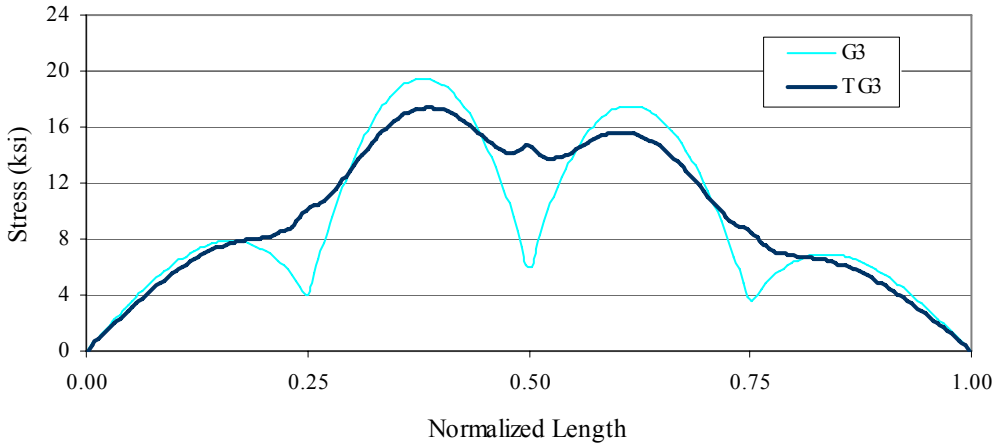

Figure 8.41 Total Normal Stress at P2 for G3 and TG3 with 5 Stiffeners (Truck Load)

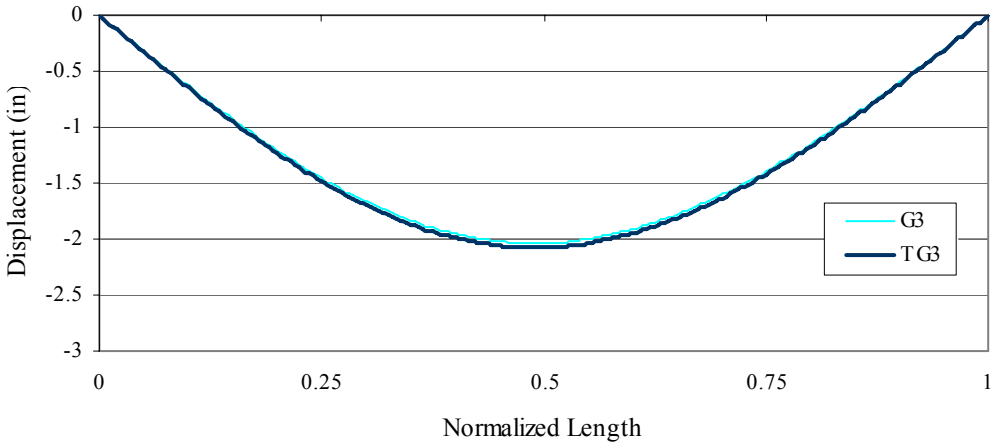

Figure 8.42 Vertical Displacement for G3 and TG3 with 5 Stiffeners (Truck Load)

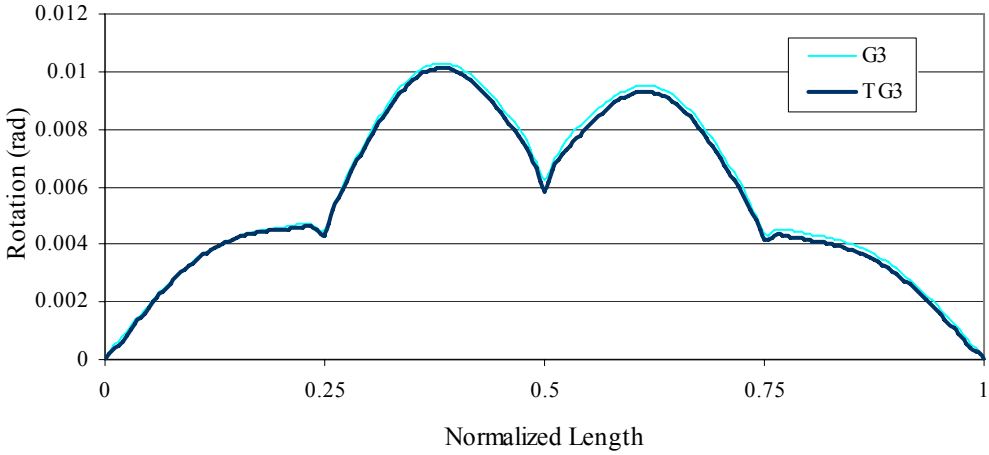

Figure 8.43 Cross Section Rotation for G3 and TG3 with 5 Stiffeners (Truck Load)

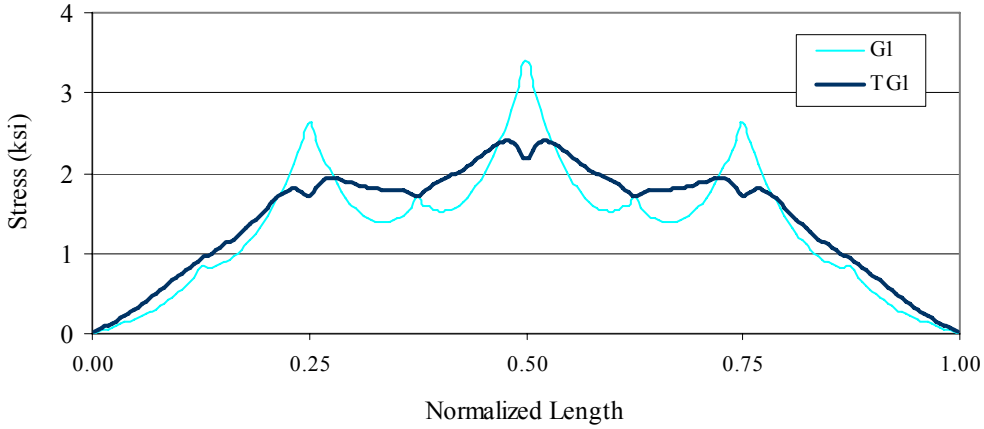

Figure 8.44 Total Normal Stress at P3 for G1 and TG1 with 9 Stiffeners (Lane Load)

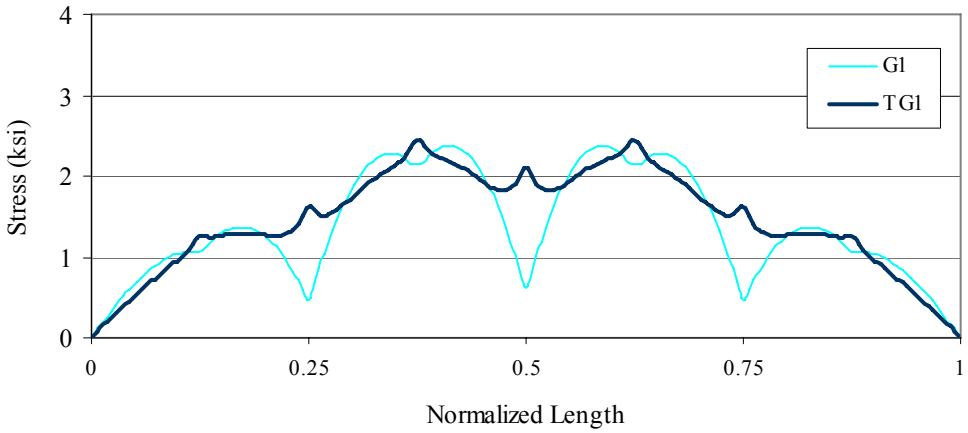

Figure 8.45 Total Normal Stress at P2 for G1 and TG1 with 9 Stiffeners (Lane Load)

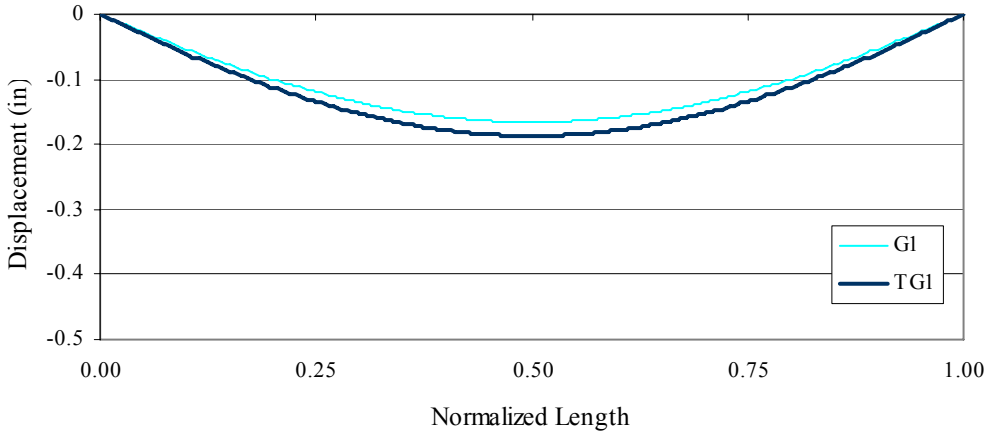

Figure 8.46 Vertical Displacement for G1 and TG1 with 9 Stiffeners (Lane Load)

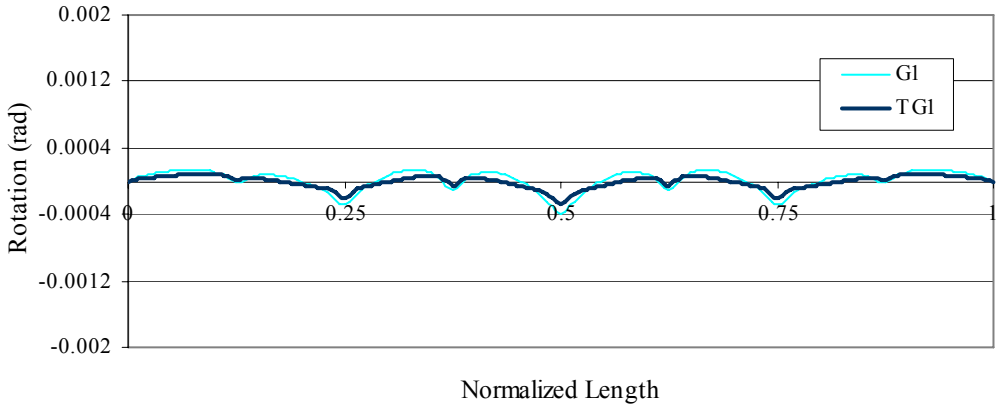

Figure 8.47 Cross Section Rotation for G1 and TG1 with 9 Stiffeners (Lane Load)

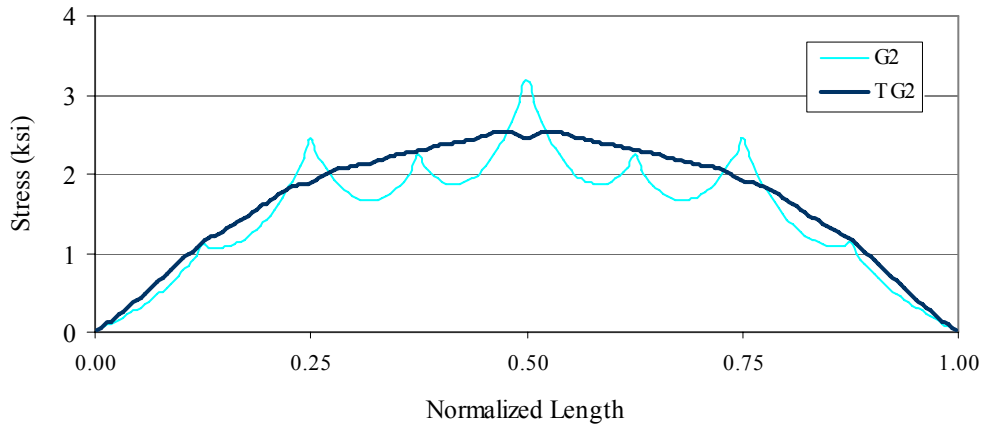

Figure 8.48 Total Normal Stress at P3 for G2 and TG2 with 9 Stiffeners (Lane Load)

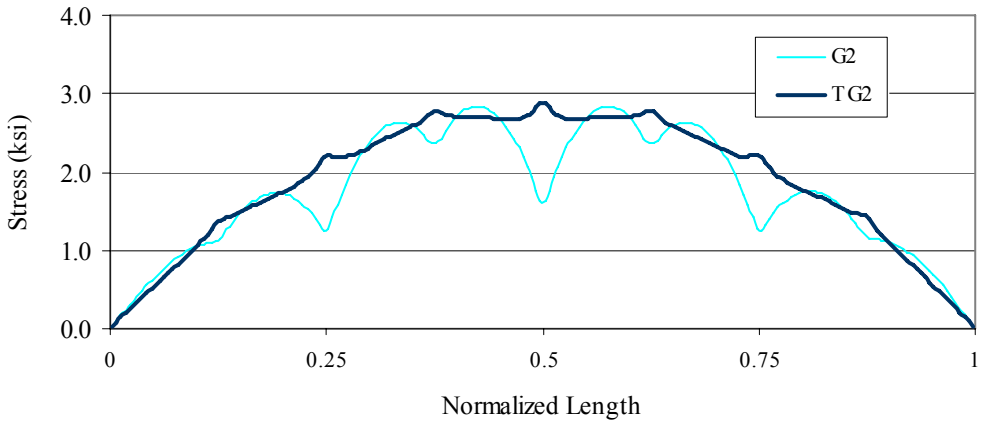

Figure 8.49 Total Normal Stress at P2 for G2 and TG2 with 9 Stiffeners (Lane Load)

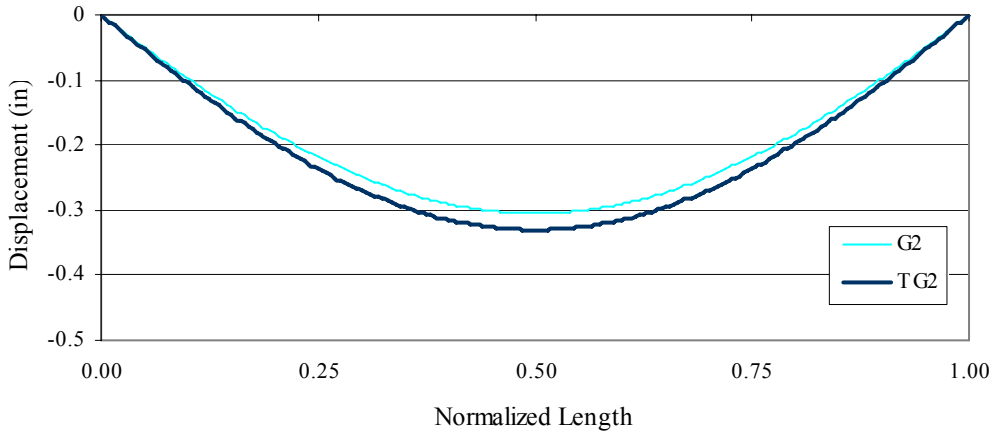

Figure 8.50 Vertical Displacement for G2 and TG2 with 9 Stiffeners (Lane Load)

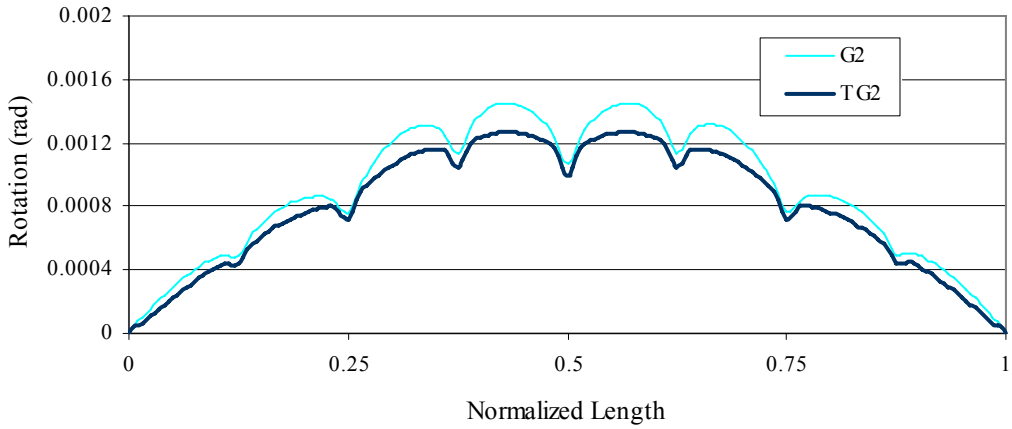

Figure 8.51 Cross Section Rotation for G2 and TG2 with 9 Stiffeners (Lane Load)

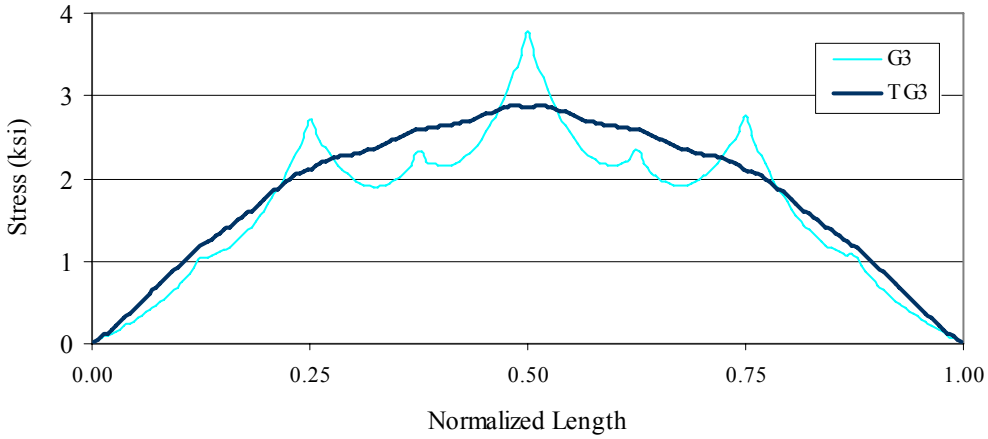

Figure 8.52 Total Normal Stress at P3 for G3 and TG3 with 9 Stiffeners (Lane Load)

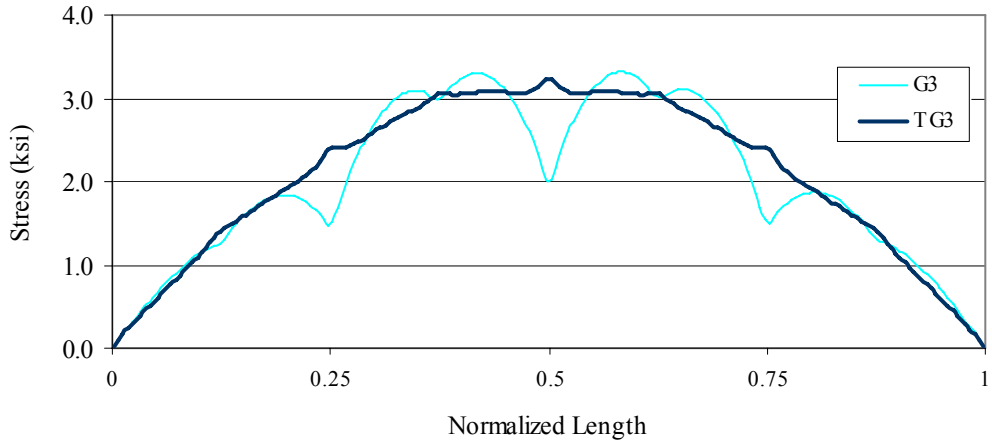

Figure 8.53 Total Normal Stress at P2 for G3 and TG3 with 9 Stiffeners (Lane Load)

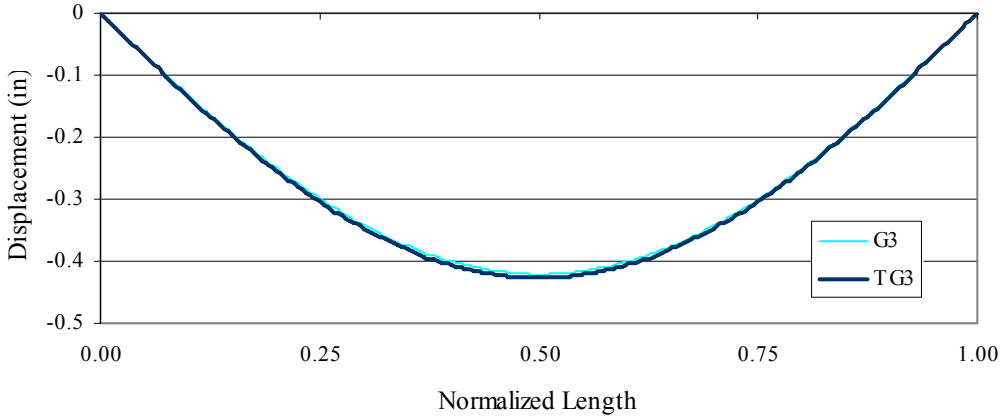

Figure 8.54 Vertical Displacement for G3 and TG3 with 9 Stiffeners (Lane Load)

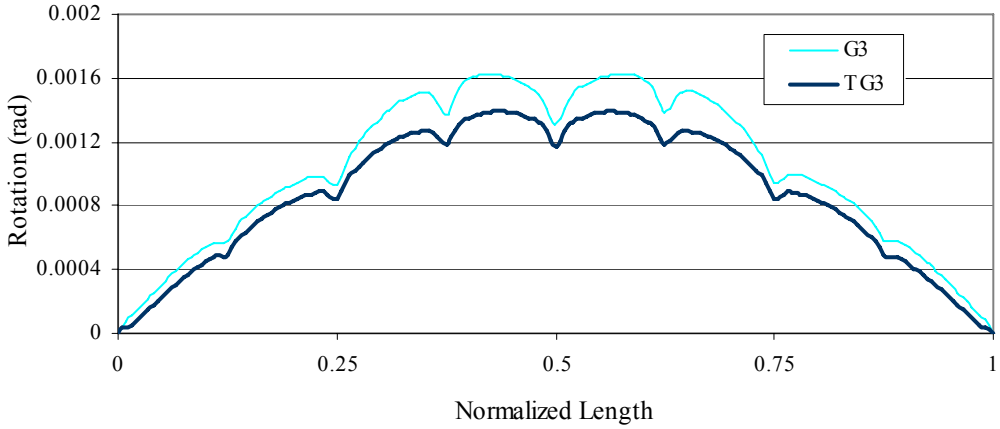

Figure 8.55 Cross Section Rotation for G3 and TG3 with 9 Stiffeners (Lane Load)

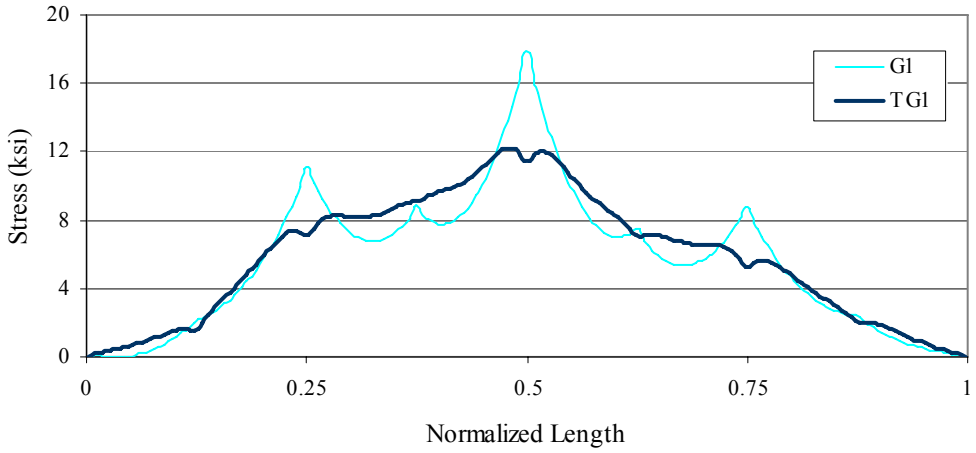

Figure 8.56 Total Normal Stress at P3 for TG1 with 9 Stiffeners (Truck Load)

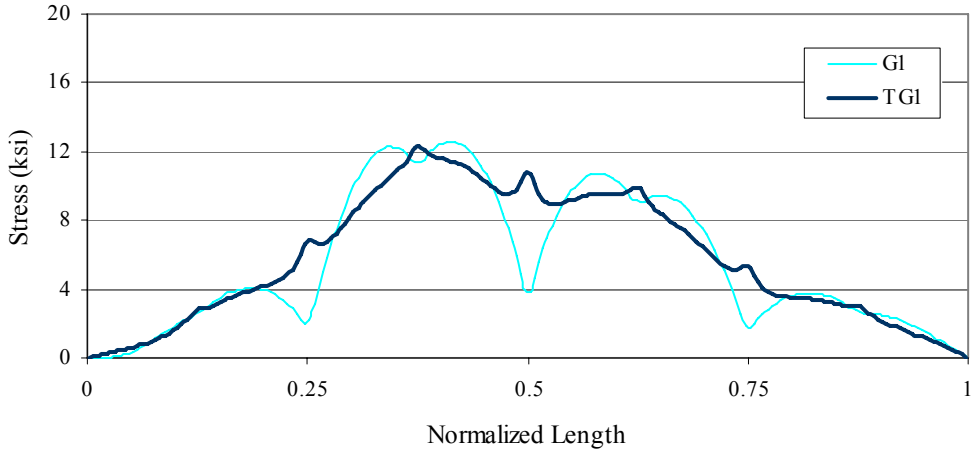

Figure 8.57 Total Normal Stress at P2 for TG1 with 9 Stiffeners (Truck Load)

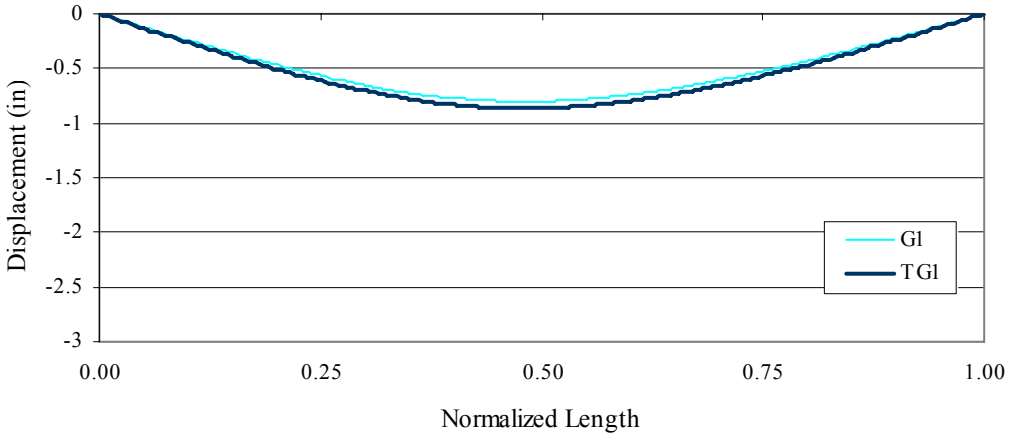

Figure 8.58 Vertical Displacement for TG1 with 9 Stiffeners (Truck Load)

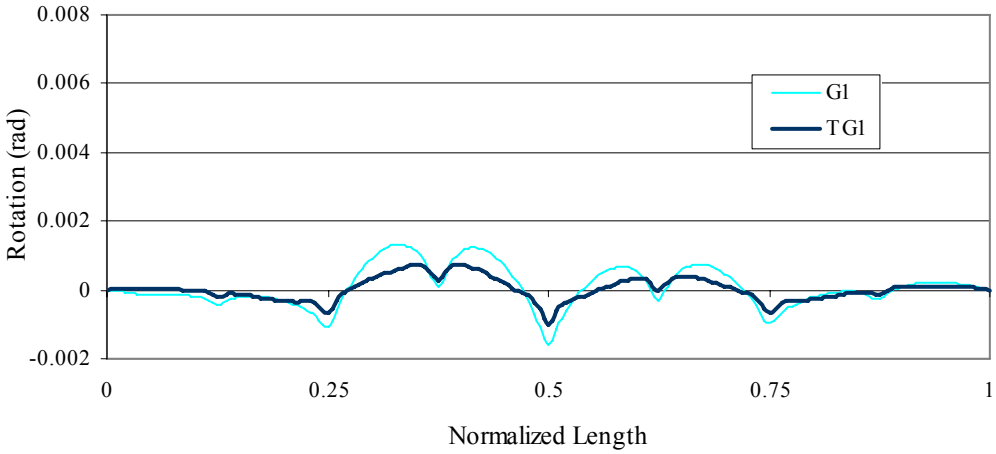

Figure 8.59 Cross Section Rotation for TG1 with 9 Stiffeners (Truck Load)

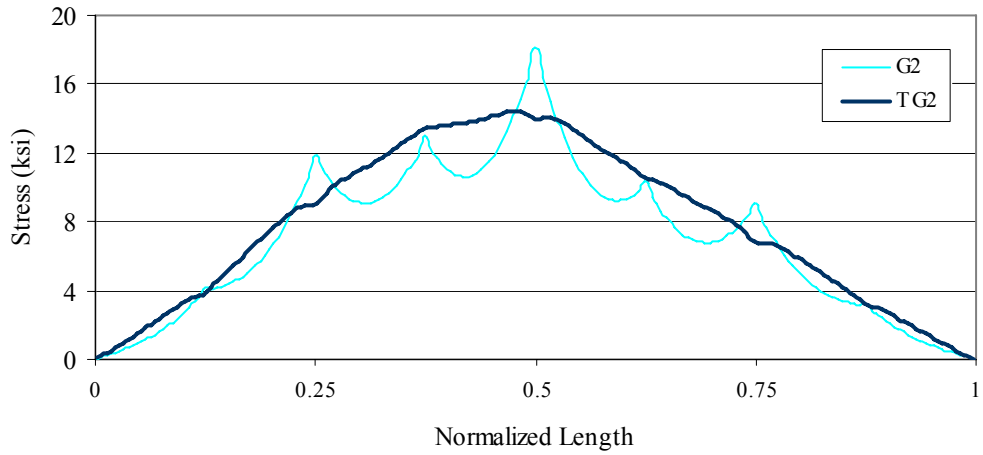

Figure 8.60 Total Normal Stress at P3 for TG2 with 9 Stiffeners (Truck Load)

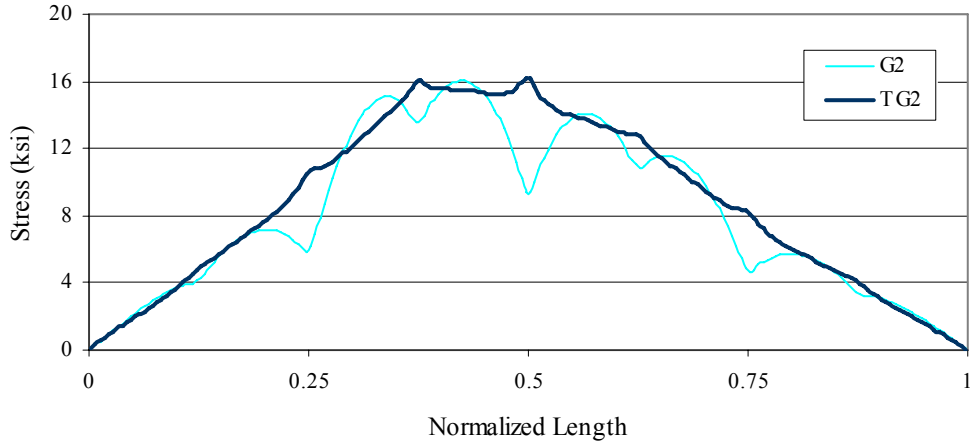

Figure 8.61 Total Normal Stress at P2 for TG2 with 9 Stiffeners (Truck Load)

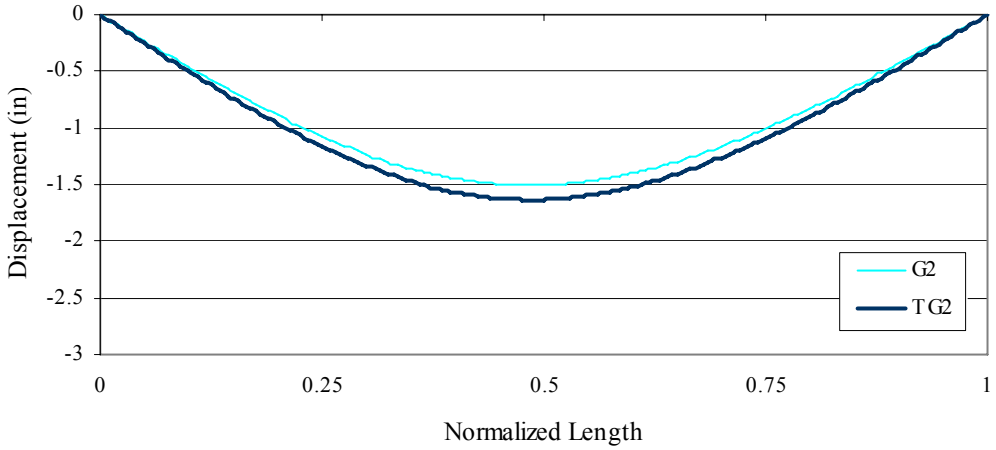

Figure 8.62 Vertical Displacement for TG2 with 9 Stiffeners (Truck Load)

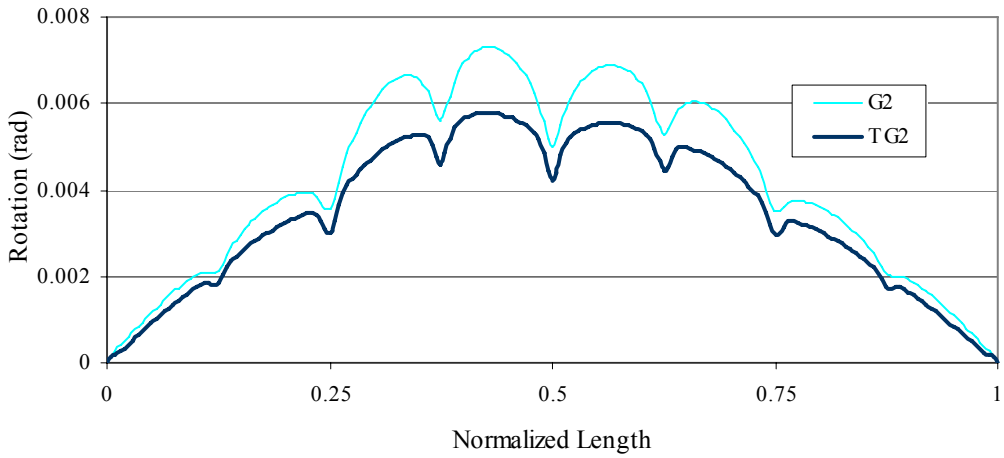

Figure 8.63 Cross Section Rotation for TG2 with 9 Stiffeners (Truck Load)

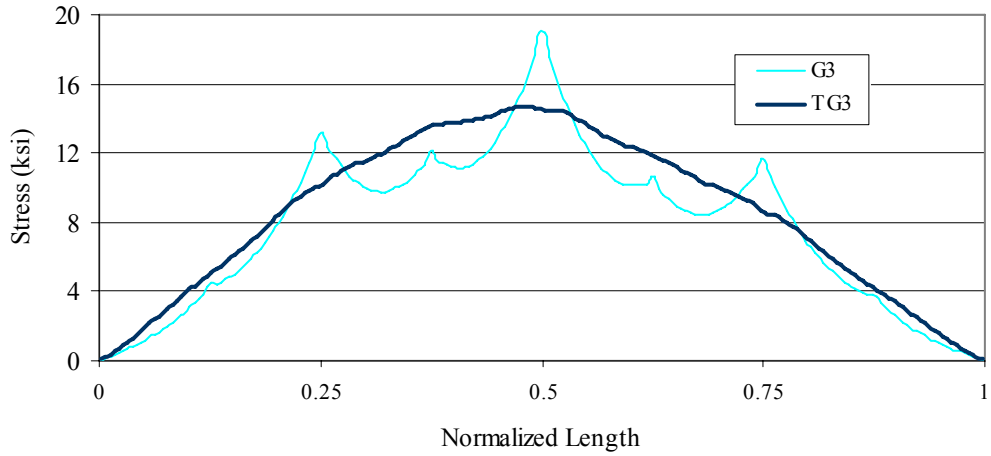

Figure 8.64 Total Normal Stress at P3 for TG3 with 9 Stiffeners (Truck Load)

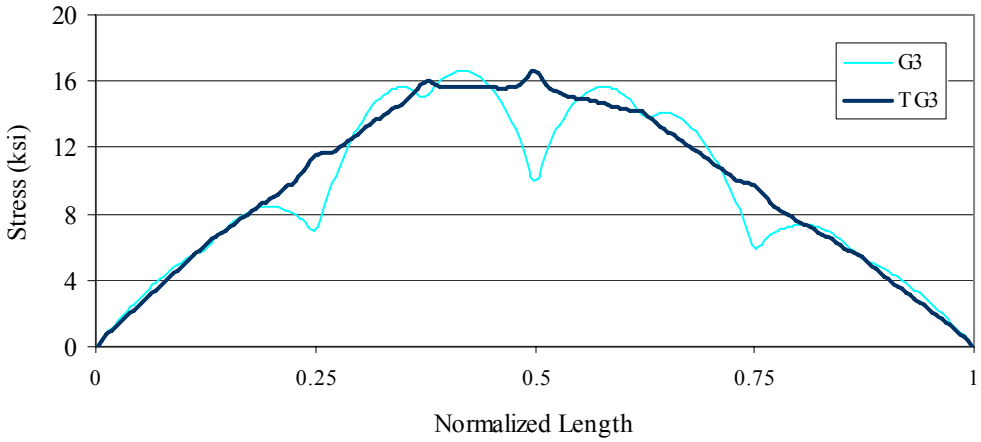

Figure 8.65 Total Normal Stress at P2 for TG3 with 9 Stiffenres (Truck Load)

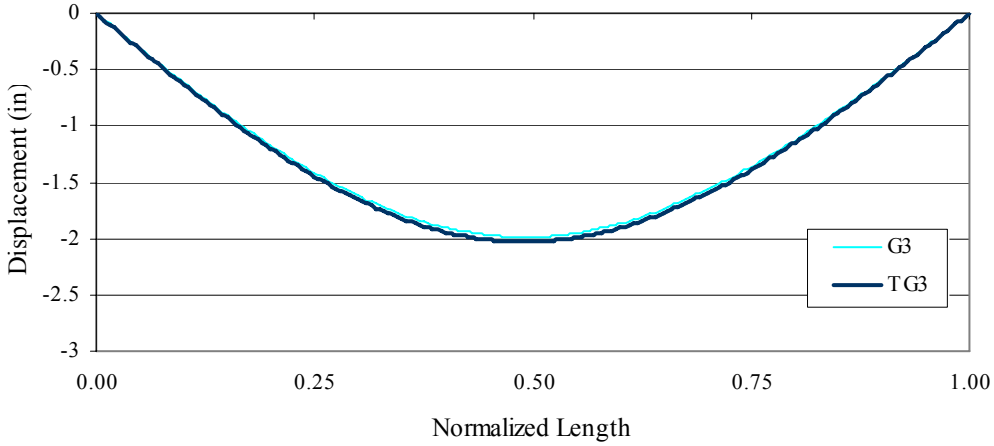

Figure 8.66 Vertical Displacement for TG3 with 9 Stiffeners (Truck Load)

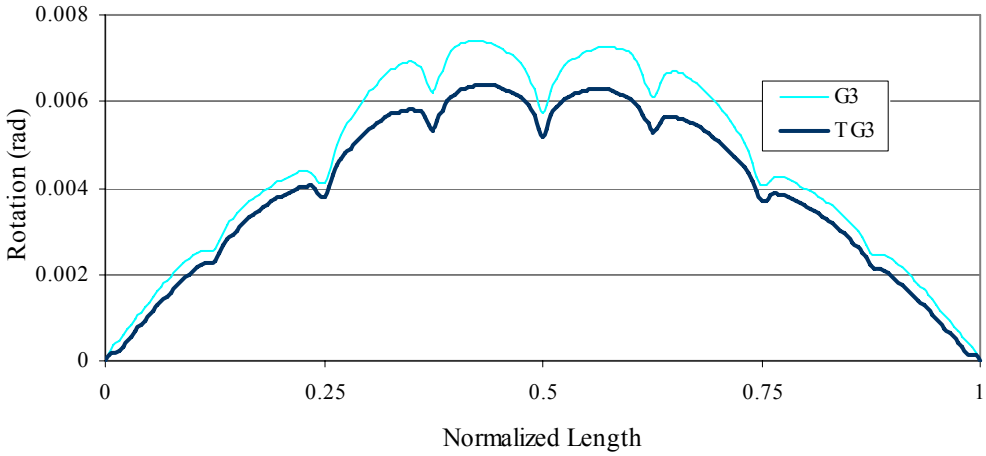

Figure 8.67 Cross Section Rotation for TG3 with 9 Stiffeners (Truck Load)

Chapter 9 Summary and Conclusions

9.1 Summary

A new type of curved girder, called a curved tubular-flange girder, is studied in this report. For the curved tubular-flange girder system that was studied, rectangular tubes are used as top and bottom girder flanges instead of the traditional plate flanges. Tubular-flange girders have much larger torsional stiffness than I-girders and less potential for cross section distortion than box-girders. Therefore, curved tubular-flange girders have potential advantages compared to curved I-girders and box-girders. Hence, theoretical and finite element analyses were carried out to investigate the behavior of curved tubular-flange girder systems.

A theoretical method was presented to study the behavior of simply supported curved tubular-flange girder bridge systems. In this theoretical method, the cross frames between the girders are assumed to be rigid. A cross section stress analysis method for tubular-flange girders was presented. A parametric study was performed using the theoretical analysis method for single curved tubular-flange girders and three-girder systems to investigate the effect of geometric parameters on the behavior of curved tubular-flange girder systems. The studied parameters include the tubular-flange width, tubular-flange depth, cross section depth, girder curvature, and the number of cross frames. The theoretical analysis results from selected cases were also compared with the results from finite element analyses to verify the parametric study results.

Finite element simulations for curved tubular-flange girder systems were performed to verify the theoretical analysis method and study the behavior of curved tubular-flange girder systems with and without a composite concrete deck. The effect of cross section distortion and the influence of the composite concrete deck were investigated. A live load analysis was carried out for both a curved tubular-flange girder system with a composite deck and a curved I-girder system with a composite deck. The finite element results for the curved tubular-flange girder system were compared with those of the corresponding curved I-girder system.

9.2 Findings

The following findings are obtained from the theoretical analyses:

- The warping of curved tubular-flange girders can be considered to consist of two parts, namely, lateral bending of each tubular-flange about the y-axis and warping of each rectangular tube about its own shear center.

- From the cross section stress analysis of tubular-flange girders, it was found that for a doubly-symmetric tubular-flange cross section, the warping moment of inertia can be simply expressed as:

$$I_w = \frac{I_{yf} \cdot h_0^2}{4} \tag{4.15}$$

- A curved tubular-flange girder is effective at resisting torsion, owing to its large torsional stiffness, and it develops relatively small warping normal stress and cross section rotation compared to a corresponding I-girder, while the corresponding curved I-girder is better at resisting bending, but develops relatively large warping normal stress and cross section rotation.

- For simply-supported single curved tubular-flange girders and multiple curved tubular-flange girder systems braced by cross frames, the following observations were made regarding stresses: the bending normal stress makes the dominant contribution to the total normal stress, relative to the warping normal stress; the St.Venant shear stress makes the dominant contribution to the total shear stress, relative to the warping shear stress and the vertical shear stress. For a single curved tubular-flange girder, the warping shear stress over the entire span is negligible. For two-girder and three-girder systems, the warping shear stress at the cross section with the maximum total shear stress is negligible, but is not negligible at other cross sections.

- A simply-supported single curved tubular-flange girder develops much smaller stresses and displacements than the corresponding single curved I-girder. The practical impact of this result is that a single curved tubular-flange girder would be easier to transport and erect than a single I-girder.

- The cross frame forces in a curved tubular-flange girder system are smaller than in the corresponding curved I-girder system. Therefore, smaller cross frame members can be used in a curved tubular-flange girder system.

The following findings are obtained from the parametric study:

- A curved tubular-flange girder with a wider and/or thicker tube results in reduced stresses and displacements. The bending and warping normal stresses are especially reduced.
- An increase in the cross section depth effectively reduces the bending normal stress, the vertical shear stress, and the vertical displacement, but the increase in the cross section depth has little effect on the St.Venant shear stress and the cross section rotation.
- An increase in the tubular-flange depth reduces the warping normal stress, the St.Venant shear stress, and the displacement.

- A single curved tubular-flange girder develops much smaller stresses and displacements than a corresponding single curved I-girder for the same bridge girder curvature.
- An increase in the curvature of bridge girders has much more influence on stresses and displacements for a single curved I-girder than for a single curved tubular-flange girder. As the girder curvature increases, the rate of increase in the stresses and displacements for a single curved I-girder is much greater than for a single curved tubular-flange girder.
- Fewer cross frames are needed for a curved tubular-flange girder system to have levels of stress that are similar to those of the corresponding curved I-girder system.

The following findings are obtained from finite element analyses:

- Cross section distortion was observed for curved tubular-flange girders under loading. The cross section distortion comes from web distortion and the distortion of the tubular flanges. The cross section distortion results in increased stresses and displacements.
- For a single curved tubular-flange girder, web distortion is the main source of cross section distortion and using transverse web stiffeners effectively reduces the effect of cross section distortion on the stresses and displacements.
- For a multiple curved tubular-flange girder system, the cross section distortion mainly results from concentrated forces and torques acting on the girders at the cross frames locations. Tubular flange distortion is the major source of cross section distortion and using transverse web stiffeners produces only a modest reduction in the effect of cross section distortion.
- For a curved tubular-flange girder system with a composite concrete deck, the composite concrete deck increases the system stiffness and reduces the warping normal stress in the girders.
- A curved tubular-flange girder with a composite concrete deck develops less warping normal stress and cross section rotation than the corresponding curved I-girder. Using an appropriate number of transverse web stiffeners on the curved tubular-flange girders of a multiple girder system with a composite concrete deck effectively reduces the effect of cross section distortion, especially, for the outer girder of the multiple girder system.

9.3 Conclusions

Based on the research on curved tubular-flange girder systems reported in this report, the following conclusions are made.

- The theoretical analysis method for curved tubular-flange girder systems presented in the report is accurate for cases without cross section distortion.

- Cross section distortion for curved single tubular-flange girders is not a major concern, since the distortion can be effectively controlled by transverse web stiffeners.
- Owing to their increased torsional stiffness, curved single tubular-flange girders should be easier to lift, transport, and erect than curved single I-girders.
- A curved tubular-flange girder system needs fewer cross frames than the corresponding I-girder system to develop similar levels of stress.
- Smaller cross frame members can be used in a curved tubular-flange girder system, compared to the corresponding I-girder system, since smaller cross frame forces develop in the curved tubular-flange girder system.
- Cross section distortion is a concern for curved tubular-flange girder systems (girders braced by cross frames) without a composite concrete deck.
- For a curved tubular-flange girder system with a composite concrete deck, the effect of cross section distortion can be effectively controlled by transverse web stiffeners.
- Bending normal stress dominates the behavior of a curved tubular-flange girder system with a composite concrete deck, when sufficient transverse web stiffeners are used, since the warping normal stress is small. On the other hand, the behavior of curved I-girder systems involves bending normal stress and significant warping normal stress, which suggests that curved tubular-flange girder systems can be designed to be more efficient than I-girder systems for curved highway bridges.

9.4 Future Research

The following future research is recommended:

- Study the nonlinear behavior of curved steel tubular-flange girder systems, including geometric and material nonlinear behavior, and investigate the ultimate strength of curved tubular-flange girder systems.
- Study and develop practical methods to restrain the cross section distortion of curved tubular-flange girders, especially the distortion of the tubular flanges.
- Develop practical methods of fabricating curved steel tubular-flange girders.
- Conduct experimental research to verify theoretical and finite element analysis results.
- Propose design criteria for preliminary and final design of curved steel tubular-flange girder systems for bridge.

References

AASHTO (2003) *AASHTO Guide Specifications for Horizontally Curved Steel Girder Highway Bridges*, American Association of State Highway Transportation Officials (AASHTO), Washington, D.C.

AASHTO (2004) *AASHTO LRFD Bridge Design Specification*, American Association of State Highway Transportation Officials (AASHTO), Washington, D.C.

ABAQUS (2003) "Standard User's Manual", v6.5. 2003.

Benscoter, S.U., (1954) "A Theory of Torsion Bending for Multicell Beams," J. Applied Mechanics, March, 25-34.

Dabrowski, R. (1968) *Curved Thin-Walled Girders, Theory and Annalysis*, Cement and Concrete Association, London.

Galambos, T. V. (1968) *Structural Members and Frames*, Prentice-Hall, Englewood Cliffs, NJ.

Kim, B. J. (2005) "High Performance Steel Girders with Tubular Flanges," Ph.D. Report, Lehigh University, Bethlehem, PA.

Richardson, Gordon, and Associate (1963) "Analysis and Design of Horizontal Curved Steel Bridge Girders," United States Steel Corporation, Pittsburgh, PA.

Wimer, M. R. (2004) "Concrete Filled Rectangular Tubular Flange Girders with Corrugated and Flat Webs," M.S. Thesis, Lehigh University, Bethlehem, PA.

U.S. Steel Corporation (1984) *V-Load Method*, Pittsburgh, PA.

Zureick A., and Naqib, R. (1999) "Horizontally Curved Steel I-Girders, State-of-the-art: Part I-Analysis Methods," Journal of Bridge Engineering, Vol. 4, No. 1, pp. 1-10.